Summer 9-5-2017

Field Mapping Investigation and Geochemical Analysis of Volcanic Units within the Dinner Creek Tuff Eruptive Center, Malheur County, Eastern Oregon

Matthew Cruz
Portland State University

Recommended Citation
Cruz, Matthew, "Field Mapping Investigation and Geochemical Analysis of Volcanic Units within the Dinner Creek Tuff Eruptive Center, Malheur County, Eastern Oregon" (2017). *Dissertations and Theses.* Paper 3837.
https://doi.org/10.15760/etd.5731

Field Mapping Investigation and Geochemical Analysis of Volcanic Units within the Dinner Creek Tuff Eruptive Center, Malheur County, Eastern Oregon

by

Matthew Cruz

A thesis submitted in partial fulfillment of the
requirements for the degree of

Master of Science
in
Geology

Thesis Committee:
Martin Streck, Chair
Michael Cummings
John Bershaw

Portland State University
2017

Abstract

The Dinner Creek Tuff is a mid-Miocene rhyolitic to dacitic ignimbrite, consisting of four cooling units with $^{40}Ar/^{39}Ar$ ages 16 – 15 Ma. Previous geologists have suspected that the source of the tuff is located in northwestern Malheur County, eastern Oregon. This broad area is called the Dinner Creek Tuff Eruptive Center.

This thesis summarizes field work, XRF/ICP-MS geochemistry, thin section petrography, and SEM feldspar analysis from the summers of 2015 and 2016. The main purpose of this study is to identify sources for the Dinner Creek Tuff units within the Dinner Creek Tuff Eruptive Center. The secondary purpose is to map lave flows that pre-date and post-date the Dinner Creek Tuff, and correlate them with regionally extensive volcanic units.

Two volcanic centers related to the Dinner Creek Tuff were identified. The southern volcanic center, centered at Castle Rock, is a caldera and source of the Dinner Creek Tuff unit 1 (DIT1). Rheomorphic, densely welded DIT1 is over 300 m thick along the east side of Castle Rock. The northwestern margin of the caldera has been uplifted along faults, showing vertically foliated tuff dikes and associated mega-breccia deposits. Up to 200 m of incipiently welded tuffs, and fluvial volcaniclastic sediments were deposited on the caldera floor, which has been uplifted due to resurgence and regional extension, creating the complex structural relationships between the volcanic units.

The northern volcanic center is located at Ironside Mountain, where densely welded rheomorphic Dinner Creek Tuff unit 2 (DIT2) is exposed in outcrops over 600 m thick. The top of the DIT2 consists of glassy, moderately welded tuff. Sources for the DIT2 are

tuff dikes along the south and western flanks of Ironside Mountain. The thick deposits of DIT2 at Ironside Mountain indicate that the mountain is an uplifted caldera, herein named the Ironside Mountain caldera. Uplift may have been due to resurgence, but it is most likely due to normal faulting along the Border Fault, a major regional normal fault that strikes across the northern margin of the caldera.

Pre-Dinner Creek Tuff lava flows occur throughout the study area, and can be correlated with the Strawberry Volcanics and the Basalt of Malheur Gorge. A distinct lava flow, herein called the Ring Butte trachy-basalt occurs within the center of the study area, and is distinct from regional lava flows. Following the eruptions of the Dinner Creek Tuff units 1 & 2, aphyric basaltic-andesite and icelandite intrude into, and overlie the intra-caldera tuffs and caldera floor sediments at both calderas. These aphyric lavas are similar in appearance and stratigraphic position with the regionally extensive Hunter Creek basalt. Porphyritic olivine basalt overlies the aphyric Hunter Creek basalt at the Castle Rock caldera. This porphyritic lava is similar in appearance and major/trace element geochemistry to the regional Tim's Peak basalt.

Acknowledgements

I would like to thank my advisor Martin Streck for his tutelage and patience. Thanks must also go to my professors and fellow graduate students at Portland State University for their insight. I would also like to extend my thanks to the ranchers and citizens of Juntura and Unity, who were kind enough to let me run around all over their property. Finally, I would like to thank my family for their unwavering support in my professional and academic career.

Table of Contents

List of Tables

List of Figures

Chapter I: Introduction, background, and methods

Introduction

The Dinner Creek Tuff is a mid-Miocene rhyolitic to dacitic ash flow tuff that is widespread across eastern Oregon. The tuff is made up of at least four cooling units that range in age from 16 to 15 Ma (Streck et al. 2015). The Dinner Creek Tuff erupted at the tail end of the Grande Ronde Basalt sequence, the most voluminous phase of the Columbia River Basalt Group (herein after abbreviated to CRBG) (Camp and Hanan, 2008; Streck et al., 2015). It is one of several regionally extensive ash flow tuffs in eastern Oregon to erupt during the eruption of the CRBG, and together with these other tuffs forms the Lake Owyhee Volcanic Field (LOVF) (Rytuba and Vander Meulen, 1991; Ferns and McClaughery, 2013; Benson and Mahood, 2016).

Despite being one of the largest tuffs within the LOVF, the source of the Dinner Creek Tuff has been poorly defined. The first geologists to study the unit believed that the tuff came from a dike exposed along the summit of Castle Rock (Haddock, 1966; Woods, 1976). However, as the size and extent of the tuff became better understood, it became clear that this one dike could not be the source for the entire unit. Later geologists suspected that a caldera was located near Castle Rock, a topographic high point at the western edge of Malheur County (Rytuba and Vander Meulen, 1991). More recently, the Dinner Creek Tuff eruptive center (DITEC) was defined as a broad source area for the tuff in between Castle Rock and Ironside Mountain (Streck et al., 2015). Due to the difficult terrain, few roads, and large plots of private land, little actual field work has been done in the area.

This thesis summarizes field work that was done during the summers of 2015 and 2016 within the DITEC (**Figure 1**). The main purpose of this thesis is to identify volcanic centers within the DITEC that were the sources for the Dinner Creek Tuff units. Characteristic features of calderas were mapped, and Dinner Creek Tuff samples were collected for XRF/ICP-MS analysis in order to separate the tuff units by major/trace element content.

The secondary purpose of this thesis is to better characterize the pre-Dinner Creek Tuff and post-Dinner Creek Tuff volcanic units in the DITEC. Some lava samples were selected for XRF and ICP-MS analysis, in order to compare to regional mafic units, such as the Basalt of Malheur Gorge, Hunter Creek basalt, Strawberry Volcanics, and Tim's Peak basalt. Thin sections were also made for select samples in order to study the petrography of the various mafic/intermediate lava flows.

The end goal of this study is to present a clearer picture of the DITEC. Silicic volcanic centers were identified as sources for Dinner Creek Tuff units, and the extent of the various mafic/intermediate units within the study area were also characterized. The data were used to create a stratigraphic column of the DITEC, and a timeline of events from pre-Dinner Creek Tuff to the present day.

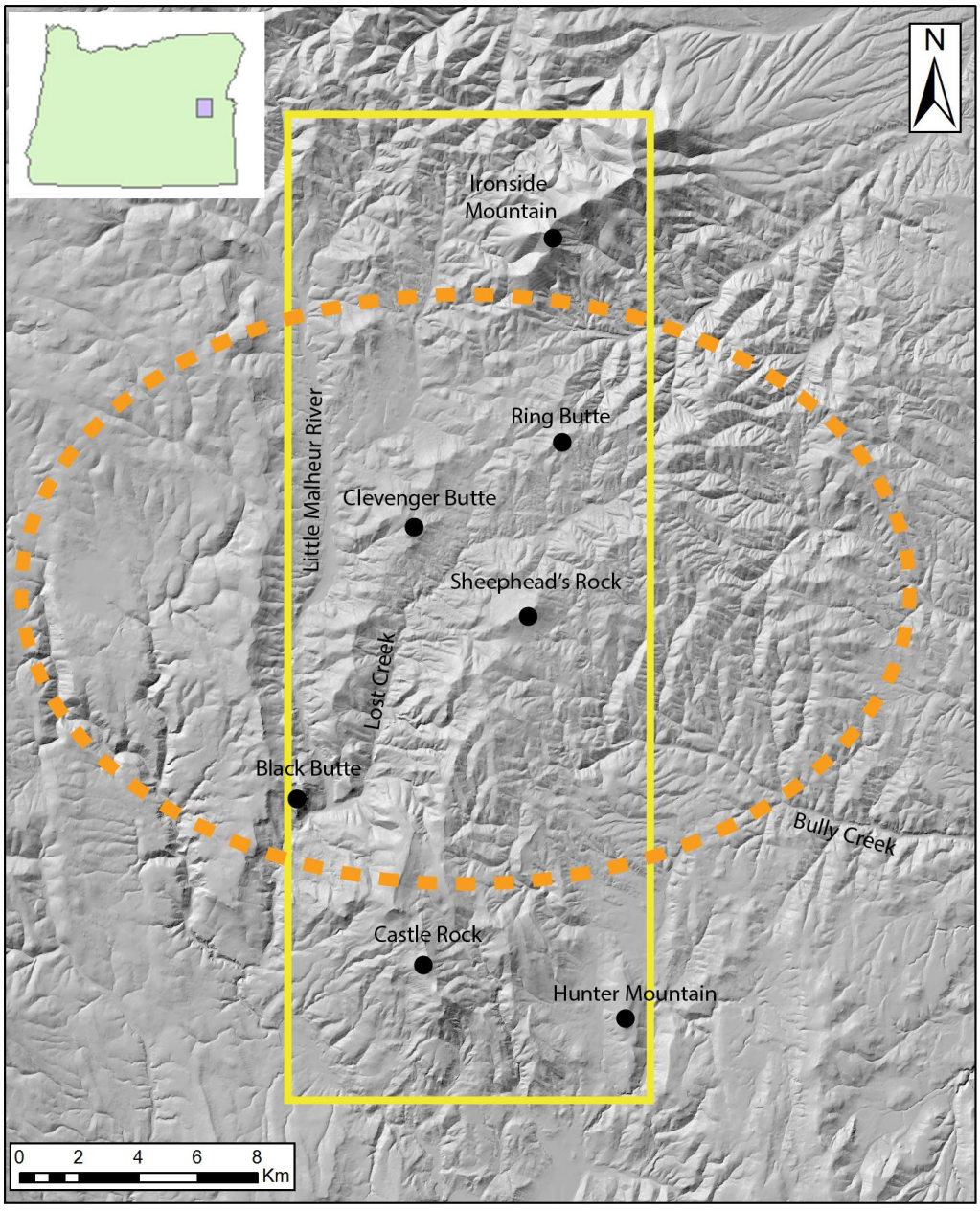

Figure 1. Location of study area (yellow rectangle. Orange dotted oval is the DITEC defined by Streck et al. 2015.

Dinner Creek Tuff

The Dinner Creek Tuff is a densely welded to moderately welded tuff that is exposed throughout the study area. It was first recognized by Kittleman et al. (1965), and mapped as the welded tuff member of the Hogback formation. Haddock (1967) mapped the tuff across the Malheur River gorge, identifying a basal moderately welded pumice lapilli tuff sequence which grades upward into a purple-red-tan densely welded, foliated, devitrified section. In his map, Lowry (1968) called the Dinner Creek Tuff the 'Dooley Rhyolite' and mapped it north of Castle Rock, and at Ironside Mountain. Woods (1976) mapped the tuff around Castle Rock, and identified source vents on the summit ridge of Castle Rock and at Black Butte, 7 km northwest of Castle Rock. On a more regional scale, the Dinner Creek Tuff was grouped with other ash-flow tuffs into the LOVF, which stretches from Castle Rock southeast towards Lake Owyhee (Rytuba and Vander Meulen, 1991; Ferns and McClaughery, 2013; Benson and Mahood, 2016). This volcanic field was linked to the CRBG, as a rhyolite ignimbrite phase contemporaneous or immediately following the eruption of the main flood basalt phase (Nash et al., 2006; Coble and Mahood, 2012; Streck et al., 2015). Rytuba and Vander Meulen (1991) interpreted younger ash-flow tuffs and tuffaceous breccia deposits that Lowry (1968) mapped as mega-breccia and caldera fill deposits, and named the Castle Rock caldera as the source for the Dinner Creek Tuff, although exact boundaries for the caldera were not defined. In these early studies, the Dinner Creek Tuff was restricted to the Castle Rock and Malheur River gorge, covering an area of 2000 km^2. Comparisons between the Dinner Creek Tuff and other regional tuffs (Bully Creek tuff, Mascall ignimbrite, and Pleasant Valley tuff) using age dates, major/trace element data, and mineral composition found that these tuffs

are actually distal outflow deposits of the Dinner Creek Tuff units, expanding the the known aerial extent to 25,000 km^2 (**Figure 2**) (Streck et al., 2015).

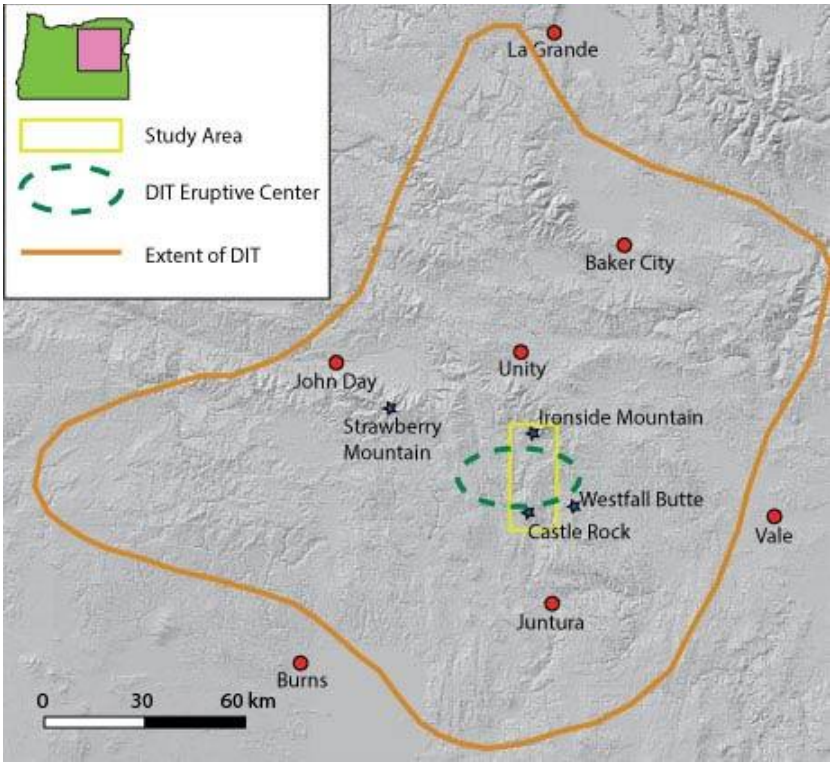

Figure 2. Map of eastern Oregon, showing the extent of the Dinner Creek Tuff, and the study area from Figure 1. Modified from Streck et al. 2015.

The Dinner Creek Tuff is best recognized in the study area and the surrounding region as a densely welded, devitrified, rheomorphic, brown-purple, cliff forming welded tuff. The tuff is eutaxitic, with pumice fragments flattened down to 1-2 mm width, creating prominent foliation planes, which causes outcrops to break into tabular fragments. As mentioned above, Haddock (1967) identified a basal pumice lapilli tuff section underneath some outcrops of the dense devitrified section. Basal vitrophyres have also been identified, although they are poorly exposed (Haddock, 1967). The phenocryst

content of the tuff is about 5% (Woods, 1976). Phenocrysts are mostly euhedral to subhedral plagioclase, which can reach lengths of 3 mm. Less common are titanomagnetite, and clinopyroxene phenocrysts (Haddock, 1967; Evans and Binger, 1997; Streck et al., 2015). Lithic fragments are also minor constituents of the tuff. Basalt, glass, and scoria are the most common lithic fragments, with minor diorite, andesite, chert, and shale fragments. Lithic fragments are typically less than 1 cm in length, and less than 5% of the unit. Within recent years, geochemical analysis and age dating has led to the realization that the Dinner Creek Tuff is made of four cooling units, hereafter referred to as DIT 1 – 4, erupted within a time span of 16 – 14.9 Ma., and decrease in silica content from rhyolitic (>75% SiO_2) to dacitic (<68% SiO_2) (Streck et al., 2015) (**Figure 3**). The geochemical distinction between these units will be further explored in Chapter 3.

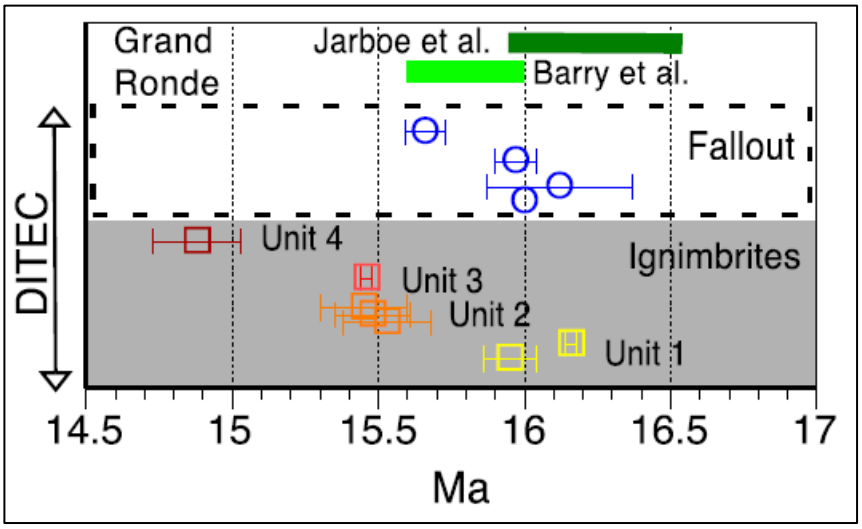

Figure 3. Age dates of Dinner Creek Tuff units and Grande Ronde basalts. Figure from Streck et al. 2015.

Calderas

Calderas form from the evacuation of large volumes (>1 km^3) of magma from a magma chamber during eruption (Smith and Bailey, 1968). As more magma is erupted, the overlying chamber roof collapses along faults, known as ring fractures (Lipman, 1984). Calderas can have different forms, ranging from almost perfectly circular to highly elliptical. The size of the underlying magma chamber, the thickness and composition of the sub-siding block, and the orientation of pre-existing faults and other structural features could all play a factor in determining the size and shape of a caldera (Lipman, 1997). This section briefly summarizes some of the most common structural/depositional features of calderas, which were recognized in the study area.

Intra-Caldera tuff

Most of the pyroclastic material that erupts during an eruption accumulates in the space that is created as the caldera forms. The tuff that is deposited within the caldera is thicker and more densely welded than the outflow deposits (Lipman, 1997). Hydrothermal alteration can also be more pervasive within intra-caldera tuff deposits than outflow deposits, due to the circulation of hot water within a geothermal system. Intra-caldera tuff can be over 100 m thick, and sometimes even on the order of several kms (Smith and Bailey, 1968; Lipman, 1984; Best et al., 1989; Lipman, 1997).

Ring fractures/dikes

Ring fractures mark the structural boundaries of calderas (Williams, 1941; Lipman, 1997; Acocella, 2006; Geyer et al., 2006). The magma erupts from these fractures, and the caldera floor collapses along them (Kennedy et al., 2004). Ring fractures are typically arcuate in shape, creating circular or elliptically shaped calderas.

More linearly shaped ring faults have been documented, and they may be influenced by the orientations of pre-existing faults (Aguirre-Diaz and Labarthe-Hernandez, 2003; Acocella, 2006). Ring dikes are best exposed in Mesozoic and Paleozoic calderas, which have been eroded down to the sub-magmatic level, beneath the overlying sedimentary and volcanic surface (Kingsley, 1931; Smith and Bailey, 1968; Lipman, 1984; Creasy and Eby, 1993; Lipman, 1997).

Mega-breccia

Mega-breccia are large, angular to sub-rounded blocks of country rock that collapse into the caldera during the climactic eruption (Shawe and Snyder, 1988). The lithic fragments can range in size from 1 m to hundreds of meters (Lipman, 1976; Lipman, 1997)

Caldera floor sediments

Since calderas are topographically lower in elevation than their surroundings, lakes often form within them (Smith and Bailey, 1968). Lacustrine and fluvial deposits are deposited along the caldera floor. Overtime, erosion, faulting, or subsequent volcanism can breach the caldera rim, and drain the lake (Smith and Bailey, 1968).

Resurgent dome

After the cataclysmic eruption, residual magma continues to rise towards the surface, and exerts a pressure against the roof of the magma chamber (Smith and Bailey, 1968). This initiates upward doming of the caldera floor. Sometimes, the doming is so intense that the resurgent dome rises higher than the surrounding caldera rim (Demant, 1984). The uplifted intra-caldera tuff and overlying volcanic rocks and lacustrine deposits are domed into a broad antiform. Faults and joints that are aligned with the long axis of

the resurgent dome can form, and in some cases, grabens can develop along the crest of the dome (Smith and Bailey, 1968).

Secondary volcanic edifices

Domes and volcanic cones are often erupted along the ring fractures of a caldera, and at faults and grabens along the resurgent dome (Smith and Bailey, 1968). The caldera forming eruption typically drains the magma chamber of its volatile content, leaving behind viscous silicic magma that then erupts as domes and flows along the ring fractures (Smith and Bailey, 1968). Post-caldera volcanism can also be intermediate to mafic in composition. The outline of these silicic domes and flows can be used to determine the locations of buried ring fractures (Lipman, 1997). **Figure 4** shows a plan view and cross section of a caldera, with the features described.

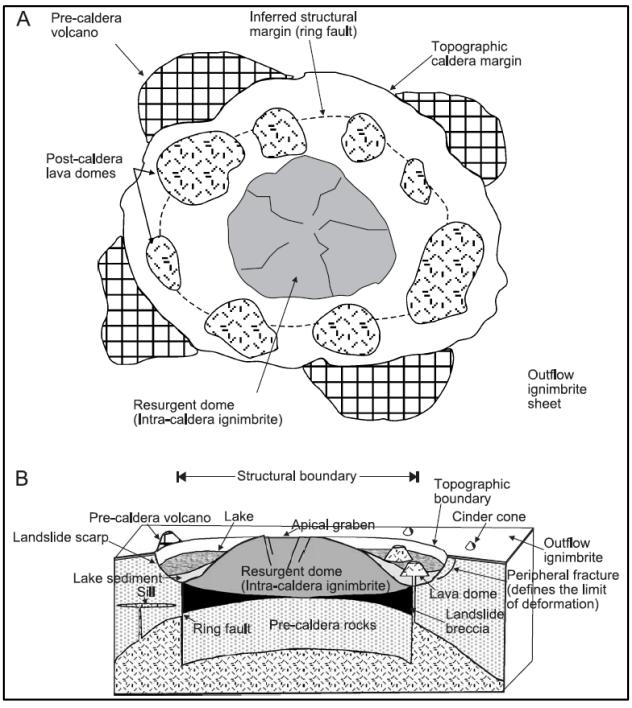

Figure 4. Plan view and cross section view of a caldera, showing the features described above. Figure from Cole et al. 2005.

Type of caldera

There are several recognized types of calderas, which can be distinguished from one another by the structure of the caldera floor and orientation of ring dikes/faults. The piston caldera forms from the collapse of a structurally coherent caldera floor into the magma chamber along steeply dipping ring faults (Smith and Bailey, 1968). This structural coherency allows for an even distribution of ash-flow tuffs within the caldera, and provides a flat surface for lakes to form within the caldera post-eruption. Resurgent domes can form in the center of the caldera, creating a structure that is similar in appearance to the one in **Figure 4**.

Piecemeal calderas are so named because the caldera floor is not a coherent structure, instead broken up into blocks which collapse to different degrees of depth (Branney and Kokelaar, 1994). Causes for this uneven collapse could be pre-caldera structures interacting with the caldera floor, or multiple eruptions of ash-flow tuffs from different ring dikes (Lipman, 1997).

Finally, trapdoor calderas form from collapse of the caldera floor along half-circular ring faults, creating a deeply subsided caldera floor along the ring fault that shallows towards a hinge line at the opposite end of the caldera (Lipman, 1997). Intra-caldera ash-flow tuffs are thickest towards ring faults, and can be less than 100 m thick at the hinge line. Trapdoor calderas are believed to form due to the shape of asymmetrical magma chambers, or from the influence of pre-caldera regional structures (Lipman, 1997). **Figure 5** shows the three types of calderas described above.

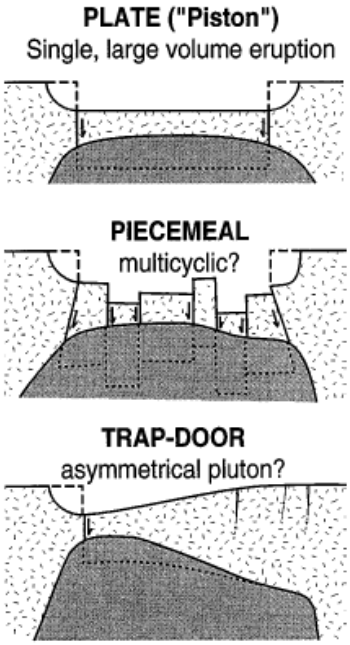

Figure 5. Cartoons of the three types of calderas described above. Figure from Lipman, 1997.

Regional Geology

Mesozoic basement

The oldest unit in the study area is the Weathersby Formation, which consists of interbedded shale, siltstone, greywacke, rhyolite tuffs, and limestone (Lowry, 1968). The Weathersby formation is exposed northwest and south of Ironside Mountain. These sedimentary rocks are part of the Izee Terrain, which was a marine fore arc basin off the coast of North America during the Mesozoic (Dorsey and LaMaskin, 2007). Amalgamation of the Wallowa Terrain to the North American continent caused deformation within the sediments (Ware, 2013). This deformation has created several major east-west trending anticlines and synclines within the study area (Lowry, 1968). U-Pb dating of zircons in interbedded tuffs east and west of the study area determined that

the sediments of the Weathersby Formation were deposited approximately 181 – 168 Ma (Ware, 2013).

The Tureman Ranch grano-diorite pluton is an 8 km by 3 km intrusive body that is elongated in a northeast-southwest direction along the southern flank of Ironside Mountain. It is a grano-diorite, with coarse plagioclase, biotite, and hornblende crystals typically 2-3 mm in size (Thayer and Brown, 1973). U-Pb ages for the Tureman Ranch grano-diorite are ~129 Ma (Ware, 2013). This age date is similar to other plutons in northeast Oregon which were intruded into the accreted terrains of the Blue Mountains (Dickinson, 2008). The Tureman Ranch grano-diorite is the oldest in a northeast trending line of plutons, and could represent migration of magmatism from eastern Oregon to Idaho, and the formation of the Cretaceous Idaho Batholith (Ware, 2013).

Early Cenozoic Strata

On a regional scale, calc-alkaline volcanic rocks of the Clarno Formation were deposited on top of the uplifted, eroded Blue Mountain terranes during the Eocene (Robyn, 1977; Felt, 2013). These volcanic rocks consist of basaltic to rhyolitic lava flows, tuff, and tuffaceous sediments (Robyn, 1979). Eocene to early Oligocene bi-modal volcanism produced ash-flow tuffs and basaltic lava flows of the John Day Formation. Vents and calderas for both the Clarno and John Day Formations occur to the north and west of the study area (McClaughery et al. 2009a; McClaughery et al. 2009b). Outcrops of late Oligocene to early Miocene calc-alkaline volcanic rocks are scattered throughout eastern Oregon. These volcanic rocks are andesite to dacite lava flows and pyroclastic material. The true extent of these rocks is difficult to determine, due to the great volume of overlying mid-Miocene flood basalts, but outcrops occur at the base of Steens

Mountain (75 km southeast of Castle Rock), at McEwen Butte quadrangle (25 km south of Castle Rock), and at Unity Reservoir (~75 km north of Castle Rock) (Brooks et al. 1979; Camp et al. 2003). Radiometric ages for the outcrops at Steens Mountain are ~24 – 17 Ma (Langer, 1991).

Within the study area, Lowry (1968) called hornblende lava flows and tuffs the 'Ring Butte andesite'. These appear to be the oldest volcanic rocks within the study area, and Lowry (1968) correlated them with Clarno Formation, based on similarities with Clarno outcrops to the west and north of the study area.

Mid-Miocene volcanics

The main phase of the CRBG consists of four members: the Steens basalt, the Imnaha basalt, the Picture Gorge basalt, and the Grande Ronde basalt. These tholeiitic lavas make up 92% of the total volume of the CRBG, and were erupted within the time span of 16.8 – 15.9 Ma (Wolf and Ramos, 2013). Silicic tuffs and lava flows were erupted contemporaneously with the flood basalts from various volcanic centers. The main silicic volcanic centers are the High Rock caldera complex in northwestern Nevada (16.4 – 15.7 Ma), the McDermitt caldera complex at the Nevada – Oregon border (16.5 – 15 Ma), and the LOVF (16 – 15 Ma) in eastern Oregon (Rytuba and Vander Meulen, 1991; Coble and Mahood, 2012, Ferns and McClaughery, 2013, Benson and Mahood, 2016). The LOVF consists of six regionally extensive tuffs, including the Dinner Creek Tuff (Rytuba and Vander Meulen, 1991). Sources for other regionally extensive tuffs occur southeast of the study area, at Lake Owyhee (Vander Meulen, 1989; Rytuba and Vander Meulen, 1991). Aside from these large silicic volcanic centers, smaller centers occur at Buchanan, along the eastern margin of the Harney Basin, and at Dooley

Mountain, 50 km north of the study area. These two volcanic centers have radiometric ages of 16.5 – 15.9 Ma and 16 – 15.2 Ma, respectively (Large, 2016). **Figure 6** shows a map of the Pacific Northwest with the distribution of CRBG lavas and silicic volcanic centers.

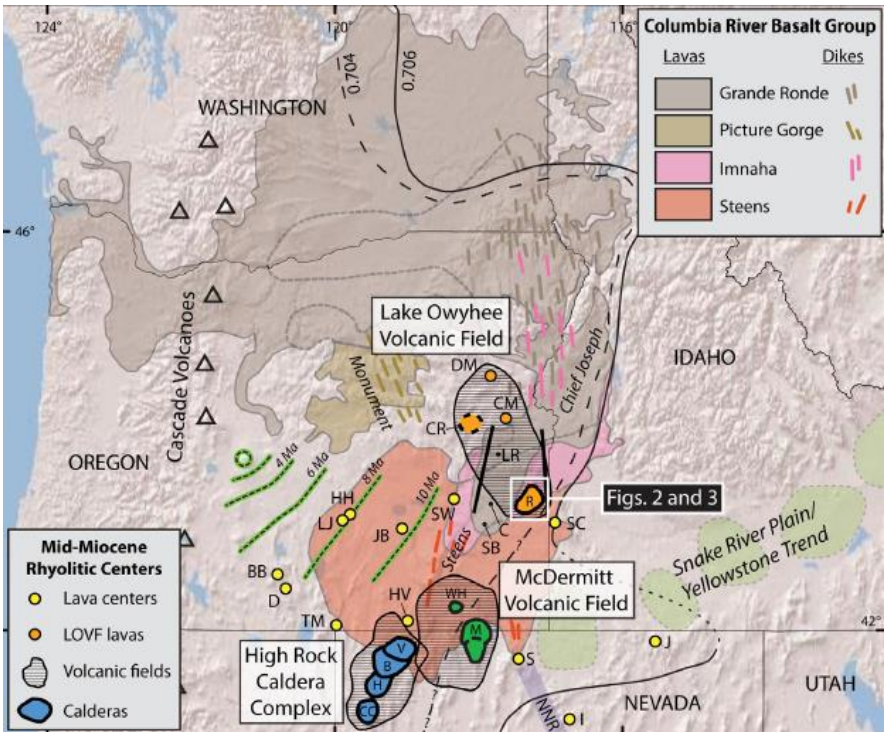

Figure 6. Map of Pacific Northwest. CRBG units and location of silicic volcanic centers, including LOVF are shown. CR is Castle Rock. Figure from Benson & Mahood, 2016.

Within the study area, previous geologists called the tholeiitic lava flows along the main ridge at Castle Rock, underneath the summit outcrop of Dinner Creek Tuff, the 'Unnamed Igneous Complex', which has been correlated with the regionally extensive Basalt of Malheur Gorge (Kittleman et al., 1965; Haddock, 1967; Woods, 1976; Evans, 1990). Radiometric dates for the Basalt of Malheur Gorge from the Malheur River Gorge area range from 16.5 – 15.7 Ma, overlapping in age with the main phase of the CRBG (Camp et al., 2003). The unit is split into three members. The Lower Pole Creek member

consists of plagioclase phyric lava flows that are geochemically and petrologically identical to the Steens Basalt (Hooper et al., 2002). The Upper Pole Creek and Birch Creek members are aphyric and have been geochemically correlated with the Imnaha and Grande Ronde Basalts, respectively (Evans and Binger, 1997). The Dinner Creek Tuff is the only LOVF unit within the study area.

Volcanic rocks overlying the Dinner Creek Tuff

In the Malheur River gorge, the Hunter Creek basalt overlies the Dinner Creek Tuff. It consists of basaltic-andesite and icelandite lava flows (Ferns and McClaughery, 2013). The Hunter Creek basalt is geochemically indistinguishable from the Birch Creek member of the Basalt of Malheur Gorge, and from the Grande Ronde Basalt (Evans and Binger, 1997). $^{40}Ar/^{39}Ar$ ages overlap with the Dinner Creek Tuff (15.7 – 15.4 Ma), and the exact relationship between the two units is unclear (Nash and Perkins, 2012). In the Jonesboro Quadrangle, 10 km southeast of the study area, a lenticular segment of Hunter Creek basalt is entrained within the Dinner Creek Tuff (Evans, 1990). There is little evidence for significant erosion below the lava flow, so it seems likely that the lava erupted shortly after the emplacement of the tuff. Major/trace element data from cognate basaltic-andesite lithic globules within the Dinner Creek Tuff are indistinguishable from the Hunter Creek basalt. This could imply that the emplacement of Hunter Creek magma at depth caused melting of continental crust and later eruption of the Dinner Creek Tuff (Streck et al., 2015).

The Dinner Creek Tuff is interbedded with the Strawberry Volcanics north and northwest of the study area. Age dates for the Strawberry Volcanics vary. Robyn identified 19 – 18 Ma dacite lava flows along the northwestern margin of the volcanic

field (Robyn, 1977). Rhyolites within the group range from 16.2 – 14.6 Ma and more mafic and intermediate lava flows range from 15.6 – 12.5 Ma, just postdating the main phase of the CRBG, and overlapping with the Dinner Creek Tuff (Steiner, 2015). The lava flows of the Strawberry Volcanics are both tholeiitic and calc-alkaline in composition. The differences in composition are believed to be due to assimilation of crustal rocks and rhyolite with CRBG tholeiitic magma at depth (Steiner, 2015). The total volume of the Strawberry Volcanics is estimated to be about 2000 km^3 (Robyn, 1979).

Within the study area, Thayer and Brown (1973) mapped much of the lava flows north of Castle Rock as Strawberry Volcanics and Woods (1976) mapped lava flows, tuffs, and volcaniclastics above the Dinner Creek Tuff as Strawberry Volcanics. Woods (1976) mapped ash fall tuffs and associated volcaniclastic sediments at Castle Rock as the sedimentary member of the Strawberry Volcanics. Lowry (1968) called these rocks the Goodwin Ranch tuff breccia. This unit consists of pumice lapilli ash-flow tuffs and volcaniclastic sandstones and conglomerates, which are 200 m thick along Lost Creek, just east of Black Butte. The unit sits directly above the Dinner Creek Tuff.

Younger Tuffs, volcaniclastic sediments, and lavas

The Tim's Peak basalt consists of olivine basalt flows that have radiometric dates of 13.5 Ma, and overlies the Hunter Creek basalt southeast of the study area (Haddock, 1967; Evans and Binger, 1997). Haddock (1967) grouped these basalt flows with sediments, calling it the Tim's Peak basalt and sediments unit. The Juntura Formation consists of mid-late Miocene sedimentary and volcaniclastic rocks that crop out mostly around Beulah Reservoir and south to Juntura (Woods, 1976; Binger, 1997). Woods (1976) mapped this unit along the southern flanks of Castle Rock. The distinction

between the sedimentary section of the Tim's Peak sediments and the Juntura Formation is difficult to determine, and both units contain Pliocene fossil leaves (Shotwell and Russell, 1963; Haddock, 1967; Binger, 1997).

The Devine Canyon tuff is a regionally extensive, late Miocene (9.7 Ma.) moderately to densely welded tuff (Green et al., 1973; Walker, 1979). It can be distinguished from other tuffs by higher phenocryst content. It has gray to light green groundmass on a fresh surface. Pumice fragments are un-flattened and up to 4 cm in length. The Devine Canyon Tuff in the study area is about 7 m thick. It is exposed along the southwest flanks of Castle Rock (Woods, 1976). The tuff thickens towards the southwest, and is believed to have been erupted from a caldera now buried beneath Harney Basin (Green et al., 1973). Sandstones and mudstones of the Drewsey Formation lie directly on top of the Devine Canyon Tuff. These sediments range in age from late Miocene to early Pliocene (Woods, 1976).

Quaternary alluvium

Faulting through the late Miocene and Pliocene has resulted in steep escarpments and ridges. Consequently, several large landslides have been mapped in the study area. A large rotational block landslide is exposed along the west side of Castle Rock, where it appears that the lower tuff breccia unit of the Basalt of Malheur Gorge acts as a slide plain (Woods, 1976). Other landslides occur along the steep ridge line that separates the Little Malheur River from Lost Creek. Major alluvial basins occur directly south of Castle Rock, in the present day Beulah Valley. Another large depositional basin sits along the southwest flank of Ironside Mountain, where alluvium sits unconformably on top of the Tureman Ranch Pluton, the Dinner Creek Tuff, and aphyric lava. The alluvial

deposits are full of cobble to boulder sized lithic fragments of the above units. **Figure 7** shows a stratigraphic column of the region and the study area from previous studies. An updated stratigraphic column created from the data in this thesis can be found in the Chapter 4.

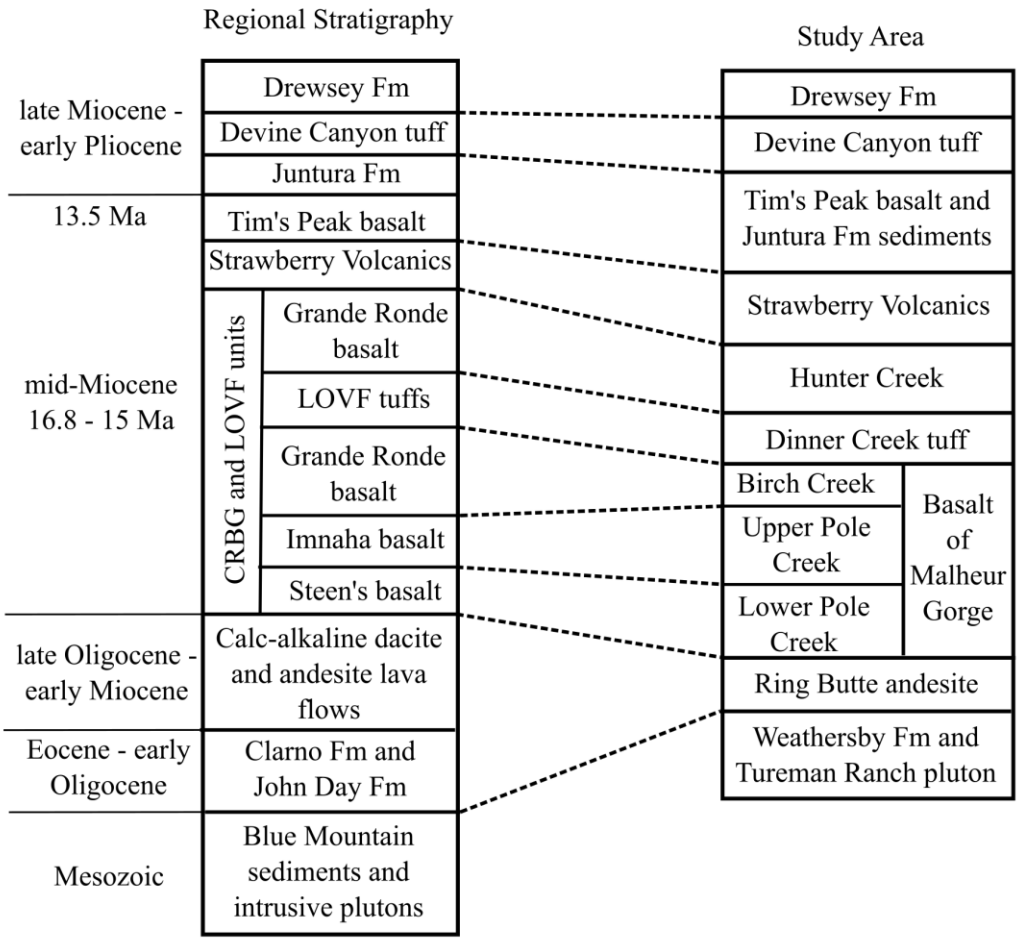

Figure 7. Stratigraphic columns showing correlation between regional geologic units, and the units described in the study area by Haddock 1966, Lowry 1968, and Woods 1976.

Field mapping occurred over four weeks in the summer of 2015, a few days in the spring of 2016, and eight weeks in the summer of 2016. The study area was accessed using dirt roads, ATV trails, and hiking. Orientations of geologic units were taken with a Brunton compass, and sample locations were marked with a GPS. A geologic map of the study area was created from the data that was acquired (Appendix A).

Geochemical analysis

Major and trace element data was acquired using the X-ray fluorescence spectrometer (XRF), and the inductively coupled plasma mass spectrometry (ICP-MS), both at Washington State University (WSU). Sample preparation for the analysis was as follows. Rock samples were crushed into chips, using the rock crusher at PSU. For tuff samples, lithic fragments were removed from the chips in order to isolate the juvenile material. For lava samples, weathered surfaces were removed from the chips so that alteration wouldn't affect the results. At WSU, the chips were further crushed into a powder in a tungsten carbide crusher. The powder was then combined with dilithium tetraborate ($Li_2B_4O_7$) in a ratio of 2:1, dilithium tetraborate to sample. The sample was then fused into a bead in an oven at a temperature of 1000° C. The beads were re-grinded into powder, and one gram of powder was separated in order to make the ICP-MS bead. Two beads per sample were then made, again at 1000° C, one for XRF and one for ICP-MS analysis. The XRF bead was analyzed in the XRF machine, and the ICP-MS bead was dissolved for final analysis. Complete geochemical data is provided in Appendix B.

Thin section petrography

Fifteen thin sections were made of samples from across the study. Billets were cut from the sample using a tile saw at PSU. The billets were 4 cm in length, 2.5 cm in width,

and 1 cm in thickness. After cutting the billets, the samples were then sent off to Spectrum Petrographics, in Vancouver, WA, who cut the thin sections from the billets. The lava samples were polished down to 40 µm, and tuff samples were polished down to 30 µm. Thin sections were analyzed in a petrographic microscope in polarized and cross polarized light. Samples were separated into units based on texture and mineral phases. Complete photos and petrographic descriptions can be found in Appendix C.

SEM feldspar analysis

Fifteen tuff samples were selected for feldspar analysis using the Zeiss Sigma SEM at Portland State University. The samples were selected in order to discriminate between individual units of the Dinner Creek Tuff. Samples were crushed in the rock crusher, and individual crystals were picked from the groundmass. The crystals were set in an epoxy plug, with five samples per plug, and 6 – 11 crystals per sample. The plugs were polished down to one micron in order to create smooth crystal surfaces, and eliminate pits and cracks. The plugs were carbon coated with a 10 nm thin coat, and grounded to the stage of the SEM using copper tape. SEM analysis was done in high vacuum mode. The accelerating voltage was set to 15 KeV. The aperture was set to 60 microns. Working distance was set to 8.5 mm. Prior to analyzing samples, the beam was calibrated on the copper tape, and the beam was set to high current mode in order to improve analysis. Spectra were taken from smooth crystal surfaces, and analyzed in Oxford Instruments Aztec software. Editing of the data involved checking elements by oxide wt. %, and removing anomalous and poor analyses. Plagioclase spectra with oxide wt. % totals below 90 were discarded. The plagioclase data were converted to atomic wt. %, and then plotted onto a ternary diagram using R, and the ggtern package.

Complete data tables of plagioclase and other phases in oxide wt. %, and backscatter electron images can be found in Appendix D. R code for plotting atomic wt. % of plagioclase data can be found in Appendix E.

Chapter II: Field Mapping Results

The main purpose of the field work was to map Dinner Creek Tuff outcrops, and identify sources for the tuff. In this section, the Dinner Creek Tuff will be considered as a whole, and no distinction will be made between the four individual cooling units. Distinction between the four cooling units will occur in Chapter 3, the sample analysis results chapter. Although faulting will be discussed, a detailed discussion about the structural history of the study area is also absent from this section. Orientations of tuffs, lavas, and faults will be mentioned in regards to alignment of dikes and resurgent doming, but a rigorous structural discussion is beyond the scope of this thesis.

Prior to discussing Dinner Creek Tuff volcanic centers, a brief section will be devoted to earlier Cenozoic volcanic rocks. **Figure 8A** shows the study area with Mesozoic basement rocks, and pre-Dinner Creek Tuff volcanic rocks.

Early Cenozoic Volcanics

Ring Butte

A short description of Ring Butte will follow. Ring Butte is notable because it is a volcanic vent that sits directly atop the Mesozoic Weathersby Formation and Tureman Ranch grano-diorite (**Figure 8B**). Dinner Creek Tuff and younger units are not present at Ring Butte, so it appears that the structure was either never covered by Dinner Creek Tuff, or was only covered by a thin enough deposit that it was easily eroded.

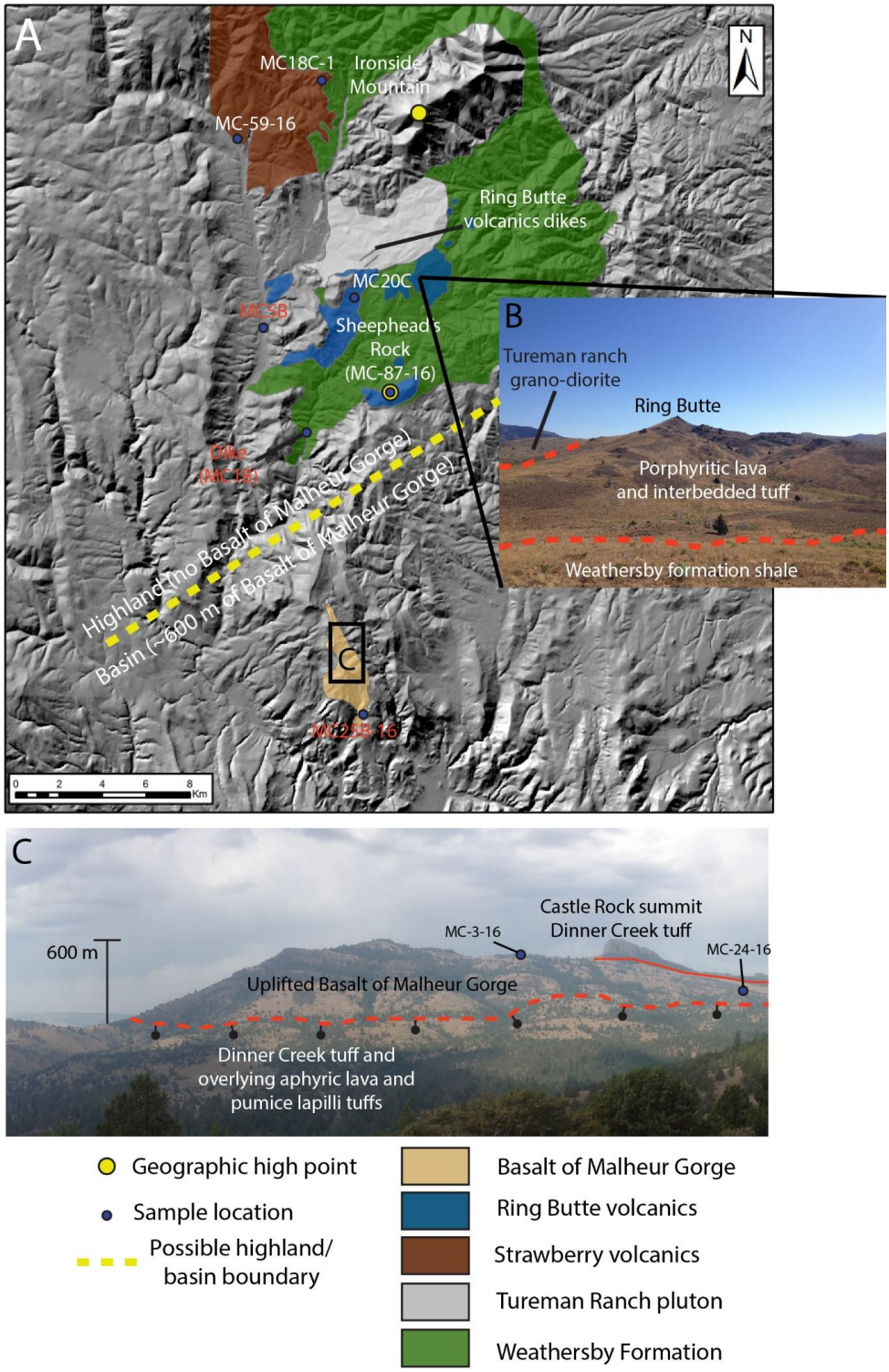

Figure 8. Map of pre-Dinner Creek Tuff units in the study area.

Ring Butte consists of interlayered lava flows and tuff breccia that sit unconformably atop Weathersby Formation sediments along the south flank and Tureman Ranch grano-diorite along the north and northeastern flanks. The tuff breccia consists of gray, ash matrix with andesite lava lithic fragments up to 20 cm in length. Euhedral-subhedral plagioclase phenocrysts make up 10 – 20% of the tuff. The lithic fragments are typically sub-rounded, and make up 50 – 60% of the rock. Tuff breccia deposits appear to be at most 2 m in thickness, and extend from Ring Butte down to Castle Rock road, a distance of 2 km.

The lava flows can be broken up into two main groups: hornblende rich flows and hornblende poor flows. The hornblende rich flows are greenish gray to gray in groundmass color, and are porphyritic. Hornblende crystals are as much as 1 cm in length, with plagioclase being common as well. The hornblende poor flows have dark gray to black groundmass, with plagioclase crystals up to 0.5 cm in length. Minor phenocrysts include pyroxene and hornblende. The hornblende poor flows are lower in the stratigraphic section. The summit consists of vertically foliated hornblende rich lava that strikes 76°. These vertically foliated lava outcrops probably are dikes from which the majority of the lava erupted. On the lower slopes, the lavas strike 27 - 45°, and dip 35 - 48° SE.

The lavas and tuffs extend west and south beyond Ring Butte. Going west, towards Clevenger Butte, 2 – 3 m of tuff is exposed in a road cut. Hornblende poor lava overlies the tuff in patchy outcrops that cover the east flanks of Clevenger Butte. In some outcrops, the lava directly overlies the Weathersby Formation, indicating that the tuff was not distributed evenly across the area, or was eroded prior to the eruption of the lava. At

Clevenger Butte, the lava sits beneath Dinner Creek Tuff, providing a clear stratigraphic relation with the younger mid-Miocene tuff. Southward at Sheephead's Rock outcrops of hornblende rich lava, exhibiting columnar jointing, cap the ridge line, sitting directly on top of the Weathersby Formation. The lava strikes 25°, and dips 50° NW at Sheephead's Rock. The western flank of Sheephead's Rock consists of andesite or basalt lava that is exposed down to the floor of the steep canyon, directly west of the ridge, 100 m below the ridge summit. In this canyon, the lava is altered such that the groundmass is pale gray. Purple stains on the basalt could be manganese alteration, and pyrite mineralization is pervasive throughout outcrops. Ring Butte lava outcrops don't extend much further north than Ring Butte, where the Tureman Ranch grano-diorite comes into sharp contact with the andesite and Weathersby Formation sediments.

Ring Butte is probably the main source for the hornblende rich andesite lava. A minor vent about 2.5 km northeast of Ring Butte, called Squaw Peak, and intrusive andesite porphyries immediately east of the study area were mapped by Lowry, and Thayer and Brown. Other potential sources for the lavas are dikes that intrude into the Tureman Ranch Grano-diorite. Two dikes strike northeast, from the southern boundary of the grano-diorite along the north flank of Clevenger Butte up towards the road along the south flank of Ironside Mountain. Dips could not be measured on the dikes, as they only appear as erosional surfaces that are about 2 - 3 m wide. The longest dike is exposed for almost half a km. These dikes are hornblende poor andesite lava, and could be the source for all the hornblende poor andesite lava in the area.

Strawberry Volcanics

As mentioned in the Regional Geology section, the Strawberry Volcanics is a large, diverse volcanic field that exists primarily to the west of the study area. In the far northwest corner of the study area, andesite and dacite lava sit unconformably atop the Weathersby Formation. The andesite occupies a small valley at the head of the Little Malheur River, and can be seen in road outcrops along National Forest Road 16. The lava is gray on weathered surfaces, and has a black groundmass on fresh surfaces. It is porphyritic, with euhedral to sub-hedral plagioclase crystals up to 1 cm in length. No orientations could be measured at the andesite, due to the poor quality of the outcrops. A dike of Dinner Creek Tuff intrudes into this andesite, which definitely makes the andesite older than the tuff.

The dacite sits atop a north-south trending ridge line, immediately west of Ironside Mountain. The dacite is aphanitic to porphyritic, with a black groundmass on fresh surfaces, and red, rusty weathered surfaces. The main phenocryst is plagioclase, with crystals up to 0.5 cm in length. Quartz veins are common within the lava. Possible flow surfaces have orientations of 51°, and dips 43° NW. Vesicles up to 1 cm in length are common within the dacite. Tuff breccia is interbedded with the dacite lava, and some scoria fragments were found as float along the hillside. Given this information, it would appear that vents for the dacite are located at, or near the ridgeline. Mapping by the state geology department in nearby quadrangles indicates that these lavas are the predominant type of volcanic rock west and northwest of the study area (Brooks and Ferns, 1979; Brooks et al., 1979). Age dates for the Strawberry Volcanics vary. Robyn (1977) mapped and age dated dacite lavas 13 km northwest of the previously mentioned dacite outcrops.

His data indicated that the dacite had ages of 19 – 18 Ma. Steiner (2015) disagreed with the association of these older dacites and andesites with the Strawberry Volcanics, due to differences in mineral assemblages with the main type Strawberry Volcanic lava flows. For convenience sake, they will be grouped with the Strawberry Volcanics in this thesis, but perhaps these andesite and dacite lavas belong to an as of yet unrecognized volcanic phase.

A dacitic dike intrudes into the Weathersby Formation near Lost Creek, just 4 km west of Sheephead's Rock. This dike is isolated from the other dacite/andesite outcrops, but is included in this section due to petrographic similarities. The dike is about 0.75 m thick, strikes 295°, and dips 36° NE. Plagioclase phenocrysts are common, and are up to 4 mm in length. Dark green minerals and rinds around crystals could be chlorite alteration.

Basalt of Malheur Gorge

The Basalt of Malheur Gorge underlies the Dinner Creek Tuff at Castle Rock (**Figure 8C**). It is rusty brown on weathered surface, with a black aphanitic groundmass. The lava is vesicular with un-stretched vesicles up to 3 cm in length. Plagioclase phenocrysts, up to 2 mm in length, are rare. Reddish brown alteration along fractures within the basalt is probably hematite. The basalt is mostly blocky to tabular, and outcrops are poorly preserved. A measurement taken from an outcrop along the east flank of the ridge gives an orientation of 10° and a dip of 29° NW, and all the aphyric lava flows have the same general trend. The total thickness of aphyric lava is ~400 m. Two beds of palagonitic tuff breccia sit below the aphyric lava, with individual thickness of 10 – 20 m. The tuff breccia is aphanitic, with pillow structures that have radii up to 0.5 m in

length. Whereas the lava above the tuff breccia is mostly aphyric, the lava below the tuff breccia is typically porphyritic, with plagioclase crystals up to 1 cm in length. These porphyritic flows are only exposed along the southern flank of Castle Rock. Orientations of the porphyritic basalt vary from 335° to 16°. Dips are mostly northwest dipping, but a couple vertical dips were measured. Quartz veins are common, and some nodules up to 0.5 cm in length were observed in the basalt. These veins and vertical dips are probably related to normal faulting along the southern flank of Castle Rock. The total thickness of pre-Dinner Creek Tuff lava flows at Castle Rock is ~600 m.

As mentioned in Chapter 1, the Basalt of Malheur Gorge has been separated into three distinct members: the Lower Pole Creek, the Upper Pole Creek, and the Birch Creek members. The porphyritic basalt flows at Castle Rock could be northern extensions of the Lower Pole Creek member. Woods (1976) postulated that the porphyritic flows were southern extensions of the Ring Butte lava, however they lack the hornblende crystals that are characteristic of the Ring Butte flows. The upper aphanitic lava flows are probably part of the Upper Pole Creek and Birch Creek members of the Basalt of Malheur Gorge. This great thickness could be due to two things: deposition within a lowland basin, or proximity to a volcanic vent. The presence of the palagonitic tuff breccia indicates that at least some of the lava flows were deposited within an aqueous environment. Lowry (1968) identified dikes at the very southern point of the Castle Rock ridge line, although no dikes were observed cutting through stratigraphy or vertical foliations were found for this study. Radiometric dates for the Basalt of Malheur Gorge range from 16.5 – 15.8 Ma (Hooper et al., 2002), meaning that the basalts erupted just prior to the Dinner Creek Tuff.

Pre-Dinner Creek Tuff topography

Prior to the eruption of the Dinner Creek Tuff, the study area was divided into a highland in the north and a basin in the south. The highland consisted of uplifted, or erosional remnant Mesozoic basement rocks, on top of which the Ring Butte volcanics erupted. Dacite and andesite lavas, tentatively correlated with the earliest phase of the Strawberry Volcanics, covered these basement rocks along the northwest margins of the study area. In the south, around the current high point of Castle Rock, a basin existed in which the of Basalt of Malheur Gorge was deposited, probably from vents further south of the study area, although possibly from more proximal vents (Lowry, 1968; Hooper et al., 2002; Camp et al., 2003). The Basalt of Malheur Gorge does not appear to be present north of Castle Rock. Aphanitic lava flows do overlie the Weathersby Formation, and mega-breccia deposits along the dividing ridge between Lost Creek and the Little Malheur River, but the prominent rust weathering, and tabular to slaty habit are more indicative of the younger, post-Dinner Creek Tuff, Hunter Creek basalt. The two units are similar petrographically and geochemically and in all likelihood represent a continuum of Grande Ronde flood basalt volcanism that was briefly interrupted by eruption of the various Dinner Creek Tuff units.

Volcanic Centers

There are two calderas within the study area. One appears to have a western boundary at Castle Rock, and extends eastward outside of the study area. This caldera is from here on referred to as the Castle Rock caldera. The second caldera is centered at Ironside Mountain, and is here on referred to as the Ironside Mountain caldera. A

description of both calderas will follow, and evidence for the above caldera characteristics will be presented for each caldera.

Castle Rock caldera

The presence of a caldera at Castle Rock as the source for the Dinner Creek Tuff was first postulated by Rytuba and Vander Meulen (1991). Prior to that, the summit outcrops of Dinner Creek Tuff at Castle Rock were believed to be a dike, and a source for the entire tuff (Haddock, 1967; Woods, 1976). Characteristic features of caldera that were identified during the field work will now be discussed.

Mega-breccia

Mega-breccia related to the collapse of the caldera during the eruption of the Dinner Creek Tuff, crops out 7 km north of Castle Rock. The mega-breccia is distributed from east to west in a thin, northeast trending outcrop from Lost Creek in the west to Clover Creek in the east (about ~13 km), ranging in width from 1 – 2.5 km (**Figure 9A**). Sheepshead Rock marks a rough northern boundary of the mega-breccia. The tuff ranges in color from tan to gray, and is incipiently welded. The only phenocrysts that can be recognized within the tuff are feldspar phenocrysts up to 2 mm in length. Hornblende rich Ring Butte lava is the most abundant type of lithic fragment within the mega-breccia. The lava lithic fragments are light gray to white in color, much lighter in color than the darker gray to black intact lava that crops out at Sheepshead Rock and Ring Butte, to the north. Aside from the lava, grano-diorite and shale lithic fragments can also be found in the mega-breccia. The lithic fragments are up to 3 m in length, and range in shape from sub-rounded to angular (**Figure 9B**).

The tuff breccia is approximately 50 m thick just south of Sheepshead Rock, where it is most prominently exposed. The tuff breccia is unconformably overlain by aphyric basaltic-andesite, palagonitic basalt, and airfall tuff. In the far east of the study area, the mega-breccia is interbedded, and grades into densely welded Dinner Creek Tuff.

On the ridgeline between Lost Creek and the Little Malheur River, the mega-breccia appears to sit unconformably atop the Weathersby Formation, although the contact is not exposed. At this site, the tuff breccia is approximately 70 m thick, and is overlain by aphyric basaltic-andesite. The mega-breccia forms prominent hoodoos within canyons along the ridge line (**Figures 9C**). It is only exposed along the east, Lost Creek facing, side of the ridge. On appearance, the mega-breccia deposits are similar to the interbedded tuffs at Ring Butte, and could be mistaken for a southern extension of the older Ring Butte volcanics. The presence of grano-diorite and shale fragments within the mega-breccia is distinct from the Ring Butte tuffs, which only have lava fragments. The lithic fragments are also larger within the mega-breccia, and the size and thickness of the mega-breccia is significantly greater than the Ring Butte tuffs. For these reasons, the mega-breccia deposits are considered to be separate from the older Ring Butte tuffs.

Other deposits which could represent mega-breccia occur within Jerry Canyon. In places, the Dinner Creek Tuff within the canyon is unconformably overlain by incipiently welded tuff that contains lithic fragments of aphyric Birch Creek Member lava up to 2 m in length (**Figure 9D**). The fragments are sub-angular to sub-round. These outcrops are not as pervasive across Jerry Canyon as the mega-breccia outcrops south of Sheepshead Rock, and in some places, particularly in the north end of Jerry Canyon, the Dinner Creek Tuff is unconformably overlain by aphyric basaltic-andesite, with no mega-breccia

deposits in between. The Castle Rock ridgeline could be the western margin of the caldera, and the mega-breccia within Jerry Canyon would have been deposited atop and within the Dinner Creek Tuff as it was erupted.

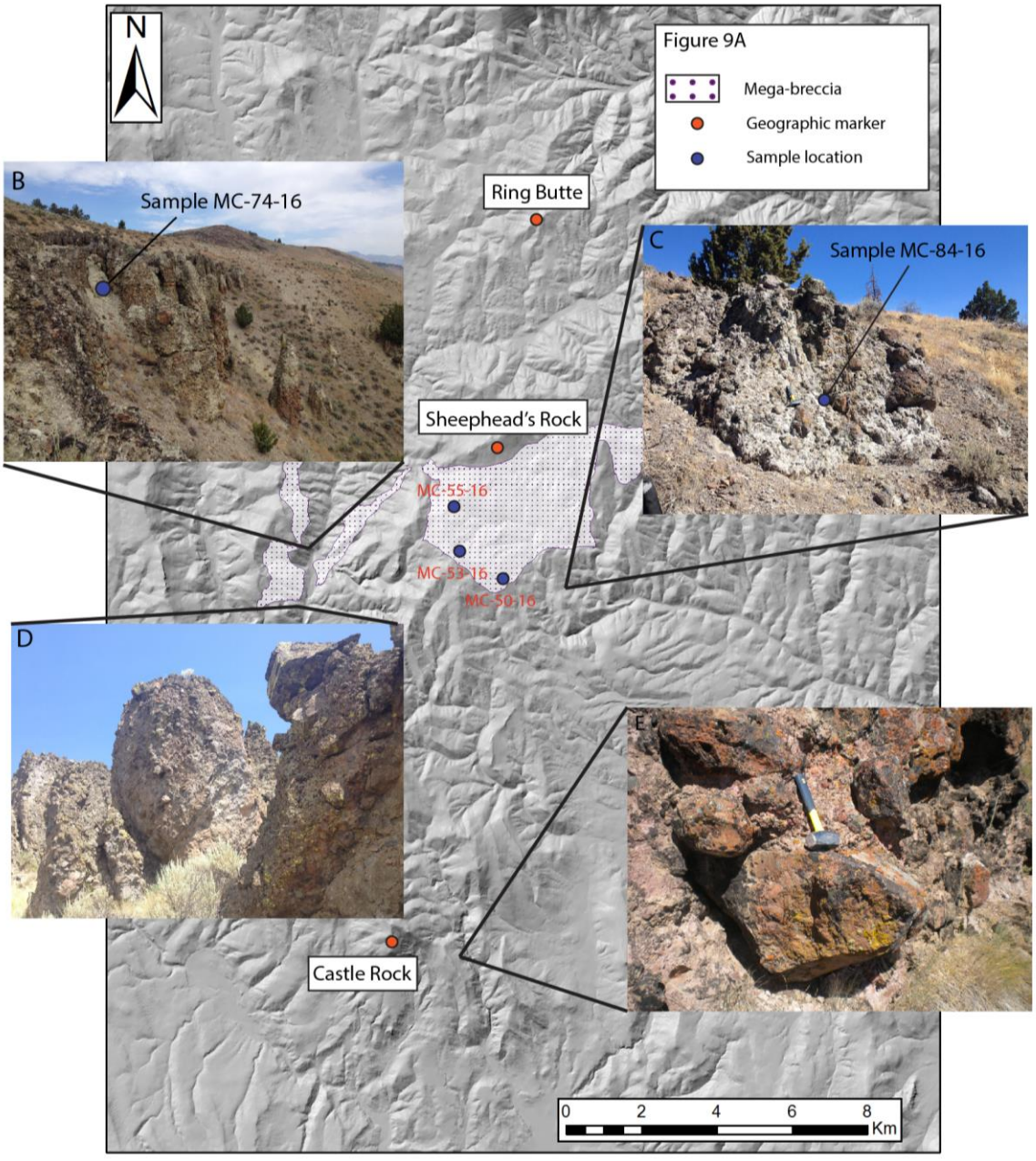

Figure 9. Map of Castle Rock caldera showing the mega-breccia outcrops, photos, and sample locations

Intra-caldera tuff

Within the Castle Rock caldera, the Dinner Creek Tuff ranges in thickness from 70 – 300 m (**Figure 10A**). The thickest accumulations of Dinner Creek Tuff occur in Jerry Canyon, immediately east of the main Castle Rock ridge, where the tuff is as much as 300 m thick (**Figure 10B**). The base is not exposed, so the outcrop could be considerably thicker. Green to white quartz veins and vugs are common within the Dinner Creek Tuff, and are probably the result of hydrothermal alteration. Orientation measurements of the tuff vary widely from 300° to 70°, and dips vary from 76° SW to 80° NE, and 63° NW. In Jerry Canyon, the Dinner Creek Tuff is densely welded and rheomorphic. The lowest outcrops at the base of Jerry Canyon sometimes lack the distinct stretched pumice foliation of most of the tuff outcrops, and may be intrusive rhyolite lava plugs, although individual plugs were not mapped. Higher up in the section, the tuff is foliated and often breaks along the pumiceous foliation planes, creating tabular, slaty float fragments. The top of the rheomorphic section has evidence of vapor phase alteration, such as spherules and lithophyasae up to 0.4 cm in length. Some outcrops along the eastern base of Castle Rock have ellipsoid shaped cavities up to 1.5 m in length. The cavities follow the general foliation trend.

Normal faulting along the west side of Hunter Mountain, ~7 km southeast of Castle Rock, exposes ~100 m Dinner Creek Tuff along Hunter Creek (**Figure 10C**). The Dinner Creek Tuff at Hunter Mountain is mostly east dipping (346°, 31° NE), and contains abundant vugs filled with quartz, up to 4 cm in length. Like in Jerry Canyon, larger cavities occur near the top of the tuff, and may represent the lithophysal, vapor phase alteration zone.

The summit of Castle Rock consists of up to 70 m of Dinner Creek Tuff. Haddock (1967) and Woods (1976) thought that this outcrop represented the source of the tuff, based on its linear, dike-like shape (**Figure 10D**). However, the outcrop is not vertically foliated, mostly striking 10° from north, and dipping 20 – 40° NW to NE. A basal vitrophyre is also present beneath the rheomorphic outcrop, striking 356° and dipping 64° NE, indicating deposition along a horizontal surface, as opposed to vertical, intrusive flow. This summit outcrop is probably a section of tuff that has been preserved along the uplifted Castle Rock fault block.

West of Castle Rock, the Dinner Creek Tuff is exposed in a faulted block just southwest of the summit, where it is up to 100 m thick, although the base is not exposed. This outcrop is uplifted relative to younger basalt and sediments to the southwest along a northwest striking (300°) normal fault. The tuff is fractured and internally displaced, which would be expected given its position along the boundary of the uplifted Castle Rock horst. The northern boundary of this outcrop is buried underneath a large landslide, but the Dinner Creek Tuff is exposed again immediately west of the summit of Castle Rock, within canyons along the ridge flank. In the largest canyon, the tuff is 50 m thick, although the base is not exposed. This outcrop is noteworthy, because it is the only outcrop that shows a gradational change from densely welded rheomorphic tuff to moderately welded tuff. The top of the rheomorphic section is lighter in color, and eventually turns tan-white in 10 m. The moderately welded section has flattened fiamme up to 9 cm in length, and 2 cm in width. Incipiently welded tuffs with un-flattened pumice overlie the dense, devitrified rheomorphic tuffs, increasing the overall thickness

of the Dinner Creek Tuff at this location to almost 100 m. The tuff strikes 333° and dips 46° SW.

The Dinner Creek Tuff is well exposed along Lost Creek, 8 km north of Castle Rock, where it is 150 - 200 m thick in the steep hillside east of Lost Creek (**Figure 10E**). Some sections of the tuff are vertically foliated with breccia, which could represent dikes, and are discussed more in the next section. Like the Jerry Canyon outcrops, the Dinner Creek Tuff at Lost Creek is densely welded and rheomorphic. Mega-breccia deposits border the tuff along the north and west, and uplifted sections of Weathersby Formation shale occasionally border the tuff. Outcrops of the Dinner Creek Tuff continue east over the ridge line, extending northwards, almost towards Sheepshead Rock.

Mega-breccia and basaltic-andesite unconformably overlie the Dinner Creek Tuff to the southeast of Sheepshead Rock, although uplifted blocks of Dinner Creek Tuff occur in the headwaters of Bully Creek. The faults trend northeast, and create ridgelines of Dinner Creek Tuff at least 200 m thick. The Dinner Creek Tuff at this location strikes northeast and dips about 30° SE, and continues to be exposed east of the study area. Lowry (1968) mapped the tuff as far as Rail Creek, 5 km east of the study area, before it’s buried underneath incipiently welded tuff and aphyric basaltic-andesite.

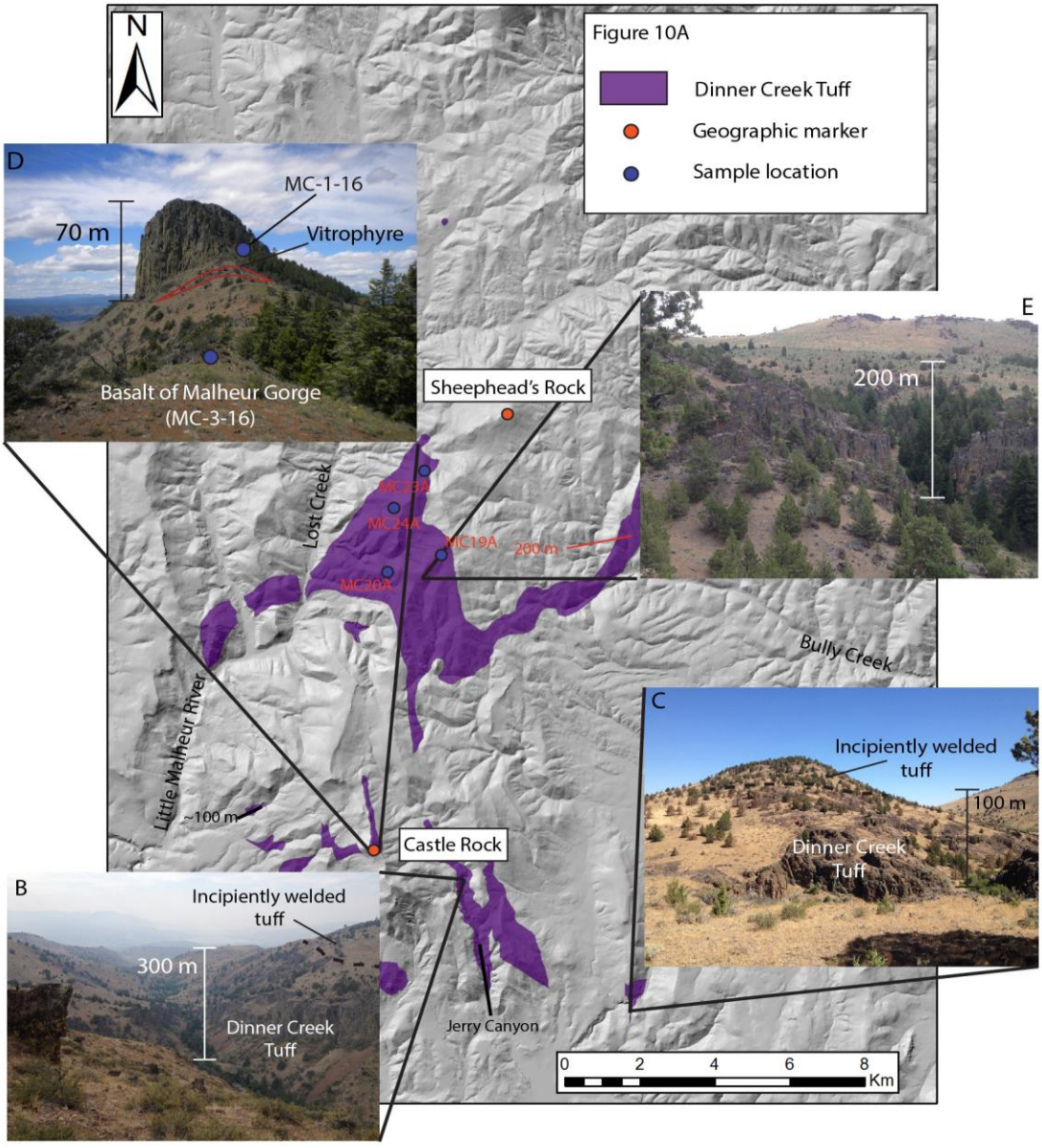

Figure 10. Map showing intra-caldera Dinner Creek Tuff outcrops across the Castle Rock caldera, with photos, sample locations, and thicknesses of outcrops.

Tuff dike/ring dike vents

As mentioned in the 'Calderas' section in Chapter 1, ring dikes are best exposed in heavily eroded Mesozoic and Paleozoic calderas, and most Cenozoic calderas have not had sufficient time for erosion to expose the ring dikes (Lipman, 1984). However, faulting along the ring dikes at some Cenozoic volcanic centers has exposed the tuff filled dikes (Aguirre-Diaz and Labarthe-Hernandez, 2003; Torres-Hernandez et al., 2006). Indicators for these tuff dikes would be vertical or near vertical foliation of the tuff, which would be indicative of magma flowing through a conduit. Vertical foliation is not totally indicative of vertical movement of magma through a dike. The rheomorphic nature of the Dinner Creek Tuff means that it is folded in some areas, and eroded, steep fold limbs can sometimes be misinterpreted as vertically flowing dikes. Generally, these fold limbs are exposed across a small area, less than 20 m. In addition to vertical foliation, tuff dikes typically have vitrophyre, and breccia from surrounding country rock entrained within the tuff. Volcanic domes or cones could also indicate the location of buried ring dikes. After caldera collapse, magma re-enters the chamber, and can use the ring dikes as pathways to the surface (Smith and Bailey, 1968). Within the study area, there are several younger volcanic structures and domes that are stratigraphically above the Dinner Creek Tuff (**Figure 11A**). Their structure and location could be surficial expressions of the underlying ring dikes that mark the structural boundaries of the caldera.

The best candidate for possible tuff dike in the study area is an outcrop of vertical to near vertically foliated Dinner Creek Tuff that trends northeast from Black Butte across Lost Creek, and up towards Sheepshead Rock, for a total exposure of 3.5 km. The

foliation of the dike is 0 - 15°, and the dip varies from vertical to 68° NW to SE. The outcrops are altered hydrothermally, with quartz filling vugs and veins within the dike. Lithic fragments of basalt and possibly shale up to 5 cm in length occur. The outcrop is bound on the northwest by incipiently welded tuff and aphyric basalt-andesite and on the southeast by rheomorphic Dinner Creek Tuff. The outcrops at Lost Creek appear to be uplifted along a northeast trending normal fault. Just west of the Dinner Creek Tuff outcrops is a linear outcrop of aphyric basaltic-andesite. This appears to be intrusive, and follows the same trend as the vertically foliated tuff. Just west of the basaltic-andesite dike is incipiently welded tuff, similar in appearance to the younger tuffs that overly the Dinner Creek Tuff, further to the south. This juxtaposition of the incipiently welded tuffs against the rheomorphic Dinner Creek Tuff further supports the presence of a normal fault, which uplifts and exposes the tuff dike, and younger basaltic-andesite dike.

South east of the above outcrops is Black Butte, a prominent hill along the confluence of the Little Malheur River and Lost Creek, about 7 km northwest of Castle Rock. The butte has an elongated, dome-like shape, which could indicate that it is a rhyolite dome (**Figure 11B**). It has a steep western flank, probably a fault contact with neighboring aphyric basaltic-andesite. The southern and northern margins are obscured by landslide debris and terrace gravels of the Little Malheur River. The Dinner Creek Tuff at Black Butte is rheomorphic, but often lacks foliation, and may in fact be rhyolite lava and not welded tuff. It appears to intrude into incipiently welded tuffs that overlie the Dinner Creek Tuff in other parts of the caldera. No contact was observed, but a vitrophyre that is poorly exposed along the eastern flank of the butte could represent an intrusive boundary between the silicic lava and the incipiently welded tuffs.

Along the high ridgeline above Castle Rock road, is another outcrop of vertically foliated Dinner Creek Tuff. It trends 5° and dips vertically to 75° NE (**Figure 11C**). This outcrop contains minor lithic fragments, unlike the outcrops at Lost Creek, although scattered vitrophyre do occur within the outcrops. Outcrops of the vitrophyre were not observed, so the actual nature of the vitrophyre (interbedded with the tuff vs. basal layer) is not known. Spires of rhyolite lava occur in the vicinity of these outcrops, so it appears that conduits for magma are located in the vicinity. These rhyolite lava spires are small, 3 – 4 m in height, 5 – 7 m in length, and about 1 – 2 m thick. They have trends similar to the previously mentioned Dinner Creek Tuff, ~5°, and vertical to near vertical dips (**Figure 11D**). The outcrop extends about 2.5 km northeastwards from Castle Rock springs until it is buried underneath aphyric basaltic-andesite. Uplift along these fractures following volcanic activity could have caused these ring dikes to be elevated to their present day positions. Uplift appears to have occurred along northeast trending normal faults that occupy the hillside between the Lost Creek valley, and the summit ridgeline. Another possibility is that these are silicic lava domes, with compositions similar to the Dinner Creek Tuff that were emplaced atop the incipiently welded tuffs. The rheomorphic nature makes it difficult to distinguish between lava and tuff. In this scenario, the vitrophyre fragments could be the mostly buried bases of these rhyolite lava flows.

Just south of these vertically foliated Dinner Creek Tuff outcrops, an aphyric basaltic-andesite plug intrudes into the Dinner Creek Tuff. Basaltic-andesite vents continue further towards the south, at the head of Jerry Canyon. The best exposed vent structure is a ridge line 2.5 km northeast of Castle Rock. It is aphyric basaltic-andesite,

with vesicular porphyritic basalt on the summit. Vertically foliated dikes are exposed along the east flank of the volcano, striking 340°. The ridge line follows the same general northerly strike of the vertically foliated Dinner Creek Tuff outcrops previously mentioned, which could indicate that this volcano erupted through the dikes that were originally conduits for the tuff. Lava outcrops are exposed further south along the ridge line on the east side of Jerry Canyon; although no vent structures were identified south of this volcano.

Just to the west of this volcano, about 3 km north and northwest of Castle Rock, vents are exposed along the high ridge line that overlooks the Little Malheur River canyon. Like the above mentioned volcano, these are aphyric basaltic-andesite vents, and are the sources for the thick accumulations of lava that cover the lower west flanks of Castle Rock. Vertically foliated dikes strike 23°. The top of the ridge consists of more porphyritic and vesicular basalt. The steep southern escarpment is probably a fault surface that laterally displaces this ridge westward from the main Castle Rock ridge to the south. The ridgeline is also bound by a fault on the eastern escarpment.

Dikes within the incipiently welded tuffs along Lost Creek, just north of the above mentioned ridge, are also vent locations for the basaltic-andesite. Not far above valley floor, a dike can be seen cutting through the incipiently welded tuff. The dike is about 4 m wide, and has a length of 60 – 70 m. At its northern terminus, it is cut by a minor westward flowing stream, and then is buried underneath alluvium and incipiently welded tuffs. The dike strikes 358°. Another basaltic-andesite dike cutting through the tuffs is located just off the Castle Rock Road, just upslope of the before mentioned dike. The dike strikes 338°, and dips vertically to 68° SW. Volcanic bombs, measuring up to 10 cm

in length occur in aphyric basaltic-andesite that is interbedded with the tuffs, proximal to the dike.

Basaltic-andesite dikes can also be observed intruding into the mega-breccia. The ridge line that separates Lost Creek from the Little Malheur River, along the west side of the study area contains several vents. Similar vents are exposed south of Sheepshead Rock, again, within the mega-breccia outcrops. The largest is an aphyric dike that exhibits sub-horizontal columnar jointing. This indicates that the basalt intruded into the mega-breccia and cooled from the margins inward (**Figure 11E**).

In other parts of the caldera, vents are less common. As mentioned in the intra-caldera sub-section, rhyolite lava intrusions occur within Jerry Canyon, although the exact size of these plugs is difficult to determine. East of Jerry Canyon, in the headwaters of Hunter Creek, the north-south trending ridge is capped by porphyritic basalt. This basalt appears to lie unconformable atop the aphyric basaltic-andesite. No vertically foliated dikes were observed, but glassy, obloid bombs were found, up to 25 cm in length. This, along with the more vesicular, porphyritic basalt would seem to indicate that this outcrop is very near the source vent.

Finally, there is an outcrop of vertically foliated Dinner Creek Tuff directly south of Hunter Mountain, in the southeast corner of the map area. The tuff emerges from underneath incipiently welded pumice-lapilli tuff and extends less than one kilometer directly south, across Hunter Creek, until it is buried underneath sediments of the Tim's Peak basalt and sediments group (**Figure 11F**). The dike trends north-south, and dips vertically to 70° east-west. Further south of the study area post Dinner Creek Tuff

sediments and tuffs overlay much of the mid-Miocene volcanics, so the likelihood of finding tuff/ring dikes in the area is low.

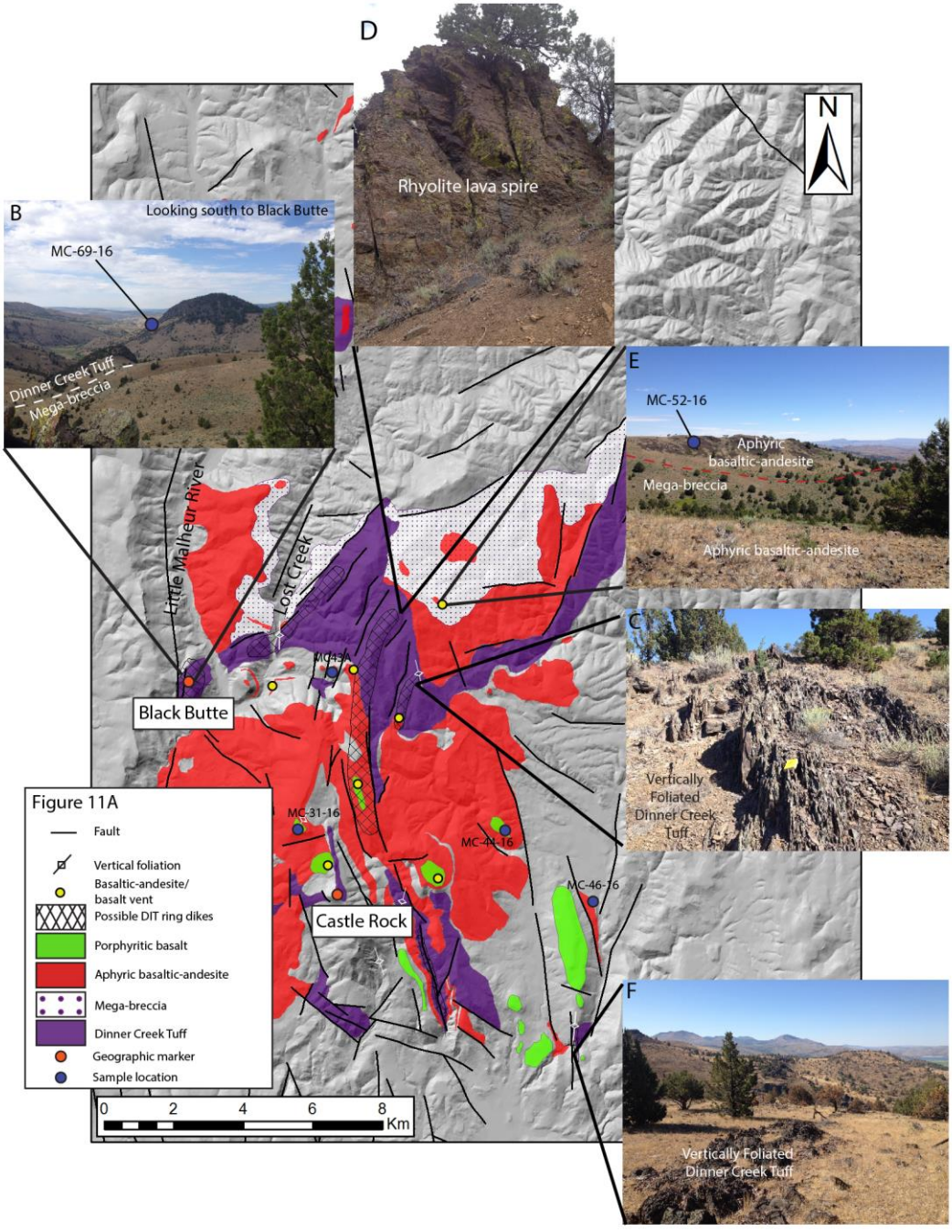

Figure 11. Map of Castle Rock caldera, showing possible vent locations for the Dinner Creek Tuff, vertical foliation, mafic vents, sample locations, and various units

Caldera floor deposits

Throughout the caldera, the rheomorphic densely welded Dinner Creek Tuff is often overlain by incipiently welded tuffs. These are best exposed along the east side of Lost Creek, just north of its confluence with the Little Malheur River. At least 20 different tuff layers are present at this site, with a total thickness of at least 200 m (**Figure 12A**). The individual tuffs range in thickness from half a meter to 20 m thick, and range in color from gray to tan to red to white. The base of this sequence consists of white-gray tuffs, with mostly un-flattened pumice fragments up to 6 cm in length. A prominent gray tuff, that is filled with 1 – 3 cm long obsidian fragments sits along the base of the incipiently welded tuff section. This gray tuff ranges in thickness from 10 – 15 m thick. Pumice fragments within the tuffs are typically white or tan in color. They are as much as 5 cm long at the base of the tuff section. Occasional gray pumice fragments make up less than 10% of the pumice fragments within these tuffs. In all tuff units, the phenocryst content is 5 – 10% of the total volume, with the pumice and ash groundmass making up the bulk of the tuff units. Phenocrysts are mostly plagioclase, with minor pyroxene. Lithic fragments are mostly basalt or basaltic-andesite. Some flow banded rhyolite fragments occur in the lower white-gray tuff beds, and are probably densely welded Dinner Creek Tuff (**Figure 12B**). At the top of the incipiently welded white-gray tuffs is a 20 – 50 cm thick fine grained ash unit, probably airfall. Above this ash sits a 40 m section of re-worked tuffs and volcaniclastic sediments, with cross-bedding and grading. Several 1 – 1.5 m thick conglomerates occur within this section (**Figure 12C**). Another airfall tuff sits atop the re-worked section, about 1.5 m thick (**Figure 12D**). The top of the section consists of tan-white-reddish brown incipiently welded tuffs with interbedded aphyric

basalt. Individual tuff thicknesses are as much as 30 – 35 m. The pumice fragments are also larger than the lower tuff beds, up to 10 cm in length. Lithic fragments of basalt are up to 30 cm in length (**Figure 12E**). The aphyric basaltic-andesite sits beneath these tuffs, and is probably derived from the intrusive, northeast trending dike mentioned in the above sub-section.

On the west side of Lost Creek white-tan, water re-worked tuffs overly southwest dipping Dinner Creek Tuff. These are correlative with the tuffs on the east side of Lost Creek. The section on the west side of Lost Creek is up to 250 m thick. The tuffs around Lost Creek appear to be within a fault bound basin. The southern boundary is a steep escarpment of mostly aphyric basalt. Northeast trending normal faults marks the east boundary of the basin, and the step faulting can be observed in vertically displaced knobs capped by basaltic-andesite that drop from Castle Rock road to Lost Creek. About 2 – 3 km south of the Lost Creek tuff beds, higher up in elevation along the flanks of Castle Rock, the white-tan tuff beds can be observed lying directly atop rheomorphic Dinner Creek Tuff.

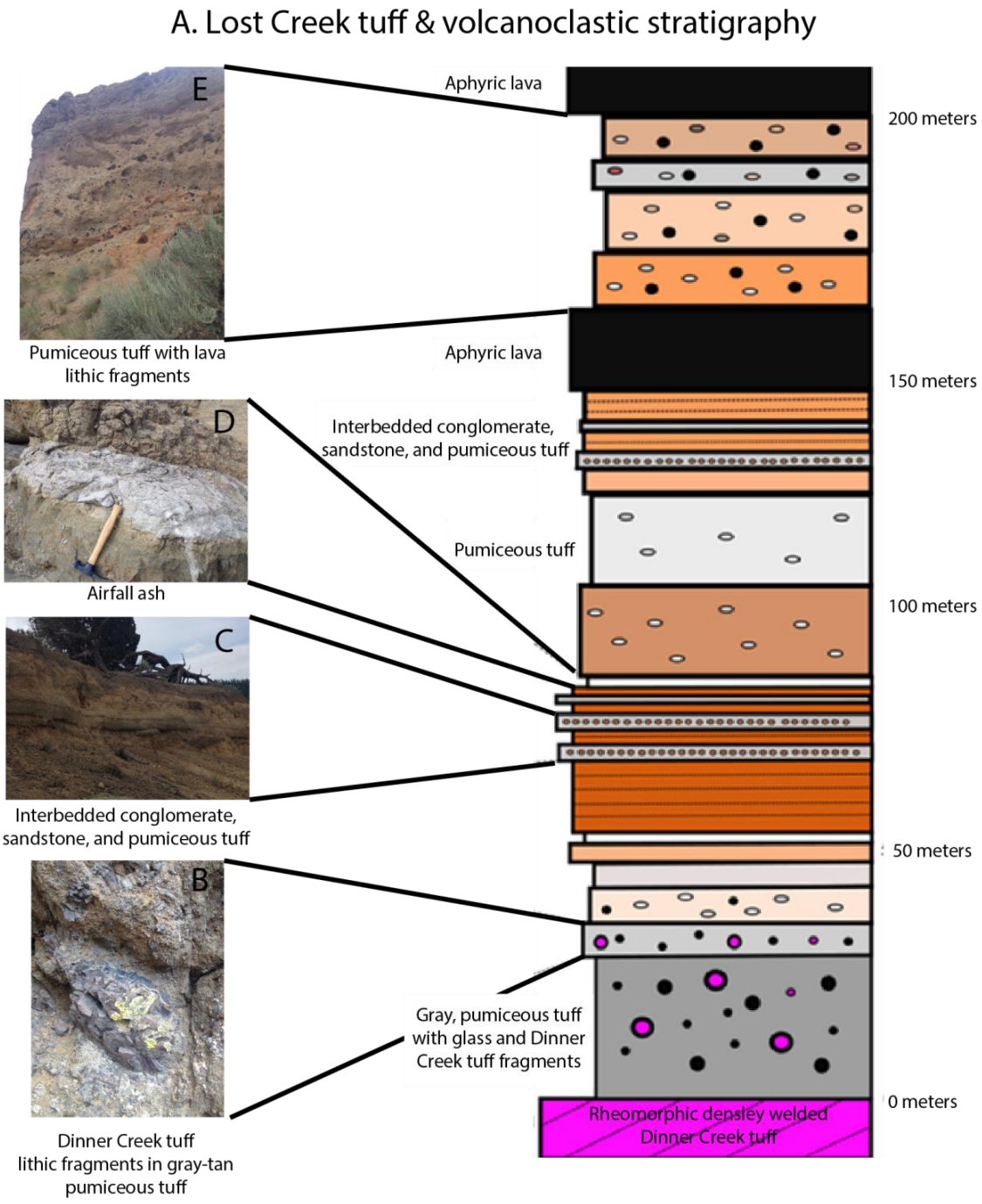

Figure 12. Stratigraphy of tuff and volcaniclastic units at Lost Creek.

Thick accumulations of incipiently welded tuffs and volcaniclastic sediments occur elsewhere other than Lost Creek (**Figure 13A**). After the outcrops at Lost Creek, the southeast flank of Castle Rock is the location of the best preserved incipiently welded tuff deposits. Just like at Lost Creek, white-tan tuffs lie directly atop the Dinner Creek Tuff. Tan, un-flattened pumice up to 15 cm in diameter are common throughout the tuff. 1 – 3 cm long vitric and basaltic-andesite fragments make up 10 – 15% of the tuff. Occasional fragments of what appears to be radiolarian chert were also found within the tuff. Ten meters of red tuff overlie the white-tan tuff, which is in turn overlain by aphyric basalt. The contact between the red tuff and the overlying basalt is a 10 cm thick tuff that consists mostly of black pumice up to 7 cm in length. The contact between the white-tan and red tuff strikes 31°, and dips 15° SE. At some outcrops, there is 5 – 8 m of fine grained airfall tuff sitting between the red tuff and the white-tan tuff (**Figure 13B**). The top of the airfall tuff strikes 7° and dips 22° SE. A conglomerate about 0.5 m thick is occasionally exposed at the base of the airfall tuff. The basalt that caps these tuffs is not exposed across the entire length of the area, and in some locations, claystone and finely laminated sandstone (<0.25 m in thickness) lie directly above the incipiently welded tuffs. The sandstone beds strike 60°, and dip 12° SE (**Figure 13C**). The claystone outcrops can be easily identified due to the 'popcorn' weathering that occurs along the fresh surface, and are the only lacustrine sediments in the study area.

These tuffs disappear underneath the aphyric basaltic-andesite further east of Castle Rock, but normal faulting along the west flank of Hunter Mountain uplift the incipiently welded tuff as much as 100 m. The tuff typically strikes 20 - 45°, and dips 5 - 30° SE, with gentler dips occurring along the southern and eastern flank of Hunter

Mountain. At the southeast end of Murray Reservoir, 26 interlayered units of tuffaceous sandstone and gray, fine, indurated tuffs are exposed in a 10 m high cliff face (**Figure 13D**). The sandstones strike 35° and dips 5° SE. Towards the north, the tuffaceous sediments are juxtaposed against basalt. The sediments are indurated and darker in color against the basalt, indicating that the basalt flowed over the tuff, or intruded into it. The basalt exhibits pillow structures, as much as 10 cm in width (**Figure 13E**). The outer rims of the pillows are glassy and contain yellow palagonite, indicating flow within an aqueous environment.

Palagonitic basaltic-andesite also occurs in the headwaters of Bully Creek, 4.5 km southeast of Sheepshead Rock. The basalt fills a minor canyon, and is glassy with vesicles up to 5 cm in length, and often times filled with yellow palagonite. Contacts with surrounding units were not observed. North of the palagonitic basaltic-andesite is aphyric basaltic-andesite and mega-breccia, and south of the palagonite, rheomorphic Dinner Creek Tuff is uplifted along northeast trending normal faults which correspond to the bed of Bully Creek. These exposed ridges of Dinner Creek Tuff are in turn overlain by re-worked tuff (**Figure 13F**).

In general, the incipiently welded tuffs and volcaniclastic sediments overly the rheomorphic Dinner Creek Tuff across the Castle Rock caldera, and in turn underlie aphyric basaltic-andesite, although the basaltic-andesite is interbedded with the tuffs at Lost Creek, as seen in **Figure 12A**. These are the ‘Strawberry Volcanics volcaniclastic unit’ and ‘Goodwin Ranch tuff breccia’ of Woods (1976) and Lowry (1968), respectively. There is a distinct pumice lapilli tuff that is interbedded with the aphyric basaltic-andesite, and separate from the lower tuffs and volcaniclastic sediments. Woods

(1976) mapped this particular tuff, and called it the ‘Strawberry Volcanics pumice lapilli marker bed’. This marker tuff generally has darker pumice fragments than the underlying tuffs, ranging from gray to dark gray, and a tan-light brown groundmass. The tuff crops out on both the west and east flanks of Castle Rock. In a canyon on the west flank of Castle Rock, the stratigraphic position of this marker tuff and older volcanic units is observable (**Figure 13G**). The thickest outcrops occur along the roadside, 0.5 km southeast of Black Butte, where the tuff is ~20 m.

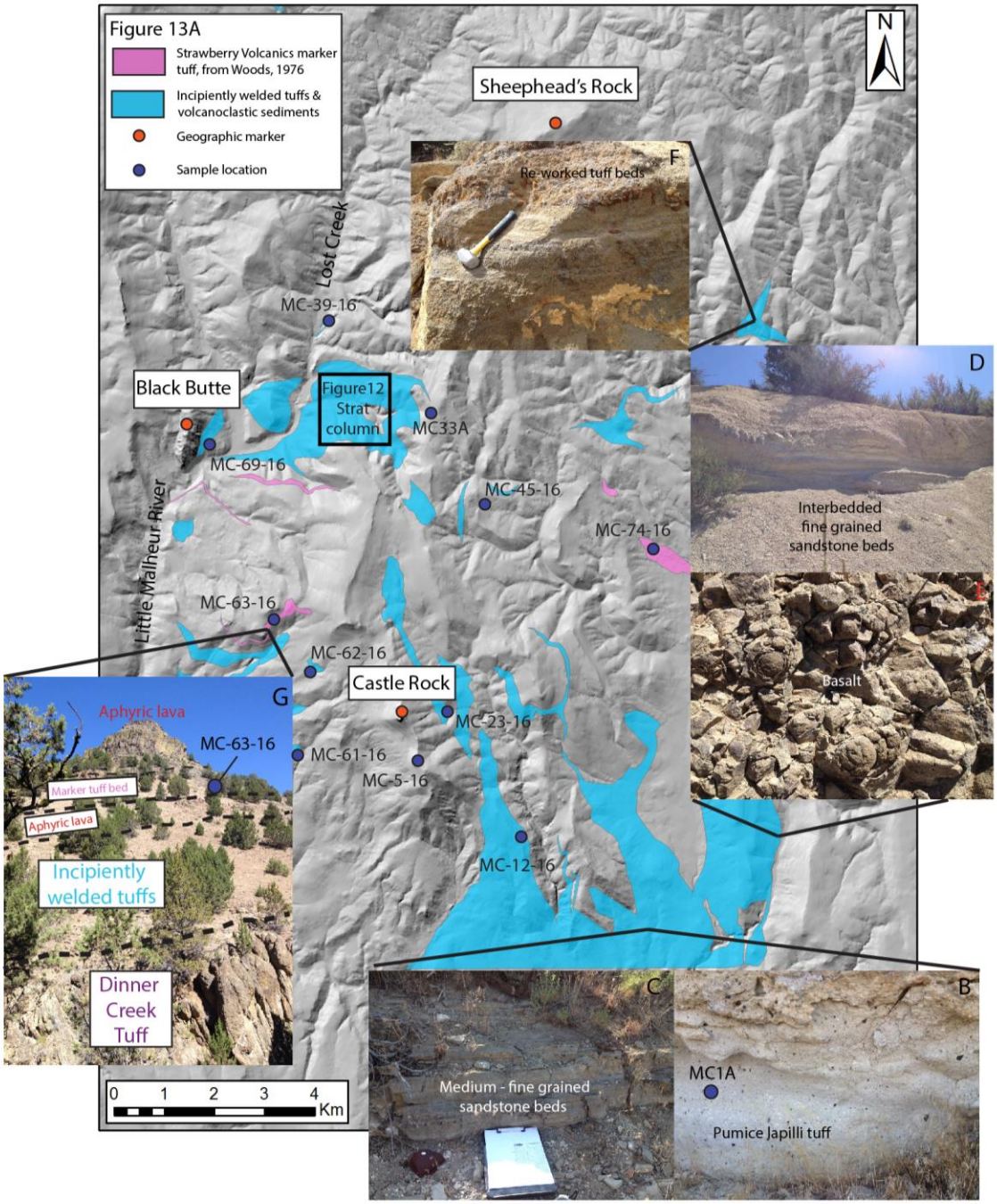

Figure 13. Map of the Castle Rock caldera showing outcrops of incipiently welded tuffs and volcaniclastic sediments across the caldera, with sample locations

Resurgence

Within the study area, the elevated ridgeline of Castle Rock and the ridgelines directly east and north of Castle Rock could be indicative of resurgent doming after caldera collapse (**Figure 14**). If doming followed the deposition of the incipiently welded tuffs and sedimentary deposits, then these deposits should be dipping away from the center of the dome. The tuffs and basalts along the southeast flank of Castle Rock, and at Hunter Mountain, dip 20 – 7° SE, however the tuffs along the northwest flanks of Castle Rock tend to dip towards the southwest. Dips are erratic across the ridgelines north and east of Castle Rock, with a predominant dip direction being northwest, and some units dipping northeast and southeast. These don't exactly conform to the idea of an uplifted resurgent dome that dips away from the center.

Some caldera resurgent domes do have uneven uplift, with tilting occurring in one predominant direction (de Silva et al., 2015). Such could be the case at the Castle Rock caldera, with uplift having occurred on the northwest margin of the caldera, titling all the intra-caldera units in a southerly direction. The focus of resurgence along the northwest corner of the caldera could explain the clustering of volcanic vents in this part of the caldera.

Much of the faulting that can be observed is probably due to regional extension and uplift. At the southern base of Castle Rock, normal faults uplift the Basalt of Malheur Gorge 600 m above the younger Dinner Creek Tuff. The ridge is also bound by faults on the west and east flanks, defining an uplifted horst. Extensional faulting occurred throughout eastern Oregon and western Idaho following the main phase of the CRBG and LOVF, and could have caused the opening of the Beulah Reservoir basin to the south of

Castle Rock, and uplift of the present day horst (Cummings et al., 2000). This extensional faulting has probably obscured the effects of resurgent doming.

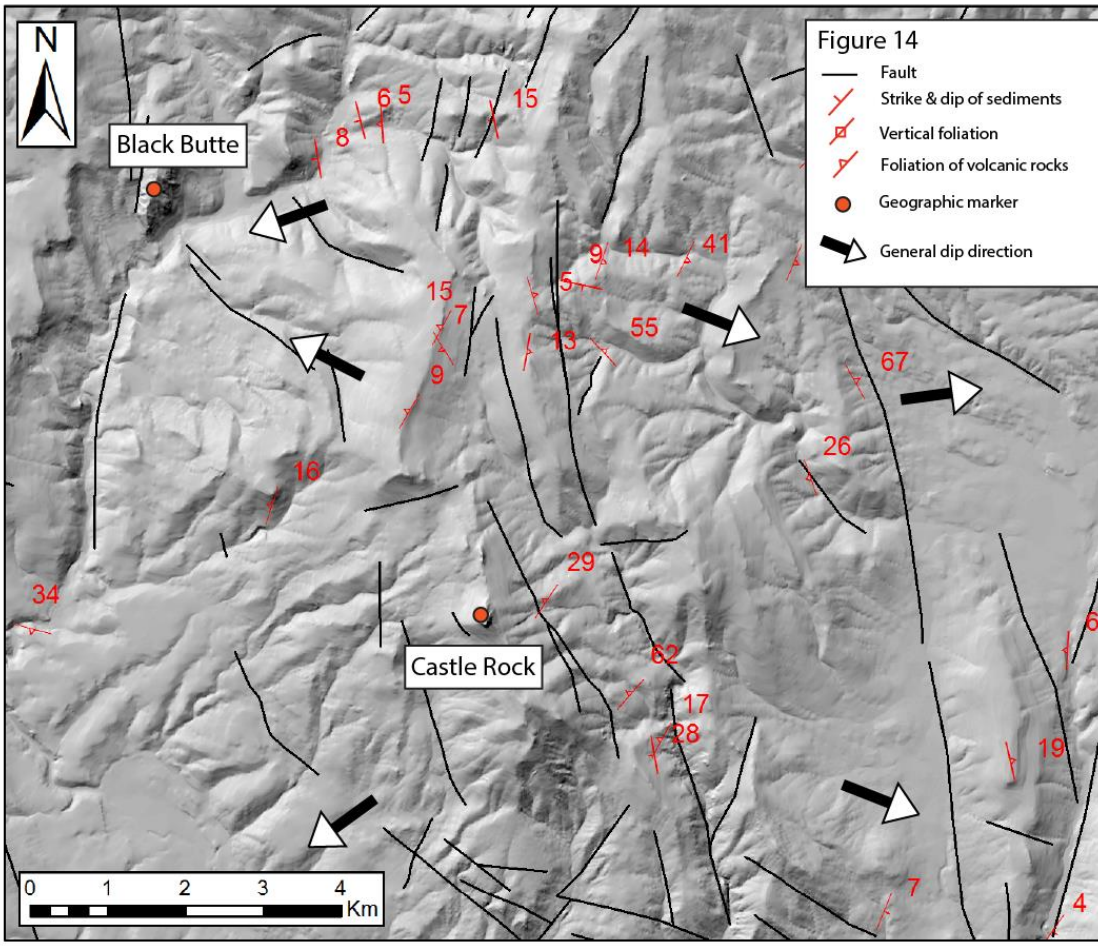

Figure 14. Map of Castle Rock showing orientation measurements.

Hydrothermal alteration

Throughout the Castle Rock caldera, there is evidence for hydrothermal alteration. Chalcedony fills vugs and forms veins within the Dinner Creek Tuff and overlying basaltic-andesite. The tuff outcrops within Jerry Canyon are particularly notable for the amount of chalcedony and quartz veins that cut through the Dinner Creek Tuff. The

mega-breccia deposits south of Sheepshead Rock also contain chalcedony fragments, up to 10 cm in length. These occur as float along the surface, with no in place veins actually observed.

The pyrite and manganese mineralization of the Ring Butte andesite lavas mentioned in the Ring Butte section, occur just north of the mega-breccia deposits, along the very northern boundary of the caldera. The lava is pale blue to light gray in color, significantly lighter than the intact, unaltered lava that occurs at Sheephead's Rock and Ring Butte. The pyrite crystals are less than 0.5 mm in size, and are distributed across the surface of the lava in clusters. Buried faults and fractures along this margin acted as conduits for water in the hydrothermal system.

Alteration is occasionally present within the units overlying the Dinner Creek Tuff. Green alteration, which could be chlorite alteration, occurs within basaltic-andesite outcrops along the western and southwestern side of Castle Rock.

Hydrothermal activity is still occurring in the region. In the Beulah Reservoir basin, directly south of the study area, hot springs occur along the length of Warm Springs Creek. These occur as small, 2-3 m long pools and at bubbling points along the creek.

Caldera margin

The outcrops of mega-breccia broadly define the northwestern margin of the caldera. Mega-breccia deposits do occur in patchy outcrops north of the ridgeline that separates the Lost Creek valley from Little Malheur river valley, seemingly outside of the proposed caldera margin. These could be basal debris flows of outflow deposits, although they are not overlain by rheomorphic Dinner Creek Tuff. About 2 km north of the

ridgeline, at Clevenger Butte, the Dinner Creek Tuff overlies hornblende poor lavas of Ring Butte. This outcrop of Dinner Creek Tuff is 50 m thick at the most, and dips towards the west/northwest. Its thickness implies that it is probably outflow facies. Therefore, the margin for the caldera must be located south, at or just north of the Lost Creek valley.

The Weathersby Formation, which is the country rock that bounds the northern margin of the caldera, is easily erodible, forming low rounded hills within the center of the study area. Any topographic margin that may have formed during the collapse of the caldera has probably been eroded away, particularly due to erosion along Lost Creek, which completely cuts through the northern margin of the caldera. The erosion of the country rock has left the more resistant intra-caldera volcanic rocks topographically higher than the surrounding country rock. A possible remnant of the topographic margin may be Sheephead's Rock. The ridgeline is capped by Ring Butte lava, which made it more resistant to erosion compared to the surrounding Weathersby Formation ridges. The ridgeline is only about 1.5 km in length. Further towards the east, the hill tops are not capped by lava, and are eroded down to the level of the mega-breccia and Dinner Creek Tuff.

The western margin of the caldera is difficult to discern, and there are two possibilities. The first possibility is that Castle Rock is the western margin of the caldera. The primary evidence for this is the juxtaposition of pre-caldera Basalt of Malheur Gorge lava flows against intra-caldera Dinner Creek Tuff and incipiently welded tuffs. As mentioned before, the Dinner Creek Tuff in Jerry Canyon, immediately east of Castle Rock is at least 300 m thick, with erratic, often vertical dips. In comparison, the Basalt of

Malheur Gorge lava flows dip gently towards the northwest. Lipman (1997) observed that intra-caldera tuff along the margins of a caldera typically display vertical to sub-vertical dips, due to interaction with the adjacent caldera wall, and that the surrounding country rock usually dips away from the caldera. The varied dips seen in the Dinner Creek Tuff at Jerry Canyon, and the opposing dips of the Basalt of Malheur Gorge could be evidence of this interaction. The stratigraphy along the Castle Rock ridge line is also varied. The summit is capped by a linear outcrop of rheomorphic Dinner Creek Tuff. Half a kilometer south of this outcrop, float fragments of pumice lapilli tuff overlie the Basalt of Malheur Gorge. These float fragments are similar in appearance to the tuffs that overlie the Dinner Creek Tuff across the study area. The absence of Dinner Creek Tuff between the pumice lapilli tuff and the Basalt of Malheur Gorge indicates that deposition of the tuff was uneven across the ridge line, or was eroded prior to the deposition of the pumice lapilli tuff, and that Castle Rock ridge was an uneven surface, such as an elevated topographic rim.

Alternatively, the western margin of the caldera could be west of Castle Rock, near the current location of the North Fork Malheur River. The primary evidence for this is the location of Black Butte, and the Lost Creek tuff section relative to Castle Rock ridge. If Castle Rock ridge is the western margin of the caldera, then we should expect to see a thinning of Dinner Creek Tuff deposits west of the ridge. However, as previously mentioned, Black Butte consists of 300 m of Dinner Creek Tuff or rhyolite lava equivalent, and is northwest of the Castle Rock ridge. At Lost Creek, the Dinner Creek Tuff is 100 – 200 m thick, and is directly north of the Castle Rock ridge. The possible ring dike at Lost Creek, mentioned in the ‘Tuff dike/ring dike vents’ subsection has

erratic vertical to sub-vertical dips, similar to the Dinner Creek Tuff outcrops at Jerry Canyon. If the Lost Creek outcrop is not representative of a dike, then it could be representative of the intra-caldera tuff interacting with the caldera floor. The Weathersby Formation on the opposite side of Lost Creek dips 17° NW, away from the caldera. The clustering of post-caldera collapse basaltic-andesite dikes and vents, are also indicative that the source vents are in this area.

As mentioned in the 'Intra-caldera tuff' subsection, over 50 m of rheomorphic Dinner Creek Tuff crops out in canyons along the western flank of the Castle ridge, further supporting the evidence that margin is further west of Castle Rock. These deposits lack the erratic dips of the Jerry Canyon and Lost Creek outcrops, dipping 46° SW, not much steeper than the Basalt of Malheur Gorge. Field mapping did not extend across the North Fork Malheur River, but the area to the west of the river consists of gently sloping basaltic-andesite hills and slopes. These aphyric lava flows continue southward towards the Beulah Reservoir. A radiometric age date for a lava sample on the west side of the North Fork Malheur river, 9 km southwest of Castle Rock is 16.3 Ma, just prior to the eruption of the first unit of the Dinner Creek Tuff (Streck et al., 2015). These older lavas could represent uplifted country rock along the western margin of the caldera.

As can be seen, the two possible western margins of the caldera have similar evidence but are separated by 4 km, from the southern terminus of Black Butte, to the northern end of the Castle Rock ridge. Sinistral transverse faulting along the southern margin of the Lost Creek tuff basin could have caused this dislocation. The Castle Rock ridge is cut by a minor sinistral fault, so sinistral step faulting along the length of the

ridge could've resulted in displacement of the margin. Alternatively, the two margins could be representative of collapse along structurally independent ring faults.

Size of the caldera beyond the study area

Mapping was restricted to the area around Castle Rock, but this section will briefly speculate about the southern and eastern extents of the caldera. At the southern end of Castle Rock, northwest trending faults displace the Basalt of Malheur Gorge and Dinner Creek Tuff against younger incipiently welded tuffs and lacustrine sediments of the Juntura Formation (Woods, 1976). These lacustrine sediments could've been deposited on the caldera floor, and uplifted to their present position due to regional extension. Woods (1976) noted that fossils recovered from the formation on the southeast side of Beulah Reservoir indicate a late Miocene to early Pliocene age. Fifteen kilometers south of Castle Rock, on the opposite side of Beulah Reservoir, the Dinner Creek Tuff crops out along the northern flanks of Beulah Peak. Haddock (1967) mapped a section that was at least 20 m thick, although the base was not exposed. This outcrop occurs at an elevation of 1522 m, approximately 500 m above the floor of the Beulah Reservoir basin. Its apparent thickness is an order of magnitude thinner than the outcrops in Jerry Canyon, 14 km north, so it would appear that the caldera margin lies somewhere along the Beulah Reservoir basin. The previously mentioned hot springs on the valley floor could mark the location of buried ring faults.

East of Beulah Peak, the Dinner Creek Tuff is largely absent. The Tim's Peak basalt is the most prominent unit, overlying the Hunter Creek basalt. Further south, along the rim of the Malheur River gorge, outflow deposits of the Dinner Creek Tuff up to 20 m thick, underlie the Hunter Creek basalt, and overlie the Basalt of Malheur Gorge

(Haddock, 1967). Thicker outcrops of Dinner Creek Tuff occur immediately northwest of Westfall Butte, 20 km southeast of Castle Rock. These outcrops occupy a canyon north of the butte, and are at least 50 m thick, with lithic fragments that make up to 50% of the rock (Evans and Binger, 1997). The abundant lithic fragments within the Dinner Creek Tuff could indicate that the tuff was erupted along a boundary, with pre-caldera country rock falling into the erupting tuff. East and south of Westfall Butte, the Dinner Creek Tuff occupies canyons, where the basal contact with the Basalt of Malheur Gorge is visible. These outcrops are 20 – 30 m thick, and continue to thin to the east (Haddock, 1967; Evans and Binger, 1997). Westfall Butte itself is a 15 – 12.5 Ma rhyolite dome complex consisting of rhyolite – basaltic tuffs and lava flows (Evans and Binger, 1997). The lava flows and tuff contains fragments of Dinner Creek Tuff, and the entire volcanic edifice could be situated atop a ring fracture of the Castle Rock caldera.

North of Westfall Butte, in the Bully Creek drainage basin, the topography is more subdued, with little indication of possible caldera margins. Isostatic gravity data shows a gravity low immediately northwest of Westfall Butte, 20 km east of Castle Rock (Griscom and Halvorson, 1994; Evans and Binger, 1997). This low could indicate buried low density intra-caldera tuffs and caldera floor deposits, beneath overlying Hunter Creek basalt (Evans and Binger, 1997).

North of Bully Creek, the topography becomes steeper. The mega-breccia outcrops were mapped by Lowry (1968) as ‘Ring Butte Andesite’, and he mapped them as far east as headwaters of Rail Creek, about 4 km east of the limits of the study area. In this drainage basin, Lowry (1968) described a volcanic vent based on tuff deposits with pumice fragments up to 2 m in length. Based on this description, the northeastern

boundary of the Castle Rock Caldera may be located at the Rail Creek headwaters. The above description defines an elliptical area, 23 km east-west and 21 km north-south. This is probably an over exaggeration of the true size of the caldera.

Caldera type

If the Castle Rock caldera were a piston type caldera, then we should see even thicknesses of intra-caldera tuff, lacustrine deposits, well defined margins, and a resurgent dome roughly in the center of the caldera. The base of the intra-caldera tuff is not exposed, so it cannot be determined whether thicknesses vary across the caldera. Lacustrine deposits are limited to the southern part of the caldera. At other locations of the caldera, namely Lost Creek, sandstone and conglomerates interbedded with the incipiently welded tuffs indicate a more fluvial environment. The margins within the study area aren't coherent, with a 4 km east-west gap between the Lost Creek – Black Butte margin, and the Castle Rock margin. Erosion of the Weathersby Formation has removed any clear indicator of a topographic rim, and the margin can only roughly defined by the mega-breccia outcrops. To the east of the study area, the subdued topography doesn't give any indication as to the location of an eastern margin. Resurgent doming, if it occurred, was focused at Castle Rock, along the western side of the caldera. Faulting in general appears to be focused mostly along the western side, far from the center. From this description it would appear that the Castle Rock caldera is not a piston type caldera. Piecemeal or trapdoor collapse seems more likely. The lack of significant amounts of lacustrine deposits across the caldera means that there was not enough of an even surface on the floor of the caldera to accommodate a significantly sized lake. The gently topography east of Castle Rock could indicate trap door collapse along the Castle

Rock/Lost Creek – Black Butte margins, and a buried, gently sloping hinge line further east in the Bully Creek drainage basin. The lack of coherence between the two western margins could indicate piecemeal collapse of the caldera during two stages of eruption: one along the Castle Rock margin, and another slightly northwest along the Black Butte margin. **Figure 15** shows the study area and surrounding region with the volcanic/sedimentary units, and structures mentioned in the previous two sub-sections.

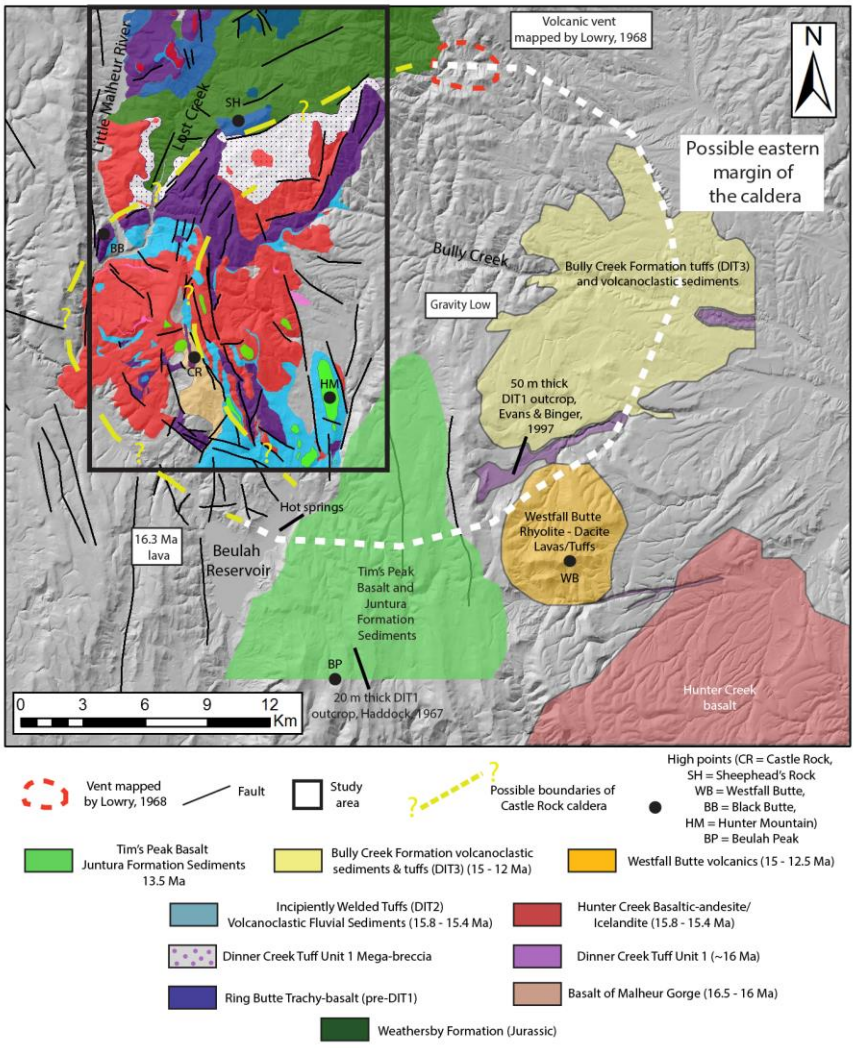

Figure 15. Map of the possible size of the Castle Rock caldera showing some of the regional volcanic units and structures described.

Ironside Mountain Caldera

Ironside Mountain is a northeast trending ridge located at the very northern part of the study area. Its southern peak is the highest topographic point in the study area at 2380 m (**Figure 16**). The mountain has long puzzled geologists, as it is an uplifted block of Tertiary volcanic rocks completely surrounded by older, mostly Mesozoic sediments and intrusive rocks. Thayer and Brown (1973) mapped the mountain in detail, and believed it was an uplifted and folded basin. The field mapping evidence presented below shows that Ironside Mountain is an uplifted, eroded caldera and a source for one of the Dinner Creek Tuff units.

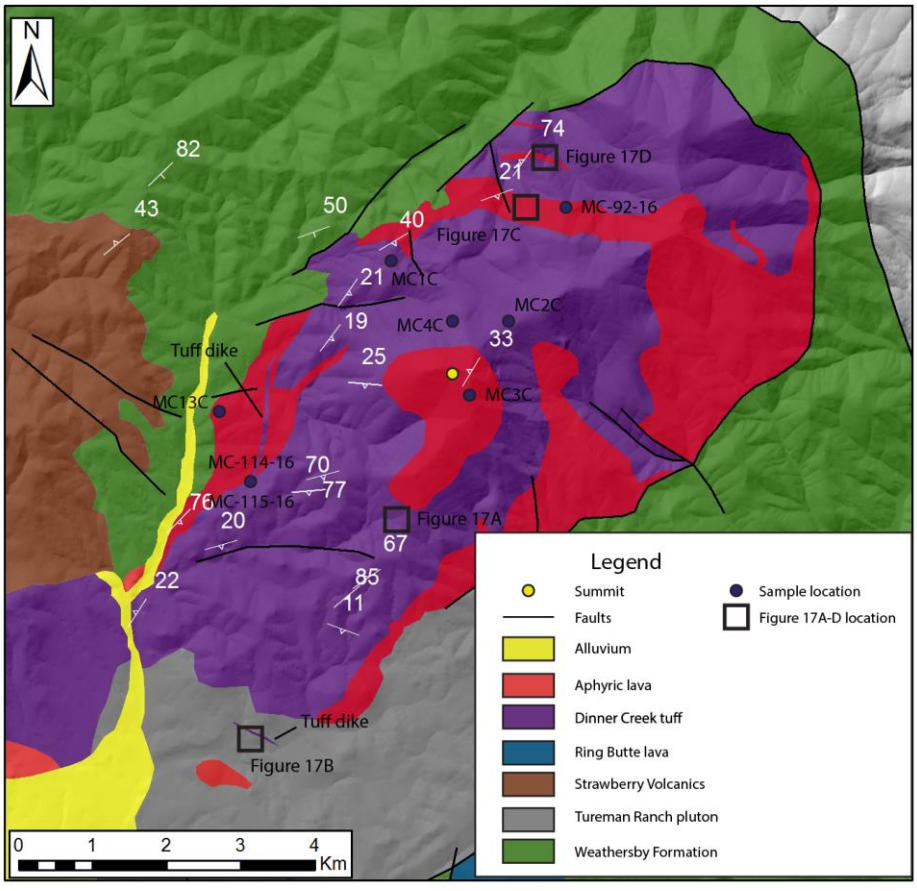

Figure 16. Geologic map of Ironside Mountain. Samples, and Figure 17 locations shown.

Intra-caldera tuff

Dinner Creek Tuff crops out across much of the south face of the mountain. It is bound on the west and east by near vertical faults, which displace the tuff against the Weathersby Formation, and occasional minor outcrops of aphyric lava. The tuff at Ironside Mountain appears to be made up of two cooling units, with the lower unit resembling the Dinner Creek Tuff at Castle Rock in color, degree of welding, rheomorphism, and phenocryst/lithic fragment content. Outcrops of rheomorphic tuff along the western flanks of the mountain dip ~20° SE, inward towards the summit. At the very southwestern edge of the mountain, rheomorphic tuff dips 22° NW, away from the mountain.

The upper unit is brown in groundmass color, and not as devitrified as the lower unit. Elongated fragments of obsidian up to 10 cm in length and 3 cm in width are present along the base of the upper unit. Occasionally, a breccia filled surge deposit lies along the upper unit's base. Clasts of the lower, rheomorphic Dinner Creek Tuff unit, up to 3 cm in length occur within the upper unit, definitively post-dating the upper unit relative to the lower unit (**Figure 17A**). The upper unit has erratic dips along the southern flanks of the mountain. It generally dips inward to the center of the mountain. Dips ranging from 70° SE to 85° NW occur along the southern flank of the mountain. Gentler dips (11° SW) occur further south, towards the contact with the Tureman Ranch grano-diorite.

The contact between the two units varies in dip. On the south flank, the contact dips 15 – 28° NE, while further upslope, towards the summit, the contact varies between 30 – 40° SW to NW. The total thickness of the two units is at least 300 m at Ironside Mountain. It is overlain by aphyric lava, which caps the summit.

Rhyolitic, white-tan, phenocryst poor tuff makes up the bulk of the mountain north of the main summit, stratigraphically beneath aphyric lava, and the Dinner Creek Tuff outcrops along the south side of the mountain. This tuff is heavily brecciated and altered. The tuff has a white, fine groundmass, with very few plagioclase phenocrysts observed. Occasional float fragments of rheomorphic tuff that look more similar to other outcrops of Dinner Creek Tuff are present, but no rheomorphic outcrops were observed in this part of the field. The tuff is cut and intruded by mafic sills and dikes. No orientation measurements could be taken on the tuff outcrops. This tuff is interpreted as Dinner Creek Tuff that has been altered by intrusive basaltic-andesite. Combined with the overlying outcrops on the south flank of the mountain, the total Dinner Creek Tuff thickness at Ironside Mountain is well over 600 m.

Tuff dike/ring dike vents

A couple of tuff dikes are exposed along the southern flanks of Ironside Mountain. One dike is exposed along the dirt road, at the base of the mountain. This dike cuts through Tureman Ranch grano-diorite, and can be traced for one km to the northwest from the roadside. It strikes 322°, and dips about 60° NE, and is about 4 m thick (**Figure 17B**). There is a sub-horizontal, northwest trending, southwest dipping joint surface that could represent cooling from the edges to the interior of the dike. The dike has a very fine grained white groundmass, with no observable phenocrysts. Thayer and Brown (1973) originally mapped the dike as an intrusive member of the Strawberry Volcanics.

Thayer and Brown (1973) mapped another dike along the southeast flank of Ironside Mountain. This dike is more brecciated, and is bound on its east side by a vitrophyre. The contact between the vitrophyre and the rheomorphic Dinner Creek Tuff,

which it appears to intrude, is near vertical. The western boundary of the dike is not very well exposed. Aphyric, mafic lava appears to border the dike on the west, and the total width of the dike is no more than 3 m. Seeing as how this dike appears to cut through aphyric basalt and rheomorphic Dinner Creek Tuff, it could be the source for the overlying glassy, moderately welded Dinner Creek Tuff unit. The dike is exposed for about 1 km in a north – northeast trend.

Mafic vents are exposed along the entire length of Ironside Mountain. These vents occur mostly along the southeastern and southwestern slopes of the mountain. The outcrops occur as 1.5 – 2 km wide ribbons between Dinner Creek Tuff in the center of the mountain, and Tureman Ranch grano-diorite/Weathersby Formation sediments in the surrounding countryside. The thickest accumulation of mafic lava occurs along the southwestern flank of the mountain, where aphyric lava sits in between Weathersby Formations sediments to the west, and rheomorphic Dinner Creek Tuff to the east. Similar aphyric lava outcrops occur in thin, 0.5 – 1 km wide outcrops along the southeastern side of Ironside Mountain. The southern summit of Ironside Mountain is capped by basaltic-andesite that overlies the Dinner Creek Tuff. The southwestern face of the summit consists of two dikes that are the source for the basalt. A 30 m thick basalt or basaltic-andesite sill is exposed about 1 km northwest of the main summit (**Figure 17C**). It is mostly aphyric, although minor 1-3 mm plagioclase crystals are present. The sill strikes 68°, and dips 21° SE, towards the center of the mountain. Two aphyric dikes cut across the altered rhyolite 1 km further north. The dikes are 10 m thick, and strike 35 – 40°, and dip from vertical to 74° NW, away from the mountain (**Figure 17D**). The east side of Ironside Mountain was not mapped in this study, but Thayer and Brown (1973)

identified more dikes along the northeast flanks of the mountain. These vents at Ironside Mountain could be due to the presence of buried ring dikes that served as conduits for upward movement of post-caldera forming Hunter Creek basalt.

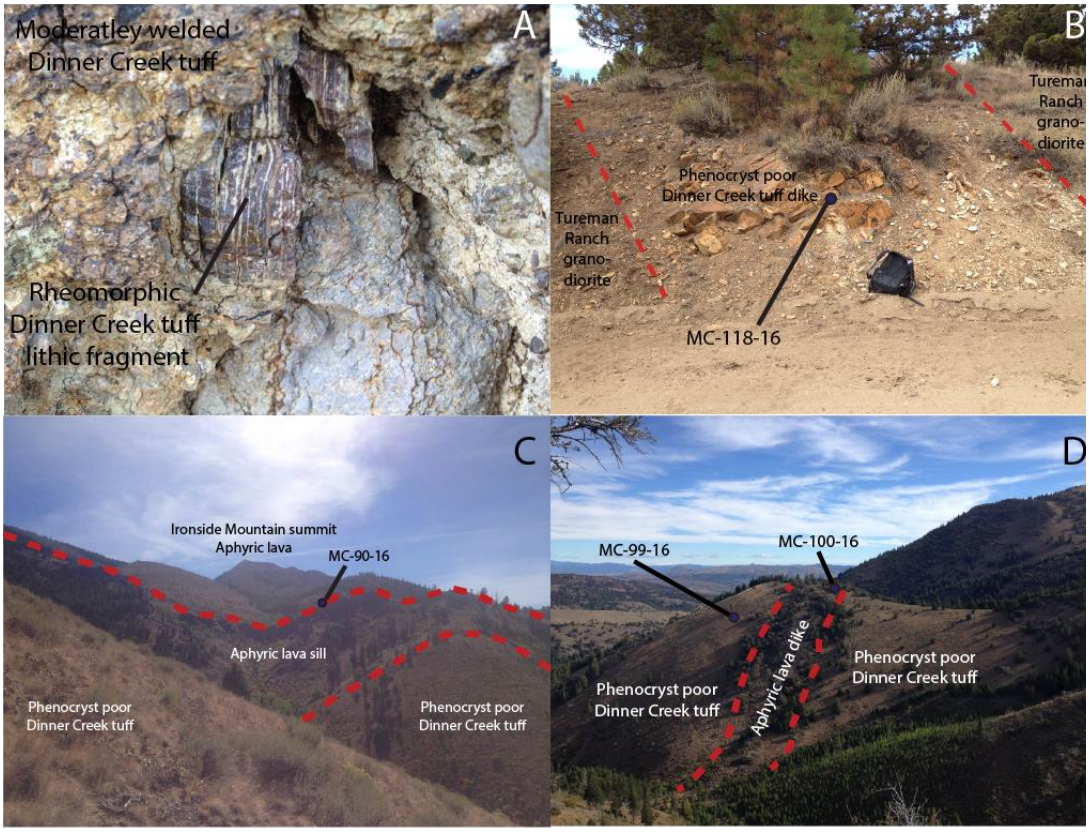

Figure 17 Photos of Ironside Mountain**. A.** Rheomorphic Dinner Creek Tuff lithic fragment within overlying moderately welded Dinner Creek Tuff. **B.** Phenocryst poor Dinner Creek dike intruding into Tureman Ranch pluton, along south flank of Castle Rock. **C.** Intrusive aphyric basalt or basaltic-andesite sill with phenocryst poor Dinner Creek Tuff below. **D.** Phenocryst poor Dinner Creek Tuff with intrusive basalt or basaltic-andesite dike.

Resurgence/uplift

Unlike at Castle Rock, pumice lapilli tuffs and volcaniclastic sediments do not overlie the Dinner Creek Tuff or summit capping aphyric lava. The absence of these types of sediments limits the amount of information that can be gained about resurgence within the caldera.

The high elevation of the mountain indicates that uplift has obviously happened. Uplift is greatest along the steep northeastern slope of the mountain, which rises ~1000 m above the Willow Creek basin to the northeast. A northwest trending ridge line extends ~20 km northwest from Ironside Mountain. This ridge line consists of uplifted Weathersby Formation sediments capped by dacite and andesite lava flows of the early Strawberry Volcanics (Robyn, 1977; Brooks et al., 1979). Southeast of Ironside Mountain, Weathersby Formation sediments are uplifted and juxtaposed against younger, undivided volcanic and sedimentary rocks. This regional uplift of the Weathersby Formation occurred along a northwest trending normal fault, which Thayer and Brown (1973) called the Border fault. The fault bounds the mountain on its northern flank, creating an arcuate shape. This arcuate shape is distinct from other sections of the fault, and could be result of re-activation of ring fractures during propagation of the Border fault. Caldera floor sediments and incipiently welded tuffs have been eroded from the mountain, probably due to the uplift, decreasing the amount of information that could be obtained about resurgence. As it stands, no obvious signs of resurgent doming are present at Ironside Mountain and current uplifted, dome like shape of the mountain is probably entirely due to uplift along the Border fault.

Margin

Despite the lack of mega-breccia, the margins of the Ironside Mountain caldera are more easily identifiable than the margins of the Castle Rock caldera. The structural boundary of the caldera consists entirely of the mountain itself, where the thick deposits of Dinner Creek Tuff and intrusive sills and dikes are confined. The northern, eastern, and western boundaries of the caldera are particularly well defined, due to uplift of the

caldera along the Border fault. Along the western-northwestern margin of the caldera, the tuff and lava deposits generally dip southeast. Thayer and Brown (1973) noted that outcrops along the eastern margin of the caldera generally dipped northwest-southwest, and that all the volcanic rocks tended to dip towards the interior of the mountain. Vertical to sub-vertical dips do occur along the southern-southeastern flanks of the mountain, and at the some parts of the northeastern end of the mountain (Thayer and Brown, 1973). Like the vertical dips at Jerry Canyon in the Castle Rock caldera, these vertical dips along the margins of the Ironside Mountain caldera could be result of intra-caldera tuff interacting with the caldera walls during deposition. The southern boundary is not as easily distinguishable. The Dinner Creek Tuff and aphyric basaltic-andesite lap up against Tureman Ranch grano-diorite on the southern flanks of the mountain, but no clear contact is exposed. Top soil, debris, and colluvium obscure the contact between the older caldera wall rocks, and the intra-caldera tuffs. The above mentioned near vertical foliations in the glassy, moderately welded upper unit could indicate interaction with the caldera wall at depth. Along the very southern and western flanks of the mountain, the Dinner Creek Tuff dips more shallowly towards away from the mountain, perhaps indicating that these outcrops already lie outside of the caldera.

The patchy distribution of Dinner Creek Tuff outcrops around Ironside Mountain Is further evidence that the boundaries of the caldera don't extend beyond the mountain. Directly south of Ironside Mountain is the Tureman Ranch grano-diorite pluton, which is about 2 km wide in a north-south direction. At the southern margin of the pluton is Clevenger Butte, where the Dinner Creek Tuff is about 50 m thick at the most, and is probably outside of the caldera. Along the west side of the caldera, lavas and tuffs occur

in sporadic patches, sitting atop the Weathersby Formation. Dinner Creek Tuff occurs in various faulted outcrops along Camp Creek, 9 kms north of Ironside Mountain, where it sits atop andesite lava. The outcrops are as much as 70 m thick, and probably represent outflow facies. Ironside Mountain is the only location north of Castle Rock where the Dinner Creek Tuff is over 100 m thick. The size of the mountain defines an 11 by 6 km uplifted caldera, filled with intra-caldera Dinner Creek Tuff and intrusive aphyric basaltic-andesite (**Figure 18**).

Like the Castle Rock caldera, the Ironside Mountain caldera is completely surrounded by Mesozoic sediments and intrusive rocks, which form low rolling hills, and produce poor outcrops along stream channels and ridge tops. Any topographic margin that existed after caldera collapse has probably been removed due to uplift of the caldera along the Border fault in the north, and the erosion that followed the uplift. In the Unity and Willow Basins to the north/northeast, water wells and wildcat oil wells that were drilled in the 1960's penetrated over 1 km of sediments without reaching basement, and the rocks that made up the topographic rim, mega-breccia deposits, and caldera floor sediments of the caldera have probably been deposited within these basins (Lowry, 1968).

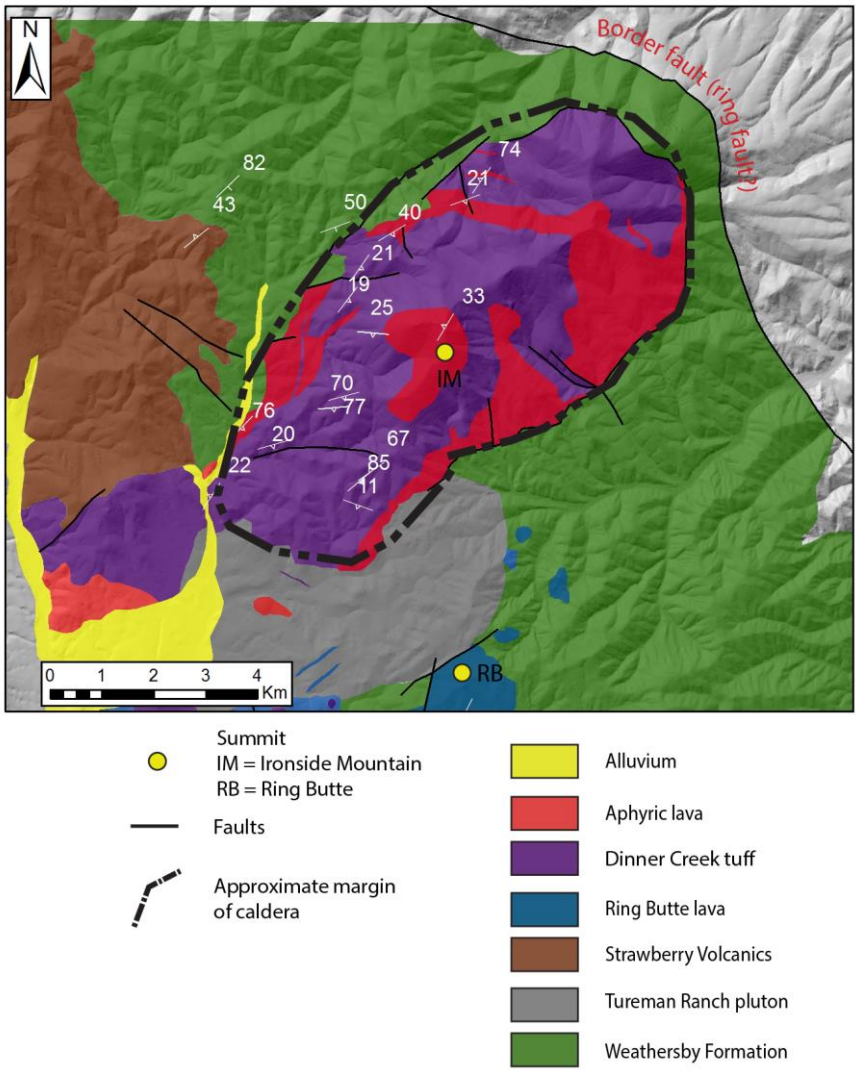

Figure 18. Map of Ironside Mountain caldera showing margin, and possible ring fault on the north flank

Caldera type

The entirety of Ironside Mountain appears to consist mostly of tuff, in various appearances: fine-grained/altered white tuff, glassy moderately welded tuff, and dense, devitrified rheomorphic tuff. The total thickness of tuff is over 600 m, with no basal contact exposed. Unlike at the Castle Rock caldera, faulting within the mountain appears minimal, less than 10 m in intrusive basalt sills and dikes. This lack of significant internal

faulting could be due to a more structurally coherent caldera floor, which collapsed along well defined ring faults. This would make the caldera a piston type caldera, as opposed to the Castle Rock caldera which is a more chaotic piecemeal type caldera.

Dinner Creek Tuff outflow deposits

A brief mention will be made of Dinner Creek Tuff outcrops that exist outside of the Castle Rock and Ironside Mountain calderas. No outflow deposits of Dinner Creek Tuff occur in the southern part of the study area. North of Sheepshead Rock, the Dinner Creek Tuff is absent, and older Weathersby Formation and Ring Butte lavas are exposed at the surface. The Dinner Creek Tuff outcrops again at Clevenger Butte, 4.5 km northwest of Sheepshead Rock. The tuff is at most 50 m thick along the east side of Clevenger Butte. The base of the tuff consists of an incipiently welded tuff with vitric glass fragments up to 6 mm in length. This basal tuff is up to 1.5 m thick. The central part of the outcrop is dense and devitrified, just like at Castle Rock and Ironside Mountain. The color varies from pale purple to purplish-brown. Some outcrops of the tuff contain many vesicles, mostly round although sometimes slightly elongated, as much as 3 cm in length (**Figure 19A**). Vesicles commonly contain quartz rinds along the edges of the vesicles and are occasionally completely filled in. Along the west flank of Clevenger Butte, the vesicles are stretched so that they are three times as long as they are wide. The overall appearance of the Dinner Creek Tuff at Clevenger Butte is lighter and paler in color than the Dinner Creek Tuff outcrops around Castle Rock. The Clevenger Butte outcrops are also noticeably harder. The paler color, increased hardness, and numerous veins and vugs filled with quartz indicate that silicification and alteration occurred at the Clevenger Butte outcrops. To the west, there is the steep escarpment along the west side

of the Little Malheur River. This is probably a fault bound escarpment, which appears to run the entire length of the river in the study area. Such a large fault could have provided a conduit for the movement of meteoric water, which could've altered the nearby Dinner Creek Tuff outcrops at Clevenger Butte.

Dinner Creek Tuff outcrops occur 9 km north of Ironside Mountain, along Camp Creek road. Northwest trending normal faults cut the volcanic rocks, creating step-like outcrops of lava and tuff that are best exposed along the confluence of Camp and King Creek. These outcrops of Dinner Creek Tuff overlie andesite lava, and the basal surge deposit is about 2 m thick. These outcrops are rheomorphic, and paler in color than the darker reddish-purple outcrops within the calderas, and have been eroded into spires along the National Forest Road 16 (**Figure 19B**). The top of the outcrops is moderately welded tuff, with stretched fiamme up to 4 cm long. Incipiently welded tuff or airfall deposits were not observed, and the tuff is overlain by aphyric lava akin to lava that overlies the Dinner Creek Tuff at the Castle Rock and Ironside Mountain calderas.

What appears to be a small dike is exposed along the Little Malheur River, where National Forest Road 16 crosses the river, at the very northwestern end of the study area. This dike is northwest of Castle Rock, and about 8 km west of Ironside Mountain, and is worth mentioning as it appears to be a source for the Dinner Creek Tuff outside of the above mentioned calderas. It shows up in a road cut, but can be traced east and west of the road for about a kilometer in both directions. The outcrop consists of Dinner Creek Tuff that is about 9 m thick, and bounded on both sides by vitrophyre that is 1 – 1.5 m thick along the boundary with Strawberry Volcanics andesite lava (**Figure 19C**). The outcrop trends 316°, and dips from 27 - 60° NE. The variance in the dips is due to the

poor exposure of the outcrop, and joint orientations being mistaken for actual foliation. Either way, these dips are much gentler than the near vertical dips of the Dinner Creek Tuff at the previously mentioned outcrops, around Castle Rock. While this would seem to argue against a dike, the presence of vitrophyre along either side of the Dinner Creek Tuff indicates that cooling occurred along a conduit through which the magma flowed through. The outcrop could have been emplaced at this angle, or could have been tilted post-eruption during regional extension in the mid-Miocene.

Finally, the Dinner Creek Tuff crops out in the Bully Creek canyon, 26 km east of Castle Rock. The Dinner Creek Tuff fills the canyon, and is as much as 50 m thick, although the base is not exposed. The tuff is densely welded and devitrified. Incipiently welded tuffs and volcaniclastic sediments of the Bully Creek Formation overlie the Dinner Creek Tuff (Ferns et al., 1993; Streck and Ferns, 2004). The Bully Creek Formation is as much as 60 m thick, and is capped by a gray, moderately welded, pumiceous tuff. It thickens towards the east. The Dinner Creek Tuff is only exposed within the steep canyon, being buried underneath the Bully Creek Formation to the north and south. This location is east of the gravity low mentioned in the Castle Rock caldera section, and is therefore probably outside of the caldera. The eastern extent of the Dinner Creek Tuff occurs at a homestead where Scott Road crosses over Bully Creek, about 9 km northwest of the town of Westfall. Beyond this point, it is buried beneath the Bully Creek formation and Hunter Creek basalt.

Figure 19 Photos of outflow Dinner Creek Tuff outcrops**. A**. Dinner Creek Tuff at Clevenger Butte, with chalcedony filled vugs and vesicles. **B.** Spires of rheomorphic Dinner Creek Tuff at King Creek, northwest of Ironside Mountain. **C.** Rheomorphic dike of Dinner Creek Tuff intruding into Strawberry Volcanics porphyritic andesite lava.

Field Mapping Summary

The field evidence indicates that two calderas are present within the study area. In the southern part of the study area is the Castle Rock caldera. Mega-breccia deposits mark the northern boundary of the caldera, and >300 m of intra-caldera tuff and 100 – 200 m of incipiently welded, re-worked tuffs and volcano-clastic sediments were deposited on the caldera floor. The structural margins of the caldera are delineated by north-northeast trending vertically foliated outcrops of Dinner Creek Tuff or rhyolite lava equivalent, faults, and mafic vents/dikes. The western margin of the caldera may be at

Castle Rock, where pre-Dinner Creek Tuff mafic lava flows are uplifted against intra-caldera deposits to the east. Alternatively, the western margin of the caldera could be located further to the west, in the valley of the Little Malheur River. The eastern and southern margins of the caldera are more poorly defined. Collapse may have occurred primarily along the north-northeast trending structures at Castle Rock and Lost Creek, creating a trap door caldera with minimal subsidence in the eastern part of the caldera.

The Ironside Mountain caldera is an 11 x 6 km northeast trending, uplifted mass of intra-caldera Dinner Creek Tuff, and intrusive mafic lava dikes and sills. The appearance of the Dinner Creek Tuff varies at Ironside Mountain, from dense, devitrified, and rheomorphic, to glassy, moderately welded, to fine-grained and altered. Tuff dikes are exposed along the southern margins of the caldera. The Border fault, a regional scale normal fault that sits just north of the caldera, has uplifted the entire structure, and titled it towards the south. This uplift has caused erosion of the surrounding Weathersby Formation, destroying the topographical rim of the caldera. Any signs of resurgence or mega-breccia/caldera floor sedimentary deposits that may have existed have probably been removed due to this erosion, leaving behind the uplifted intra-caldera tuff and intrusive mafic lavas.

Lava flows pre-date and post-date the Dinner Creek Tuff within the DITEC. The oldest lava flows occur at Ring Butte in the center of the study area. These lava flows unconformably overlie the Mesozoic basement rocks. Andesite and dacite lavas, similar in appearance to the 19 – 18 Ma early Strawberry Volcanics occur in the very northwest corner of the study area (Robyn, 1977). In the Castle Rock caldera, pre-Dinner Creek Tuff tholeiitic lava flows of the Basalt of Malheur Gorge have been uplifted over 600 m

above the Beulah Reservoir basin. Post-Dinner Creek Tuff lava flows consist mostly of aphyric basaltic-andesite, similar in appearance to the regionally extensive Hunter Creek basalt. These lavas intrude into Dinner Creek Tuff at both calderas. They are the highest stratigraphic unit at the Ironside Mountain caldera. At the Castle Rock caldera, a distinct pumice lapilli tuff is interbedded with the aphyric lava. Porphyritic basalt flows overlie the aphyric lava at Castle Rock. Mid-Miocene to early Pliocene volcaniclastic sediments of the Juntura and Drewsey Formations crop out along the southern margins of the study area. The 9.7 Ma Devine Canyon tuff is interbedded with these sediments along the southwestern flank of Castle Rock.

In the next section of the thesis, XRF, ICP-MS, SEM-EDS, and petrographic analysis of samples taken from the study area will be used to discriminate between different Dinner Creek Tuff units in order to determine which units erupted from which caldera. Mafic lavas and other tuff units will also be analyzed in order to provide a better understanding of the volcanic units within the DITEC.

Chapter III: Sample Analysis Results

In this section, the results of the geochemical, petrographic, and mineral compositional data will be discussed. Samples will be separated into tuffs and basalts, and they will be grouped together into units.

Dinner Creek Tuff units

Of the 58 samples collected in this study, 36 of them are tuff samples. All the tuff samples collected within the field area were compared to geochemical data from Streck et al (2015), which separated the Dinner Creek Tuff into four cooling units. Streck et al. (2015) separated the four Dinner Creek Tuff units by SiO_2, trace element concentrations, and mineral composition. A brief description of the distinguishing features of the various Dinner Creek Tuff units from Streck et al. (2015) follows.

The first unit, DIT1, has SiO_2 over 75 wt. %, and lower FeO*, MgO, TiO_2, and Al_2O_3 compared to the other units. The DIT1 is elevated in just about all trace elements, with the notable exception of Sr (<60 ppm). Streck et al. (2015) determined that the age is 16.1 – 15.9 Ma using $^{40}Ar/^{39}Ar$ analysis, with a preferred age of 16.15 Ma.

The second and third units, DIT2 and DIT3, range in SiO_2 from 70 – 75 wt. %. In general, these two units are higher in FeO*, MgO, TiO_2, and Al_2O_3, but lower in SiO_2, than DIT1. They are mostly depleted in trace elements compared to DIT1 (i.e. 400 >Zr > 300 pm), although the La, Ce, U, and Rb content is the same as DIT1. DIT2 and DIT3 are enriched in Sr, Ba, and Ta. DIT2 is more enriched in Sr than DIT3, but any other distinguishing traits between the two units are difficult to discern. The primary distinction between DIT2 and DIT3 is the composition of feldspar crystals, with DIT2 containing

more oligoclase plagioclase feldspars and DIT3 containing more anorthoclase K-feldspars (Streck et al., 2015). The distinction between these two units will be further explored in the 'Feldspar Analysis' section. Ages for the DIT2 -3 overlap and range from 15.5 – 15.4 Ma.

The DIT4 has SiO_2 lower than 68 wt. %, and is a dacite tuff. It is lower in K_2O and higher in the other major elements relative to the rhyolitic Dinner Creek Tuff units. In terms of trace elements, the DIT4 is enriched in Eu, Sr, and is generally depleted in the other trace elements. One $^{40}Ar/^{39}Ar$ radiometric date for the DIT4 yielded 15 Ma.

Table 1 shows the Dinner Creek Tuff units defined by Streck et al. (2015), with variations of major and trace elements mentioned above.

Table 1. Variations of select major and trace elements in the Dinner Creek Tuff units, from Streck et al. 2015.

Major/Trace Element	DIT1	DIT2-3	DIT4
SiO_2 wt. %	> 75	70 - 74	< 68
FeO* wt. %	< 2.5	2 - 5	> 5
TiO_2 wt. %	< 0.2	0.2 - 0.7	> 0.9
Al_2O_3 wt. %	12.3 - 13.6	13.2 - 14.3	> 14 - 15
K_2O wt. %	3.7 - 6.1	3.3 - 6.1	< 3.4
CaO wt. %	0.3 - 1	0.5 - 4.4	2.7 - 3.6
Zr ppm	> 400	300 - 400	< 275
Nb ppm	22 - 26	13 - 24	16 - 18
Hf ppm	> 11	11 - 8	< 8
Ta ppm	1.2 - 1.5	0.9 - 1.4	1 - 1.1
Y ppm	86 - 93	50 - 84	46 - 55
Eu ppm	1.5 - 1.8	1.6 - 2.7	> 2.3
Sr ppm	25 - 70	71 - 256	233 - 271
La ppm	42 - 49	29 - 54	30 - 34

Tuff Sample Geochemistry

Table 2 shows the samples that were analyzed in this section, and **Figure 20** shows a location map of the samples. Sample MC-88B-16 is considerably more mafic

than the other samples (wt. % SiO_2 is 51), and is discarded from this section. Based on the geochemistry, it is more likely that this sample is a basal tuff related to the eruption of overlying basalt. It is included with the other samples in Appendix B.

Table 2. Samples selected for XRF/ICP-MS analysis. Columns show sample name, rock type, geologic unit that it had been previously identified with, and location. CR = Castle Rock and IM = Ironside Mountain

Sample	Rock Type	Previously mapped as	Location
MC-107-16	Rheomorphic devitrified tuff	Strawberry Volcanics	King/Camp Creek
MC-114-16	Moderately welded glassy tuff	Strawberry Volcanics	IM Caldera
MC-115-16	Moderately welded glassy tuff	Strawberry Volcanics	IM Caldera
MC-1-16	Rheomorphic devitrified tuff	Dinner Creek Tuff	CR Caldera
MC-118-16	Aphyric tuff	Strawberry Volcanics	IM Caldera
MC-12-16	Pumice lapilli tuff	Tsvv	CR Caldera
MC19A	Rheomorphic devitrified tuff	Dooley rhyolite	CR Caldera
MC1A	Pumice lapilli tuff	Juntura Formation	CR Caldera
MC-1-BC	Rheomorphic devitrified tuff	?	Bully Creek Canyon
MC1C	Rheomorphic devitrified tuff	Strawberry Volcanics	IM Caldera
MC20A	Rheomorphic devitrified tuff	Dooley rhyolite	CR Caldera
MC-23-16	Pumice lapilli tuff	Tsvv	CR Caldera
MC23A	Rheomorphic devitrified tuff	Dooley rhyolite	CR Caldera
MC24A	Rheomorphic devitrified tuff	Dooley rhyolite	CR Caldera
MC-2-BC	Vitrophyre	?	Bully Creek Canyon
MC2C	Moderately welded glassy tuff	Strawberry Volcanics	IM Caldera
MC33A	Pumice lapilli tuff	Tsvv	CR Caldera
MC-37-16	Rheomorphic devitrified tuff	Dooley rhyolite	CR Caldera
MC-39-16	Pumice lapilli tuff	GR tuff breccia	CR Caldera
MC-3-BC	Pumice lapilli tuff	?	Bull Creek Canyon
MC-45-16	Pumice lapilli tuff	Tsvv	Castle Rock Caldera
MC4C	Moderately welded glassy tuff	Strawberry Volcanics	IM Caldera
MC-50-16	Mega-breccia	Ring Butte Andesite	CR Caldera
MC-5-16	Pumice lapilli tuff	?	CR Caldera
MC-53-16	Mega-breccia	Ring Butte Andesite	CR Caldera
MC-55-16	Mega-breccia	Ring Butte Andesite	Castle Rock Caldera
MC-58-16	Rheomorphic devitrified tuff	Strawberry Volcanics	Little Malheur River
MC-61-16	Pumice lapilli tuff	Tsvv	CR Caldera
MC-62-16	Pumice lapilli tuff	Tsvv	CR Caldera
MC-63-16	Pumice lapilli tuff	Tsvm	CR Caldera
MC-69-16	Pumice lapilli tuff	Tsvv	CR Caldera
MC-73-16	Pumice lapilli tuff	GR tuff breccia	CR Caldera
MC-74-16	Mega-breccia	Ring Butte Andesite	CR Caldera
MC-84-16	Mega-breccia	Ring Butte Andesite	CR Caldera
MC-99-16	Aphyric tuff	Strawberry Volcanics	IM Caldera

Strawberry Volcanics, from Thayer & Brown, 1973

Dooley Rhyolite, Ring Butte Andesite, GR (Goodwin Ranch) tuff breccia, from Lowry, 1968

Dinner Creek Tuff, Juntura Formation, Tsvv (Strawberry Volcanics Volcaniclastics), Tsvm (Strawberry Volcanics Marker), from Woods, 1976

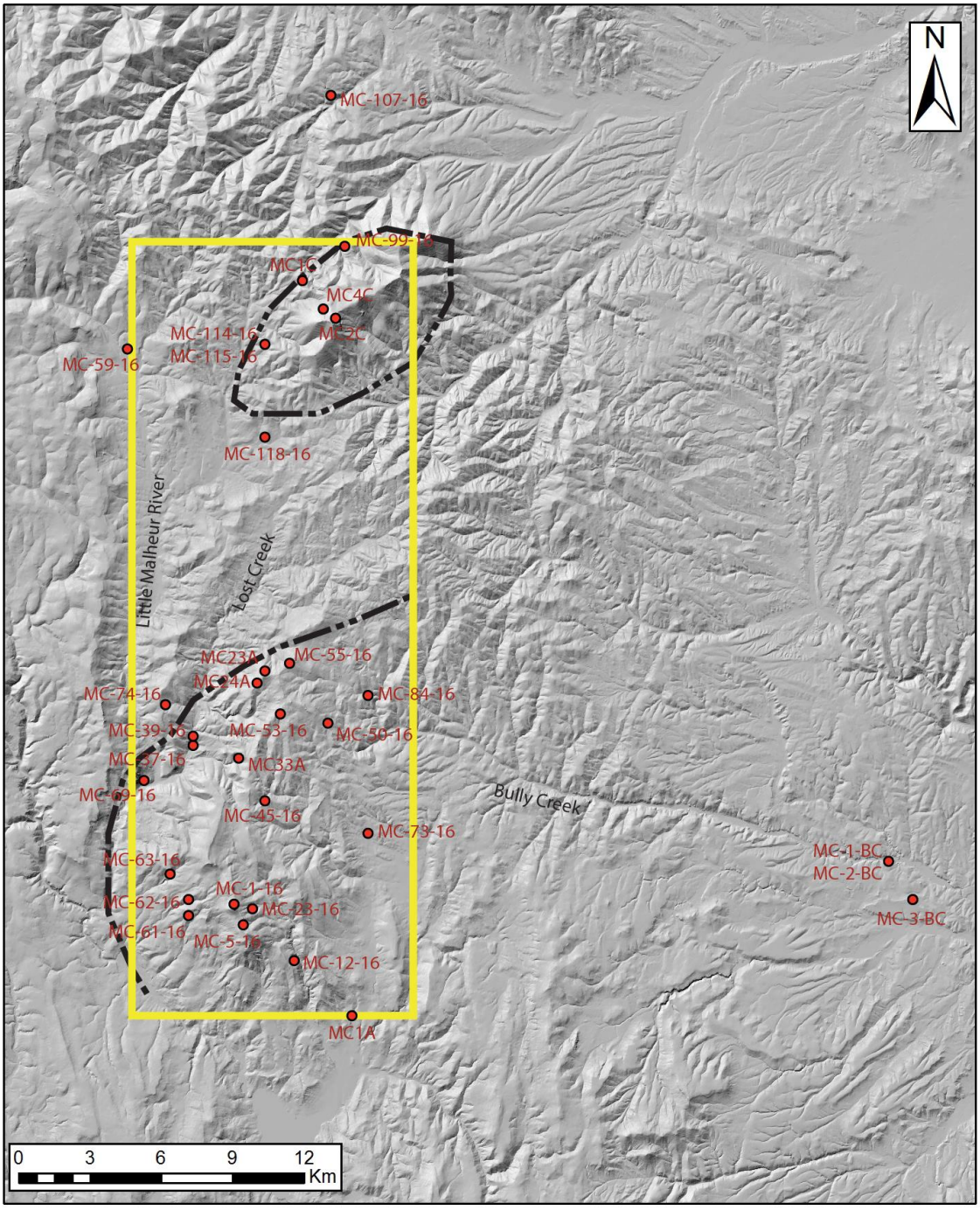

Figure 20. Map of the study area with tuff sample locations Yellow rectangle is the study area, and black outlines are Castle Rock and Ironside Mountain caldera margins.

Major elements

In this section, the tuff samples will be grouped with the DIT1 – 4 units based on their major element geochemistry. **Figure 21** shows the tuff samples in a TAS plot. **Figure 22** consists of Harker diagrams of samples from this study compared with the units from Streck et al. (2015).

Samples MC-19A – MC-24A, MC1C, MC-1-BC, MC-1-16, MC-58-16, and MC-107-16 are all very similar in major element composition, with wt. % SiO_2 ranging from 76.41 – 77.61. The wt. % Al_2O_3 content ranges from 11.97 – 12.76. MC1C has lower wt. % SiO_2, of 74.72 and wt. % Al_2O_3 of 13.21, and higher wt. % CaO of 1.05. They are all rheomorphic, devitrified tuff samples. Almost all of them group with the DIT1 samples in the Harker diagrams and TAS plot. The one exception is MC1C, the sample from the west flank of Ironside Mountain. This sample groups with the DIT2-3

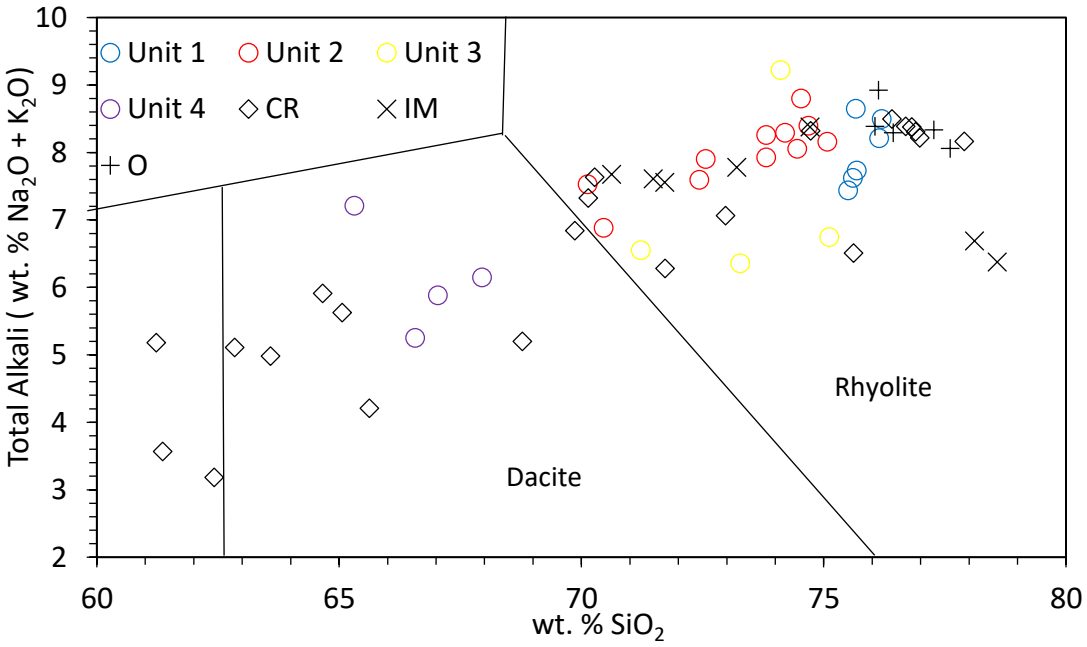

Figure 21. TAS diagram of tuff samples from this study with units from Streck *et al*. 2015. CR = tuffs from Castle Rock caldera, IM = tuffs from Ironside Mountain caldera, O = outflow deposits.

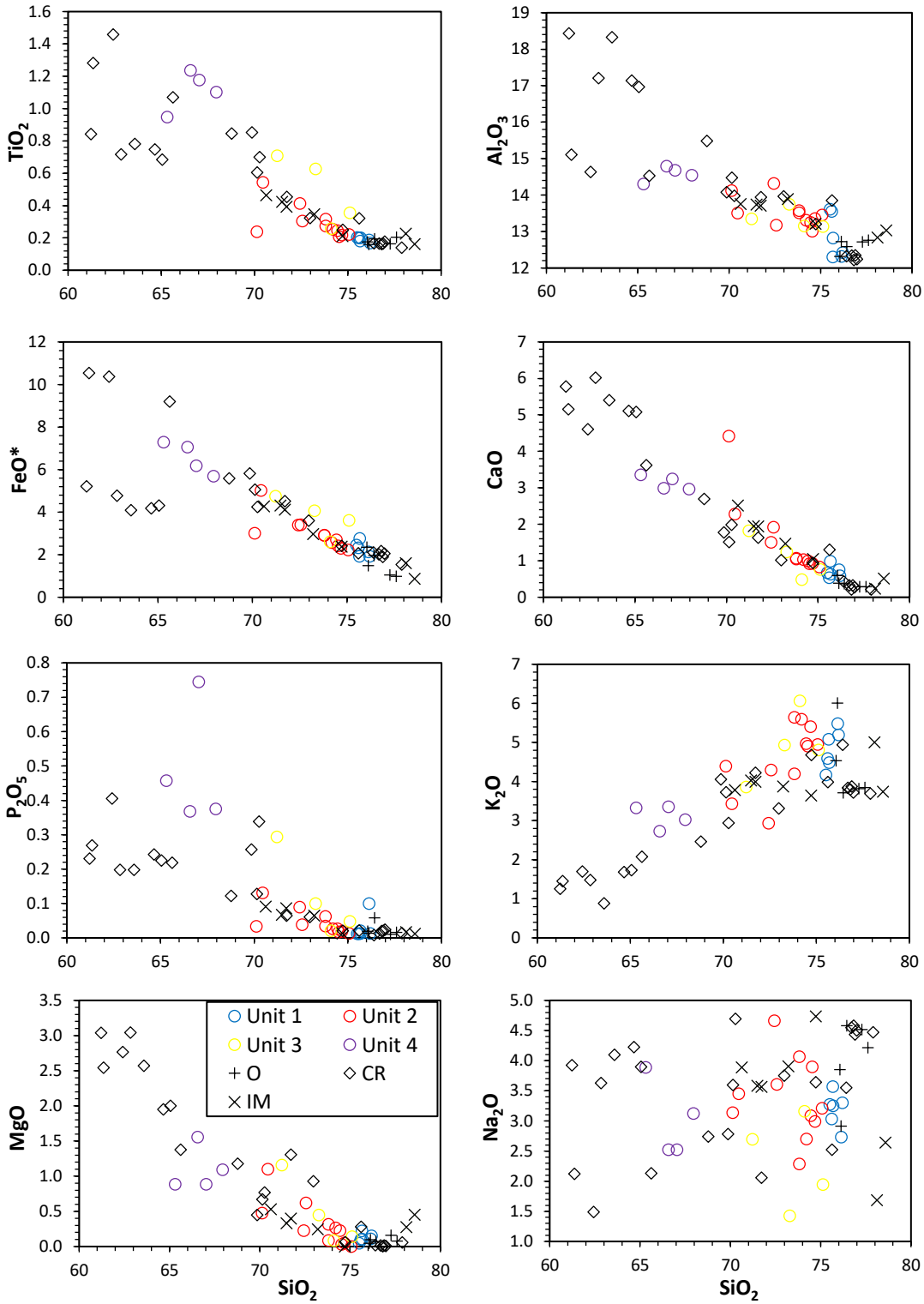

Figure 22. Harker variation diagrams of the tuff samples from this study. Dinner Creek Tuff units from Streck et al. 2015. Major elements are in wt. %. CR = Castle Rock caldera tuffs, IM = Ironside Mountain caldera tuffs. O = outflow deposits of Dinner Creek Tuff

The vitrophyre sample from the Bully Creek canyon, MC-2-BC, has wt. % SiO_2 76.08, and most major element compositions are similar to the DIT1 cluster. The only elements that the sample differs from the DIT1 is MgO, FeO*, and CaO which it is slightly higher in relative to typical DIT1.

The phenocryst poor white-tan rhyolite dike (MC-118-16) shown in **Figure 17B** has wt. % SiO_2 of 78.58, and most other major element compositions are similar to DIT1, although it has higher wt. % Al_2O_3 of 13.03.The other phenocryst poor tuff sample from the northwest flank of Ironside, MC-99-16, also has high wt. % SiO_2 of 78.12. The total alkali content is notably lower than the other DIT1 samples, and is more akin to the DIT2-3 group.

The four samples of moderately welded, glassy tuff from Ironside Mountain (MC2C, MC4C, MC-114-16, MC-115-16) have wt. % SiO_2 ranging from 70.62 to 73.21, wt. % Al_2O_3 of ~13.70, wt. % TiO_2 ranging from 0.34 – 0.46, and wt.% K_2O of 3.72 – 4.03, putting these samples in the DIT2-3 cluster.

The five samples taken from the mega-breccia deposit just south of Sheephead's Rock, have wt. % SiO_2 ranging from 62.84 – 65.06. On the TAS plot, the samples mostly plot in the dacite section, although two of them (MC-55-16 and MC-84-16) plot in the andesite section. In general, samples of the tuffaceous matrix of the mega-breccia deposits are higher in the major elements than any of the units, with the exception of wt. % K_2O (0.5 – 2). When compared to the DIT4, the mega-breccia deposits are depleted in MnO, P_2O_5, FeO*, and TiO_2.

The pumice lapilli tuffs vary greatly in major element composition, with wt. % SiO_2 ranges from 61.36 – 75.62 and wt. % Al_2O_3 ranges from 13 – 15. Still, the samples

can be broken up into two main groups. Samples MC1A, MC33A, MC-3-BC, MC-23-16, MC39-16, and MC-61-16, MC-62-16, MC-63-16 cluster with the DIT2 - 3 group. Samples MC-5-16, MC-12-16, MC-45-16, MC-63-16, MC-69-16, and MC-73-16 have wt. % SiO_2 ranging from 61.35 – 70.34, plotting in the andesite section of the TAS plot. The wt. % Al_2O_3 ranges from 14.08 – 15.49, which groups these samples closer to the DIT4 cluster, although the major elements concentrations are pretty variable, sometimes putting these samples closer to the DIT2 – 3 group. Most of these samples sit directly atop aphyric basaltic-andesite, which sits directly atop older pumice lapilli tuff and rheomorphic Dinner Creek Tuff, indicating that these are younger tuffs, and more likely part of the DIT4.

Trace elements

Trace element geochemistry of the tuff samples, obtained from ICP-MS analysis, will now be discussed. **Figure 23** shows bivariate plots of wt. % SiO_2 vs various trace elements. Like with the major element compositions, the tuff samples from this study fall nicely into place with these four units, for the most part. Some samples that correlate with one Dinner Creek Tuff unit in the major elements group with different units when looking solely at trace elements.

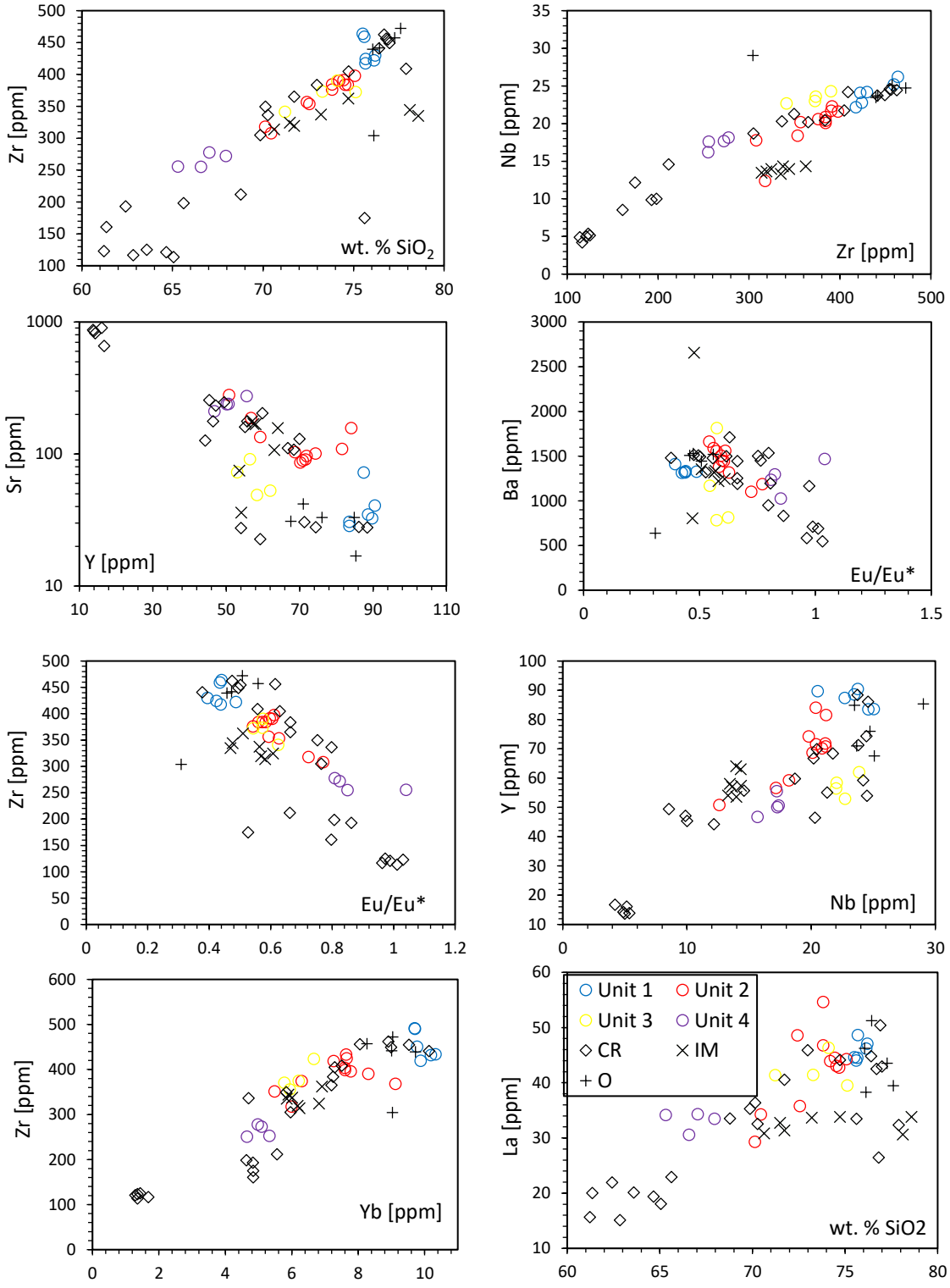

Figure 23. Bivariate trace element plots of tuff samples from this study and DIT 1 – 4 units from Streck et al. 2015.

The rheomorphic tuff samples again, for the most part, groups mostly with DIT1. Zr is greater than 400 ppm. Nb and Hf are generally more enriched than in the other units, with Nb greater than 20 ppm, and Hf over 10 ppm. Y ranges between 53 – 88 ppm, and is generally more enriched than in other Dinner Creek Tuff units. The samples are depleted in Sr (<41 ppm). Like with the major elements, the rheomorphic sample from Ironside Mountain, MC1C, groups better with the DIT2 – 3 group. The Zr, Nb, Hf, and Y concentrations are lower than the DIT1 (362, 14, 9, and 63 ppm, respectively), and the Sr is significantly higher than in the DIT1 (107 ppm). The rheomorphic dike sample from **Figure 19C** (MC-58-16) has Zr (454 ppm), Nb (25 ppm), Hf (12 ppm), Y (67 ppm), and Sr (31 ppm) which is similar to the DIT1 group.

The vitrophyre from the Bully Creek Canyon (MC-2-BC) has Zr (440 ppm), Hf (11.7 ppm), Y (85 ppm), and Sr (33 ppm), which is similar to the DIT1 group.

The phenocryst poor tuff samples, MC-99-16 and MC-118-16, are similar to the DIT1 in major element composition but differ from the DIT1 in trace elements. MC-118-16 has Zr (335 ppm), Nb (13 ppm), Hf (9 ppm), Y (54 ppm), and Sr (36 ppm) concentrations, and MC-99-16 has Zr (344 ppm), Nb (14 ppm), Hf (9 ppm), Y (53 ppm), and Sr (75 ppm). MC-99-16 also has the highest concentration of Ba (2657 ppm) of all the samples in the study. All in all, these two tuffs group with the DIT2 – 3 when it comes to trace element geochemistry.

The moderately welded glassy tuffs from Ironside Mountain (MC2C, MC4C, MC-114-16, and MC-115-16) also group with the DIT2 – 3. These samples have Zr (319 – 338 ppm), Nb (13 – 14 ppm), Hf (8 – 9 ppm), Y (57 – 64 ppm), and Sr (157 – 177 ppm).

Most of the pumice lapilli tuffs and glassy moderately welded tuffs appear to group with DIT 2 – 3, with Zr (300 – 400 ppm), Nb (10 – 20 ppm), Hf (5 – 10 ppm), Y (50 – 70 ppm), and Sr (100 – 200 ppm). These samples include MC1A, a pumice lapilli tuff on the southeast flank of Castle Rock, and MC33A, a gray, pumice lapilli tuff that is exposed in the thick, re-worked tuff section east of Lost Creek. Samples MC-61-16 and MC-62-16 are from outcrops in canyons along the western flank of Castle Rock. These tuff samples appear to lie directly above rheomorphic DIT1, therefore making their grouping with the younger DIT2 - 3 more plausible.

The other pumice lapilli tuff samples (MC-12-16, MC-23-16, MC-45-16, MC-63-16, MC-69-16, MC-73-16) group better with DIT4. The concentration of Zr (150 – 250 ppm) is much lower than the other Dinner Creek Tuff units. The other HFSE are Nb (8 – 23 ppm), Hf (4 – 9 ppm), and Y (45 – 60 ppm). Sr content is significantly higher than other Dinner Creek Tuff units, between 120 – 220 ppm. These samples don't cluster as well with the DIT4 as the other samples do with their respective groups, but the stratigraphic (tan-gray pumice lapilli tuff with mostly dark gray pumices unconformably overlying aphyric basaltic-andesite) and geochemical correlation is still strong enough to conclude that these samples are part of the DIT4.

In the multi-element plot, all the Dinner Creek Tuff units have peaks at Ba, U, K, Pb and troughs at Th, Nb, Ta, La, Ce, Sr, P, and Ti (**Figure 24**). In general, the DIT1 is more enriched in the incompatible elements than the other units, although it is depleted in Sr, P, Eu, and Ti. The DIT1 is also more enriched in the REE elements, except Eu, where it has a prominent negative Eu anomaly (**Figure 25**). The DIT2 – 3 follows the same trend as the DIT1 on the multi-element plot. The concentrations of Rb – Pr are generally

the same between the two groups, but the DIT2 – 3 is more enriched in Sr, P, and T. The group is depleted in Zr, Hf, Sm, and Tb – Lu. Like the DIT1, the DIT2 – 3 the samples have a negative Eu anomaly, although not as pronounced as the DIT1. The phenocryst poor tuff, moderately welded glassy tuff, and certain pumice lapilli tuffs tend to group with this DIT2 – 3 group. Some samples (MC-118-16, MC-99-16, MC1C, MC-39-16) do differ somewhat from the trend. Stratigraphic relations still warrant putting these samples in the DIT2 – 3 group. The DIT4 is more depleted than the other samples, but enriched in Sr, P, and Ti. In the REE plot, the DIT4 tends to lack a Eu anomaly, although slight troughs can be seen in the samples. Some of the samples vary from this trend, and are enriched in depleted in Sr and P.

The five mega-breccia samples appear to be different from the rest of the samples, and don't fit neatly with any of the Dinner Creek Tuff units. The concentration of the trace elements is depleted when compared to all the other samples and the Dinner Creek Tuff units of Streck et al. (2015), with Zr (113 – 125 ppm), Nb (4 – 6 ppm), Hf (3 – 4 ppm), and Y (13 – 17 ppm). The Sr concentrations are way more elevated than the other samples (600 - 900 ppm), the Ba concentrations are more depleted (< 1000 ppm). **Figure 26** shows a REE plot of mega-breccia samples and DIT1 – 4, and **Figure 27** is a multi-element plot. When looking at the multi-element plot, the mega-breccia samples have similar element trends in the most incompatible elements, with Ba, U, K, and Pb peaks, and a prominent Nb-Ta trough. The mega-breccia does differ significantly in Sr and P concentrations, which are more enriched when compared to the Dinner Creek Tuff units. The mega-breccia also lacks a Ti trough. On an REE plot, the mega-breccia samples lack a Eu anomaly, and are depleted when compared to all of the Dinner Creek Tuff units.

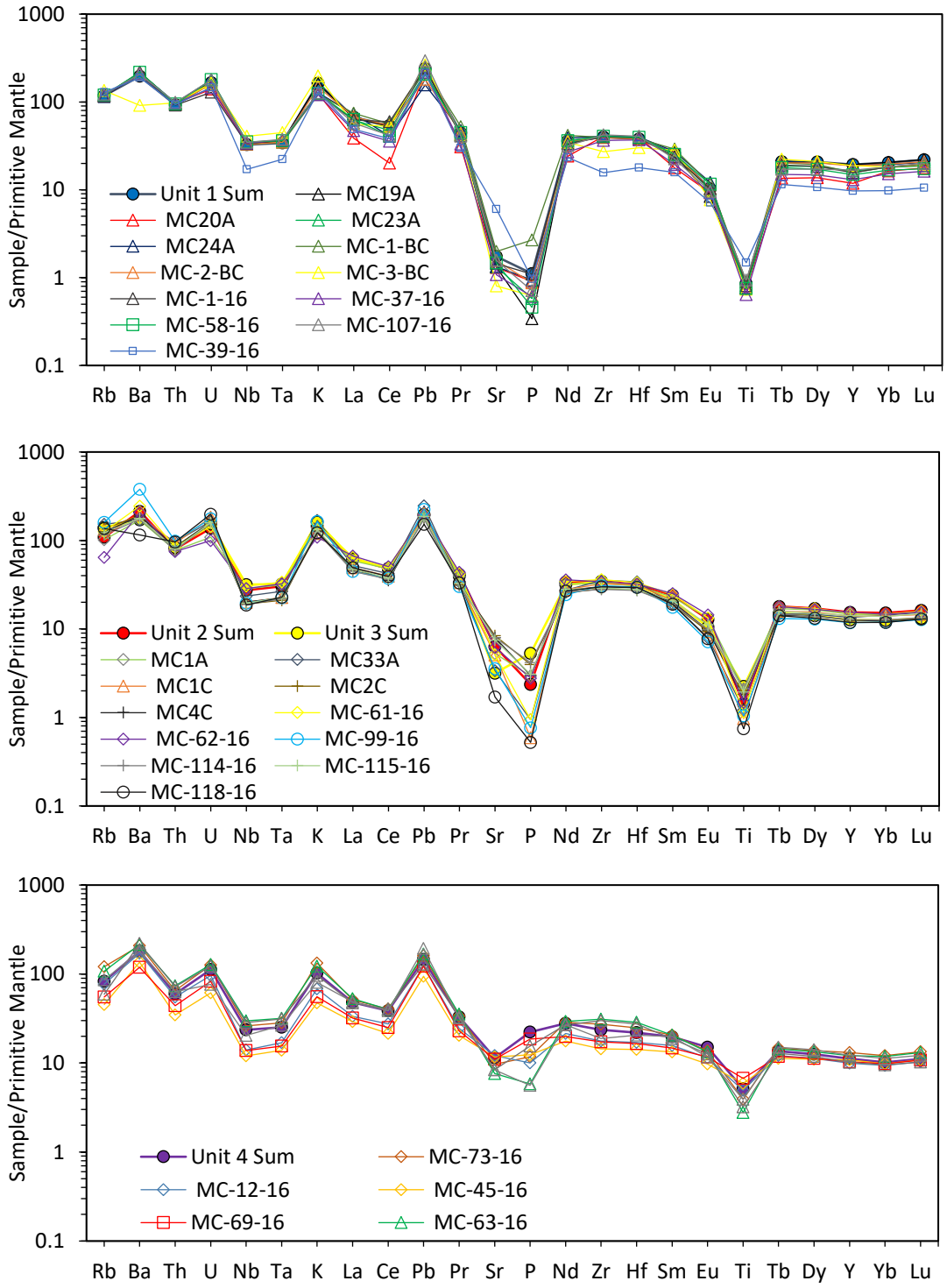

Figure 24. Multi-element plots of various Dinner Creek units and samples. Mantle normalized values from Sun & McDonough, 1989.

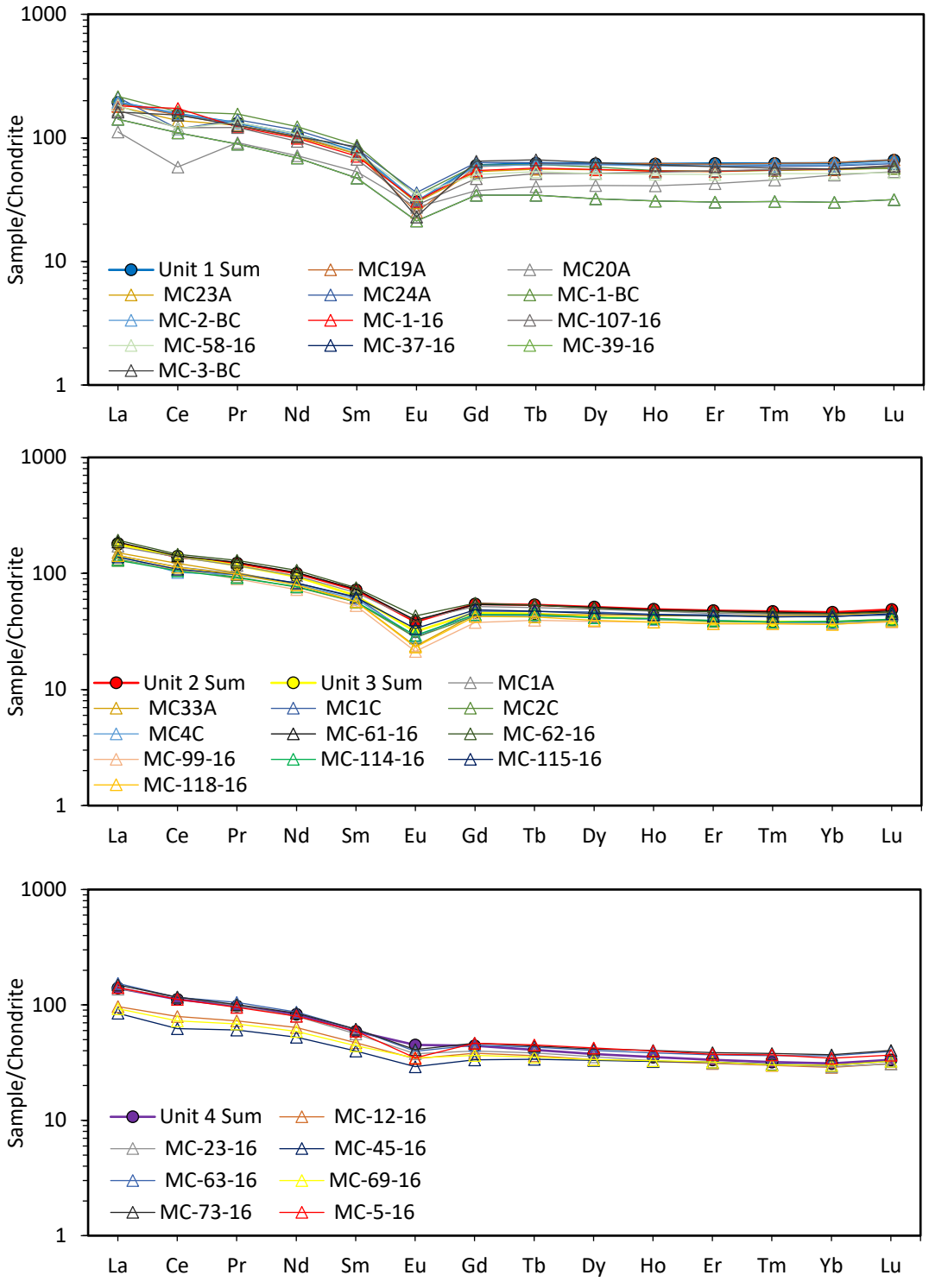

Figure 25. Chondrite normalized REE plot of samples and Dinner Creek units. Chondrite values from McDonough & Sun, 1995.

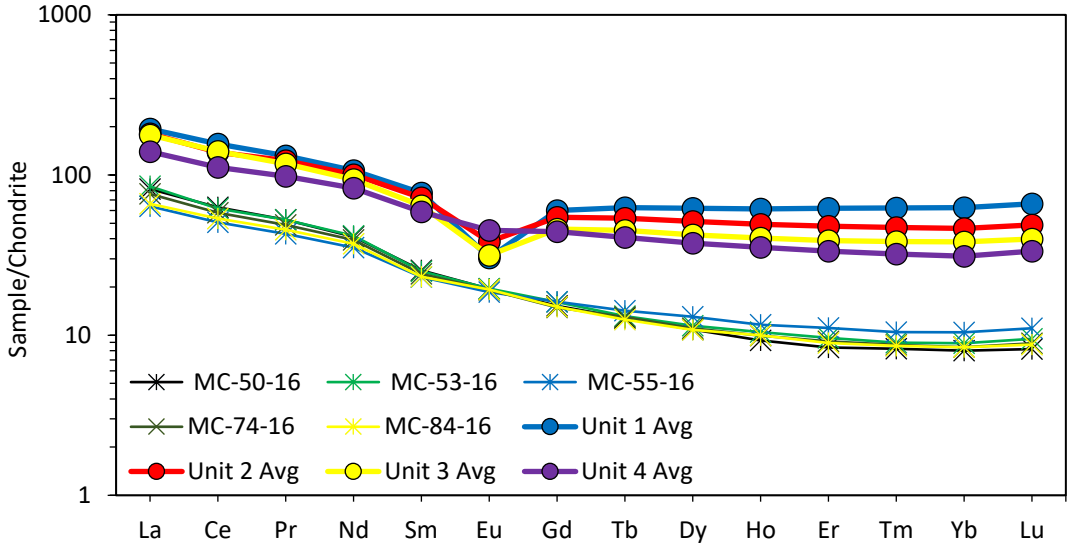

Figure 26. REE plot showing average values for DIT units, and the mega-breccia samples normalized against Chondrite. C1 chondrite values from McDonough and Sun, 1995.

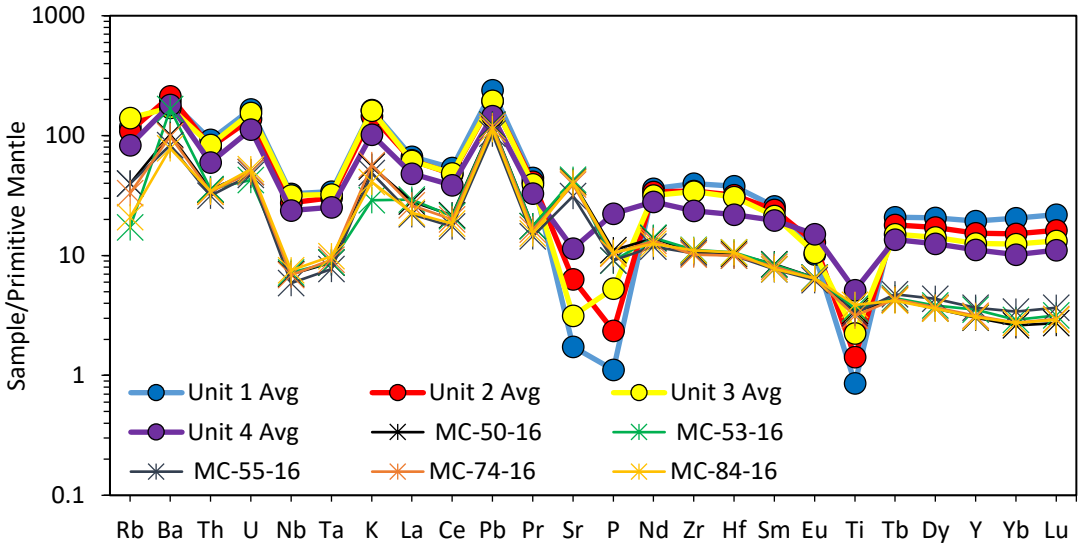

Figure 27. Multi-element plot showing average values for DIT units, and the mega-breccia samples normalized against primitive mantle. Primitive mantle values from Sun & McDonough 1989.

Feldspar Analysis

Streck et al. (2015) made use of subtle compositional differences in feldspar composition to distinguish among individual Dinner Creek Tuff units. They determined that the DIT1 and DIT2 had Na-rich plagioclase while the DIT3 and DIT4 had anorthoclase as the main feldspar phase. Feldspar crystals were picked from fifteen samples from this study, mounted in an epoxy plug, and analyzed in the Zeiss Sigma SEM at Portland State University. The EDS data from the analysis was used to answer several questions.

Table 3 shows the samples from which the feldspar crystals were taken, and **Figure 28** is an image of the feldspar ternary diagram from Streck et al. (2015), showing Dinner Creek Tuff units.

Table 3. Samples from which feldspar crystals were extracted for analysis

Sample	Rock Type	Geochemical Data?
MC-1-16	Rheomorphic devitrified tuff	Yes
MC-114-16	Moderately welded glassy tuff	Yes
MC-115-16	Moderately welded glassy tuff	Yes
MC4B	Rheomorphic devitrified tuff	No
MC1C	Rheomorphic devitrified tuff	Yes
MC2B	Mega-breccia	No
MC4C	Moderately welded glassy tuff	Yes
MC-37-16	Rheomorphic devitrified tuff	Yes
MC-39-16	Pumice lapilli tuff	Yes
MC-5-16	Pumice lapilli tuff	Yes
MC-63-16	Pumice lapilli tuff	Yes
MC-68-16	Rheomorphic devitrified tuff	No
MC-73-16	Pumice lapilli tuff	Yes
MC-3-BC	Pumice lapilli tuff	Yes
MC-84-16	Mega-breccia	Yes

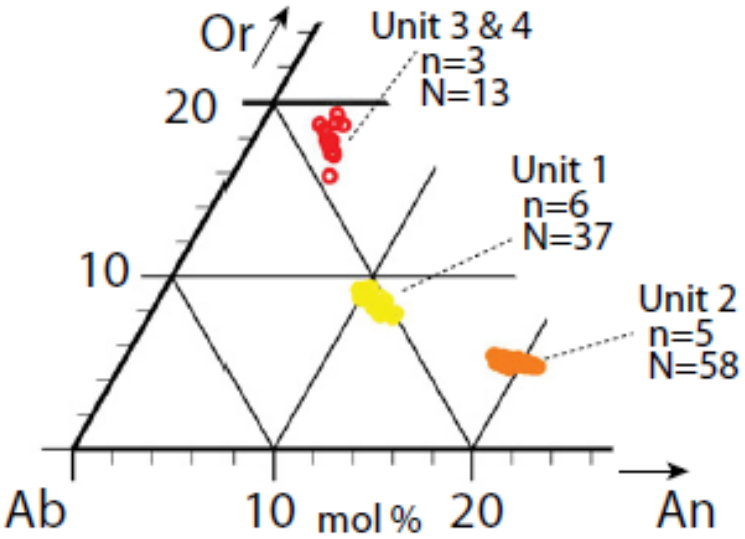

Figure 28. Feldspar ternary diagram from Streck et al. 2015. Diagram shows the different composition of feldspar crystals from the various Dinner Creek Tuff units. Or = Orthoclase, Ab = Albite, and An = Anorthoclase.

Feldspar crystals for all samples are generally pitted, which is a preparation artifact, with common fractures that follow cleavage planes. Zoning is rare, although some zoning can be seen in samples MC-5-16 and MC-63-16, where anorthoclase (Na rich alkali feldspar) inclusions occur within oligoclase. Ba is a common constituent of the feldspar crystals, with BaO ranging between 0.1 and 1.5 wt %. Minor phases and inclusions within the feldspars include zircon, Fe-oxide's, and apatite. Some samples contain apatite crystals that are enriched in REE's, such as La, Ce, Nd, Dy, Sm, and Y.

The EDS data for feldspar crystals shows that there is an agreement with the geochemical data. Crystals from samples MC-1-16 and MC-37-16 plot in the same area as DIT1 crystals from Streck et al. (2015) (An_{7-10}), and match up with the DIT1 from the geochemical data (**Figure 29A**). MC-68-16 and MC4B, which do not have geochemical

data, also group with DIT1 crystals. Sample MC-68-16 is devitrified rhyolite or lava from Black Butte, and sample MC4B is silicified devitrified tuff from Clevenger Butte.

Like DIT1 feldspars, DIT2 feldspars are mostly oligoclase, although they have higher An contents, ranging from An_{18-20} (Streck et al., 2015). Samples MC-39-16 and MC-5-16 plot perfectly with the crystal samples from Streck et al. (2015). Sample MC-39-16 matches with the DIT2 from the geochemical data, although MC-5-16 groups better with the DIT4. Samples MC-114-16, MC-115-16, MC1C, and MC4C plot a little further towards the An side of the plot (An_{25-35}), from oligoclase to andesine (**Figure 29B**). These samples all group with the DIT2-3 from the geochemical data, but have feldspar crystals that match more with the DIT2. Therefore, it can be concluded that the samples are DIT2 and not DIT3, since the feldspar crystals are oligoclase-andesine and not anorthoclase, as the Streck et al. (2015) data would suggest that DIT3 feldspar crystals should be.

The only sample that could possibly represent DIT3 is MC-3-BC, which has considerable scatter among the EDS data, but plots in the anorthoclase area of the feldspar ternary diagram. Geochemically, the tuff is similar to the DIT1 group. Samples MC-63-16 and MC-73-16 also plot in the anorthoclase part of the ternary diagram, but geochemically are similar to the DIT4. **Figure 29C** shows the above mentioned samples in the feldspar ternary diagram.

The samples MC2B and MC-84-16 come from the mega-breccia outcrops. The crystals have An_{39-57}, ranging from andesine to labradorite (**Figure 29D**). The EDS data is most similar to the DIT2, but the geochemical data is distinct from most of the DIT

units, with the same trend, but much more depleted trace element contents, with the notable exception of Sr.

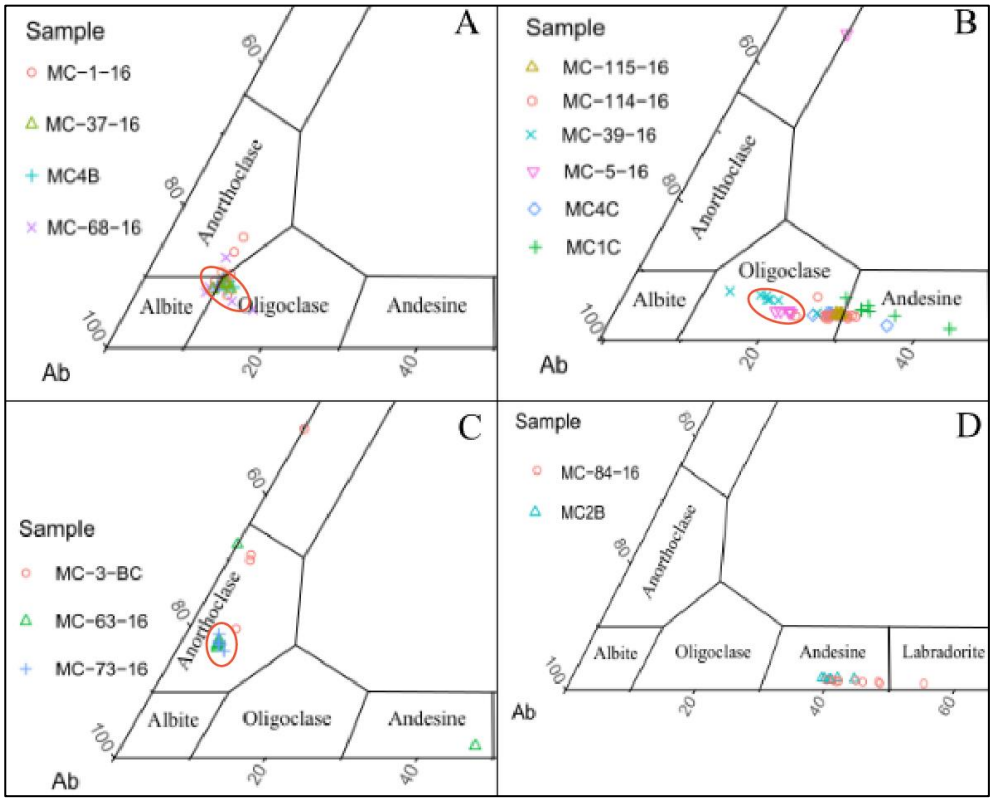

Figure 29. Feldspar ternary diagrams for the EDS data from this study. A) Crystals from this study that group with the DIT1, with the oval area being the group defined by Streck et al. 2015. B) Crystals from this study that group with the DIT2, with the oval area being the group defined by Streck et al. 2015. C) MC-3-BC, which could potentially be DIT3, and the samples that group with DIT4, with the oval area being the group defined by Streck et al. 2015. D) Crystals from the mega-breccia.

DIT Unit Assignment of Samples

When looking at the major/trace element geochemistry, and feldspar EDS data most of the samples can be grouped with the units defined by Streck et al. (2015). **Table 4** shows the samples, rock type, location, data type, and the Dinner Creek Tuff unit that they have been grouped with. The rheomorphic samples from the Castle Rock caldera are grouped with the DIT1, and represent intra-caldera deposits. The SEM-EDS feldspar data

for sample MC-68-16, which is from Black Butte, shows that Black Butte is either intra-caldera DIT1 or a rhyolite lava dome equivalent. Outflow deposits of the DIT1 occur at Bully Creek canyon (MC-1-BC and MC-2-BC), at Clevenger Butte (MC4B), and northwest of Ironside Mountain, at Camp Creek (MC-107-16). The dike from **Figure 19C**, which is MC-58-16, groups with DIT1, although it lies well outside of the Castle Rock caldera. If it is indeed a dike, it could indicate that the extent of the Castle Rock caldera is larger than the field data indicates.

The rheomorphic tuff sample from the Ironside Mountain caldera (MC1C) and the moderately welded glassy tuffs (MC4C, MC-114-16, MC-115-16) from the Ironside Mountain caldera groups with DIT2-3 from the major/trace element geochemistry, and more specifically group with the DIT2 from the SEM-EDS feldspar data. The phenocryst poor tuff samples from Ironside Mountain (MC-99-16 and MC-118-16) are part of the DIT2, based on the major/trace element geochemistry. Incipiently welded DIT2 outcrops occur within the Castle Rock caldera, along the west flanks of Castle Rock (MC-61-16 and MC-62-16), at Lost Creek (MC33A), and along the southeast flank of Castle Rock (MC1A).

The tuff samples that directly overlie the aphyric lava flows in the Castle Rock caldera (MC-12-16, MC-23-16, MC-45-16, MC-63-16, MC-69-16, MC-73-16) group with the DIT4 in both major/trace element geochemistry and EDS feldspar data.

Some samples don't group so well with the units, or they group with one unit when looking at the geochemistry and another when looking at the EDS data. These discrepancies will now be discussed.

The pumice lapilli tuff from Bully Creek, MC-3-BC, has geochemical data akin to the DIT1. The EDS feldspar data shows that the crystals are mostly anorthoclase, which is more akin with the DIT3, although there is considerable scatter within the crystals. While it would seem likely that this is an incipiently welded member of the DIT1, the outcrop sits stratigraphically above other incipiently welded, re-worked tuffs and aphyric lava flows, which all sit directly atop rheomorphic and vitric DIT1 (samples MC-1-BC and MC-2-BC). The stratigraphic position of this tuff would imply that it is younger than the DIT1. It could be DIT3, based on the feldspar data, or it could be part of the Westfall Butte volcanic center, about 12 km southeast of the outcrop. This volcanic center consists of rhyolite lava flows and tuffs that are late Miocene in age (Evans and Binger, 1997).

Sample MC-5-16 shows affinity with the DIT4 in the major/trace element geochemistry, but the feldspar data indicates that it is similar to the DIT2 (oligoclase). The tuff sits atop aphyric basaltic-andesite on the Castle Rock ridge, about 0.5 km south of the rheomorphic DIT1 outcrops. There is no outcrop of tuff, just float fragments. Based on the feldspar data, this sample is being grouped with the DIT2, and represents outflow deposits of tuff. Its position atop the Castle Rock ridge indicates that the ridge was not uplifted at the time of the eruption of the DIT2 at ~15.4 Ma.

Sample MC-39-16 groups with the DIT2 in the feldspar EDS data, and overlaps with the DIT1 in the major/trace element data. In the field, it is juxtaposed against rheomorphic DIT1 along the east side of Lost Creek. Its position adjacent to the DIT1 would indicate that it is part of the DIT1, but the slightly depleted trace element geochemistry, and the feldspar data indicates that it is outflow deposit of DIT2. Normal

faulting along the DIT1 outcrops has uplifted the DIT1 so that it is adjacent to the DIT2 outflow deposits. Quartz veining within the DIT1 is indicative of this faulting.

The mega-breccia samples (MC2B, MC-50-16, MC-53-16, MC-55-16, MC-74-16, MC-84-16) differ from the above tuff samples and the Dinner Creek Tuff units in major/trace element geochemistry and SEM-EDS feldspar data. In terms of major element geochemistry, the mega-breccia is depleted in SiO_2 and elevated in the other elements when compared with the Dinner Creek Tuff units. In the multi-element plot, the mega-breccia has a similar trend with the Dinner Creek Tuff units, although it has a noticeable spike in Sr and P, whereas the DIT 1-4 has troughs. The SEM-EDS data show that the feldspars within the mega-breccia have the highest anorthite content of all the samples, ranging from andesine to labradorite (An_{39-57}).

There are several possible reasons for these discrepancies between the mega-breccia and the DIT 1 – 4. First, contamination of the juvenile material with lithic fragments could be the cause of differences in the geochemical data. As mentioned in the 'Methods' section, the tuff samples were crushed into chips, and lithic fragments were removed, so that juvenile material would be the only thing analyzed. However, the mega-breccia is clast supported, and the lower SiO_2 values, and depletion in trace element geochemistry could be the result of Ring Butte lithic fragments not being successfully removed from the juvenile material. These lithic fragments could also account for the high Sr concentrations.

Alternatively, it is possible that the mega-breccia could be an older tuff related to the Ring Butte volcanic episode. Similar block and ash deposits are interbedded with lavas at Ring Butte, as mentioned in the 'Early Cenozoic Volcanics' section. There are

some differences between these Ring Butte tuffs, and the mega-breccia. The Ring Butte tuff deposits are smaller in scale than the mega-breccia, only about 3 m thick when compared to the 50 m thick mega-breccia. The grano-diorite and shale lithic fragments within the mega-breccia also distinguish it from the Ring Butte tuffs. The outcrops appear to sit stratigraphically atop the Weathersby Formation along the ridgeline west side of Lost Creek, but do not appear on the other side of the ridgeline, which could indicate that the mega-breccia is mantled up against the Weathersby Formation, not sitting atop it.

Finally, the mega-breccia could be landslide deposits, with no tuffaceous material in between the clasts. These landslides could have occurred along the steep topographic rim of the caldera, and consist entirely of Ring Butte volcanic material, hence the low SiO_2, and high Sr values.

Despite the discrepancies in the major/trace element geochemistry and feldspar data, the mega-breccia deposits are probably related to the Castle Rock caldera. The great size, thickness, and extent differentiate the mega-breccia from the Ring Butte tuffs, and the position of the mega-breccia between older Weathersby Formation and Ring Butte volcanics to the north and thick intra-caldera DIT1 to the south indicates that it lies along the northern boundary of the Castle Rock caldera.

Table 4. Samples from this study grouped into Dinner Creek Tuff units, based on geochemistry data.

Sample	Rock Type	Unit	Location	Data
MC19A	Rheomorphic tuff	1	Castle Rock Caldera	Geochemistry
MC20A	Rheomorphic tuff	1	Castle Rock Caldera	Geochemistry
MC23A	Rheomorphic tuff	1	Castle Rock Caldera	Geochemistry
MC24A	Rheomorphic tuff	1	Castle Rock Caldera	Geochemistry
MC4B	Rheomorphic tuff	1	Clevenger Butte	SEM-EDS
MC-1-BC	Rheomorphic tuff	1	Bully Creek	Geochemistry
MC-2-BC	Vitrophyre	1	Bully Creek	Geochemistry
MC-1-16	Rheomorphic tuff	1	Castle Rock Caldera	Both
MC-37-16	Rheomorphic tuff	1	Castle Rock Caldera	Both
MC-68-16	Rheomorphic tuff	1	Castle Rock Caldera	SEM-EDS
MC-58-16	Rheomorphic tuff	1	Little Malheur River	Geochemistry
MC-107-16	Rheomorphic tuff	1	King/Camp Creek	Geochemistry
MC1A	Pumice lapilli tuff	2	Castle Rock Caldera	Geochemistry
MC33A	Pumice lapilli tuff	2	Castle Rock Caldera	Geochemistry
MC1C	Rheomorphic tuff	2	Ironside Mountain Caldera	Both
MC2C	Mod-welded glassy tuff	2	Ironside Mountain Caldera	Geochemistry
MC4C	Mod-welded glassy tuff	2	Ironside Mountain Caldera	Both
MC-5-16	Pumice lapilli tuff	2	Castle Rock Caldera	Both
MC-39-16	Pumice lapilli tuff	2	Castle Rock Caldera	Both
MC-61-16	Pumice lapilli tuff	2	Castle Rock Caldera	Geochemistry
MC-62-16	Pumice lapilli tuff	2	Castle Rock Caldera	Geochemistry
MC-99-16	Aphyric tuff	2	Ironside Mountain Caldera	Geochemistry
MC-114-16	Mod-welded glassy tuff	2	Ironside Mountain Caldera	Both
MC-115-16	Mod-welded glassy tuff	2	Ironside Mountain Caldera	Both
MC-118-16	Aphyric tuff	2	Ironside Mountain Caldera	Geochemistry
MC-3-BC	Pumice lapilli tuff	3(?)	Bully Creek Canyon	Both
MC-12-16	Pumice lapilli tuff	4	Castle Rock Caldera	Geochemistry
MC-23-16	Pumice lapilli tuff	4	Castle Rock Caldera	Geochemistry
MC-45-16	Pumice lapilli tuff	4	Castle Rock Caldera	Geochemistry
MC-63-16	Pumice lapilli tuff	4	Castle Rock Caldera	Both
MC-69-16	Pumice lapilli tuff	4	Castle Rock Caldera	Geochemistry
MC-73-16	Pumice lapilli tuff	4	Castle Rock Caldera	Both
MC2B	Mega-breccia	1(?)	Castle Rock Caldera	SEM-EDS
MC-50-16	Mega-breccia	1(?)	Castle Rock Caldera	Geochemistry
MC-53-16	Mega-breccia	1(?)	Castle Rock Caldera	Geochemistry
MC-55-16	Mega-breccia	1(?)	Castle Rock Caldera	Geochemistry
MC-74-16	Mega-breccia	1(?)	Castle Rock Caldera	Geochemistry
MC-84-16	Mega-breccia	1(?)	Castle Rock Caldera	Both

Lava Samples XRF/ICP-MS Analysis

Twenty one samples were taken from mafic/intermediate lava flows across the study area for XRF and ICP-MS analysis. The major and trace element data were acquired in order to break the mafic units up into groups. In this section, geochemical data from various regional mafic lava flows will be compared with the samples from this study in order to see if there are any similarities. Data from the three members (Lower Pole Creek, Upper Pole Creek, Birch Creek) of the Basalt of Malheur Gorge and the Hunter Creek basalt come from Hooper et al. (2002). The Birch Creek Member is older than the Dinner Creek Tuff, and the Hunter Creek is younger, although both basaltic-andesites are geochemically equivalent to lava flows of the Grande Ronde Basalt member of the CRBG (Camp et al., 2003). Data from the Strawberry Volcanics come from Steiner (2015). This volcanic unit is believed to be derived from CRBG magma mixed with accreted terrain (Steiner, 2015). Finally, data from the Juniper Gulch Basalt was taken from Johnson et al. (1998). This basalt occurs directly south of the study area and is likely late Miocene in age. It is part of the larger Tim's Peak basalt unit. **Figure 30** shows a map of the study area with sample locations. **Figure 31** shows Harker Variation diagrams of the samples from this study and the regional mafic units. **Figure 32** shows a TAS plot of the samples from this study. **Figure 33** shows a tholeiitic series vs calc-alkaline series discrimination plot from Myashiro (1974).

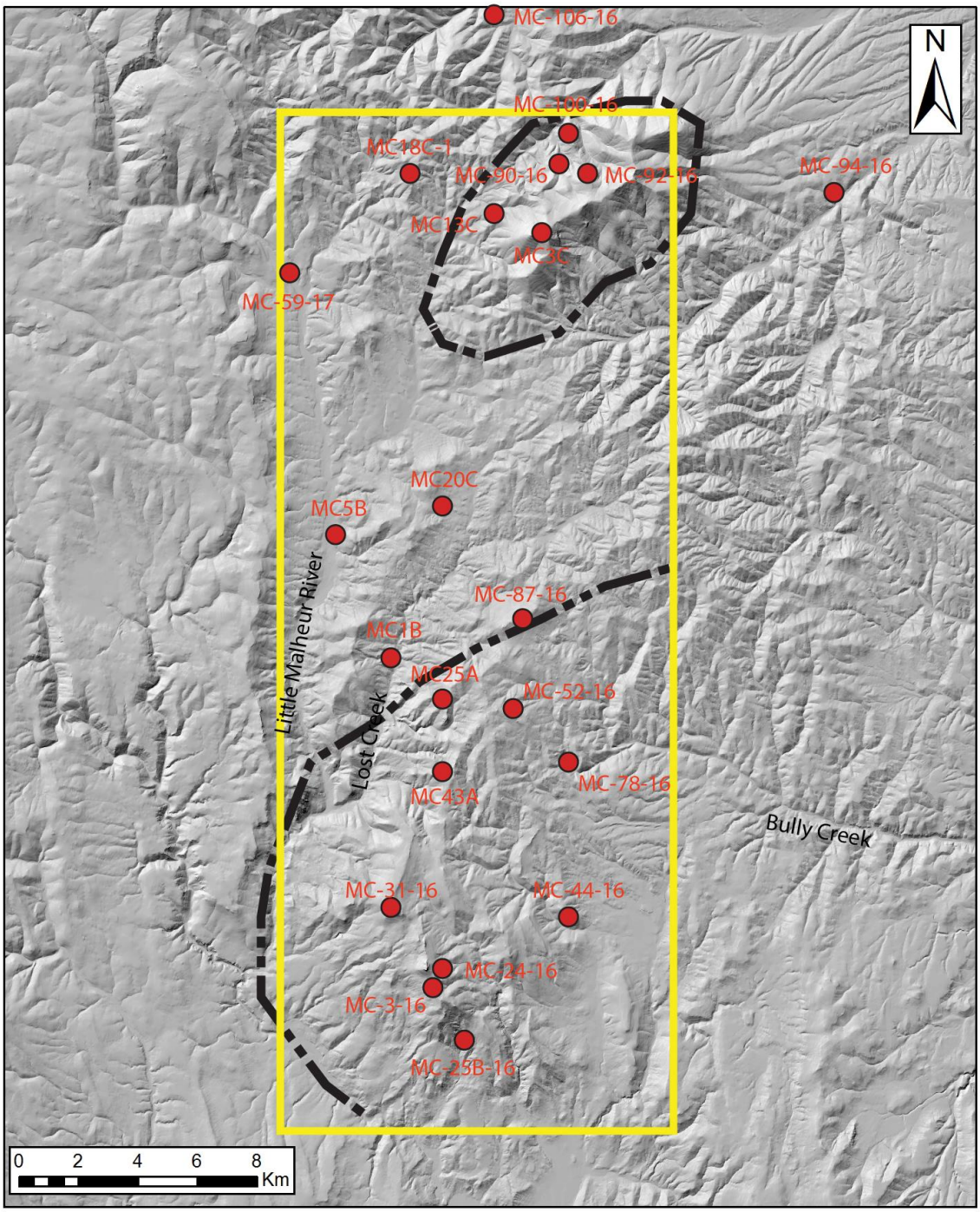

Figure 30. Map of the study area with mafic lava flow sample locations. Yellow rectangle is the study area, and black outlines are Castle Rock and Ironside Mountain caldera margins

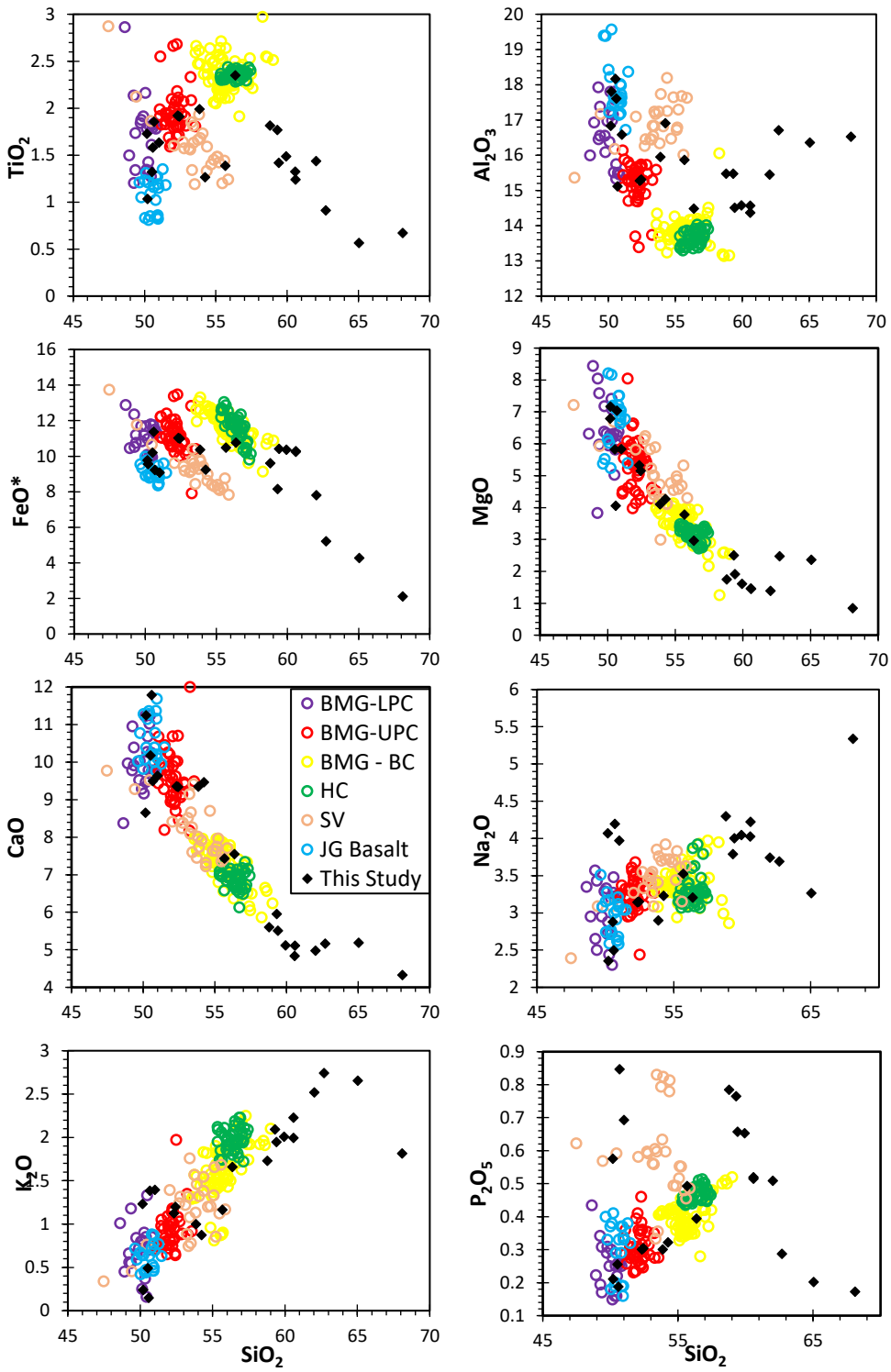

Figure 31. Harker diagrams showing samples from this study and four regional mafic units. HC = Hunter Creek Basalt, BMG-LPC = Lower Pole Creek member of the Basalt of Malheur Gorge, BMG-UPC = Upper Pole Creek member of the Basalt of Malheur Gorge, BMG-BC = Birch Creek member of Basalt of Malheur Gorge, SV = Strawberry Volcanic, finally JG Basalt = Basalt of Juniper Gulch.

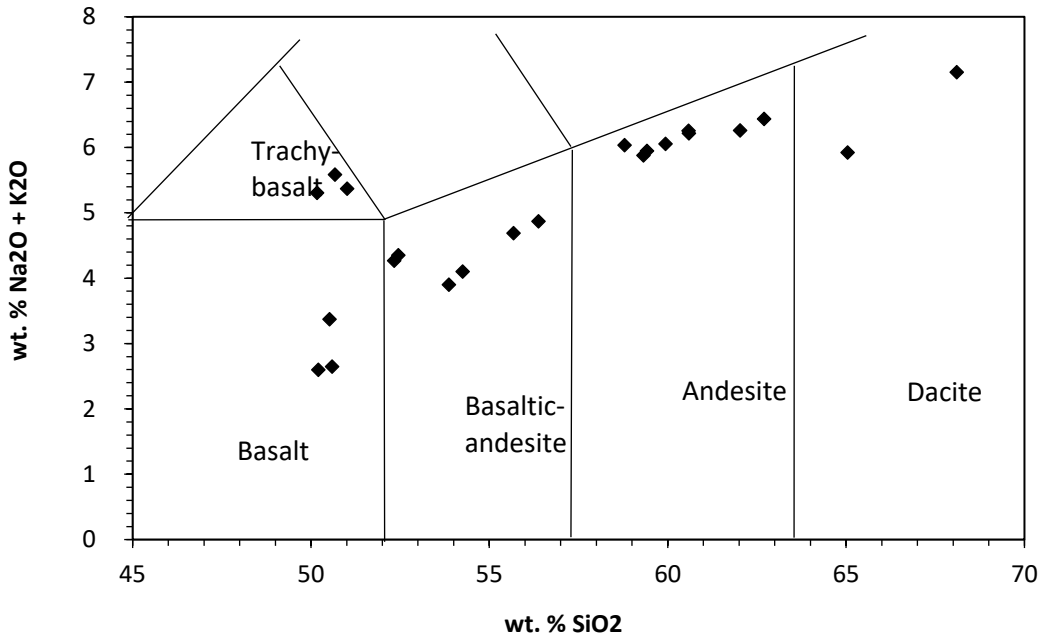

Figure 32. TAS plot of the lava samples from this study.

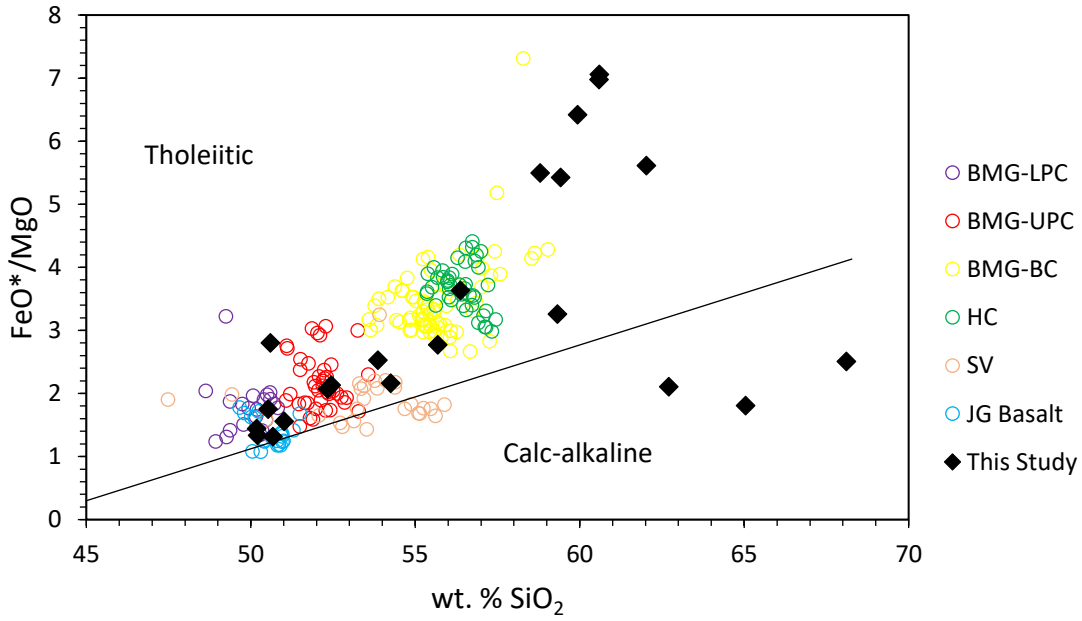

Figure 33. Tholeiitic vs. Calc-alkaline diagram of the samples from this study and regional mafic/intermediate units, from Miyashiro, 1974.

Major elements

The basaltic-andesite/andesite group ranges in wt. % SiO_2 from 52 – 62. These lavas mostly occupy the same stratigraphic position, and in hand sample, these rocks are indistinguishable from one another, so they will all be considered as one group. On the Harker variation diagrams, these samples mostly group separately from the other regional mafic units. The samples appear to all be tholeiitic according to **Figure 33**. The samples are depleted in wt. % CaO, TiO_2, MgO, and enriched in wt. % FeO*, K_2O, Na_2O, Al_2O_3, and P_2O_5 relative to the Birch Creek Member and the Hunter Creek basalt, the regional units that these samples are most similar to. One sample, MC-3-16, does plot with the Birch Creek Member and Hunter Creek basalt in all the graphs. Its stratigraphic position on Castle Rock, directly below the DIT1 would mean that it is older than the Dinner Creek Tuff, and therefore part of the Birch Creek Member of the Basalt of Malheur Gorge. Sample MC-92-16 plots with the Birch Creek Member and the Hunter Creek basalt in all plots except Al_2O_3 vs. SiO_2, and TiO_2 vs. SiO_2, where it is enriched and depleted, respectively, when compared to the regional units. This sample comes from the sill in **Figure 17C**, and is stratigraphically bound by tuff that appears to be DIT2, making it age equivalent with the Hunter Creek basalt.

Six samples (MC25A, MC43A, MC3C, MC13C, MC-94-16, MC-100-16, and MC-106-16) have wt. % SiO_2 greater than 59, and wt. % FeO* greater than 10. These are high FeO* andesites and can be called icelandites, based on the description by Carmichael (1967). These samples all come from sills, dikes, and extrusive flows from Ironside Mountain and the east side of Lost Creek.

The three samples that are basalt have wt. % SiO_2 of ~50, and the highest wt. % Al_2O_3 (~17 – 18) and wt. % CaO (~10 – 12) of all the samples. Sample MC-25B-16 was taken from the southern base of the Castle Rock ridge. On the Harker variation diagrams this sample groups best with the Lower Pole Creek member of the Basalt of Malheur Gorge, with wt. % MgO, FeO*, and TiO_2 of 4.06, 11.38, and 1.58, respectively. In **Figure 33** it plots in the tholeiitic side, with the Lower Pole Creek Member. MC-31-16 comes from the ridgeline 5 km north of Castle Rock, and MC-44-16, come from ridges line just east of Hunter Creek, 5 km northeast of the main Castle Rock ridge. These two samples plot with the Juniper Gulch Basalt in all the variation diagrams.

The three trachy-basalt samples range in wt. % SiO_2 from 50 - 51. The wt. % MgO is generally higher than in other samples (~5.8 – 7.0), as the wt. % Na_2O is (3.97 – 4.07) which is higher than the other basalt samples. The samples plot in the tholeiitic series with the Strawberry Volcanics in **Figure 33** (wt. % P_2O_5 0.576 – 0.847). The trachy-basalts plot best with the Basalt of Juniper Gulch in the SiO_2 vs FeO* and the SiO_2 vs MgO graphs. The MC20C sample is from the east flank of Clevenger Butte, directly overlying the Weathersby Formation and underneath the DIT1. The sample MC-87-16 is from a Ring Butte lava outcrop on Sheephead's Rock. Sample MC5B is from an outcrop along the Little Malheur River, immediately west of Clevenger Butte. These trachy-basalts sit unconformably atop Weathersby Formation and Tureman Ranch grano-diorite, and appear to be the oldest Tertiary unit in the study area.

The two dacite samples (MC1B and MC18C-1) don't fit very well with the other samples; particularly sample MC1B, which plots distal from all the regional mafic units in the Harker diagrams. Sample MC1B is from the dike that intrudes into the Weathersby

Formation, about 4 km west of Sheephead's Rock along Lost Creek. It is a dacite that has wt. % SiO_2 68.10, and is depleted in wt. % TiO_2 (0.67), MgO (0.85), and FeO* (2.12) relative to the other samples. The other dacite sample, MC18C-1, is from the ridgeline directly west of Ironside Mountain. It has wt. % SiO_2 of 65.04. Like MC1B, MC18C-1 is depleted in wt. % TiO_2 (0.56) and FeO* (4.28). Both of these samples plot in the calc-alkaline series in **Figure 33**. Sample MC-59-16 is andesite from the northwestern part of the map area, along the Little Malheur River. It is intruded by the DIT1 dike in **Figure 19C**. Like the dacites, it does not group very well with any of the regional mafic units in the variation diagrams.

Trace elements

Figure 34 shows bivariate plots of the samples from this study and the regional mafic units. **Figures 35 and 36** show mantle normalized multi-element and C1-chondrite normalized REE plots of the samples. The basaltic-andesites/andesites/icelandites show some variability in their trace element geochemistry. The basaltic-andesite samples (MC-24-16, MC-52-16, MC-78-16, MC-90-16, MC-92-16) have Zr, Nb, Rb, La, and Y of 107 – 150, 6 – 8, 17 – 22, 12 – 26, and 28 – 40 ppm, respectively. Samples MC-24-16, MC-52-16, and MC-78-16 plot with the Upper Pole Creek member of the Basalt of Malheur Gorge in most of the bivariate plots while samples MC-90-16 and MC-92-16 plot closer to the Birch Creek Member/Hunter Creek basalt, although there is some overlap in the samples. Sample MC-3-16 plots with the Birch Creek member/Hunter Creek basalt on the bivariate plots. The icelandite and andesite samples (MC25A, MC43A, MC3C, MC13C, MC-94-16, MC-100-16, MC-106-16) have Zr, Nb, Rb, and Y of 180 – 220, 9 –

11.5, 33 – 59, and 46 – 53 ppm, respectively. These samples plot closest with the Birch Creek member and Hunter Creek basalt in the bivariate plots.

On a multi-element plot, the samples have peaks of Ba, U, K, Pb, and troughs at Th, Nb, Ta, and Ti. There is variation in the samples at Sr, P, and Ti. The basaltic-andesite samples are depleted relative to the icelandites/andesite samples in the LREE Ba – Pr. These samples have minor peaks at Sr, and small troughs at P and Ti. Samples MC-90-16 and MC-92-16 have more pronounced troughs at Ti than the other basaltic-andesite samples. MC-3-16 is more enriched in the HREE elements than the other basaltic-andesites, and plots more closely with the icelandites/andesite samples on the right side of the plot. The icelandite samples (MC25A, MC43A, MC3C, MC13C, MC-94-16, MC-100-16) are more enriched in LREE and HREE when compared to the basaltic-andesite samples, with a peak at P, and troughs at Sr and Ti. The one true andesite sample, MC-100-16, has a similar trend to the icelandites. On a REE plot, the icelandites/andesite samples have negative Eu anomalies and are more enriched in REE than the other basaltic-andesite samples. The basaltic-andesite samples lack any Eu anomaly for the most part, with MC-92-16 being the only exception. MC-3-16 is more enriched in REE than the other basaltic-andesite samples, and plots with the icelandites, except for the lack of a Eu anomaly.

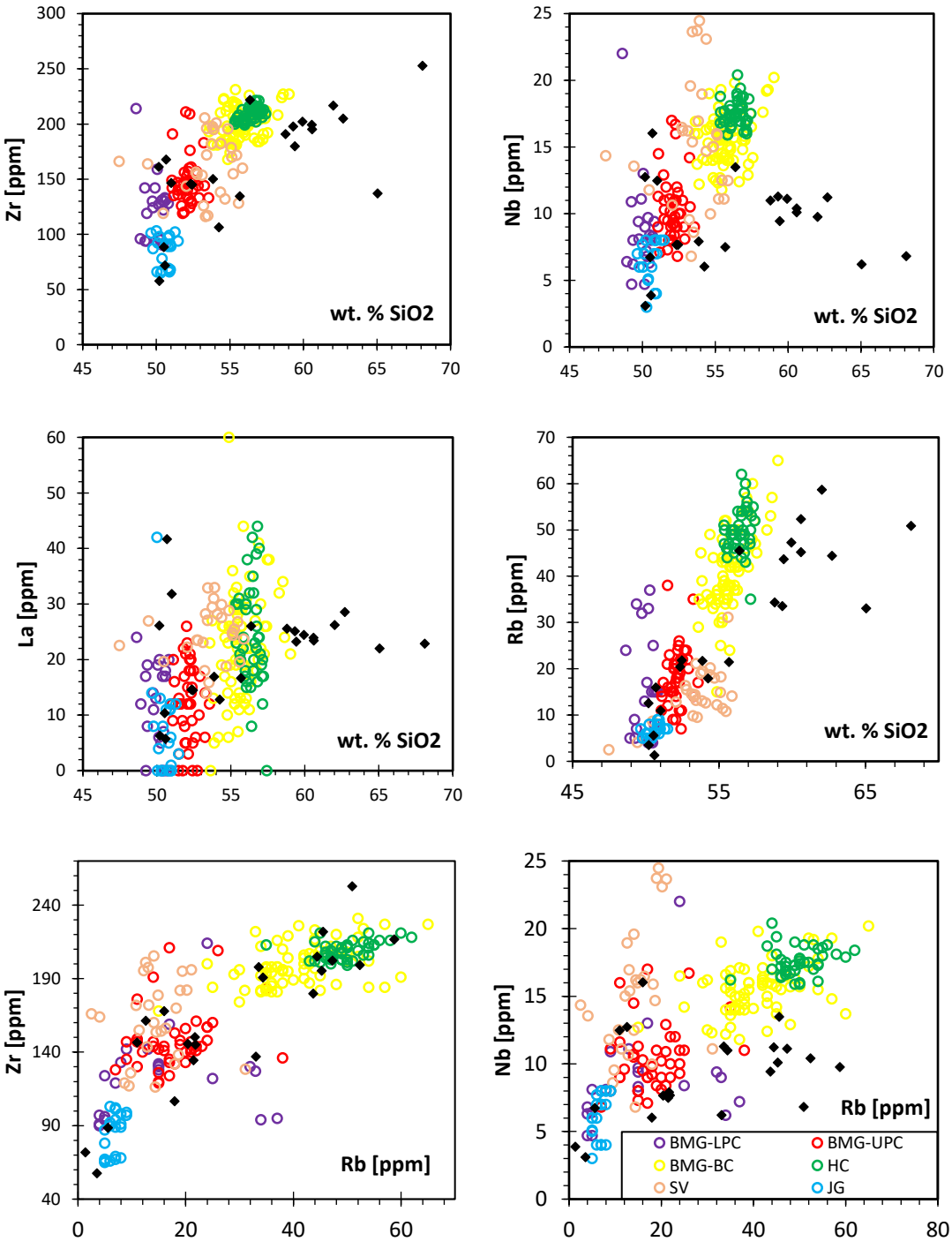

Figure 34. Trace element bivariate plots of the samples from this study and regional mafic units. BMG-LPC = Lower Pole Creek member of the Basalt of Malheur Gorge, BMG-UPC = Upper Pole Creek member of the Basalt of Malheur Gorge, BMG-BC = Birch Member of Basalt of Malheur Gorge, HC = Hunter Creek Basalt, SV = Strawberry Volcanics, JG = Basalt of Juniper Gulch.

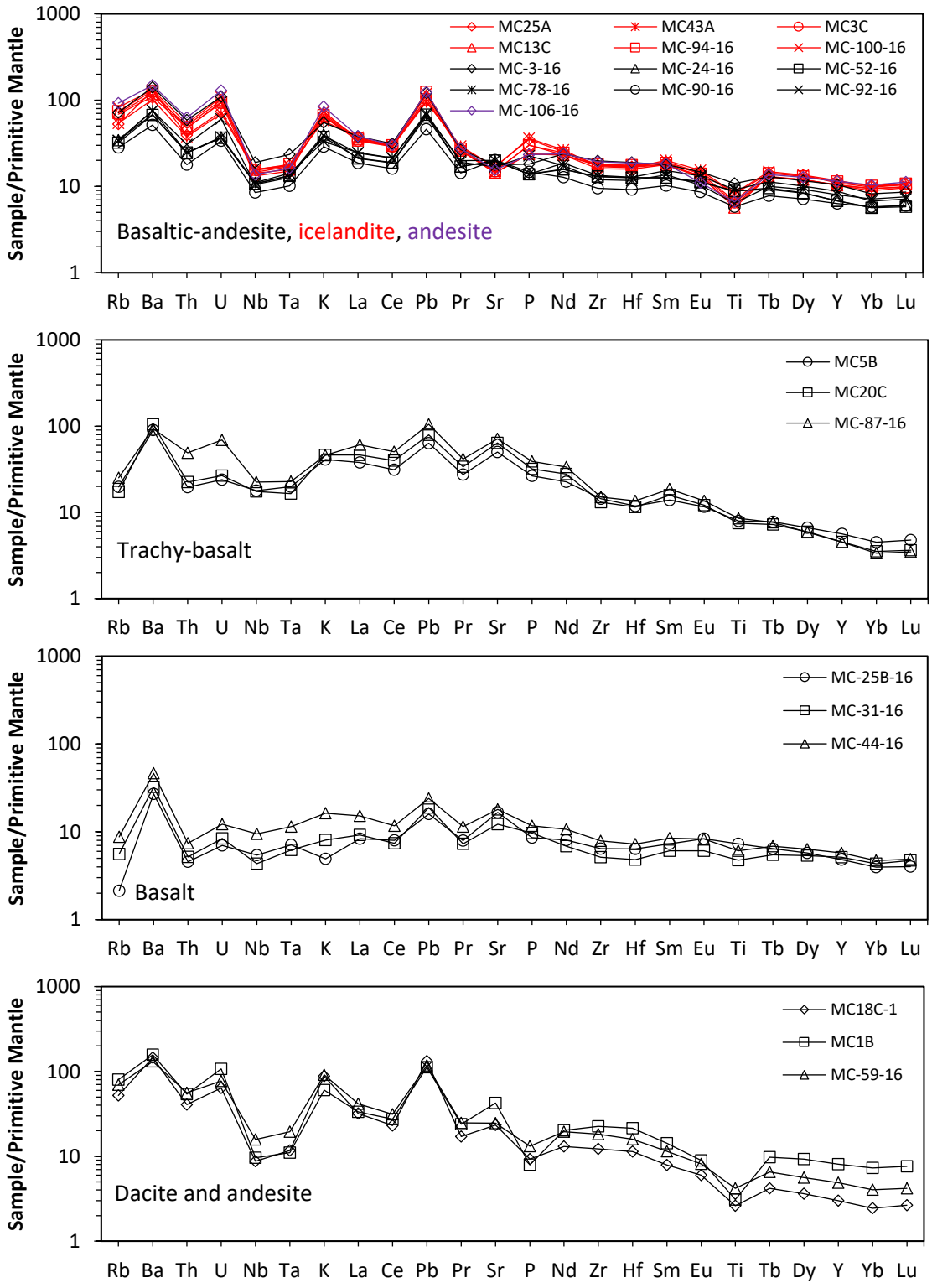

Figure 35. Multi-element plot of the samples from this study. Mantle normalized values from Sun and McDonough, 1989.

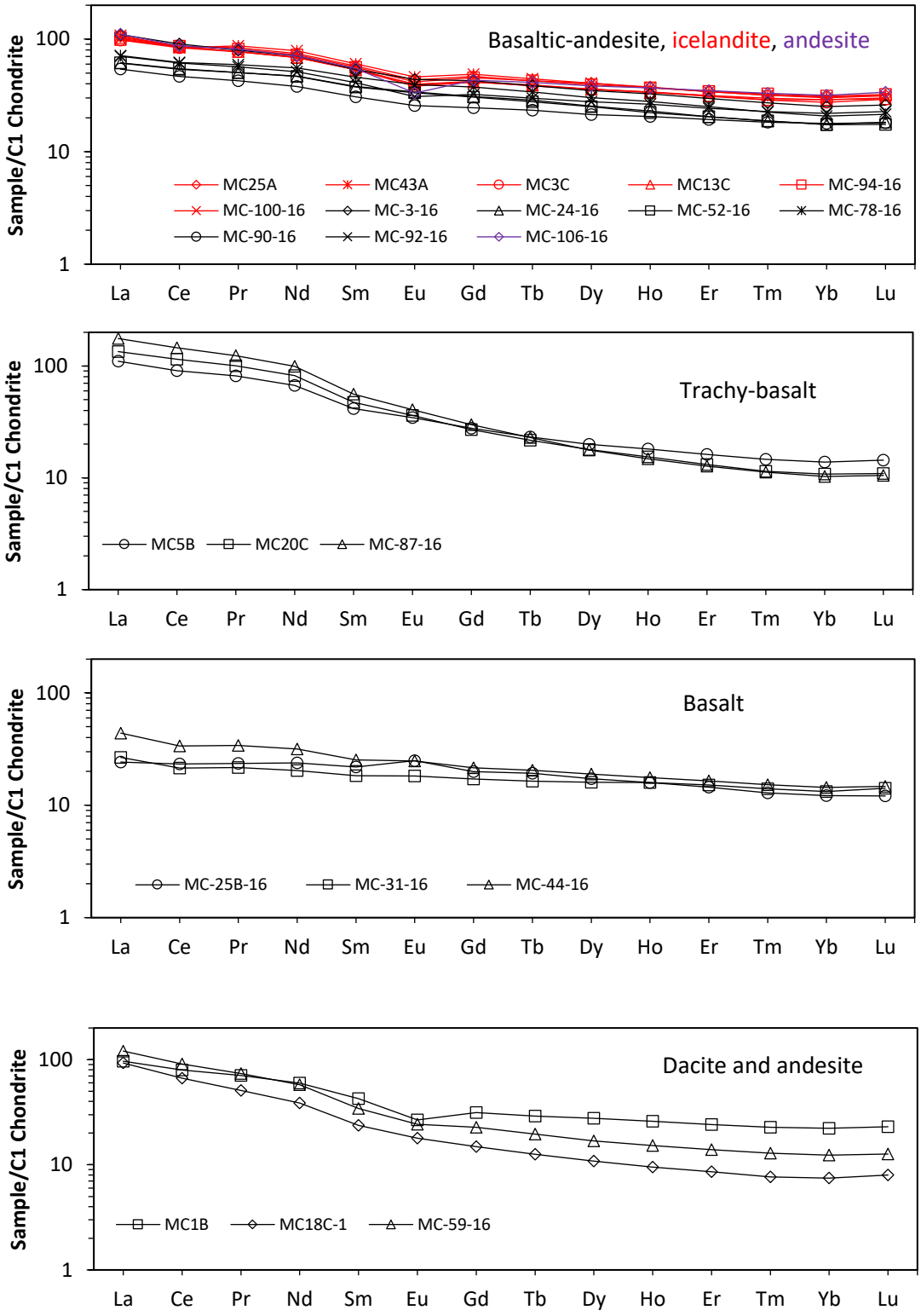

Figure 36. REE plot of the samples from this study. Chondrite values from McDonough and Sun, 1995.

The basalt samples are depleted in trace elements when compared to all the other samples, with Zr, Nb, Rb, La, and Y of 60 – 90, 3 – 7, 1 – 6, 5 – 10, and 21 – 26 ppm, respectively. The samples plot very closely with the Lower Pole Creek and Juniper Gulch basalts in every single trace element plot. On a multi-element graph, the samples have spikes in Ba, Pb, and Sr. The Ba spike is especially notable due to the depletion of Rb, resulting in a prominent spike. The samples have Th, Nb, and Pr troughs. MC-31-16 and MC-44-16 have Ti troughs but MC-25B-16 lacks this trough. On REE plots, the samples decrease in concentrations from La to Lu, lacking any pronounced negative Eu anomaly. MC-31-16 and MC-44-16 have a flat trend at Eu, but MC-25B-16 has a positive Eu anomaly.

The trachy-basalts have Zr, Nb, Rb, La, and Y of 145 – 170, 12 – 16, 11 – 16, 26 – 42, and 20 – 26 ppm, respectively. They have much higher Sr concentrations than the other samples, with Sr of 1000 – 1500 ppm. The samples group with the Lower and Upper Pole Creek members of the Basalt of Malheur Gorge, and the Strawberry Volcanics in the bivariate plots. On a multi-element plot, the samples have spikes in Ba, La, Pb, Sr, and Sm, and MC-87-16 has a spike in U. Troughs occur at Th, Nb, Ta, and Hf. On the REE graph, the samples all have steep negative slopes after the LILE, between Nd and Dy. After Dy, the slopes still are negative but tend to flatten out. There is no Eu anomaly.

The two dacite samples are enriched in Zr and depleted in Nb when compared to the other samples (137 – 253, and 6 – 7 ppm, respectively). The Rb and La concentrations are about the same as the basaltic-andesite/andesite group. In the multi-element plot, the samples have Ba, U, K, Pb, and Sr spikes. Troughs are at Th, Nb, Ta,

Ce, Pr, P, and Ti. The samples have a similar trend to the basaltic-andesite and andesite samples, such as Nb-Ta trough, although the Sr peak, P trough, and the rounded trend from Nd – Eu are characteristic enough to differentiate them from the other samples. On the REE plot, the samples have different trends from each other. MC1B looks similar to the basaltic andesite and andesite group, with a well-developed Eu anomaly while MC18C-1 decreases across its entire length, and looks similar to the trachy-basalt group. Sample MC-59-16, which plots with the basaltic andesite-andesite group in the TAS plot, looks similar to the dacites in the multi-element plot, although it does lack the Sr peak. On the REE plot, the sample is similar to MC18C-1, although slightly depleted.

Petrography

Thin sections of fifteen samples were made to investigate petrographic characteristic of the different mafic/intermediate units. Of the samples that were used for XRF/ICP-MS analysis, two trachy-basalt (MC20C, MC-87-16), two andesites (MC-59-16, MC-106-16), two basaltic-andesites (MC-24-16, MC-52-16), and one basalt sample were used for thin sections. Other samples that were selected for thin section analysis include MC-89-16, MC-15-16, MC-18-16, MC-26-16, MC-46-16, MC-76-16, MC-98-16, and MC-101-16.

The trachy-basalt samples are porphyritic, consisting mostly of plagioclase lathes in the groundmass and about 30 – 40% phenocrysts. Opaque magnetite crystals are common. Larger phenocrysts consist mostly of plagioclase, and clinopyroxene. Olivine is a minor phenocryst in both samples. Crystals are euhedral to subhedral. Some crystals are skeletal in appearance, with opaque Fe-oxides on the surface. MC-87-16 has common hornblende crystals, which have opaque alteration rinds around the edges. The

plagioclase lathes are generally aligned in the same orientation. Simple twinning is common in the pyroxene and plagioclase. Some plagioclase crystals exhibit concentric zoning, but most of them do not. MC-89-16 is similar in appearance to the above samples. It comes from a dike that intrudes into the Tureman Ranch grano-diorite pluton, about 3 km west of Ring Butte. As mentioned in the Regional Geology section, this dike could be a potential source for the Ring Butte trachy-basalt, and the petrographic similarities reinforce that idea.

The two andesite samples differ greatly from each other. MC-59-16 has porphyritic texture akin to the above mentioned trachy-basalt samples, with a groundmass consisting of plagioclase lathes, and opaque magnetite phenocrysts. Larger phenocrysts consist mostly of plagioclase, which often form glomerocrysts. Plagioclase crystals are mostly euhedral. Simple twinning is dominant, but albite twinning does occur in some crystals. Alkali-feldspar phenocrysts also occur, and can be distinguished from the plagioclase by the negative biaxial interference figures. After plagioclase, clinopyroxene is the most common phenocryst. The phenocrysts are subhedral to anhedral, and are commonly twinned.

In contrast to this, MC-106-16 has a microlitic texture consisting of plagioclase lathes and opaque minerals. Tiny phenocrysts of crystals with higher interference colors could be pyroxenes, although they are too small to properly analyze even under highest magnification. Only four phenocrysts of simply twinned plagioclase can be observed in the sample. MC-98-16 comes from an icelandite dike on the west flank of Ironside Mountain. Like MC-106-16, this sample has a microlitic texture with rare plagioclase phenocrysts. MC-15-16 and MC-18-15 are also aphyric under the petrographic

microscope, even lacking sparse plagioclase phenocrysts that occur in MC-106-16 and MC-98-16. All four of these samples occur stratigraphically above the DIT1, with MC-15-16 and MC-18-16 occurring within the Castle Rock caldera, and MC-98-16 and MC-106-16 occurring at the Ironside Mountain caldera. The two MC-101-16 samples come from the western flank of Ironside Mountain. These samples were taken from altered, phenocryst poor DIT2 with intrusive aphyric icelandite lava. In thin section, the tuff and basalt groundmass are too fine to distinguish crystals, but the lava has a brown color in PP, while the rhyolite is tan to light brown in color. Both are dark in XP. Calcite is common within the icelandite veins, and could represent hydrothermal alteration of the glass/plagioclase within the icelandite. Green minerals could be chlorite or actinolite, products of olivine alteration. Zeolites are also present as small circular growths along the tuff margins.

The basaltic-andesite and basalt samples are similar in that they have a subophitic texture, with plagioclase lathes being the predominant phenocryst. Pyroxene phenocrysts fill the spaces between the plagioclase lathes, and are subhedral to anhedral in habit. Glass, ranging in color from black to brown, fills spaces between pyroxenes. The basalt samples have larger pyroxene phenocrysts than the basaltic-andesites, which have more interstitial glass. Three basaltic-andesite samples come from the Basalt of Malheur Gorge at Castle Rock: MC-26-16 comes from the southern base of the mountain, MC-76-16 midway up the mountain, and MC-24-16 coming from 200 m below the summit. All of these samples sit below the DIT1. MC-31-16 is basalt that comes from a ridgeline north of Castle Rock, where it sits atop aphyric basaltic-andesite/icelandite. MC-46-16 comes from lava flows that are interbedded with incipiently welded tuffs on the north flank of

Hunter Mountain, and MC-52-16 comes from a plug that intrudes into the mega-breccia deposits, just south of Sheephead's Rock. These samples occur below and above the DIT1 at the Castle Rock caldera. No subophitic lavas occur around the Ironside Mountain caldera.

Lava Samples and Regional Units

Table 5 shows the lava samples, the type of rock they are, the unit that they have been grouped with, and their stratigraphic position relative to Dinner Creek Tuff units. When compared with the stratigraphic data from the FIELD MAPPING section, a timeline of the mafic/intermediate lava flows can be determined. The oldest regional unit is the 19 – 18 Ma dacites and andesites of the Strawberry Volcanics, which occur immediately west/northwest of the study area (Robyn, 1976; Steiner, 2015). Within the study area, MC-59-16 and MC18C-1 could represent an eastern extension of this volcanic phase. MC18C-1 sits directly atop the Weathersby Formation, and MC-59-16 is intruded by DIT1, so both outcrops definitely predate the Dinner Creek Tuff. The other dacite sample, MC1B, is being grouped with this early Strawberry Volcanic group, despite the fact that it is geographically separated The samples don't group well with any of the regional units, including the Strawberry Volcanics, and they vary amongst each other in trace element geochemistry. They do have similar multi-element and REE plots.

The trachy-basalts, which are the Ring Butte Andesite of Lowry, appear to be the oldest extrusive mafic units entirely within the study area. Like the Strawberry Volcanics, they sit directly atop the Weathersby Formation and Tureman Ranch grano-diorite, in between the Castle Rock and Ironside Mountain calderas. They group with the Strawberry Volcanics and the Lower Pole Creek member of the Basalt of Malheur Gorge

from the major/trace element geochemistry. The petrographic analysis shows that the trachy-basalt has a porphyritic texture with groundmass consisting of plagioclase lathes and magnetite crystals and larger plagioclase, pyroxene, and hornblende phenocrysts, which is very similar to the Strawberry Volcanics. They differ from the Strawberry Volcanics in trace element geochemistry, with the highest Sr concentrations of all the samples. The multi-element plot for the trachy-basalts is somewhat different from the Strawberry Volcanics, with depletions in Th, U, and Rb, and spikes in Sr and Sm. Unlike the Strawberry Volcanics, the Ring Butte trachy-basalts lack a Ti trough. The two units have similar REE plot trends, although the Ring Butte trachy-basalts are more enriched in REE when compared to the Strawberry Volcanics. Both units also plot in the tholeiitic side of the plot in **Figure 33.** The Ring Butte trachy-basalt could be an eastern, more mafic, extension of the early Strawberry Volcanic phase. Age dates would help to clear up the matter, and since there are none for the Ring Butte Volcanics, they will be kept separate from the Strawberry Volcanics, and considered as their own unit.

Around the Ironside Mountain caldera, the icelandites and andesite that intrude into, and sit atop the Dinner Creek Tuff plot on the tholeiitic side of the diagram in **Figure 33**. Unlike the older lavas mentioned above, these samples are aphyric in both hand sample and in thin section, consisting mostly of a plagioclase lathe groundmass, with opaque magnetite crystals. This is similar to the Hunter Creek basalt, more widespread to the southeast of the study area. On the bivariate major/trace element plots, the icelandites and andesite don't typically group with any regional unit, due to the high wt. % SiO_2, although they fall along the same trend as the Birch Creek and Hunter Creek units. The aphyric lava flows at the Castle Rock caldera are probably southern extensions

of the icelandites. Icelandite does occur regionally in eastern Oregon, generally overlying rhyolite lava or tuffs (Wallace et al., 1980; Cummings et al., 2000; Starkel, 2014; Streck et al., 2015). The icelandites probably represent mixing of Hunter Creek basalt magma with Dinner Creek Tuff rhyolite magma at depth (Streck et al., 2015).

The subophitic basaltic-andesite and basalt flows from the Castle Rock caldera come from various regional units. The oldest lava flows are basalts at the base of Castle Rock, which are geochemically similar to the Lower Pole Creek member of the Basalt of Malheur Gorge. These basalt flows are depleted in major and trace elements when compared to the other units. These are in turn overlain by basaltic-andesite flows of the Upper Pole Creek and Birch Creek members of the Basalt of Malheur Gorge. These lava flows sit beneath the Dinner Creek Tuff and the Hunter Creek basalt/icelandite. The basaltic-andesite lavas have similar multi-element and rare earth trends with the icelandites, although they are depleted in trace elements. The youngest lavas are again subophitic, and are exposed along the high ridgelines north and east of Castle Rock. These youngest basalts are geochemically similar to the Juniper Gulch member of the Tim's Peak basalt, which is ~13.5 Ma (Binger, 1997).

Table 5. Mafic/intermediate lava samples from this study, grouped into regional units. Thin section only samples lack XRF/ICP-MS data, and have question marks in the SiO2 and Ca vs. Th columns.

Sample	Rock type	Unit	wt.% SiO2	CA vs. Th	Stratigraphy
MC-31-16	Basalt	Juniper Gulch	50.2	Th	
MC-44-16	Basalt	Juniper Gulch	50.52	Th	
MC25A	Icelandite	Hunter Creek	59.32	Th	Below DIT4
MC43A	Icelandite	Hunter Creek	58.79	Th	
MC3C	Icelandite	Hunter Creek	59.42	Th	
MC13C	Icelandite	Hunter Creek	60.6	Th	
MC-78-16	Basaltic-andesite	Hunter Creek	53.86	Th	
MC-90-16	Basaltic-andesite	Hunter Creek	54.25	Th	
MC-92-16	Basaltic-andesite	Hunter Creek	55.68	Th	
MC-94-16	Icelandite	Hunter Creek	59.93	Th	
MC-100-16	Icelandite	Hunter Creek	60.58	Th	
MC-98-16	Icelandite	Hunter Creek	?	?	
MC-101-16-A	Icelandite	Hunter Creek	?	?	
MC-101-16-B	Icelandite	Hunter Creek	?	?	
MC-106-16	Andesite	Hunter Creek	62.02	Th	Below DIT2
MC-15-16	Icelandite	Hunter Creek	?	?	
MC-18-16	Icelandite	Hunter Creek	?	?	
MC-52-16	Basaltic-andesite	Hunter Creek (?)	52.33	Th	
MC-46-16	Basaltic-andesite	Hunter Creek (?)	?	?	
MC-3-16	Basaltic-andesite	Birch Creek	56.38	Th	Below DIT1
MC-24-16	Basaltic-andesite	Upper Pole Creek	52.44	Th	
MC-76-16	Basaltic-andesite	Upper Pole Creek	?	?	
MC-25B-16	Basalt	Lower Pole Creek	50.59	Th	
MC-26-16	Basalt	Lower Pole Creek	?	?	
MC5B	Trachy-basalt	Ring Butte	50.17	Th	
MC20C	Trachy-basalt	Ring Butte	51.01	Th	
MC-87-16	Trachy-basalt	Ring Butte	50.67	Th	
MC-89-16	Trachy-basalt	Ring Butte	?	?	
MC18C-1	Dacite	Strawberry	65.04	Calc-alk	
MC-59-16	Andesite	Strawberry	62.71	Calc-alk	
MC1B	Dacite	Strawberry	68.10	Calc-alk	

Chapter IV: Discussion and Conclusion

In this section, the results from the previous sections will be used to create a general stratigraphic section and a timeline of events for the field area. First, a brief discussion about possible source areas for the DIT3 and DIT4.

DIT3 and DIT4 sources

Within the study area, calderas were identified at Castle Rock and Ironside Mountain. Based on the major/trace element and feldspar composition data, these calderas are the sources for the DIT1 and DIT2, respectively. The two other Dinner Creek Tuff units were erupted from vents outside of the study area.

The DIT3 was not identified within the study area. It probably is interbedded with the incipiently welded tuff beds and volcaniclastic sediments that overlie the DIT1, but the similar geochemistry and age with the DIT2 makes it difficult to identify. The only true way to distinguish between the two units is to analyze the feldspar composition. Since no pumice lapilli tuffs overlying the DIT1 have anorthoclase as their main mineral phase, it cannot be said for sure whether the DIT3 is present at the Castle Rock caldera. Prior to Streck et al. (2015), the tuff was known as the tuff of the Bully Creek formation, because it is interbedded with the extensive volcaniclastic sediments east of the study area, around the town of Westfall (Streck and Ferns, 2004). An outcrop was sampled in Bully Creek canyon (MC-3-BC), 26 km east of Castle Rock. This one outcrops appears to be only identifiable DIT3 outcrop from this study, with major/trace element composition similar to the DIT2, and anorthoclase as its main mineral phase. This DIT3 outcrop

overlies volcaniclastic sediments and interbedded lava flows of the Bully Creek formation. Streck et al. (2015) identified most of the DIT3 in the area around Westfall.

The DIT4 was identified in the study area, and was originally mapped by Woods (1976), who called it the 'Strawberry Volcanics marker tuff bed'. Unlike the DIT3, it is stratigraphically separated from the DIT2 and other incipiently welded tuff beds by aphyric basaltic-andesite/icelandite lava flows. This is best observed in the canyons along the west flank of Castle Rock (**Figure 13G**). The DIT4 is also visibly more distinct, due to the abundance of dark gray to black un-flattened pumice fragments when compared to the younger Dinner Creek Tuff units. Outside of the study area, it has a wider distribution than the DIT3. Streck et al. (2015) identified samples 54 km north of the study area, near the town of Sumpter.

Sources for the DIT3 and DIT4, probably lie east of the study area. The previously mentioned Westfall Butte volcanic center could be a source. This structure consists of rhyolite lava flows, tuffs, and basalt flows with common DIT1 lithic fragments, and the volcanic center has an estimated age range of 15 – 12.5 Ma (Evans and Binger, 1997).

During their mapping of the Westfall Butte quadrangle, Evans and Binger (1997) mapped a pumice lapilli tuff with lithic fragment up to a meter in length, and which they interpreted to be a vent proximal deposit. They speculated that the source for the tuff could be in the De Armond Mountain quadrangle, directly southeast of Castle Rock. Lowry (1968) mapped a similar 60 m thick tuff in the southern part of his map, which corresponds to the northern part of the De Armond Mountain quadrangle. He noted that

the tuff's main phenocryst is potassium feldspar, which could be anorthoclase just like in the DIT3 and DIT4.

The outcrops of DIT4 at Unity reservoir and Sumpter could indicate that its source vent is north or northeast of the study area. Rhyolitic tuff and tuff breccia occur along the Unity reservoir, and further east in the Beaverdam Creek quadrangle (Reef, 1983; Evans, 1995). The tuff breccia consists of rhyolitic tuff matrix with 60% lithic fragments up to 1.5 m in length. Evans (1993 and 1995) believed that this outcrop was mega-breccia along the margins of a caldera, and he identified similar outcrops in the nearby Brannan Gulch quadrangle. **Figure 37** shows a map of the region with the possible DIT3 and DIT4 sources mentioned above.

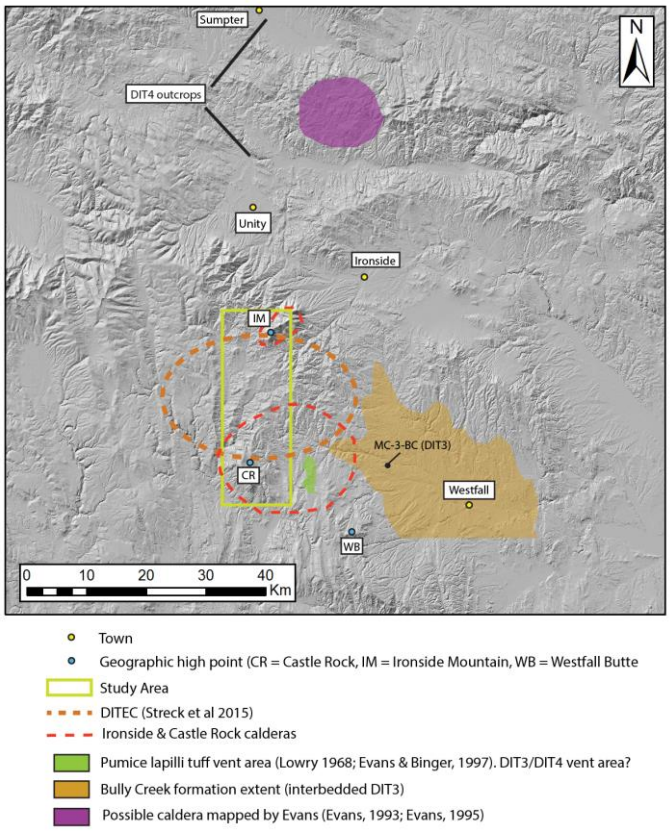

Figure 37. Map of the region with possible DIT3 and DIT4 source areas

Stratigraphy and Timeline

With all of this data, it is now possible to make a revised stratigraphic column for the study area within the DITEC, and a possible timeline of events. **Figure 38** shows the stratigraphic column, and **Figure 39A-G** shows the timeline.

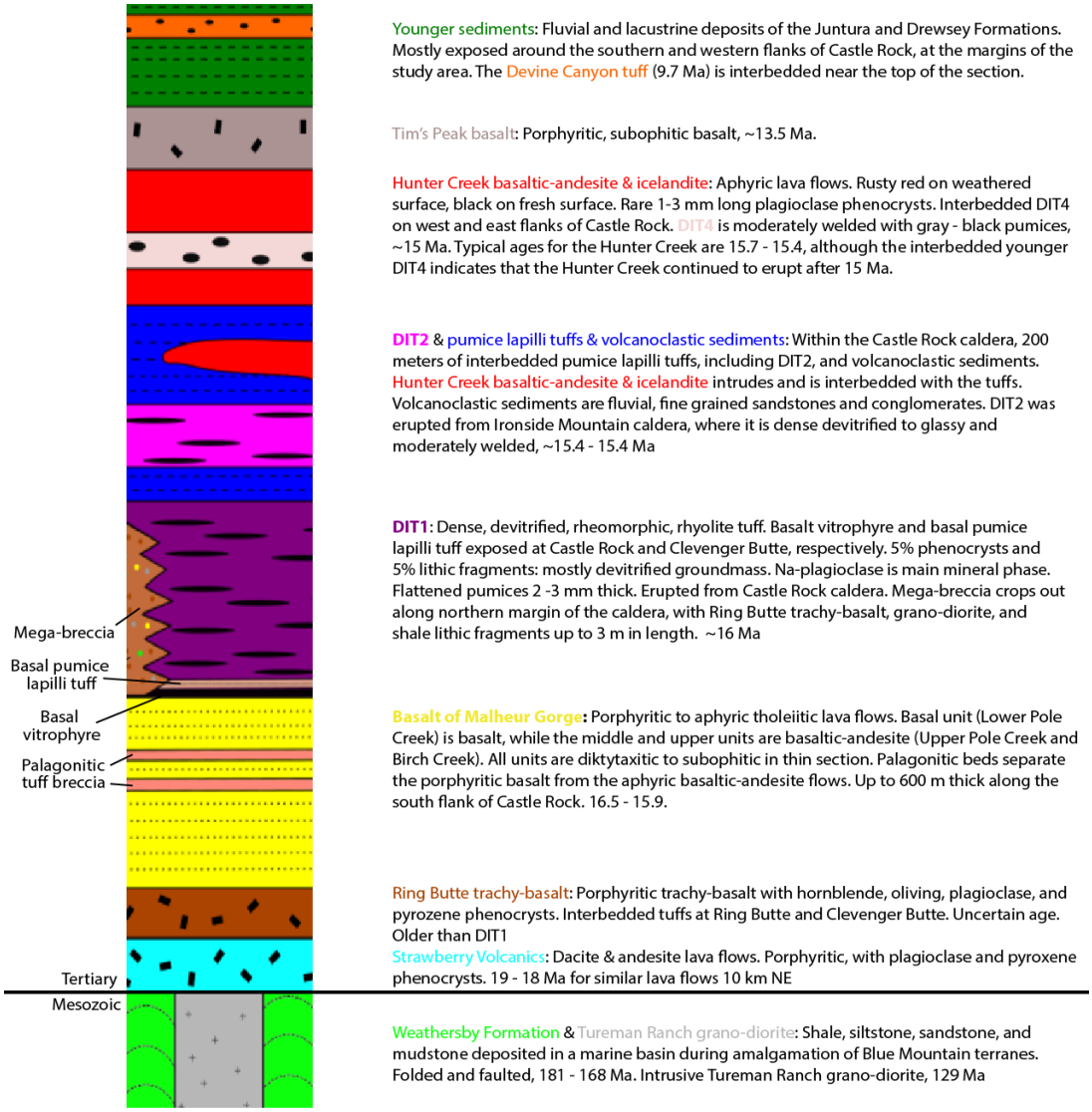

Figure 38. Stratigraphic column of geologic units in the study area.

The oldest rocks in the study area are the Jurassic Weathersby Formation sedimentary units, which are part of the Izee Terrain. These rocks formed in an offshore marine environment, just to the west of a volcanic arc, and were faulted and folded into northeast-southwest trending folds during amalgamation of the Blue Mountain terranes (Ware, 2013). In the early Cretaceous (129 Ma), the Tureman Ranch grano-diorite pluton intruded into the Weathersby Formation in a northeast-southwest trend, which parallels older folds and faults within the Weathersby Formation (Lowry, 1966; Brown and Thayer, 1966; Ware, 2013) (**Figure 39A**).

There is an unconformity between the Mesozoic rocks and the later mid-late Cenozoic rocks. This indicates that during the early Cenozoic, the study area was an uplifted, erosional highland. The earliest Cenozoic rocks in the study area are calc-alkaline andesite and dacite lava flows of the Strawberry Volcanics. These lava flows occur along the northwestern boundary of the study area, along the Little Malheur River. Radiometric age dates of similar lava flows 10 km northwest of the study area are 19 – 18 Ma. (Robyn, 1977; Steiner, 2015).

In the center of the study area is the Ring Butte trachy-basalt and interbedded tuffs. These rocks are similar to the Strawberry Volcanics in their porphyritic texture and main mineral phases, but differ in major/trace element geochemistry. The Ring Butte trachy-basalts were originally identified as andesite by Lowry (1968), and grouped with the Eocene/Oligocene Clarno Formation based on similarities with Clarno Formation lava flows outside of the study area. Although no age dates exist for the trachy-basalt, it will be considered as similar in age to the Strawberry Volcanics based on its stratigraphic position above the Mesozoic sediments/intrusives, and below the DIT1.

In the southern part of the study area, subophitic lava flows of the Basalt of Malheur Gorge are the oldest rocks. These lava flows consist of the basal Lower Pole Creek basalt member, the middle Upper Pole Creek basaltic-andesite member, and the upper Birch Creek basaltic-andesite member. The base of the unit is not exposed at Castle Rock. The geochemical data suggests that all three members of the Basalt of Malheur Gorge are present at Castle Rock, although exact stratigraphic boundaries between the units were not determined, and so the entire unit will be presented undivided. The Basalt of Malheur Gorge ranges in age from 16.5 – 15.9 Ma (Hooper et al., 2002; Camp et al., 2003). The Basalt of Malheur Gorge is over 600 m thick at Castle Rock, but does not crop out further north. This indicates that the southern part of the study area could have been a basin, in which the thick outcrops of the Basalt of Malheur Gorge were deposited (**Figure 39B**). Interbedded palagonitic tuff breccia is also indicative of a basin environment.

At ~16 Ma, the Castle Rock caldera formed as a result of the eruption of the DIT1. The caldera collapsed along arcuate, north-northeast trending ring fractures that follow bound the eastern edge of Castle Rock, and extend northeast up towards the Bully Creek headwaters. Subsidence occurs mostly along the western margin of the caldera where over 300 m of DIT1 accumulated. Rheomorphic DIT1 covers the entire study area, with the possible exception of Ring Butte, which must have been a high enough point that tuff had to flow around it. Outflow thicknesses range from at least 50 m in Bully Creek Canyon and at Clevenger Butte, to 70 m at El Dorado campsite, 9 km northwest of Ironside Mountain. The DIT1 sits directly atop the Birch Creek member of the Basalt of Malheur Gorge on the Castle Rock ridge. At Clevenger Butte, it sits directly atop the

Ring Butte trachy-basalt. A basal vitrophyre is preserved at the base of the Castle Rock outcrop, and basal surge deposits and pumice lapilli tuff members are present at Clevenger Butte. Mega-breccia deposits occur within Lost Creek and Bully Creek. The mega-breccia contains sub-rounded to sub-angular fragment of mostly Ring Butte Trachy-basalt, up to 3 m in length. Shale, grano-diorite, and basalt samples are also present. Inter-fingering of the mega-breccia with the DIT1 can be seen in the headwaters of Bully Creek, indicating that they are related. The DIT1 is a rhyolitic ignimbrite, enriched in trace elements relative to the other Dinner Creek Tuff units. The mega-breccia member is depleted in trace elements, with the exception of Sr. Differences in the mega-breccia could be due to the large abundance of trachy-basalt fragments within the tuff. The main mineral phase of the DIT1 is Na-rich plagioclase.

Within the Castle Rock caldera, up to 200 m of incipiently welded tuffs and interbedded volcaniclastic sediments overlie the DIT1. These outcrops are best exposed on the eastside of Lost Creek, and along the southeast flank of Castle Rock, near Hunter Mountain. The tuff beds range in color from white to gray to red to tan. Pumices are un-flattened and can be as much as 10 cm in length. Lithic fragments are minor, and consist mostly of basalt, glass, shale, chert, and rheomorphic DIT1. The volcaniclastic sediments are best seen at Lost Creek, and include fine grained sandstone and conglomerates with individual beds up to 1 m in thickness. Cross-bedding within sandstones is poorly preserved, but does indicate a fluvial environment. Minor mudstone is present along the southeastern flank of Castle Rock, which indicates a lacustrine environment. Previous geologists had grouped these incipiently welded tuffs and volcano-clastic sediments with various regional sedimentary units, however the mostly volcanic nature, and great

thickness around Castle Rock indicates that they are caldera filling deposits following the collapse of the Castle Rock caldera.

At ~15.5 Ma, the Ironside Mountain caldera forms from the eruption of the DIT2. Tuff dikes along the southern/southwestern flanks of the mountain could be sources for the tuff. Within the caldera, the tuff consists of two members: a lower rheomorphic devitrified member that is similar in appearance to the DIT1, but with compositional characteristics of DIT2, and an overlying glassy, moderately welded member which contains lithic fragments of the lower devitrified member. On the northwestern side of the mountain the tuff is altered by intrusive icelandite and hydrothermal activity, so that is tan – white in color, and aphyric. Zeolite crystals and calcite veins in thin section samples are evidence of hydrothermal alteration. Outside of the Ironside Mountain caldera, the DIT2 is one of the incipiently welded tuffs that fills the Castle Rock caldera at Lost Creek, and along the southeastern flank of Castle Rock. Within the Castle Rock caldera, the tuff is white to light gray, with un-flattened gray to white pumice. The tuff is slightly depleted in most trace elements relative to the DIT1, but enriched in Sr. Its main mineral phase is oligoclase plagioclase. No tuffs within the study area specifically match up with the DIT3. The only tuff from this study that did match with the DIT3 was an incipiently welded tuff from Bully Creek canyon, outside of the study area. This tuff has trace element trends similar to the DIT2, but the main mineral phase is anorthoclase instead of plagioclase. It is likely that incipiently welded DIT3 is present within the tuff beds that fill the Castle Rock caldera. The DIT2 has $^{40}Ar/^{39}Ar$ ages ranging from 15.5 – 15.4 Ma, and the DIT3 has ages of about 15.46 Ma (Streck et al., 2015).

Volcanism continued within both calderas following collapse. Black Butte, along the northwestern margin of the Castle Rock caldera could be an intrusive rhyolite dome. Incipiently welded tuffs continued to be deposited near Lost Creek, creating the thick successions of tuffs and volcaniclastic sediments seen in **Figure 12**. Resurgence may have also occurred at both calderas, although later faulting and erosion has obscured this. The most voluminous post-caldera volcanism is the eruption of aphyric basaltic-andesite and icelandite lava. Dikes for the lava intrude into and are interbedded with the incipiently welded tuffs at Lost Creek, and intrude through intra-caldera DIT2 at Ironside Mountain. Along the southwestern flank of Ironside Mountain, an outcrop of aphyric lava is cut but a tuff dike that is probably one of the sources for the moderately welded glassy member of the DIT2, indicating that these lavas may have started erupting concurrently with the DIT2. The lava is black in hand sample, and have a microlitic texture in thin section, with occasional visible plagioclase phenocrysts. These lavas are similar in appearance to the regionally extensive Hunter Creek basalt, and so will be grouped with them in this study. Ages are 15.7 – 15.4 Ma, which overlap with the DIT2-3 (Nash and Perkins, 2012). Palagonitic Hunter Creek basalt in the Bully Creek headwaters, and at Murphy Reservoir indicate some lacustrine environments along the southern and eastern extents of the Castle Rock caldera.

The DIT4 is interbedded with Hunter Creek basalt/icelandite along the west and east flanks of Castle Rock. The tuff is an incipiently welded tuff, ranging in color from gray to dark gray, and pumices ranging in color from red to gray to black. The outcrops of tuff are as much as 20 m thick along the western flank of Castle Rock. The main mineral phase is anorthoclase. The tuff is depleted in trace elements relative to the other

Dinner Creek Tuff units, although it is enriched in Sr. The thicknesses and spotty distribution of the tuff across the study area indicates that the DIT4 has a source outside of the study area, and flowed into the Castle Rock caldera where it ponded. The age of the DIT4 is about 15 Ma (Streck et al., 2015).

Porphyritic basalt unconformably overlies the Hunter Creek basalt in the Castle Rock caldera. These outcrops occur along the ridge lines east and north of Castle Rock, atop vents that erupted Hunter Creek basalt and icelandite. This basalt is black in hand sample with plagioclase phenocrysts up to 3 mm in length. In thin section, the basalt is subophitic and similar in appearance to the older Basalt of Malheur Gorge unit, although pyroxene crystals are larger. Geochemically, the basalt is depleted relative to all the other mafic units, and groups with the Juniper Gulch member of the Tim's Peak basalt, which is regionally extensive immediately southeast of the study area. $^{40}Ar/^{39}Ar$ ages for the Tim's Peak basalt are ~13.5 Ma (Binger, 1997).

Regional faulting followed the eruption of the Tim's Peak basalt. The Castle Rock ridgeline was uplifted along pre-existing ring fractures and faults, and younger, north-northwest trending faults to create the high ridgeline that is present today. The southern flank of Castle Rock was uplifted 600 m along a northwest striking normal fault. The ridgeline just east of Castle Rock was also uplifted along a northwest normal fault that occupies the present day Jerry Canyon, uplifting 300 m of DIT1. Another northwest trending fault cuts through the incipiently welded tuffs and aphyric basalt, and creates Hunter Mountain in the southeast corner of the map. Just north of the study area, the northwest trending Border fault cuts through early Pliocene sediments of the Unity and Willow Creek Basin, creating the present day Ironside Mountain, Bullrun Mountain, and

Monument Rock ridge line (Brown and Thayer, 1966; Lowry, 1968; Thayer and Brown, 1973). The sediments of the Weathersby Formation and the grano-diorite of the Tureman Ranch pluton have been eroded more thoroughly than the intra-caldera fill of the Ironside Mountain Caldera, creating the gently sloping hills to the northwest and southeast of the caldera. This contrasts strongly with the rheomorphic/altered tuff and intrusive icelandite sills and dikes within the caldera, which are a topographic high relative to the older sediments and intrusive stocks. Any incipiently welded tuffs, volcaniclastic sediments, or mega-breccia deposits have probably been eroded from the caldera. The current day Beulah Basin opened along the southern part of the study area, and was filled in by Juntura Formation sediments. The 9.7 Ma Devine Canyon tuff, which erupted from the Harney Basin to the southwest, was deposited along the southwestern flanks of Castle Rock, overlying volcaniclastic sediments of the Juntura Formation (Green et al., 1973; Woods, 1976). The lack of Devine Canyon tuff immediately east of Castle Rock suggests that the ridgeline was already a structural barrier by the time the tuff was erupted. Drewsey Formation sediments overlie the Devine Canyon tuff, and are the top of the stratigraphic section in the study area.

Faulting continued after the deposition of the Drewsey Formation. The relief created by the faulting resulted in landslides along the Castle Rock ridge and the ridge line between the Little Malheur River and the Lost Creek Valley. Large sedimentary basins formed in the present day Beulah Basin, at the valley directly southwest of Ironside Mountain, and at the basin directly east of Castle Rock. Uplift, erosion, and deposition of these sediments has continued to the present day, creating the existing topography of the study area.

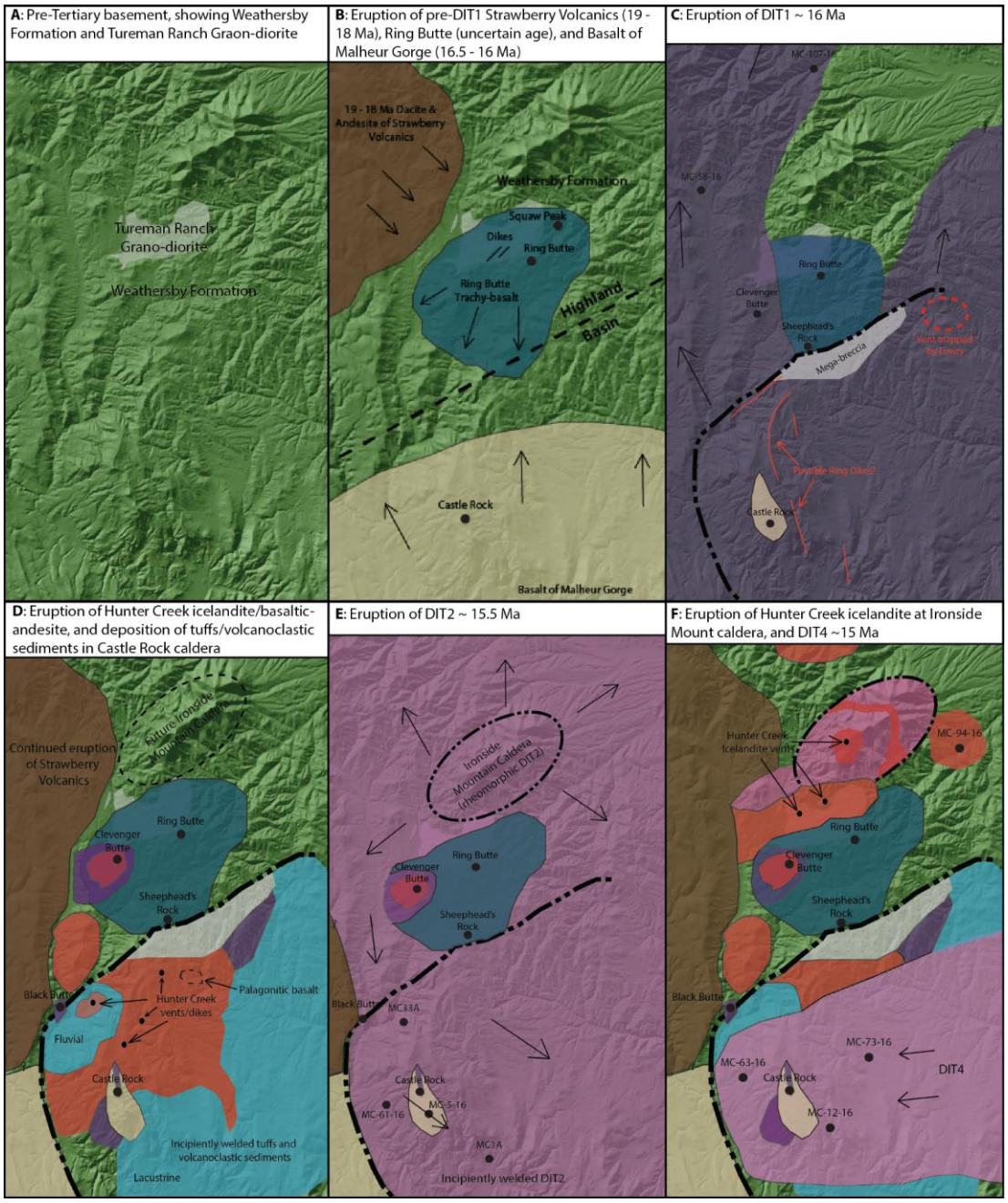

Figure 39. Timeline of events in the study area. Samples from outflow DIT1, DIT2, and DIT4 shown in panels **C**, **E**, and **D**.

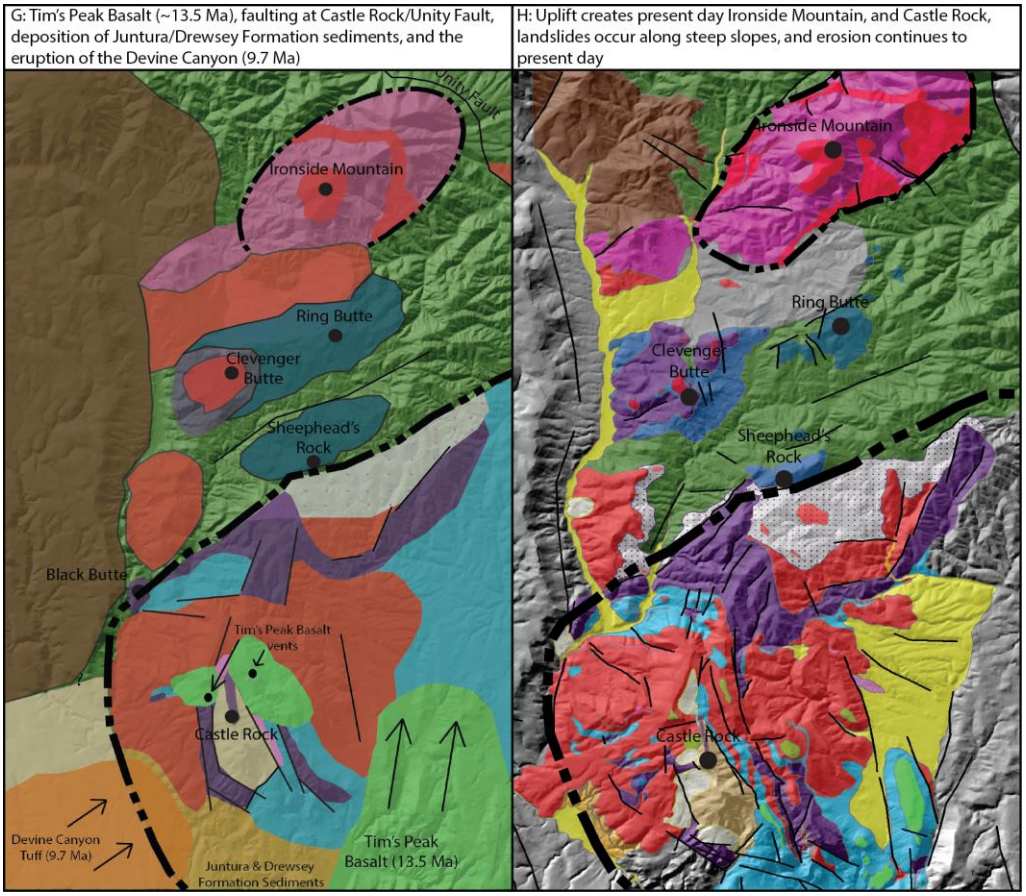

Figure 39 continued.

Conclusion

Within the DITEC are two calderas: the Castle Rock caldera, and the Ironside Mountain caldera. The Castle Rock caldera is a trap door caldera that resulted in the eruption of the DIT1, ~16 Ma. The caldera is filled with over 300 m of dense, devitrified, rheomorphic DIT1, which is overlain my incipiently welded tuffs. Mega-breccia deposits, consisting of incipiently welded tuff filled with older Ring Butte trachy-basalt and Mesozoic sediments/grano-diorite lithic fragments up to 3 m in length occur along the northern margin of the caldera. The tuff is phenocryst poor, with phenocrysts making up

less than 5% of the rock. The main phenocryst is a Na-rich plagioclase, with minor phases being titanomagnetite and clinopyroxene. The tuff is rhyolitic (wt. % SiO_2 > 75), and is enriched in HFSE such as Zr (>400 ppm), Nb (>20 ppm), and Y (>60 ppm), and depleted in the LILE Sr (<40 ppm). Samples have prominent negative Eu anomalies on REE plots. The mega-breccia has a similar trend as the rheomorphic tuff on multi-element plots, although it is depleted in everything but Sr, which it has a major spike. This is probably due to the abundant trachy-basalt fragments within the breccia. Following collapse, streams re-worked some of the incipiently welded tuffs, creating minor sandstones and conglomerates. Palagonitic basalt is further evidence that the caldera floor contained bodies of water at some point. Dikes of aphyric Hunter Creek basalt and silicic domes intruded into the caldera floor along the ring faults, creating minor volcanic cones, such as Black Butte. Later Dinner Creek Tuff units flowed into the caldera, becoming interbedded with volcaniclastic sediments and Hunter Creek basalt/icelandite. Resurgence probably occurred along ring faults, at the present location of Castle Rock.

The Ironside Mountain caldera is the source for the DIT2. The DIT2 erupted 15.5 – 15.4 Ma, causing the initial collapse of the caldera. The rheomorphic DIT2 is up to 600 m thick within the caldera. A second tuff was erupted from vents that cut through the icelandite and rheomorphic tuff along the southwest flank of the mountain. This tuff is moderately welded and glassy, with common lithic fragments of the older rheomorphic unit. Outside of the caldera, the DIT2 is a tan-gray incipiently welded tuff with white – tan pumices. The main phenocryst is Na-rich plagioclase (oligoclase – andesine), although it only makes up about 5% of the tuff. The DIT2 is rhyolitic (wt. % SiO_2 70 –

74), and is more depleted in the HFSE than the DIT1, although it is enriched in Sr (>70 ppm). It extends as far south as the southeast flanks of Castle Rock. Following the eruption of the DIT2, aphyric basaltic-andesite and icelandite, similar in appearance to the regionally widespread Hunter Creek basalt, intruded into the caldera, creating sills and dikes within the caldera, and along the margins. These intrusions probably caused resurgence within the caldera.

The DIT3 erupted from vents outside of the study area, probably near Westfall Butte. This tuff has similar geochemistry to the DIT2, but its main mineral phase is anorthoclase. Its age overlaps with the DIT2. The DIT4 erupted ~ 14.5 Ma, also from a caldera/vent outside of the study area, perhaps from Bully Creek canyon to the east, or the Dooley Mountain Volcanic Center, to the north. It is a dacitic tuff (wt. % SiO_2 <68), and is depleted in HFSE relative to all the other tuffs, and enriched in Sr (>200 ppm). The tuff is preserved within the Castle Rock caldera, where it is interbedded with the Hunter Creek basalt. It is a tan – gray tuff that is filled with gray to black pumices. The tuff ranges in thickness from 5 – 10 m, with the thickest outcrops occurring along the west flank of Castle Rock.

The last phase of volcanism within the DITEC was the eruption of porphyritic Tim's Peak basalt, along the southern rim of the caldera, ~13.5 Ma. Following this, regional faulting uplifted the Castle Rock caldera, creating the present day topography, and causing erosion of the topographic rim of the caldera. In the northern part of the study area, uplift along the Border fault created Ironside Mountain, and caused erosion of the topographic rim and any intra-caldera mega-breccia and sediments.

This information provides a clearer picture of the size and extent of the DITEC, but further research in the study area and the surrounding region would be beneficial. In particular, mapping east and south of the study area could serve to better define the boundaries of the Castle Rock caldera. An investigation of nearby volcanic vents, such as Westfall Butte, could expand the size of the DITEC. Field mapping immediately west of the study area would be very useful in expanding the size of the DITEC. Age dating of the volcanic units sampled in this study would also help constrain the age of the DITEC. Age dating of the Ring Butte trachy-basalt in particular could provide the earliest age dates for volcanism within the study area. Finally, detailed mapping of the northern flanks of Ironside Mountain would shed more light on the margins of the caldera, and structure of the ring faults.

References

Acocella, V., 2006, *Caldera types: How end-members relate to evolutionary stages of collapse*, American Geophysical Union, Geophysical Research Letters, September 2006, vol. 33, p. 1 - 5

Aguirre-Diaz, G.J. and Labarthe-Hernandez, G., 2003, *Fissure Ignimbrites: Fissure-Source Origin for Voluminous Ignimbrites of the Sierra Madre Occidental and its Relationship with Basin and Range Faulting*, Geology, v. 31, no. 9, p. 773 - 776

Benson, T.R. and Mahood, G.A., 2016, *Geology of the Mid-Miocene Rooster Comb Caldera and Lake Owyhee Volcanic Field, eastern Oregon: Silicic volcanism associated with Grande Ronde flood basalt*, Journal of Volcanology and Geothermal Research, v. 309, p. 96 – 117, doi:10.1016/j.jvolgeores.2015.11.011

Best, M.G., Christiansen, E.H., Deino, A.L., Gromme, C.S., McKee, E.H., Noble, D.C., 1989, *Eocene through Miocene Volcanism in the Great Basin of the Western United States*, New Mexico Bureau of Mines and Mineral Resources Memoir 47, p. 91 - 133

Binger, G.B., 1997, *The volcanic stratigraphy of the Juntura region, eastern Oregon*, Washington State University, M.S. thesis, 206 p.

Branney, M.J., and Kokelaar, P., 1994, *Volcanotectonic faulting, softstate deformation, and rheomorphism of tuffs during development of a piecemeal caldera, English Lake District*. Geol. Soc. Am. Bull. 106, p. 507–530

Brooks, H.C. and Ferns, M.L., 1979, *Geologic Map of the Bullrun Rock Quadrangle, Oregon*, Department of Geology and Mineral Industries, Geologic Map Series 0-79-6, scale 1:24,000.

Brooks, H.C., M.L. Ferns, Nusbaum, R.W., Kovich, P.M., 1979, *Geologic Map of the Rastus Mtn. Quadrangle, Oregon*, Department of Geology and Mineral Industries, Geologic Map Series 0-79-7, scale 1:24,000.

Brown, C.E., and Thayer, T.P., 1966, *Geologic Map of the Canyon City Quadrangle, Northeastern Oregon*, USGS, Map I-447, 1:250,000

Camp, V.E., Ross, M.E., Hanson, W.E., 2003, *Genesis of Flood Basalts and Basin and Range Volcanic Rocks from Steens Mountain to the Malheur River Gorge, Oregon*, GSA Bulletin, January 2003; v. 115; no. 1; p. 105–128.

Camp, V.E. and Hanan, B.B., 2008, *A Plume Triggered Delamination Origin for the Columbia River Basalt Group*, Geosphere, v. 4, no. 3, p. 480–495.

Carmichael, I.S.E., 1964, *The Petrology of Thingmuli, a Tertiary Volcano in Eastern Iceland*,
Journal of Petrology 5, 435–460. doi:10.1093/petrology/5.3.435

Coble, M.A., and Mahood, G.A., 2012, *Initial impingement of the Yellowstone plume located by widespread silicic volcanism contemporaneous with Columbia River flood basalts*, Geology, vol.40, p. 655–658, doi: 10 .1130/G32692 .1 .

Cole, J.W., Milner, D.M., Spinks, K.D., 2005, *Calderas and caldera structures: a review*, Earth Science Reviews, February 2005, vol. 69, 26 p.

Creasy, J. W., and Eby, G. N., 1993, *Ring dikes and plutons: a deeper view of calderas as illustrated by the White Mountain igneous province, New Hampshire*, in Cheney, J. T., and Hepburn, J. C., eds., 'Field Trip Guidebook for the Northeastern United States: 1993 Boston GSA', Volume 1: Department of Geology, University of Massachusetts, Contr. no. 67, p. N1-N25.

Cummings, M.L., Evans, J.G., Ferns, M.L., and Lees, K.R., 2000, *Stratigraphic and structural evolution of the middle Miocene synvolcanic Oregon-Idaho graben*: Geological Society of America Bulletin, vol. 112, no. 5, p. 668-682.

De Silva, S.L., Mucek, A.E., Gregg, P.M., Pratomo, I., 2015, *Resurgent Toba – Field, Chronologic, and Model Constraints on Time Scales and Mechanisms of Resurgence at Large Calderas*, Frontiers in Earth Science, June 2015, vol. 3, 17 p., doi: 10.3389/feart.2015.00025

Demant, A., 1984, *The Reforma Caldera, Santa Rosalia Area, Baja California, A volcanological, petrographical and mineralogical study*: in V. Malpica-Cruz, S. Celis-Gutiérrez, J. Guerrero-Garcia, and L. Ortlieb, eds., 'Neotectonics and sea level variations in the Gulf of California area, a Symposium', pp. 77-96, University National Auton. México, Inst. Geologia, México, D. F., 1984.

Dickinson, W.R., 2008, *Accretionary Mesozoic – Cenozoic Expansion of the Cordilleran Continental Margin in California and Oregon*: Geosphere, v. 4, p. 1268 – 1280, doi:10.1130/GES00105.1.

Dorsey, R.J., and LaMaskin, T.A., 2007, *Stratigraphic record of Triassic-Jurassic collisional tectonics in the Blue Mountains Province, Northeastern Oregon*: American Journal of Science, v. 307, p. 1167-1193.

Dorsey, R.J., and LaMaskin, T.A., 2008, *Mesozoic collision and accretion of oceanic terranes in the Blue Mountains province of north-eastern Oregon: new insights from the stratigraphic record*. In Spencer, J. E., and Titley, S. R., eds. 'Circum-Pacific Tectonics, Geologic Evolution, and Ore deposits'. Tucson, AZ, Arizona Geol. Soc. Dig. 22.

Evans, J.G., 1990, *Geologic map of the Jonesboro quadrangle, Malheur County, Oregon*: Oregon Department of Geology and Mineral Industries Geological Map Series GMS-66, scale 1:24,000.

Evans, J.G., 1992, *Geologic map of the Dooley Mountain7 ½ Quadrangle, Baker County, Oregon*: Oregon Department of Geology and Mineral Industries Geological Map Series GQ-1694, scale 1:24,000.

Evans, J.G., 1993, *Geologic map of the Brannan Gulch 7$^{1/2}$ Quadrangle, Baker County, Oregon*: Oregon Department of Geology and Mineral Industries Geological Map series GQ-1744, scale 1:24,000.

Evans, J.G., 1995, *Geologic map of the Beaverdam Creek Quadrangle, Baker County, Oregon*: Oregon Department of Geology and Mineral Industries Geological Map series MF-2299, scale 1:24,000.

Evans, J.G. and Binger, G.B., 1997, *Geologic Map of the Westfall Butte Quadrangle, Malheur County, Oregon*, USGS, Open-File Report 97-481, scale 1:24,000

Felt, K.J., 2013, *Volcanogenic sedimentation and volcano-tectonic evolution of the Clarno Formation in the Blue Mountains Region, NE Oregon*, Washington State University, MS thesis, 79 p.

Ferns, M.L., Brooks, H.C., Evans, J.G., and Cummings, M.L., 1993, *Geologic map of the Vale 30′ × 60′ quadrangle,Malheur County, Oregon and Owyhee County, Idaho*, Oregon Department of Geology and Mineral Industries Geologic Map Series GMS-77, scale 1:100,000.

Ferns, M.L., and McClaughry, J.D**.,** 2013, *Stratigraphy and volcanic evolution of the middle Miocene La Grande – Owyhee eruptive axis in eastern Oregon*, in Reidel, S.P., Camp, V. Ross, M.E., Wolff, J.A., Martin, B.E., Tolan, T.L., and Wells, R.E., eds., 'The Columbia River Flood Basalt Province', Geological Society of America Special Paper 497, p. 401-427, doi:10.1130/2013.2497(16).

Green, R.C., Walker, G.W., Corcoran, R.E., 1972, *Geologic Map of the Burns Quadrangle, Oregon, USGS*, Map I-680, 1:250,000

Geyer, A., Folch, A., Martì, J., 2006, *Relationship between caldera collapse and magma chamber withdrawal: an experimental approach*: Journal of Volcanology and Geothermal Research 157, p. 375–386.

Griscom, A. and Halvorson, P.P., 1994, *Geophysical interpretation of the Malheur, Jordan, and Andrews Resource Areas, southeastern Oregon*, in Smith, C.L., eds., 'Quantitative mineral resource assessment of BLM's Malheur, Jordan, and Andrews

Resource Areas, southeastern Oregon': USGS Administrative Report to the Bureau of Land Management

Haddock, G.H., 1967, *The Dinner Creek Welded Ash-Flow Tuff (Miocene) of the Malheur Gorge Area, Malheur County, Oregon*, Portland State University, PhD thesis, 111 p.

Hooper, P.R. Binger, G.B., Lee, K.R., 2002, *Ages of the Steens and Columbia River flood basalts and their relationship to extension-related calc-alkalic volcanism in eastern Oregon*. Geological Society of America, Bulletin, 114, 43-50.

Johnson, J.A., Hooper, P.R., Hawkesworth, C.J., G.B., Binger, 1998, *Geologic Map of the Stemler Ridge Quadrangle, Malheur County, Eastern Oregon,* USGS Open-file report 98-105

Kennedy, B., Stix, J., Vallance, J.W., Lavallee, Y., Longpre, M.A., 2004, *Controls on caldera structure: Results from analogue sandbox modeling*, Geological Society of America, GSA Bulletin, May/June 2004, vol. 116, no. 5/6, p. 515 - 524

Kingsley, L., 1931, *Cauldron subsidence of the Ossipee Mountains*, American Journal of Science vol. 22, p. 139–168

Kittleman, L.R., Green, A.R., Hagood, A.R., Johnson, A.M., McMurray, J.M., Russell, R.G., Weeden, D.A., 1965, *Cenozoic Stratigraphy of the Owyhee Region, Southeastern Oregon*, Museum of Natural History, University of Oregon, Bulletin no. 1, 45 p.

Langer, V., 1991, *Geology and petrologic evolution of the silicic to intermediate volcanic rocks underneath Steens Mountain basalt, southeastern Oregon*, Oregon State University, MS thesis, 109 p.

Large, A., 2016, *Silicic Volcanism at the Northern and Western Extent of the Columbia River Basalt Rhyolite Flare-up: Rhyolites of Buchanan Volcanic Complex and Dooley Mountain Volcanic Complex, Oregon*, Portland State University, MS thesis, 190 p.

Lipman, P.W., 1976, *Caldera-collapse breccias in the western San Juan Mountains, Colorado*, Geological Society of America, GSA Bulletin, October 1976, vol. 87, p. 1397 - 1410

Lipman, P.W., 1984, *The roots of ash-flow calderas in North America: windows into the tops of granitic batholiths*, Journal of Geophysics Research, September 1984, vol. 80, p. 8801 - 8841

Lipman, P.W., 1997, *Subsidence of ash-flow calderas: relation to caldera size and magma-chamber geometry*, Bulletin of Volcanology, August 1997, vol. 59, p. 198 - 218

Lowry, W.D., 1968, *Geology of the Ironside Mountain Quadrangle, Oregon*, Department of Geology and Mineral Industries, Open-file Report, 76 p.

McClaughry, J. D., Gordon, C. L., and Ferns, M. L., 2009a, *Field trip guide to the middle Eocene Wildcat Mountain Caldera, Ochoco National Forest, Crook County, Oregon*: Oregon Geology, v. 69, no. 1, p. 5–24.

McClaughry, J. D., Ferns, M. L., Gordon, C. L., and Patridge, K. A., 2009b, *Field trip guide to the Oligocene Crooked River caldera: Central Oregon's Supervolcano, Crook, Deschutes, and Jefferson Counties, Oregon*, Oregon Geology, v. 69, no. 1, p. 25–44.

McDonough, W. F. and Sun, S.S., 1995, *The composition of the Earth*. Chemical Geology 120, p. 223-253.

Miyashiro, A., 1974, *Volcanic rock series in island arcs and active continental margins*, American Journal of Science, 274, p. 321–355.

Nash, B.P., Perkins, M.E., Christensen, J.N., Lee, D.-C., and Halliday, A.N., 2006, *The Yellowstone hospot in space and time: Nd and Hf isotopes in silicic magmas*: Earth and Planetary Science Letters, v. 247, p. 143–156, doi: 10.1016 /j .epsl .2006 .04 .030 .

Nash, B.P., and Perkins, M.E., 2012, *Neogene fallout tuffs from the Yellowstone hotspot in the Columbia Plateau region, Oregon, Washington, and Idaho, USA*: PLoS ONE, v. 7, no. 10, p. e44205, doi: 10 .1371 /journal .pone.0044205 .

Robyn, T. L., 1977, *Geology and petrology of the Strawberry Mountain volcanic series, Central Oregon*. University of Oregon, Unpublished PhD thesis, 189 p.

Robyn, T. L., 1979, *Miocene volcanism in eastern Oregon—An example of calc-alkaline volcanism unrelated to subduction*. Journal of Volcanology and Geothermal Research, 5, 149-161.

Rytuba, J.J., Vander Meulen, D.B., Plouff, D., Minor, S.A., 1985, *Geology of the Mahogany Mountain Caldera*, Oregon. Geological Society of America Abstracts with Programs 17, 4, p. 263.

Rytuba, J.J., Vander Meulen, D.B.,Minor, S.A., 1989, *Geologic evolution of the Three Fingers caldera, Malheur County, Oregon*. Geological Society of America Abstracts with Programs 21, 5 p. 138.

Rytuba, J.J. and Vander Meulen, D.B., 1991, *Hot-spring precious-metal systems in the Lake Owyhee volcanic field, Oregon-Idaho*: in Raines, G.L., Lisle, R.E., Schafer, R.W., Wilkinson, W.H., eds., 'Geology and ore deposits of the Great Basin', Reno, Geological Society of Nevada, Symposium Proceedings, April 1 - 5, 1990, v. 2, p. 1085 – 1096.

Shawe, D.R. and Snyder, D.B., 1988, *Ash-flow Eruptive Megabreccias of the Manhattan and Mount Jefferson Calderas, Nye County, Nevada*: USGS Professional Paper 1471, 33 p.

Shervais J.W. and Hanan B.B., 2008, *Lithospheric topography, tilted plumes, and the track of the Snake River-Yellowstone hot spot*. Tectonics 27, TC5004.

Shotwell, J.A., and Russell, D.E., 1963, *Mammalian Fauna of the Upper Juntura Formation*: in Shotwell, J.A., 1963, 'The Juntura Basin: Studies in Earth History and Paleontology', Am. Philos. Soc. Trans.,v. 53 (new ser.), pt. 1, 77 p.

Smith, R.L. and Bailey, R.A., 1968, *Resurgent Cauldrons*: in Coats, R.R., Hay, R.L., Anderson, C.A., eds., 'Studies in Volcanology – A memoir in honor of Howell Williams', Geological Society of America Memoir 116, p. 613 – 662.

Starkel, W.A., 2014, *Mapping, Geologic Evolution, and Petrogenesis of the McDermitt Caldera Center, Northern Nevada and Southern Oregon, USA*, Washington State University, PhD Thesis, 407 p.

Steiner, A, 2015, *Field Geology and Petrologic Investigation of the Strawberry Volcanics, Northeast Oregon*, Portland State University, PhD Thesis, 229 p.

Streck, M.J. and Ferns, M.L., 2004, *The Rattlesnake Tuff and other Miocene Silicic Volcanism in Eastern Oregon*, in Haller, K.M., Wood, S.H., eds., 'Geological Field Trips in Southern Idaho, Eastern Oregon, and Northern Nevada' USGS Open-file report 2004 - 1222

Streck, M.J., Ferns, M.L., and McIntosh, W., 2015, *Large, Persistent Rhyolitic Magma Reservoirs above Columbia River Basalt Storage Sites: The Dinner Creek Tuff Eruptive Center, Eastern Oregon*, Geosphere, April 2015, v. 11, no. 2, 10 p.

Sun, S.S. and McDonough, W.F., 1989, *Chemical and isotopic systematics of oceanic basalts: implications for mantle composition and processes*. Geological Society of London Special Publication, 42(1), p. 313-345.

Thayer, T.P. and Brown, C.E., 1973, *Ironside Mountain, Oregon: A Late Tertiary Volcanic and Structural Enigma*, Geological Society of America, GSA Bulletin 01/1973

Torres-Hernandez, J.R., Labarthe-Hernandez, G., Aguillon-Robles, A., Gomez-Anguiano, M., Mata-Segura, J.L., 2006, *The pyroclastic dikes of the Tertiary San Luis Potosi volcanic field: Implications on the emplacement of Panalillo ignimbrite*, Geofisica Internacional, vol. 45, n. 4, p. 243 - 253

Vander Meulen, D.B., 1989, *Intracaldera Tuffs and Central-Vent Intrusion of the Mahogany Mountain Caldera, Eastern Oregon*: U.S. Geological Survey Open-File Report 89-77, 69 p., 2 plates, map scale 1:72,750.

Walker G. W., 1979, *Revisions to the Cenozoic stratigraphy of Harney basin, southeastern Oregon*, USGS Bulletin 1475, 35 p.

Wallace, A.B., Noble, C.D., Grant, N.K., 1980, *Icelandite and aenigmatite-bearing pantellerite from the McDermitt caldera complex, Nevada-Oregon*: Geology, v. 8, p. 380–384.

Ware, B.D., 2013, *Age, Provenance, and Structure of the Weathersby Formation, Eastern Izee Sub-basin, Blue Mountains Province, Oregon and Idaho*, Boise State University, M.S. thesis, 265 p.

Williams, H., 1941, *Calderas and their origin*, University of California Publishing Department Geological Sciences vol. 25, p. 239–346

Wolff, J.A., and Ramos, F.C., 2013, *Source materials for the main phase of the Columbia River Basalt Group: Geochemical evidence and implications for magma storage and transport*, in Reidel, S.P., *et al*.., eds., 'The Columbia River flood basalt province', Geological Society of
America Special Paper 497, p. 273–291, doi: 10 .1130/2013 .2497 (11) .

Woods, J.D., 1976, *The Geology of the Castle Rock Area, Grant, Harney, and Malheur Counties, Oregon*, Portland State University, M.S. thesis, 89 p.

Appendix A

Geologic Map of Study Area

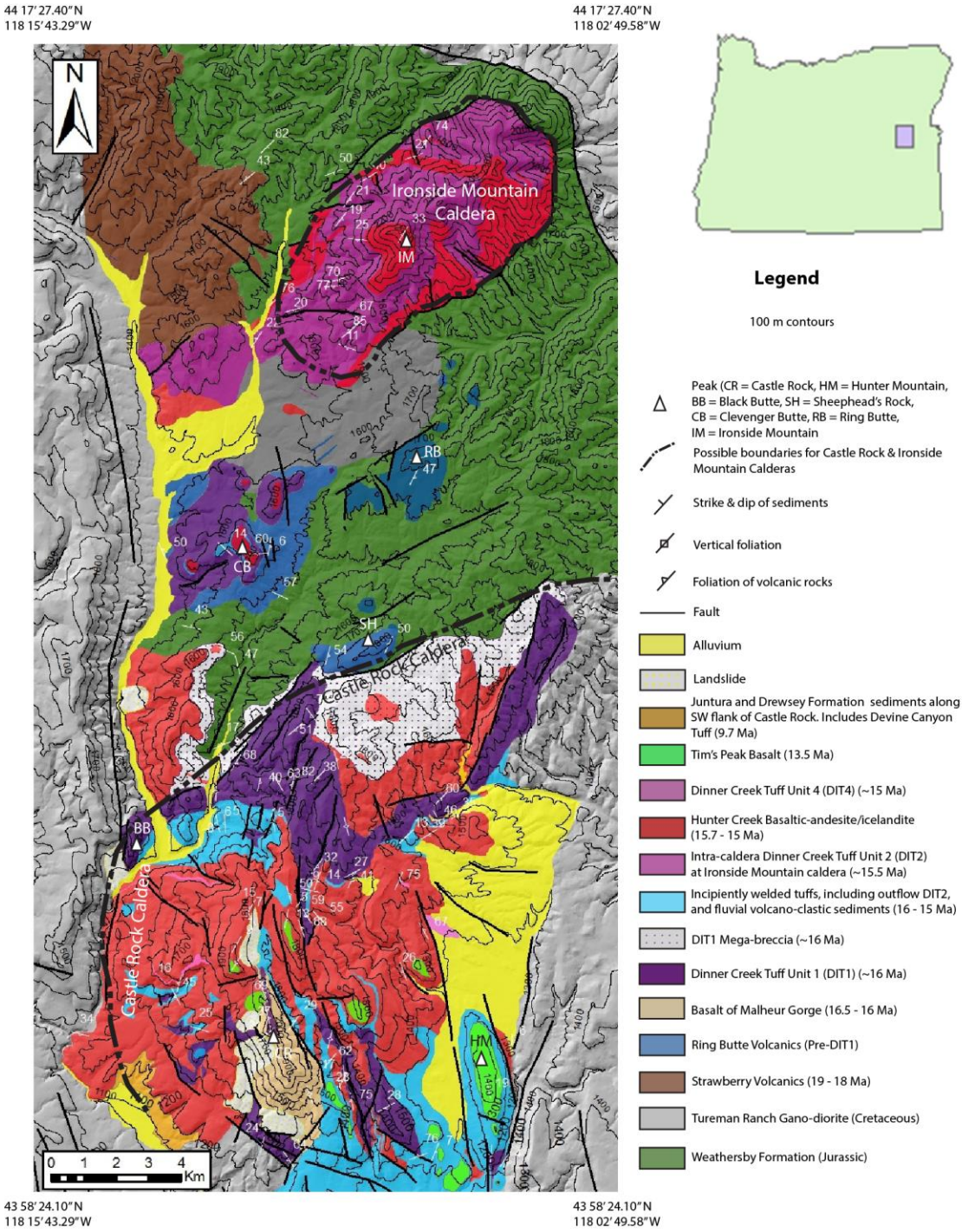
44 17' 27.40"N
118 15' 43.29"W
44 17' 27.40"N
118 02' 49.58"W
N
Ironside Mountain Caldera
IM
RB
CB
SH
Castle Rock Caldera
BB
Castle Rock Caldera
HM
0 1 2 3 4 Km
43 58' 24.10"N
118 15' 43.29"W
43 58' 24.10"N
118 02' 49.58"W
Legend
100 m contours
Peak (CR = Castle Rock, HM = Hunter Mountain, BB = Black Butte, SH = Sheephead's Rock, CB = Clevenger Butte, RB = Ring Butte, IM = Ironside Mountain
Possible boundaries for Castle Rock & Ironside Mountain Calderas
Strike & dip of sediments
Vertical foliation
Foliation of volcanic rocks
Fault
Alluvium
Landslide
Juntura and Drewsey Formation sediments along SW flank of Castle Rock. Includes Devine Canyon Tuff (9.7 Ma)
Tim's Peak Basalt (13.5 Ma)
Dinner Creek Tuff Unit 4 (DIT4) (~15 Ma)
Hunter Creek Basaltic-andesite/icelandite (15.7 - 15 Ma)
Intra-caldera Dinner Creek Tuff Unit 2 (DIT2) at Ironside Mountain caldera (~15.5 Ma)
Incipiently welded tuffs, including outflow DIT2, and fluvial volcano-clastic sediments (16 - 15 Ma)
DIT1 Mega-breccia (~16 Ma)
Dinner Creek Tuff Unit 1 (DIT1) (~16 Ma)
Basalt of Malheur Gorge (16.5 - 16 Ma)
Ring Butte Volcanics (Pre-DIT1)
Strawberry Volcanics (19 - 18 Ma)
Tureman Ranch Gano-diorite (Cretaceous)
Weathersby Formation (Jurassic)

Appendix B

Whole Rock Geochemical Data

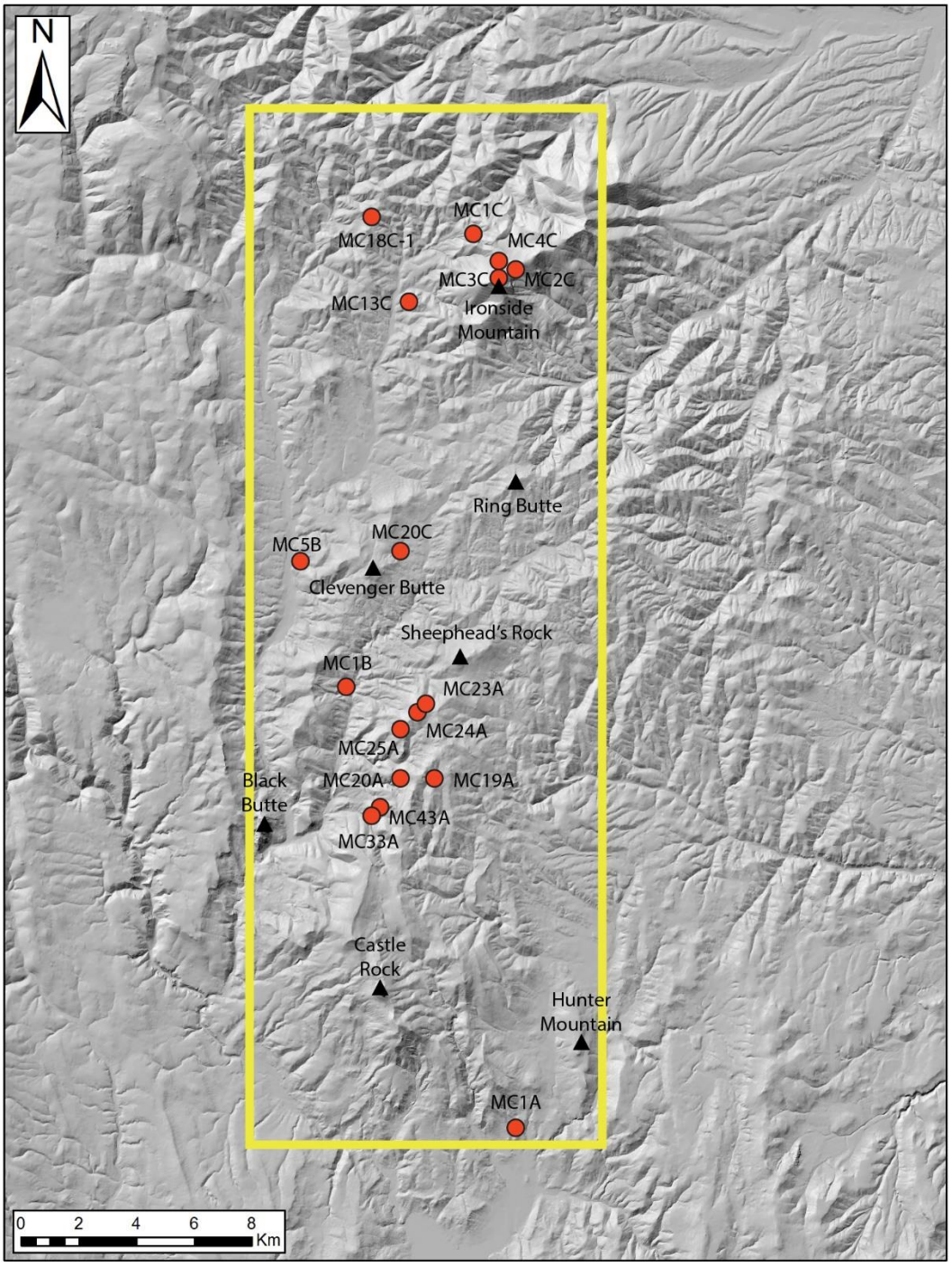

Location of samples from summer 2015 field work.

Summer 2015						
Sample	**MC1A**	**MC19A**	**MC20A**	**MC23A**	**MC24A**	**MC25A**
Lat	43.9789	44.0900	44.0901	44.1090	44.1066	44.1049
Long	-118.1172	-118.1644	-118.1750	-118.1690	-118.1724	-118.1761
Rock type	mod-welded tuff	vitrophyre	rheomorphic tuff	rheomorphic tuff	rheomorphic tuff	icelandite
Unit	DIT2	DIT1	DIT1	DIT1	DIT1	HCB
XRF						
Wt. % normalized						
SiO2	71.73	76.41	76.82	76.70	76.90	59.32
TiO2	0.453	0.166	0.162	0.166	0.165	1.769
Al2O3	13.94	12.32	12.22	12.34	12.35	15.47
FeO*	4.51	2.10	2.17	2.02	1.89	8.17
MnO	0.083	0.057	0.020	0.041	0.031	0.172
MgO	1.30	0.02	0.00	0.01	0.01	2.51
CaO	1.63	0.43	0.21	0.33	0.32	5.96
Na2O	2.06	3.55	4.58	4.55	4.44	3.79
K2O	4.22	4.94	3.80	3.84	3.87	2.09
P2O5	0.064	0.007	0.020	0.013	0.020	0.765
ppm						
Ni	4	1	1	2	2	2
Cr	4	2	1	2	3	0
Sc	11	4	4	4	4	24
V	72	4	8	6	9	132
Ba	1170	1466	1474	1486	1475	896
Rb	67	80	78	78	76	35
Sr	110	27	26	26	27	358
Zr	357	438	448	450	447	194
Y	68	90	55	75	88	53
Nb	21.1	24.8	24.8	24.7	25.7	11.5
Ga	21	20	21	22	21	19
Cu	10	2	3	3	3	4
Zn	140	155	152	132	103	158
Pb	16	19	17	16	14	8
La	40	47	24	41	53	23
Ce	87	93	32	87	66	48
Th	7	8	8	8	7	3
Nd	42	46	32	46	49	33
U	2	4	3	3	2	2

	Summer 2015					
Sample	**MC1A**	**MC19A**	**MC20A**	**MC23A**	**MC24A**	**MC25A**
Lat	43.9789	44.0900	44.0901	44.1090	44.1066	44.1049
Long	-118.1172	-118.1644	-118.1750	-118.1690	-118.1724	-118.1761
Rock type	mod-welded tuff	vitrophyre	rheomorphic tuff	rheomorphic tuff	rheomorphic tuff	icelandite
Unit	DIT2	DIT1	DIT1	DIT1	DIT1	HCB
ICP-MS ppm						
La	40.56	44.83	26.49	42.54	50.43	25.14
Ce	84.98	93.54	35.71	84.39	72.35	53.26
Pr	10.88	11.73	8.49	11.76	13.02	7.78
Nd	43.50	47.02	32.80	46.28	52.56	34.14
Sm	10.13	11.09	7.87	10.97	12.08	8.54
Eu	2.23	1.41	1.55	1.68	2.03	2.45
Gd	10.35	11.62	7.44	10.60	12.56	9.26
Tb	1.83	2.21	1.46	2.01	2.28	1.54
Dy	12.10	15.13	10.11	13.55	15.13	10.00
Ho	2.58	3.39	2.23	2.94	3.30	2.05
Er	7.23	9.79	6.83	8.53	9.45	5.46
Tm	1.11	1.53	1.13	1.35	1.46	0.79
Yb	7.19	10.13	8.05	8.91	9.53	4.94
Lu	1.14	1.63	1.31	1.40	1.52	0.78
Ba	1191	1483	1500	1515	1495	901
Th	6.56	7.93	8.16	8.32	8.31	3.34
Nb	20.21	23.74	24.51	24.46	24.58	11.29
Y	66.80	88.45	53.99	74.39	86.13	53.43
Hf	9.54	11.84	12.22	12.38	12.28	5.22
Ta	1.29	1.46	1.49	1.51	1.51	0.72
U	2.29	3.55	2.94	3.67	3.74	1.55
Pb	13.99	17.43	15.36	15.16	11.12	6.95
Rb	64.6	75.6	74.6	75.5	72.6	33.6
Cs	2.64	3.02	1.53	2.24	2.46	1.42
Sr	111	28	28	28	28	356
Sc	10.9	3.4	3.7	3.6	3.6	23.4
Zr	365	441	456	463	455	198

Summer 2015						
Sample	**MC33A**	**MC43A**	**MC1B**	**MC5B**	**MC1C**	**MC2C**
Lat	44.0777	44.0788	44.1159	44.1532	44.2568	44.2477
Long	-118.1850	-118.1831	-118.1984	-118.2257	-118.1494	-118.1308
Rock type	mod-welded tuff	icelandite	dacite lava	trachy-basalt	rheomorphic tuff	mod-welded tuff
Unit	DIT2	HCB	SBV?	RB?	DIT2	DIT2
XRF						
Wt. % normalized						
SiO2	74.23	58.79	68.10	50.17	74.72	71.72
TiO2	0.265	1.813	0.671	1.728	0.211	0.393
Al2O3	13.16	15.47	16.53	16.83	13.21	13.71
FeO*	3.53	9.61	2.12	9.78	2.37	4.11
MnO	0.138	0.146	0.077	0.165	0.047	0.082
MgO	0.72	1.75	0.85	6.79	0.00	0.40
CaO	1.23	5.61	4.33	8.66	1.05	1.94
Na2O	1.56	4.30	5.34	4.07	4.74	3.56
K2O	5.15	1.73	1.81	1.23	3.64	3.99
P2O5	0.021	0.785	0.173	0.576	0.013	0.086
ppm						
Ni	1	4	6	144	1	2
Cr	0	0	6	189	1	3
Sc	5	25	15	23	3	8
V	21	140	79	200	2	24
Ba	1163	715	1085	637	1338	1324
Rb	101	36	55	14	88	89
Sr	69	354	895	1071	104	173
Zr	389	186	253	159	356	316
Y	61	50	37	24	64	57
Nb	17.4	11.0	6.7	13.4	14.1	14.0
Ga	18	20	17	18	20	20
Cu	2	5	29	66	1	3
Zn	128	159	89	90	136	149
Pb	18	7	8	4	16	13
La	34	25	26	27	32	28
Ce	70	53	44	52	64	63
Th	9	4	5	3	8	7
Nd	35	36	27	29	34	33
U	3	2	4	2	4	2

Summer 2015						
Sample	**MC33A**	**MC43A**	**MC1B**	**MC5B**	**MC1C**	**MC2C**
Lat	44.0777	44.0788	44.1159	44.1532	44.2568	44.2477
Long	-118.1850	-118.1831	-118.1984	-118.2257	-118.1494	-118.1308
Rock type	mod-welded tuff	icelandite	dacite lava	trachy-basalt	rheomorphic tuff	mod-welded tuff
Unit	DIT2	HCB	SBV?	RB?	DIT2	DIT2
ICP-MS ppm						
La	35.77	25.57	22.88	26.11	33.85	31.40
Ce	74.88	51.23	48.71	55.60	69.90	65.79
Pr	9.42	8.11	6.58	7.56	9.24	8.65
Nd	37.21	35.99	27.32	30.53	37.77	34.87
Sm	8.47	8.92	6.31	6.15	9.30	8.41
Eu	1.33	2.59	1.50	1.95	1.56	1.58
Gd	8.81	9.69	6.26	5.51	9.39	8.53
Tb	1.60	1.60	1.05	0.84	1.70	1.55
Dy	10.82	9.95	6.81	4.89	11.46	10.32
Ho	2.36	2.03	1.42	0.99	2.43	2.20
Er	6.95	5.45	3.86	2.59	7.05	6.18
Tm	1.08	0.79	0.56	0.36	1.04	0.94
Yb	7.07	4.85	3.58	2.22	6.91	6.17
Lu	1.14	0.77	0.57	0.35	1.08	0.98
Ba	1187	711	1098	630	1355	1335
Th	8.20	3.20	4.60	1.67	7.83	6.81
Nb	16.76	11.00	6.83	12.75	14.33	13.64
Y	61.45	50.10	36.85	25.70	63.10	57.05
Hf	10.54	5.07	6.62	3.67	9.74	8.59
Ta	1.09	0.71	0.45	0.82	0.93	0.86
U	3.47	1.47	2.25	0.50	3.88	3.24
Pb	17.45	6.73	7.95	4.49	14.32	12.83
Rb	96.7	34.3	50.9	12.6	85.0	86.2
Cs	3.54	1.63	3.07	0.38	3.81	4.10
Sr	71	353	894	1057	108	177
Sc	4.9	23.7	13.8	21.8	2.7	6.5
Zr	397	191	253	161	362	319

	Summer 2015				
Sample	**MC3C**	**MC4C**	**MC13C**	**MC18C-1**	**MC20C**
Lat	44.2429	44.2501	44.2502	44.2566	44.1606
Long	-118.1365	-118.1375	-118.1601	-118.1937	-118.1770
Rock type	icelandite	mod-welded tuff	icelandite	dacite lava	trachy-basalt
Unit	HCB	DIT2	HCB	SBV	RB
XRF					
Wt. % normalized					
SiO2	59.42	73.21	60.60	65.04	51.01
TiO2	1.419	0.347	1.239	0.566	1.632
Al2O3	14.51	13.89	14.36	16.35	16.58
FeO*	10.42	2.97	10.29	4.28	9.08
MnO	0.203	0.031	0.211	0.076	0.158
MgO	1.92	0.25	1.46	2.37	5.83
CaO	5.51	1.47	5.11	5.19	9.64
Na2O	4.00	3.91	4.22	3.27	3.97
K2O	1.95	3.87	2.00	2.66	1.39
P2O5	0.658	0.065	0.520	0.203	0.693
ppm					
Ni	6	2	4	29	143
Cr	0	3	0	46	169
Sc	30	7	32	10	22
V	63	22	46	91	193
Ba	779	1290	824	1023	738
Rb	44	80	47	35	13
Sr	310	164	300	485	1343
Zr	178	332	192	139	148
Y	47	58	47	13	20
Nb	10.1	14.6	9.9	5.5	13.2
Ga	18	20	20	17	18
Cu	8	3	6	32	56
Zn	165	165	173	71	96
Pb	7	13	8	10	5
La	22	34	26	24	29
Ce	52	58	55	40	65
Th	4	8	4	4	3
Nd	31	35	33	19	37
U	1	3	3	2	1

	Summer 2015				
Sample	**MC3C**	**MC4C**	**MC13C**	**MC18C-1**	**MC20C**
Lat	44.2429	44.2501	44.2502	44.2566	44.1606
Long	-118.1365	-118.1375	-118.1601	-118.1937	-118.1770
Rock type	icelandite	mod-welded tuff	icelandite	dacite lava	trachy-basalt
Unit	HCB	DIT2	HCB	SBV	RB
ICP-MS ppm					
La	23.24	33.69	23.45	22.01	31.85
Ce	51.23	62.64	52.25	40.80	70.59
Pr	7.16	9.08	7.19	4.73	9.30
Nd	31.41	36.76	31.24	17.66	37.57
Sm	7.96	8.90	7.88	3.51	7.00
Eu	2.23	1.63	2.23	1.01	2.03
Gd	8.40	8.73	8.25	2.97	5.37
Tb	1.38	1.56	1.41	0.45	0.78
Dy	8.84	10.33	8.85	2.66	4.39
Ho	1.84	2.19	1.83	0.52	0.84
Er	4.97	6.33	5.01	1.37	2.10
Tm	0.71	0.94	0.71	0.19	0.28
Yb	4.42	6.01	4.67	1.20	1.74
Lu	0.72	0.96	0.73	0.20	0.27
Ba	765	1319	824	1016	732
Th	4.07	7.19	4.29	3.44	1.91
Nb	9.45	14.35	10.11	6.22	12.49
Y	46.87	57.42	46.87	13.66	20.64
Hf	4.90	9.00	5.19	3.51	3.56
Ta	0.62	0.92	0.65	0.48	0.68
U	1.95	3.39	2.10	1.34	0.56
Pb	7.43	13.17	8.03	9.37	5.63
Rb	43.7	79.3	45.2	33.1	11.0
Cs	1.95	4.74	2.10	1.06	0.18
Sr	315	169	304	494	1344
Sc	28.5	6.0	32.8	11.0	21.3
Zr	180	337	195	137	147

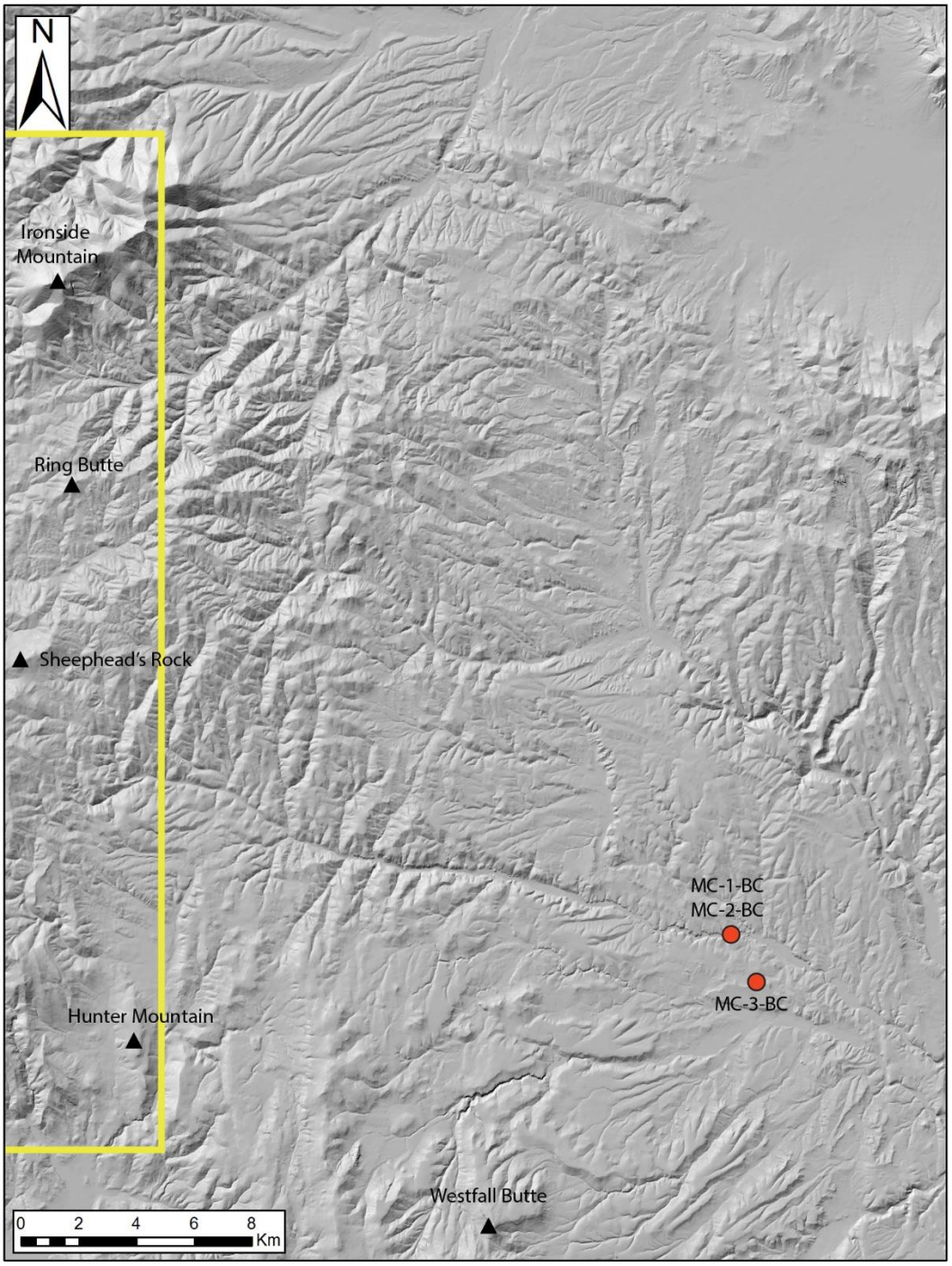

Location of samples from spring 2016 trip to Bully Creek Canyon.

	Spring 2016		
Sample	**MC-1-BC**	**MC-2-BC**	**MC-3-BC**
Lat	44.0397	44.0397	44.0276
Long	-117.8447	-117.8447	-117.83
Rock Type	rheomorphic tuff	vitrophyre	mod-welded tuff
Unit	DIT1	DIT1	DIT3?
XRF			
Wt. % normalized			
SiO2	76.44	76.06	76.13
TiO2	0.194	0.175	0.159
Al2O3	12.59	12.32	12.73
FeO*	1.97	2.35	1.49
MnO	0.025	0.057	0.076
MgO	0.07	0.04	0.10
CaO	0.37	0.59	0.39
Na2O	4.58	3.85	2.91
K2O	3.71	4.53	6.01
P2O5	0.058	0.019	0.014
ppm			
Ni	6	3	4
Cr	2	2	2
Sc	5	5	5
V	12	5	9
Ba	1508	1493	641
Rb	75	76	88
Sr	41	32	16
Zr	447	438	309
Y	74	87	88
Nb	24.6	23.9	30.1
Ga	22	21	20
Cu	7	6	12
Zn	138	147	103
Pb	17	14	20
La	50	41	40
Ce	93	92	91
Th	8	8	8
Nd	52	43	44
U	3	5	4

	Spring 2016		
Sample	**MC-1-BC**	**MC-2-BC**	**MC-3-BC**
Lat	44.0397	44.0397	44.0276
Long	-117.8447	-117.8447	-117.83
Rock Type	rheomorphic tuff	vitrophyre	mod-welded tuff
Unit	DIT1	DIT1	DIT3?
ICP-MS			
ppm			
La	51.27	46.27	38.32
Ce	99.63	95.79	93.68
Pr	14.46	12.31	11.67
Nd	56.44	48.59	46.81
Sm	12.93	11.33	12.53
Eu	1.93	1.73	1.29
Gd	11.92	11.74	12.86
Tb	2.19	2.19	2.40
Dy	14.28	14.89	15.51
Ho	2.97	3.24	3.28
Er	8.62	9.49	9.33
Tm	1.35	1.49	1.41
Yb	9.01	9.72	9.03
Lu	1.40	1.55	1.45
Ba	1529	1510	640
Th	8.02	7.91	8.31
Nb	23.68	23.50	29.05
Y	71.00	84.88	85.34
Hf	11.77	11.68	9.33
Ta	1.42	1.43	1.84
U	3.45	3.38	3.43
Pb	16.66	12.83	18.74
Rb	74.5	75.0	85.8
Cs	2.37	2.90	3.20
Sr	42	33	17
Sc	4.5	4.3	4.6
Zr	442	440	304

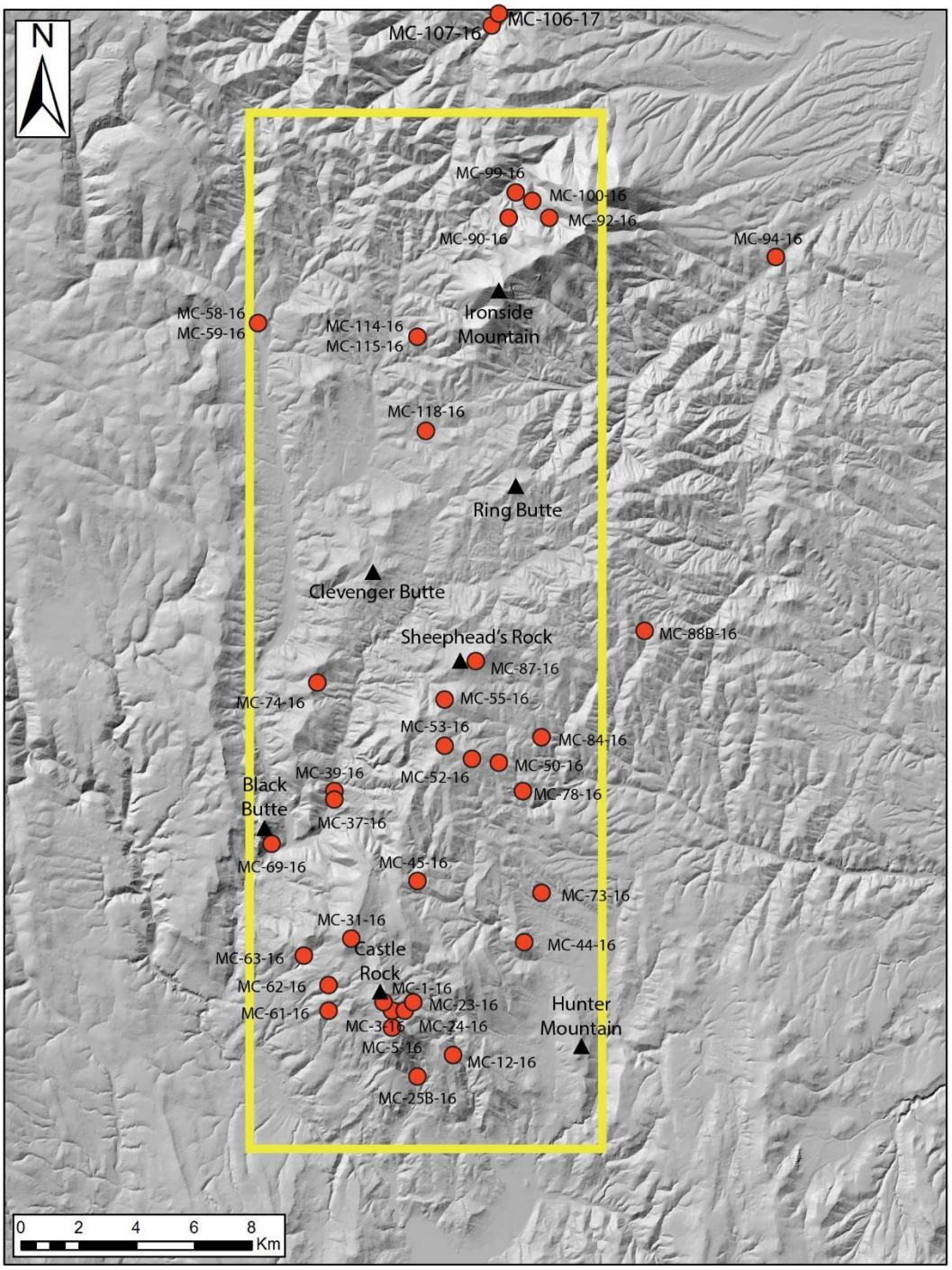

Location of samples from summer 2016 field work.

	Summer 2016					
Sample	**MC-1-16**	**MC-3-16**	**MC-5-16**	**MC-12-16**	**MC-23-16**	**MC-24-16**
Lat	44.02	44.018	44.013	44.006	44.0191	44.0178
Long	-118.182	-118.179	-118.179	-118.1562	-118.1710	-118.1731
Rock Type	rheomorphic tuff	basaltic andesite	mod-welded tuff	mod-welded tuff	mod-welded tuff	basaltic andesite
Unit	DIT1	BMG-BC	DIT4 (?)	DIT4	DIT4	BMG-BC
XRF						
Wt. % normalized						
SiO2	76.99	56.38	68.78	65.62	70.27	52.44
TiO2	0.176	2.348	0.845	1.069	0.700	1.912
Al2O3	12.24	14.49	15.49	14.53	13.98	15.30
FeO*	2.05	10.77	5.58	9.20	4.24	11.00
MnO	0.026	0.243	0.105	0.157	0.083	0.196
MgO	0.01	2.96	1.18	1.38	0.77	5.15
CaO	0.27	7.55	2.70	3.62	1.98	9.34
Na2O	4.50	3.21	2.74	2.13	4.69	3.15
K2O	3.72	1.66	2.46	2.08	2.94	1.20
P2O5	0.024	0.394	0.122	0.219	0.338	0.304
ppm						
Ni	2	7	14	2	2	52
Cr	3	5	25	12	8	131
Sc	3	33	18	24	11	34
V	9	375	120	30	35	306
Ba	1445	981	1223	1176	1476	479
Rb	75	45	55	50	38	22
Sr	32	364	178	254	178	408
Zr	436	210	207	189	323	140
Y	72	47	56	46	48	30
Nb	24.6	13.6	15.1	9.6	21.1	7.4
Ga	21	22	20	18	20	20
Cu	3	51	50	9	5	136
Zn	137	137	102	157	118	101
Pb	19	8	13	8	10	4
La	43	23	29	21	32	14
Ce	102	58	66	49	72	37
Th	8	6	5	5	6	3
Nd	44	32	36	29	35	23
U	3	2	1	3	2	2

	Summer 2016					
Sample	**MC-1-16**	**MC-3-16**	**MC-5-16**	**MC-12-16**	**MC-23-16**	**MC-24-16**
Lat	44.0194	44.0293	44.0175	44.006	44.0191	44.0178
Long	-118.1756	-118.1746	-118.1743	-118.1562	-118.1710	-118.1731
Rock Type	rheomorphic tuff	basaltic andesite	mod-welded tuff	mod-welded tuff	mod-welded tuff	basaltic andesite
Unit	DIT1	BMG-BC	DIT4 (?)	DIT4	DIT4	BMG-BC
ICP-MS ppm						
La	42.98	26.02	33.54	22.92	32.57	14.49
Ce	105.97	55.55	68.53	48.82	71.94	33.07
Pr	11.36	7.38	8.83	6.75	9.13	4.69
Nd	45.29	32.35	36.48	29.16	36.57	21.45
Sm	10.50	7.93	8.78	6.97	8.31	5.63
Eu	1.73	2.47	1.96	1.93	2.13	1.91
Gd	10.83	8.47	9.24	7.60	7.93	6.13
Tb	2.05	1.40	1.62	1.31	1.39	1.03
Dy	13.63	8.58	10.42	8.28	8.74	6.23
Ho	2.94	1.78	2.17	1.77	1.80	1.25
Er	8.57	4.75	5.96	4.97	5.02	3.27
Tm	1.37	0.67	0.91	0.74	0.75	0.46
Yb	8.99	4.05	5.56	4.63	4.70	2.82
Lu	1.47	0.64	0.91	0.76	0.76	0.45
Ba	1510	986	1255	1197	1536	478
Th	7.83	4.99	5.37	4.70	6.12	2.07
Nb	23.80	13.49	14.60	10.02	20.32	7.68
Y	71.27	47.69	55.71	45.40	46.45	30.87
Hf	12.02	5.87	6.37	5.27	8.49	3.88
Ta	1.51	0.96	1.09	0.69	1.29	0.55
U	2.71	2.29	1.60	2.03	2.57	0.78
Pb	17.38	8.57	13.71	8.76	9.14	4.57
Rb	73.7	45.5	54.6	48.9	37.6	21.8
Cs	1.17	1.56	1.86	3.10	0.84	0.73
Sr	31	374	177	256	177	413
Sc	3.6	34.8	19.3	25.1	11.2	35.5
Zr	449	222	212	198	336	145

Summer 2016						
Sample	**MC-25B-16**	**MC-31-16**	**MC-37-16**	**MC-39-16**	**MC-44-16**	**MC-45-16**
Lat	44.0009	44.0377	44.0843	44.0865	44.0368	44.0603
Long	-118.1648	-118.1955	-118.2031	-118.2023	-118.1226	-118.1680
Rock Type	basalt	basalt	rheomorphic tuff	mod-welded tuff	basalt	mod-welded tuff
Unit	LPCB	TPB	DIT1	DIT2	TPB	DIT4
XRF						
Wt. % normalized						
SiO2	50.59	50.20	77.90	75.62	50.52	61.36
TiO2	1.581	1.033	0.139	0.321	1.323	1.281
Al2O3	17.61	17.80	11.97	13.85	18.16	15.10
FeO*	11.38	9.57	1.53	2.07	10.21	10.54
MnO	0.155	0.159	0.010	0.032	0.152	0.185
MgO	4.06	7.17	0.06	0.28	5.82	2.54
CaO	11.79	11.25	0.21	1.30	10.18	5.16
Na2O	2.50	2.36	4.47	2.52	2.88	2.12
K2O	0.15	0.24	3.69	3.99	0.49	1.45
P2O5	0.188	0.211	0.013	0.021	0.256	0.269
ppm						
Ni	169	168	2	9	122	11
Cr	337	294	4	7	66	10
Sc	34	34	4	8	30	27
V	300	252	5	26	244	182
Ba	195	234	1405	1268	321	936
Rb	3	4	75	82	7	29
Sr	345	255	22	127	374	242
Zr	72	60	391	170	88	154
Y	22	24	60	45	27	49
Nb	3.5	3.4	24.7	12.4	6.7	7.4
Ga	19	16	22	17	19	19
Cu	132	101	1	7	142	15
Zn	75	79	151	61	94	129
Pb	1	0	16	17	2	7
La	8	6	29	33	12	20
Ce	16	15	62	63	21	36
Th	1	1	8	7	2	4
Nd	12	10	34	29	14	24
U	1	0	3	4	1	2

	Summer 2016					
Sample	**MC-25B-16**	**MC-31-16**	**MC-37-16**	**MC-39-16**	**MC-44-16**	**MC-45-16**
Lat	44.0009	44.0377	44.0843	44.0865	44.0368	44.0603
Long	-118.1648	-118.1955	-118.2031	-118.2023	-118.1226	-118.1680
Rock Type	basalt	basalt	rheomorphic tuff	mod-welded tuff	basalt	mod-welded tuff
Unit	LPCB	TPB	DIT1	DIT2	TPB	DIT4
ICP-MS						
ppm						
La	5.75	6.32	32.38	33.51	10.40	20.06
Ce	14.25	13.16	63.11	67.43	20.70	38.26
Pr	2.19	2.01	9.16	8.25	3.16	5.63
Nd	10.88	9.31	36.52	31.41	14.51	23.97
Sm	3.25	2.71	8.63	6.99	3.76	5.92
Eu	1.40	1.02	1.57	1.20	1.39	1.64
Gd	3.97	3.41	8.48	6.84	4.28	6.67
Tb	0.70	0.59	1.62	1.24	0.74	1.22
Dy	4.23	3.94	10.92	7.90	4.66	8.12
Ho	0.87	0.87	2.43	1.69	0.96	1.77
Er	2.32	2.42	7.19	4.84	2.64	5.11
Tm	0.32	0.35	1.14	0.75	0.38	0.76
Yb	1.96	2.13	7.50	4.83	2.32	4.83
Lu	0.30	0.35	1.20	0.78	0.36	0.80
Ba	189	226	1477	1322	324	950
Th	0.39	0.44	8.15	7.93	0.63	2.95
Nb	3.88	3.10	24.20	12.18	6.75	8.55
Y	21.89	23.40	59.26	44.29	26.23	49.46
Hf	1.97	1.49	11.41	5.54	2.24	4.38
Ta	0.29	0.26	1.52	0.92	0.47	0.57
U	0.15	0.18	3.04	3.08	0.26	1.29
Pb	1.13	1.34	15.40	15.25	1.71	6.68
Rb	1.4	3.5	75.7	82.1	5.6	28.7
Cs	0.15	0.08	1.80	2.62	0.33	1.21
Sr	351	258	23	127	379	247
Sc	34.9	36.2	3.3	6.8	30.8	28.0
Zr	72	58	409	175	89	161

Summer 2016						
Sample	**MC-50-16**	**MC-52-16**	**MC-53-16**	**MC-55-16**	**MC-58-16**	**MC-59-16**
Lat	44.0962	44.1035	44.1004	44.1133	44.2357	44.2357
Long	-118.1354	-118.1465	-118.1587	-118.1564	-118.2485	-118.2485
Rock Type	mega-breccia	basaltic andesite	mega-breccia	mega-breccia	rheomorphic tuff	andesite lava
Unit	DIT1	HCB	DIT1	DIT1	DIT1	SBV
XRF						
Wt. % normalized						
SiO2	64.66	52.33	63.59	62.84	77.28	62.71
TiO2	0.747	1.922	0.781	0.717	0.164	0.912
Al2O3	17.14	15.27	18.33	17.20	12.71	16.70
FeO*	4.18	11.03	4.09	4.78	1.04	5.22
MnO	0.066	0.186	0.060	0.088	0.015	0.097
MgO	1.95	5.33	2.57	3.04	0.16	2.47
CaO	5.11	9.36	5.41	6.02	0.28	5.16
Na2O	4.23	3.14	4.10	3.63	4.52	3.69
K2O	1.68	1.12	0.88	1.48	3.82	2.75
P2O5	0.242	0.301	0.198	0.198	0.010	0.287
ppm						
Ni	28	51	41	27	2	12
Cr	40	134	45	26	3	21
Sc	11	33	12	14	3	12
V	98	311	87	113	7	106
Ba	685	470	1121	573	1451	897
Rb	24	20	12	26	78	45
Sr	870	412	902	665	29	517
Zr	120	141	124	116	446	201
Y	13	30	16	18	68	22
Nb	5.3	8.2	5.2	4.2	25.9	11.3
Ga	20	20	20	18	22	19
Cu	25	136	29	32	2	19
Zn	64	101	68	61	78	83
Pb	9	5	10	7	16	8
La	19	15	22	17	40	26
Ce	39	32	38	32	70	54
Th	4	4	3	3	9	6
Nd	20	20	18	17	46	26
U	2	2	1	2	4	2

	Summer 2016					
Sample	**MC-50-16**	**MC-52-16**	**MC-53-16**	**MC-55-16**	**MC-58-16**	**MC-59-16**
Lat	44.0962	44.097	44.1004	44.1133	44.5504	44.5504
Long	-118.1354	-118.147	-118.1587	-118.1564	-118.5854	-118.5854
Rock Type	mega-breccia	basaltic andesite	mega-breccia	mega-breccia	rheomorphic tuff	andesite lava
Unit	DIT1	HCB	DIT1	DIT1	DIT1	SBV
ICP-MS						
ppm						
La	19.39	14.59	20.15	15.11	43.54	28.58
Ce	38.48	33.50	37.81	30.98	72.78	55.62
Pr	4.87	4.69	4.87	3.98	12.40	6.85
Nd	18.84	21.35	19.11	16.10	49.09	26.33
Sm	3.76	5.56	3.70	3.41	11.21	5.09
Eu	1.10	1.87	1.10	1.05	1.95	1.36
Gd	3.03	6.08	3.21	3.22	10.08	4.53
Tb	0.46	1.00	0.47	0.51	1.92	0.70
Dy	2.67	6.19	2.82	3.20	12.61	4.14
Ho	0.51	1.21	0.57	0.63	2.78	0.83
Er	1.34	3.27	1.54	1.77	8.08	2.23
Tm	0.20	0.46	0.22	0.26	1.27	0.32
Yb	1.29	2.79	1.43	1.68	8.26	1.99
Lu	0.20	0.43	0.23	0.27	1.29	0.31
Ba	712	471	1165	583	1520	915
Th	3.01	2.10	3.05	2.68	8.04	4.76
Nb	5.00	7.67	5.15	4.20	25.10	11.24
Y	13.75	30.93	16.11	16.74	67.57	22.16
Hf	3.20	3.93	3.29	3.09	12.24	4.89
Ta	0.36	0.54	0.36	0.32	1.49	0.80
U	1.04	0.77	0.89	0.99	3.76	1.62
Pb	8.76	4.83	8.63	7.35	14.63	8.35
Rb	25.2	20.4	10.9	25.3	76.2	44.4
Cs	0.95	0.63	0.91	0.87	2.23	1.20
Sr	874	420	905	661	31	519
Sc	11.8	35.5	12.9	14.8	3.3	12.2
Zr	121	146	125	117	458	205

Summer 2016						
Sample	**MC-61-16**	**MC-62-16**	**MC-63-16**	**MC-69-16**	**MC-73-16**	**MC-74-16**
Lat	44.0182	44.023	44.0345	44.0686	44.0531	44.1166
Long	-118.2075	-118.2065	-118.2166	-118.2327	-118.1159	-118.2147
Rock Type	mod-welded tuff	mod-welded tuff	mod-welded tuff	mod-welded tuff	mod-welded tuff	mega-breccia
Unit	DIT2	DIT2	DIT4	DIT4	DIT4	DIT1
XRF						
Wt. % normalized						
SiO2	74.73	72.98	70.14	62.42	69.86	65.06
TiO2	0.250	0.322	0.604	1.458	0.852	0.684
Al2O3	13.20	13.96	14.48	14.64	14.08	16.97
FeO*	2.42	3.60	5.06	10.36	5.82	4.31
MnO	0.056	0.069	0.074	0.159	0.064	0.051
MgO	0.06	0.93	0.67	2.76	0.45	2.00
CaO	0.94	1.02	1.51	4.61	1.78	5.08
Na2O	3.64	3.75	3.60	1.49	2.78	3.89
K2O	4.68	3.31	3.73	1.70	4.06	1.73
P2O5	0.020	0.061	0.127	0.405	0.256	0.225
ppm						
Ni	3	4	3	3	4	31
Cr	2	4	6	0	5	36
Sc	5	6	11	22	14	12
V	4	17	21	143	45	101
Ba	1660	1402	1471	822	1422	677
Rb	82	42	69	35	78	22
Sr	108	132	160	230	205	821
Zr	397	376	338	185	292	115
Y	69	70	56	46	59	14
Nb	22.7	21.4	21.9	9.9	19.5	5.1
Ga	23	23	20	18	21	19
Cu	3	7	4	7	5	27
Zn	136	124	153	177	146	63
Pb	16	14	13	10	11	8
La	43	42	34	20	35	14
Ce	87	87	72	44	65	37
Th	6	6	7	4	6	4
Nd	45	45	36	27	35	18
U	4	3	3	1	4	1

	Summer 2016					
Sample	**MC-61-16**	**MC-62-16**	**MC-63-16**	**MC-69-16**	**MC-73-16**	**MC-74-16**
Lat	44.0182	44.023	44.0345	44.0686	44.0531	44.1166
Long	-118.2075	-118.2065	-118.2166	-118.2327	-118.1159	-118.2147
Rock Type	mod-welded tuff	mod-welded tuff	mod-welded tuff	mod-welded tuff	mod-welded tuff	mega-breccia
Unit	DIT2	DIT2	DIT4	DIT4	DIT4	DIT1
ICP-MS ppm						
La	44.16	45.92	36.39	21.97	35.29	18.06
Ce	86.86	89.88	71.15	44.48	71.55	35.58
Pr	11.59	12.05	9.77	6.34	9.33	4.53
Nd	46.58	48.72	39.69	26.97	38.77	17.99
Sm	10.83	11.18	9.15	6.57	9.12	3.58
Eu	2.23	2.42	2.23	1.96	2.31	1.08
Gd	10.75	11.06	8.92	7.28	9.28	2.96
Tb	1.93	1.92	1.56	1.28	1.59	0.47
Dy	12.55	12.34	9.91	8.28	10.21	2.72
Ho	2.66	2.61	2.10	1.79	2.21	0.54
Er	7.61	7.50	5.91	5.13	6.18	1.46
Tm	1.15	1.13	0.90	0.75	0.94	0.21
Yb	7.29	7.24	5.83	4.83	5.96	1.35
Lu	1.17	1.15	0.97	0.80	0.99	0.22
Ba	1712	1445	1502	832	1452	690
Th	7.16	6.37	6.29	3.74	5.54	2.88
Nb	21.76	20.46	21.29	9.88	18.70	4.89
Y	68.44	69.95	55.14	47.15	59.86	14.29
Hf	10.35	9.91	8.89	5.12	7.66	3.09
Ta	1.39	1.33	1.31	0.64	1.16	0.38
U	3.01	2.10	2.70	1.74	2.64	1.04
Pb	14.00	13.81	11.91	8.73	11.42	8.53
Rb	80.1	40.8	68.3	35.0	76.5	21.0
Cs	3.06	1.16	2.49	4.93	2.38	0.76
Sr	108	131	161	233	204	824
Sc	4.3	6.2	11.4	21.4	14.0	11.2
Zr	405	384	350	193	305	114

Summer 2016						
Sample	**MC-78-16**	**MC-84-16**	**MC-87-16**	**MC-88B-16**	**MC-90-16**	**MC-92-16**
Lat	44.0865	44.1026	44.1273	44.1402	44.264	44.2666
Long	-118.1242	-118.1129	-118.1450	-118.0725	-118.1326	-118.1233
Rock Type	basaltic andesite	mega-breccia	trachy-basalt	mod-welded tuff	basaltic andesite	basaltic andesite
Unit	HCB	DIT1	RB	?	HCB	HCB
XRF						
Wt. % normalized						
SiO2	53.86	61.23	50.67	51.66	54.25	55.68
TiO2	1.988	0.842	1.854	1.880	1.265	1.388
Al2O3	15.95	18.43	15.12	15.78	16.90	15.86
FeO*	10.38	5.21	9.24	12.37	9.25	10.49
MnO	0.166	0.065	0.152	0.193	0.167	0.181
MgO	4.11	3.04	7.04	5.62	4.27	3.78
CaO	9.35	5.78	9.50	8.86	9.46	7.44
Na2O	2.90	3.92	4.20	2.72	3.23	3.52
K2O	1.00	1.25	1.39	0.69	0.87	1.16
P2O5	0.301	0.231	0.847	0.220	0.322	0.493
ppm						
Ni	35	29	151	71	5	23
Cr	136	29	209	92	28	38
Sc	36	12	22	36	29	27
V	315	119	243	306	273	176
Ba	534	546	656	311	363	522
Rb	22	15	18	16	19	22
Sr	417	864	1484	371	417	353
Zr	144	125	165	131	106	131
Y	40	13	20	32	28	37
Nb	7.7	5.6	16.0	6.4	5.5	7.6
Ga	21	20	21	19	19	19
Cu	135	25	76	178	7	14
Zn	102	70	146	99	119	141
Pb	7	8	7	5	2	5
La	16	14	40	11	14	16
Ce	39	33	90	29	33	40
Th	3	3	6	3	2	3
Nd	25	17	45	19	19	23
U	1	2	3	0	1	1

Summer 2016						
Sample	**MC-78-16**	**MC-84-16**	**MC-87-16**	**MC-88B-16**	**MC-90-16**	**MC-92-16**
Lat	44.0865	44.1026	44.1273	44.1402	44.264	44.2666
Long	-118.1242	-118.1129	-118.1450	-118.0725	-118.1326	-118.1233
Rock Type	basaltic andesite	mega-breccia	trachy-basalt	mod-welded tuff	basaltic andesite	basaltic andesite
Unit	HCB	DIT1	RB	?	HCB	HCB
ICP-MS						
ppm						
La	16.92	15.67	41.69	12.37	12.82	16.67
Ce	38.01	32.75	89.32	29.02	28.53	37.62
Pr	5.50	4.22	11.45	4.10	3.95	5.27
Nd	25.36	17.02	45.40	19.09	17.31	23.47
Sm	6.81	3.43	8.27	5.51	4.55	6.06
Eu	2.22	1.08	2.29	1.83	1.45	1.74
Gd	7.47	3.00	5.95	5.99	4.88	6.41
Tb	1.23	0.45	0.83	1.01	0.84	1.08
Dy	7.44	2.65	4.34	6.30	5.26	6.82
Ho	1.52	0.54	0.81	1.30	1.12	1.44
Er	4.01	1.43	2.04	3.46	3.10	3.88
Tm	0.55	0.21	0.28	0.49	0.45	0.56
Yb	3.33	1.35	1.65	2.96	2.87	3.52
Lu	0.53	0.22	0.26	0.46	0.44	0.56
Ba	528	549	654	305	359	527
Th	2.09	2.92	4.17	1.69	1.52	2.61
Nb	7.92	5.37	16.03	6.90	6.04	7.50
Y	40.11	13.93	20.44	31.91	28.87	36.44
Hf	3.96	3.28	4.19	3.63	2.84	3.63
Ta	0.58	0.40	0.93	0.50	0.42	0.52
U	0.78	1.10	1.45	0.59	0.71	1.27
Pb	4.76	8.05	7.46	3.57	3.28	4.97
Rb	21.7	13.3	16.0	15.2	17.9	21.5
Cs	0.82	0.60	0.55	0.51	0.90	0.50
Sr	425	856	1507	376	428	357
Sc	35.9	13.4	23.2	36.1	30.3	27.5
Zr	150	123	168	134	107	135

Summer 2016						
Sample	**MC-94-16**	**MC-99-16**	**MC-100-16**	**MC-106-16**	**MC-107-16**	**MC-114-16**
Lat	44.2548	44.2709	44.2688	44.3318	44.3296	44.2316
Long	-118.0170	-118.1265	-118.1231	-118.1334	-118.1329	-118.1636
Rock Type	icelandite	tuff	icelandite	andesite lava	rheomorphic tuff	mod-welded tuff
Unit	HCB	DIT2	HCB	HCB	DIT1	DIT2
XRF						
Wt. % normalized						
SiO2	59.93	78.12	60.58	62.02	77.61	70.62
TiO2	1.488	0.227	1.325	1.435	0.204	0.464
Al2O3	14.57	12.84	14.56	15.45	12.76	13.75
FeO*	10.37	1.60	10.25	7.81	0.98	4.26
MnO	0.190	0.004	0.201	0.136	0.009	0.089
MgO	1.62	0.28	1.47	1.39	0.08	0.53
CaO	5.12	0.23	4.84	4.98	0.29	2.51
Na2O	4.05	1.69	4.03	3.74	4.21	3.89
K2O	2.01	5.00	2.23	2.52	3.84	3.78
P2O5	0.653	0.017	0.516	0.509	0.015	0.091
ppm						
Ni	2	2	4	2	2	2
Cr	0	3	2	0	4	5
Sc	24	5	30	21	4	8
V	80	4	67	113	9	44
Ba	889	2540	900	1024	1382	1191
Rb	46	104	52	59	78	75
Sr	310	73	299	323	33	168
Zr	192	336	192	208	457	302
Y	51	53	47	52	76	59
Nb	11.0	14.4	10.7	10.0	25.4	14.2
Ga	21	19	20	24	22	19
Cu	6	3	10	6	3	3
Zn	174	111	179	223	103	152
Pb	8	17	9	9	22	13
La	27	30	24	23	39	32
Ce	52	64	54	56	70	69
Th	4	9	5	5	8	7
Nd	32	29	30	33	41	35
U	3	4	4	3	3	4

Summer 2016						
Sample	**MC-94-16**	**MC-99-16**	**MC-100-16**	**MC-106-16**	**MC-107-16**	**MC-114-16**
Lat	44.2548	44.2709	44.2688	44.3318	44.3296	44.2316
Long	-118.0170	-118.1265	-118.1231	-118.1334	-118.1329	-118.1636
Rock Type	icelandite	tuff	icelandite	andesite lava	rheomorphic tuff	mod-welded tuff
Unit	HCB	DIT2	HCB	HCB	DIT1	DIT2
ICP-MS ppm						
La	24.46	30.65	23.95	26.23	39.46	30.83
Ce	53.02	66.29	52.57	53.39	73.98	64.72
Pr	7.55	8.34	7.20	7.56	11.25	8.52
Nd	33.21	33.12	31.43	32.42	42.85	35.25
Sm	8.31	7.82	7.95	8.11	9.93	8.46
Eu	2.35	1.20	2.15	1.86	1.60	1.65
Gd	9.04	7.51	8.26	8.57	9.31	8.81
Tb	1.54	1.42	1.39	1.49	1.85	1.60
Dy	9.62	9.51	8.84	9.43	12.72	10.19
Ho	2.01	2.09	1.85	2.01	2.88	2.25
Er	5.48	5.89	5.06	5.60	8.64	6.29
Tm	0.81	0.91	0.74	0.81	1.37	0.94
Yb	5.01	5.89	4.66	5.10	9.04	6.23
Lu	0.80	0.94	0.74	0.83	1.47	0.99
Ba	889	2657	919	1040	1444	1222
Th	3.99	8.35	4.56	5.34	8.43	6.62
Nb	11.13	13.99	10.41	9.76	24.74	13.47
Y	51.92	53.58	47.63	52.21	76.05	58.03
Hf	5.46	9.21	5.34	5.77	12.54	8.40
Ta	0.74	0.93	0.70	0.67	1.54	0.90
U	2.01	3.69	2.27	2.71	3.72	3.30
Pb	8.84	15.87	8.45	8.77	20.85	12.44
Rb	47.3	101.8	52.3	58.7	78.1	73.5
Cs	2.45	2.93	2.37	2.38	2.55	3.42
Sr	318	75	305	328	33	168
Sc	25.2	4.1	30.8	22.1	4.3	8.8
Zr	202	344	199	217	472	314

Summer 2016		
Sample	**MC-115-16**	**MC-118-16**
Lat	44.2316	44.1985
Long	-118.1636	-118.1706
Rock Type	mod-welded tuff	tuff
Unit	DIT2	DIT2
XRF		
Wt. % normalized		
SiO2	71.49	78.58
TiO2	0.422	0.162
Al2O3	13.74	13.03
FeO*	4.31	0.87
MnO	0.084	0.000
MgO	0.33	0.45
CaO	1.95	0.52
Na2O	3.58	2.64
K2O	4.03	3.74
P2O5	0.067	0.011
ppm		
Ni	4	2
Cr	4	3
Sc	8	4
V	27	0
Ba	1222	771
Rb	79	87
Sr	154	36
Zr	313	326
Y	65	55
Nb	14.0	13.4
Ga	20	20
Cu	5	2
Zn	155	42
Pb	14	13
La	33	32
Ce	63	63
Th	7	9
Nd	35	33
U	4	3

Summer 2016		
Sample	**MC-115-16**	**MC-118-16**
Lat	44.2316	44.1985
Long	-118.1636	-118.1706
Rock Type	mod-welded tuff	tuff
Unit	DIT2	DIT2
ICP-MS		
ppm		
La	32.77	33.84
Ce	66.59	69.51
Pr	9.12	9.15
Nd	37.90	36.45
Sm	9.22	8.45
Eu	1.88	1.31
Gd	9.66	8.48
Tb	1.71	1.52
Dy	11.13	9.73
Ho	2.41	2.08
Er	6.91	5.90
Tm	1.05	0.91
Yb	6.82	5.85
Lu	1.11	0.96
Ba	1245	806
Th	6.85	8.19
Nb	13.96	13.31
Y	64.08	54.07
Hf	8.58	9.09
Ta	0.92	0.94
U	3.34	4.17
Pb	13.26	10.78
Rb	77.9	86.8
Cs	3.34	1.64
Sr	158	36
Sc	7.6	3.6
Zr	325	335

Appendix C

Thin Sections

Fourteen samples were collected for thin section analysis. The table below shows the samples, sample locations, and whether there is XRF/ICP-MS data for the samples

Sample	Latitude	Longitude	XRF/ICP-MS Data?
MC-106-16	44.3318	-118.1334	Yes
MC-15-16	44.0105	-118.1574	No
MC-18-16	44.0461	-118.167	No
MC-98-16	44.2738	-118.128	No
MC-52-16	44.1035	-118.1465	Yes
MC-46-16	44.0193	-118.0894	No
MC-31-16	44.0377	-118.1955	Yes
MC-26-16	44.0009	-118.1648	No
MC20C	44.1606	-118.177	Yes
MC-87-16	44.1273	-118.145	Yes
MC-89-16	44.1799	-118.1683	No
MC-59-16	44.2357	-118.2485	Yes
MC-24-16	44.0178	-118.1731	Yes
MC-76-16	44.0068	-118.1636	No

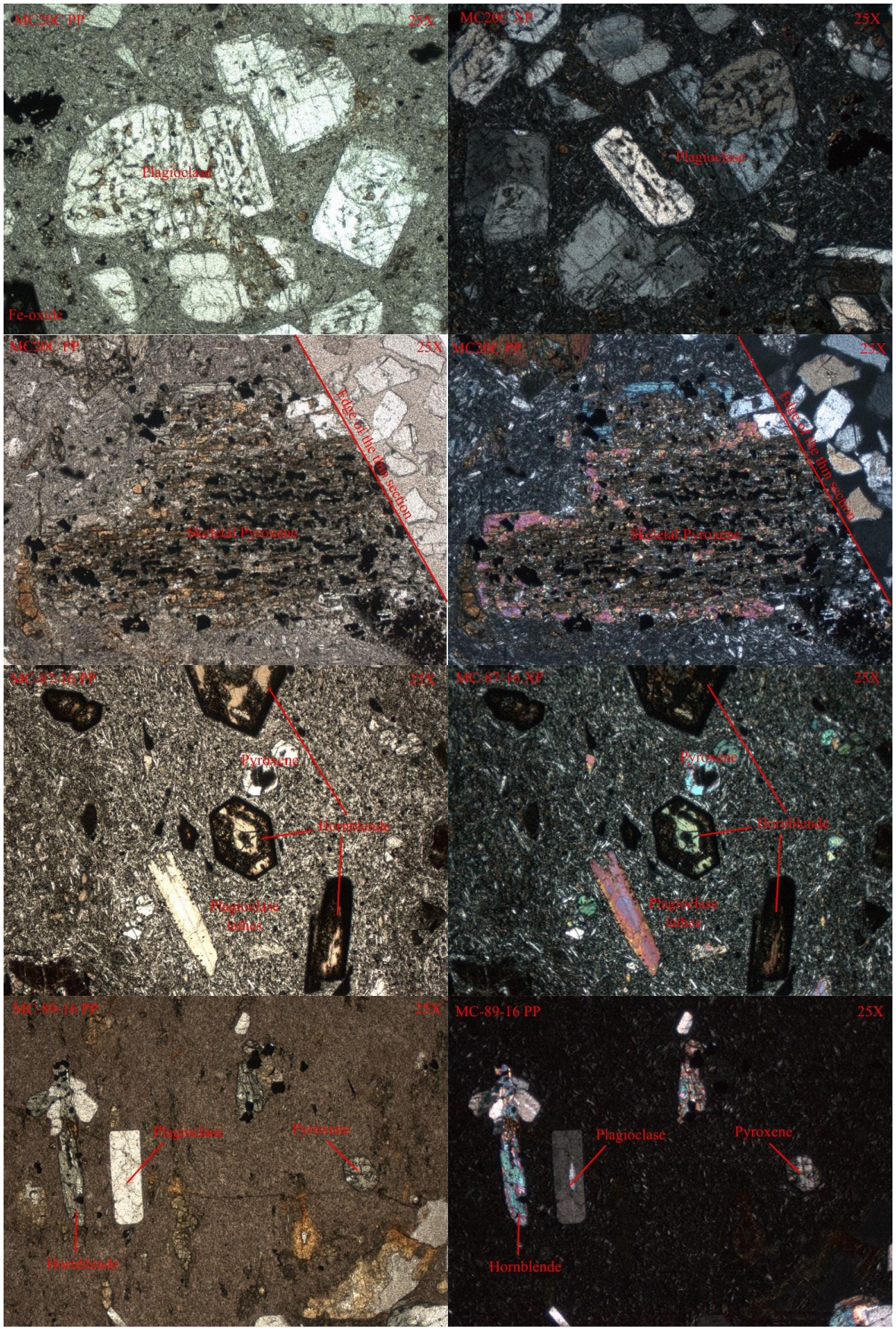
MC20C PP
25X
Plagioclase
Fe-oxide
MC20C XP
25X
Plagioclase
MC20C PP
25X
Edge of the thin section
Skeletal Pyroxene
MC20C PP
25X
Edge of the thin section
Skeletal Pyroxene
MC-87-16 PP
25X
Pyroxene
Hornblende
Plagioclase laths
MC-87-16 XP
25X
Pyroxene
Hornblende
Plagioclase laths
MC-89-16 PP
25X
Plagioclase
Pyroxene
Hornblende
MC-89-16 PP
25X
Plagioclase
Pyroxene
Hornblende

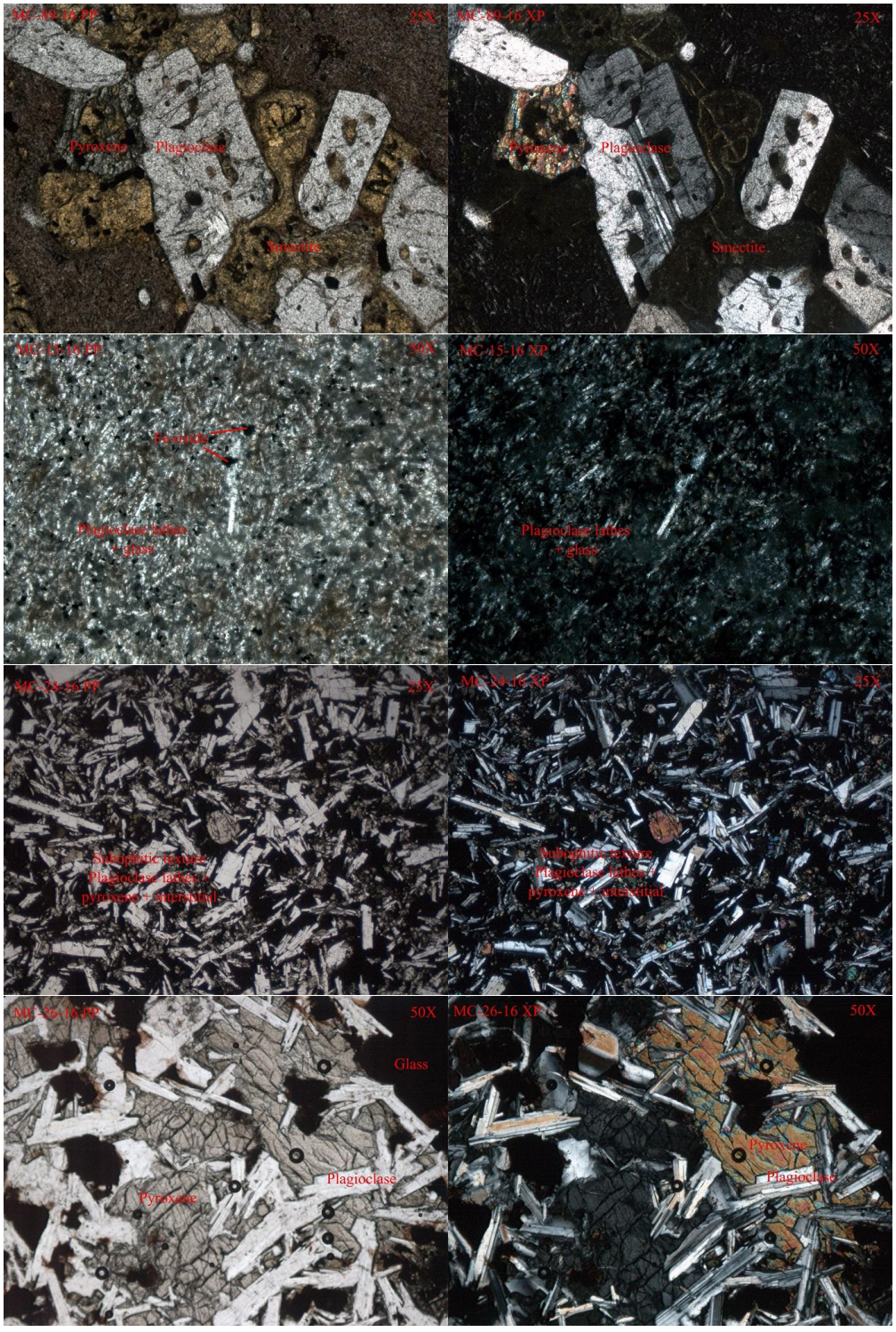
MC-89-16 PP
25X
Pyroxene
Plagioclase
Smectite
MC-89-16 XP
25X
Pyroxene
Plagioclase
Smectite
MC-15-16 PP
50X
Fe-oxide
Plagioclase lathes + glass
MC-15-16 XP
50X
Plagioclase lathes + glass
MC-24-16 PP
25X
Subophitic texture Plagioclase lathes + pyroxene + interstitial
MC-24-16 XP
25X
Subophitic texture Plagioclase lathes + pyroxene + interstitial
MC-26-16 PP
50X
Glass
Plagioclase
Pyroxene
MC-26-16 XP
50X
Pyroxene
Plagioclase

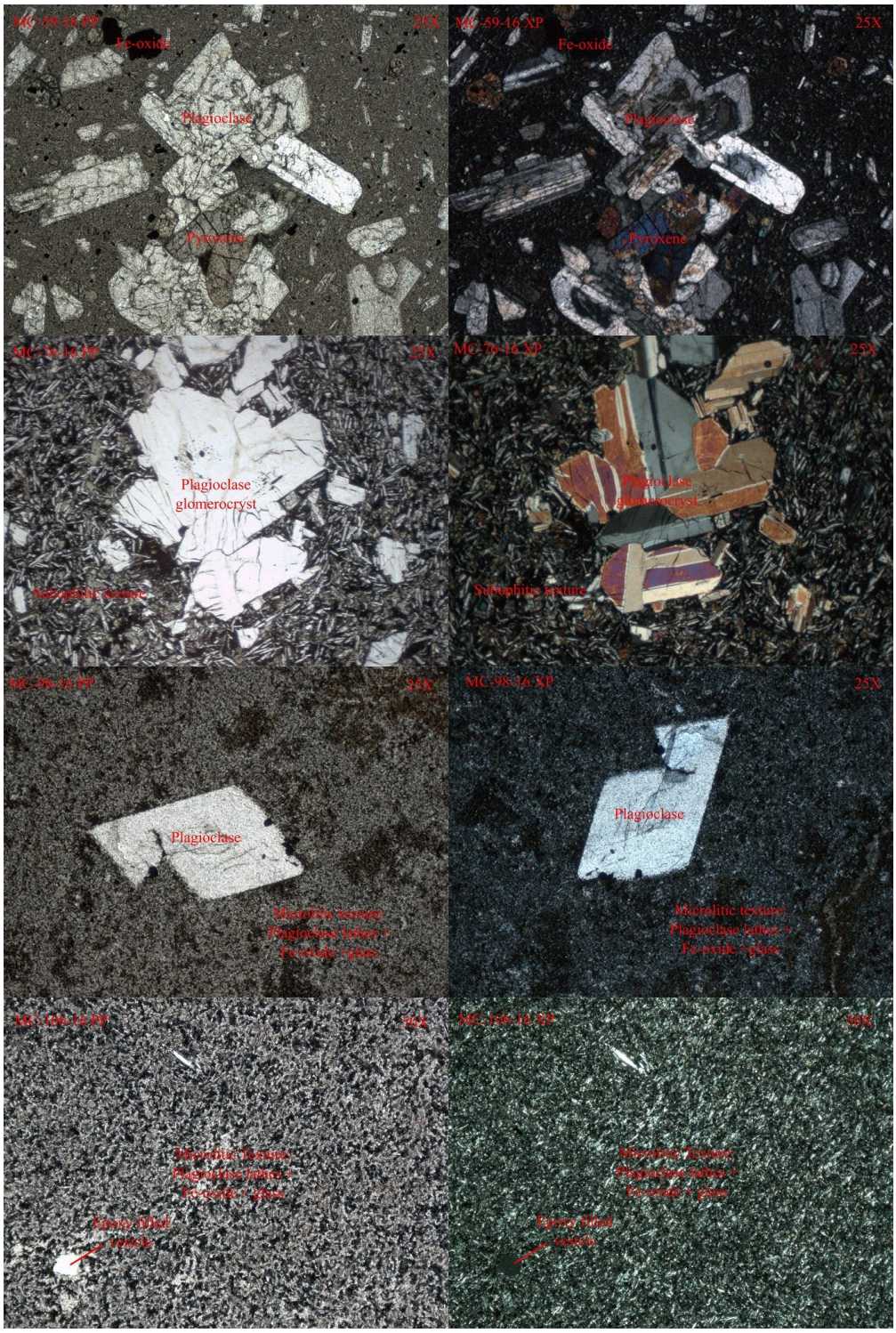
MC-59-16 PP
25X
Fe-oxide
Plagioclase
Pyroxene
MC-59-16 XP
25X
Fe-oxide
Plagioclase
Pyroxene
MC-70-16 PP
25X
Plagioclase glomerocryst
Subophitic texture
MC-70-16 XP
25X
Plagioclase glomerocryst
Subophitic texture
MC-98-16 PP
25X
Plagioclase
Microlitic texture: Plagioclase laths + Fe-oxide +glass
MC-98-16 XP
25X
Plagioclase
Microlitic texture: Plagioclase laths + Fe-oxide +glass
MC-106-16 PP
50X
Microlitic Texture: Plagioclase laths + Fe-oxide + glass
Epoxy filled vesicle
MC-106-16 XP
50X
Microlitic Texture: Plagioclase laths + Fe-oxide + glass
Epoxy filled vesicle

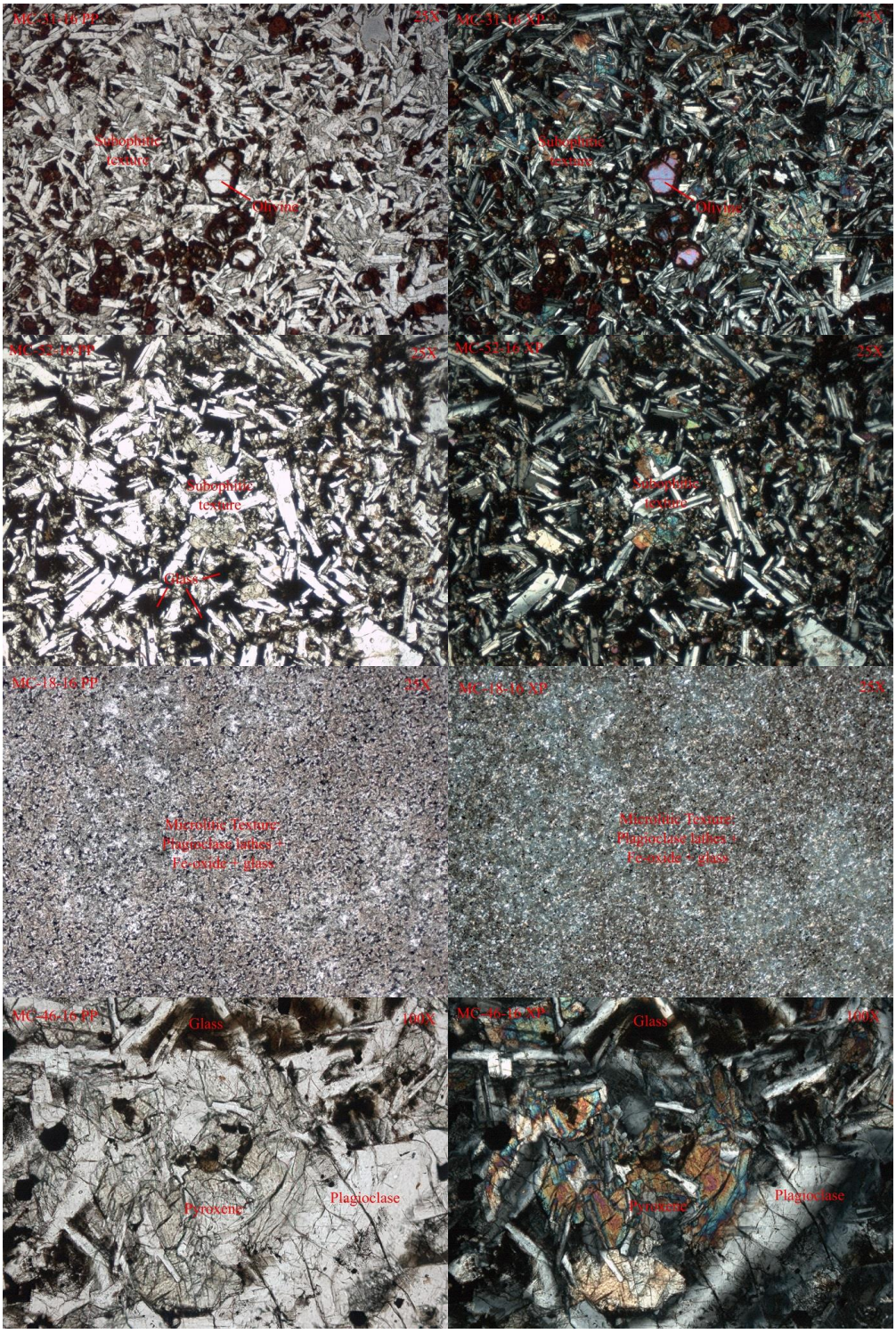
MC-31-16 PP
25X
Subophitic texture
Olivine
MC-31-16 XP
25X
Subophitic texture
Olivine
MC-32-16 PP
25X
Subophitic texture
Glass
MC-32-16 XP
25X
Subophitic texture
MC-18-16 PP
25X
Microlitic Texture: Plagioclase lathes + Fe-oxide + glass
MC-18-16 XP
25X
Microlitic Texture: Plagioclase lathes + Fe-oxide + glass
MC-46-16 PP
Glass
100X
Pyroxene
Plagioclase
MC-46-16 XP
Glass
100X
Pyroxene
Plagioclase

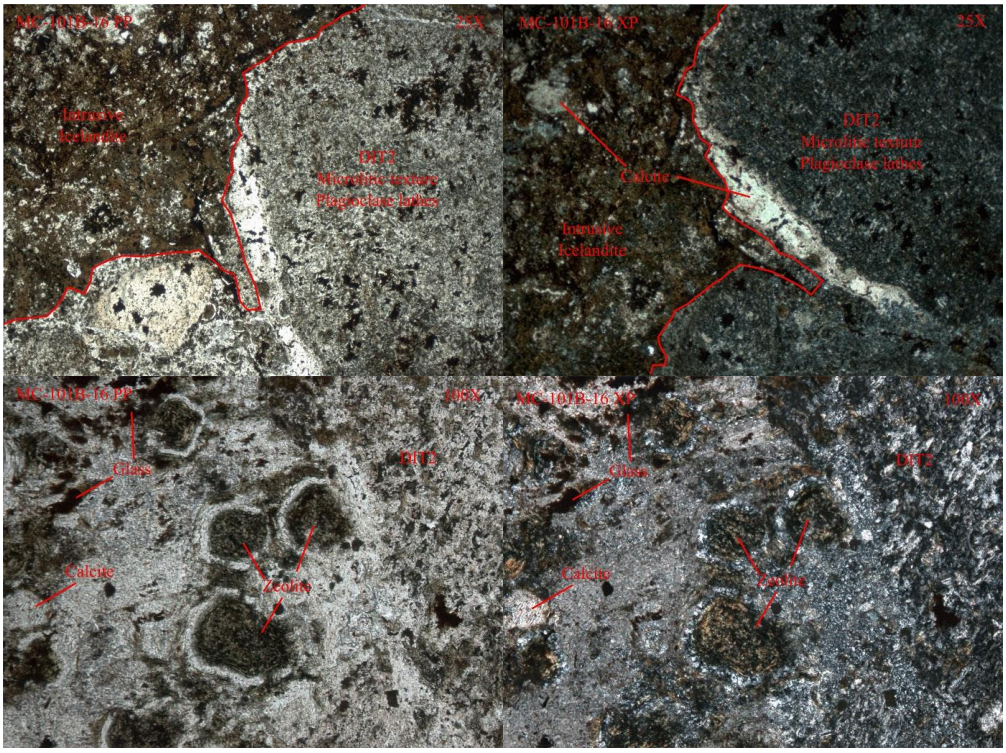

Sample	Unit	Description
MC20C	Ring Butte Volcanics	Porphyritic texture. Gray-white plagioclase lathe groundmass in PP, dark gray in XP. 40% phenocrysts. Plagioclase is white, light gray, and tan in PP, gray in XP. Euhedral to subhedral, occasional concentric zoning, and simple twinning. Some samples are skeletal, with opaque minerals growing over the surface and in fractures. Pyroxenes are light green in PP 1st - 2nd order yellow, brown, and blue in XP. Subhedral. Opaque minerals are probably magnetite. Small crystals with high interference colors are probably Olivine.
MC-87-16	Ring Butte Volcanics	Porphyritic texture. Gray-white-brown plagioclase lathe groundmass in PP, dark gray in XP. Plagioclase lathes are somewhat aligned in a specific orientation. 30 - 40% phenocrysts. Hornblende is tan - brown in PP, 1st - 2nd order green - blue - yellow in XP. Subhedral habit, with opaque alteration rinds around edges. Pyroxenes are light green in PP, 1st - 2nd order yellow, brown, and blue in XP. Subhedral. Opaque minerals are probably magnetite.
MC-89-16	Ring Butte Volcanics	Porphyritic texture. Brown groundmass in PP, dark gray to black in XP. 30% phenocrysts. Plagioclase is white-tan in PP, and gray - white in XP. Euhedral to subhedral. Simple & albite twinning. Hornblende is tan - brownish green in PP, 1st - 2nd order green - blue - yellow in XP. Subhedral habit, with opaque alteration rinds around edges. Pyroxenes are light green in PP, 1st - 2nd order yellow, brown, and blue in XP. Subhedral. Opaque minerals are probably magnetite.

MC-15-16	Hunter Creek Basalt/icelandite	Microlitic texture. Gray fine plagioclase lathe and brown-black glass groundmass in PP, dark gray in XP. Opaque minerals are probably magnetite.
MC-24-16	Basalt of Malheur Gorge	Subophitic/diktytaxitic texture. Euhedral plagioclase lathes, simple twinning, overprinting subhedral - anhedral pyroxene with interstitial black glass. Plagioclase lathes aren't completely entrained within pyroxene, so the texture may be best described as a middle ground between subophitic and diktytaxitic.
MC-26-16	Basalt of Malheur Gorge	Subophitic texture. Euhedral plagioclase lathes, simple & albite twinning, overprinting subhedral - anhedral pyroxene with interstitial black glass.
MC-31-16	Tim's Peak Basalt	Subophitic texture. Euhedral-subhedral plagioclase lathes, simple albite twinning, overprinting subhedral - anhedral pyroxene with interstitial brown glass. Small, anhedral, phenocrysts with 2nd order interference colors, probably olivine.
MC-52-16	Hunter Creek Basalt/icelandite	Subophitic/diktytaxitic texture. Euhedral plagioclase lathes, simple twinning, overprinting subhedral - anhedral pyroxene with interstitial black glass. Plagioclase lathes aren't completely entrained within pyroxene, so the texture may be best described as a middle ground between subophitic and diktytaxitic.
MC-18-16	Hunter Creek Basalt/icelandite	Microlitic texture. Gray fine plagioclase lathe and brown-black glass groundmass in PP, dark gray in XP. Opaque minerals are probably magnetite.
MC-46-16	Hunter Creek Basalt/icelandite	Subophitic texture. Euhedral-subhedral plagioclase lathes, simple twinning, overprinting subhedral - anhedral pyroxene with interstitial black glass.
MC-59-16	Strawberry Volcanics	Porphyritic texture. Gray-brown groundmass in PP, dark gray in XP. 20 - 30% phenocrysts. Plagioclase is white, light gray in PP, gray in XP. Euhedral to subhedral, simple twinning. Pyroxenes are light green-brown in PP, 1st - 2nd order yellow-blue in XP. Subhedral. Plagioclase and pyroxene commonly form clusters (glomerocrysts). Opaque minerals are probably magnetite.
MC-76-16	Basalt of Malheur Gorge	Subophitic texture. Euhedral plagioclase lathes, simple & albite twinning, overprinting subhedral - anhedral pyroxene with interstitial black glass. Plagioclase lathes often form clusters of crystals (glomerocrysts).
MC-98-16	Hunter Creek Basalticelandite	Microlitic texture. Gray fine plagioclase lathe and brown-black glass groundmass in PP, dark gray in XP. 0 - 5 % euhedral plagioclase phenocrysts, simple twinning. Opaque minerals are probably magnetite.
MC-101B-16	Hunter Creek Basalt/icelandite intruding into DIT2	Microlitic texture. Brown glass, with calcite replacing plagioclase and/or glass. Circular zeolite along contact with DIT2.Opaque minerals are probably magnetite.
MC-106-16	Hunter Creek Basalt/icelandite	Microlitic texture. Gray fine plagioclase lathe and brown-black glass groundmass in PP, dark gray in XP. 0 - 5 % euhedral plagioclase phenocrysts, simple twinning. Opaque minerals are probably magnetite.

Appendix D

Feldspar SEM-EDS Data

Sample	Plug	Sites	Lat	Long
MC-63-16	Plug 1	1 - 10	44.0345	-118.2166
MC-73-16	Plug 1	11 - 15	44.0531	-118.1159
MC-5-16	Plug 1	16 - 22	44.0175	-118.1743
MC-3-BC	Plug 1	23 - 27	44.0276	-117.83
MC2B	Plug 1	28 - 33	44.1283	-188.2077
MC1C	Plug 2	34 - 40	44.2568	-118.1494
MC4C	Plug 2	41 - 48	44.2501	-118.1375
MC-115-16	Plug 2	49 - 55	44.2316	-118.1636
MC4B	Plug 2	56 - 62, 121 – 122*	44.1465	-118.221
MC-114-16	Plug 2	63 - 71, 123 – 130*	44.2316	-118.1636
MC-1-16	Plug 3	72 - 79, 118, 119 – 120*	44.0194	-118.1756
MC-68-16	Plug 3	80 - 87, 117*	44.0684	-118.2333
MC-84-16	Plug 3	88 - 96	44.1026	-118.1129
MC-37-16	Plug 3	97 - 107	44.0843	-118.2031
MC-39-16	Plug 3	108 - 115	44.0865	-118.2023

* During the first session of testing, charging of the surface due to inadequate carbon coating disturbed the backscatter images of the individual sites. The plugs were re-coated and analyzed again in order to get better images. New spectra was taken during the second session, but the data from the first section was kept.

Plug 1: MC-63-16

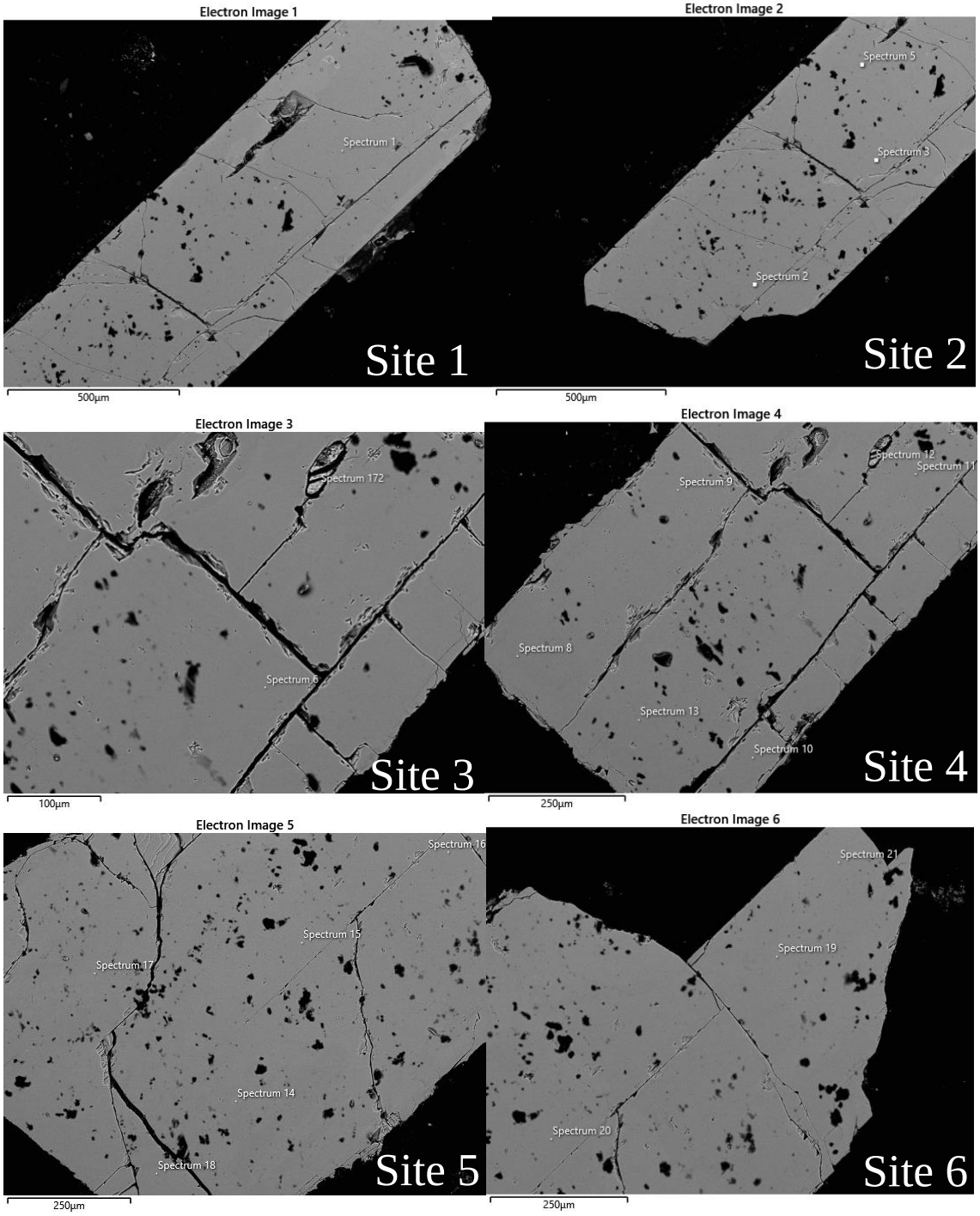

Plug 1: MC-63-16

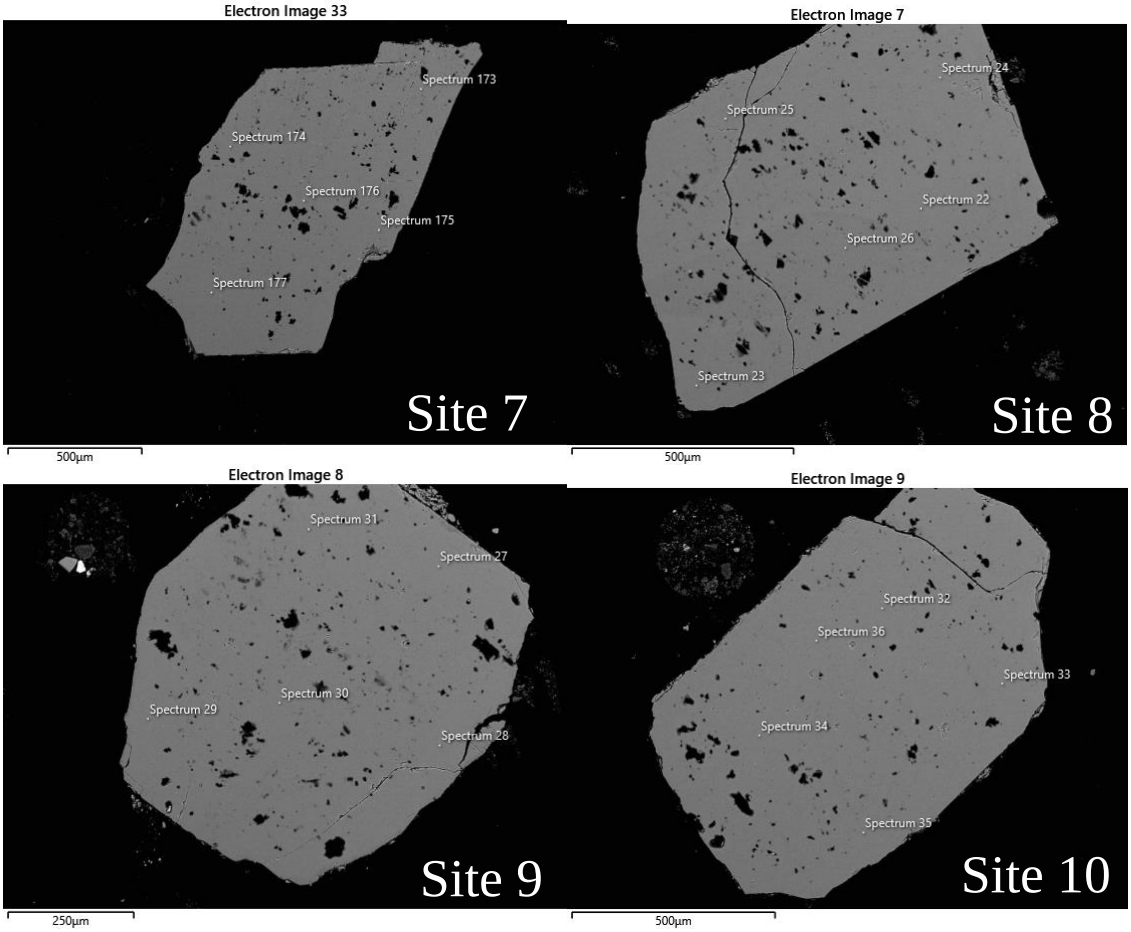

Plug 1: MC-63-16

Spectrum	Na	Mg	Al	Si	K	Ca	Ti	Fe	Ba	Total	Phase	Site
1	5.31		25.1	54.1	0.28	8.56		0.29		93.6	Anorthoclase	1
2	5.05		23.6	51.2	0.33	8.24		0.39		88.88	Anorthoclase	2
3	5.28		24.4	53.5	0.3	8.2				91.7	Anorthoclase	2
5	5.46		25.8	55	0.33	8.62		0.34		95.53	Anorthoclase	2
6	7.49		18.6	61.5	2.62	0.93			1.09	92.2	Anorthoclase	3
8	7.56		18.2	61	2.51	0.88			1.17	91.29	Anorthoclase	4
9	7.86		19.2	63.5	2.81	0.94			1.17	95.47	Anorthoclase	4
10	7.37		18	59.5	2.47	0.91			0.86	89.04	Anorthoclase	4
11	7.82		19	62.8	2.67	0.86			1.1	94.22	Anorthoclase	4
12		2.69	9.64	53.2	1.08	1.12	0.64	19.6		87.96	Ilmenite	4
13	7.54		18.4	60.7	2.62	0.86		0.27	1.06	91.49	Anorthoclase	4
14	7.67		18.7	61.5	2.5	0.92		0.32	1.16	92.74	Anorthoclase	5
15	7.89		19.2	62.6	2.49	1.02			1.27	94.44	Anorthoclase	5
16	8.04		19	63.7	2.61	0.85			1.09	95.36	Anorthoclase	5
17	7.82		18.9	63	2.64	0.88			1.13	94.39	Anorthoclase	5
18	7.3		17.7	59.1	2.39	0.93			1.06	88.52	Anorthoclase	5
19	7.85		19.1	63.1	2.74	0.97			1.15	94.89	Anorthoclase	6
20	7.51		18.1	60.5	2.42	0.87			1.14	90.49	Anorthoclase	6
21	8.05		19.5	64.1	2.7	0.95			1.16	96.41	Anorthoclase	6
173	7.96		19.1	64	2.84	0.75		0.33	1	95.92	Anorthoclase	7
174	7.83		19	63.3	2.66	0.94			1	94.73	Anorthoclase	7
175	7.41		18.4	61	2.59	0.93		0.29	1.02	91.53	Anorthoclase	7
176	7.82		19.1	62.8	2.58	0.93			1.24	94.45	Anorthoclase	7
177	7.39		18	59.8	2.46	0.87			1.12	89.65	Anorthoclase	7
22	7.68		19.1	62.4	2.65	0.95			1.26	93.93	Anorthoclase	8
23	6.89		17.8	59.3	2.44	0.89			1.06	88.4	Anorthoclase	8
24	7.68		19.4	64	2.61	0.92			1.27	95.82	Anorthoclase	8
25	7.62		19.1	63.5	2.76	0.83			1.03	94.79	Anorthoclase	8
26	7.76		18.8	63.4	2.81	0.71			1.15	94.63	Anorthoclase	8
27	6.99		18.4	65.5	4.96				0.47	96.29	Anorthoclase	9
28	6.67		17.5	62.1	4.74					90.96	Anorthoclase	9
29	6.43		18	63.8	5.23				0.55	94.07	Anorthoclase	9
30	6.86		18	63.6	4.87					93.26	Anorthoclase	9
31	6.99		18.3	64.9	5.02			0.37	0.64	96.3	Anorthoclase	9
32	7.92		19.1	63.4	2.66	0.92			0.98	94.96	Anorthoclase	10
33	7.77		18.7	62.4	2.64	0.85		0.36	0.92	93.65	Anorthoclase	10
34	8.33		19.6	65.2	2.74	0.95			1.12	98.02	Anorthoclase	10
35	7.44		18	59.7	2.5	0.87		0.27	1.06	89.82	Anorthoclase	10
36	7.81		19.1	63	2.64	0.92			1.18	94.71	Anorthoclase	10

Plug 1: MC-73-16

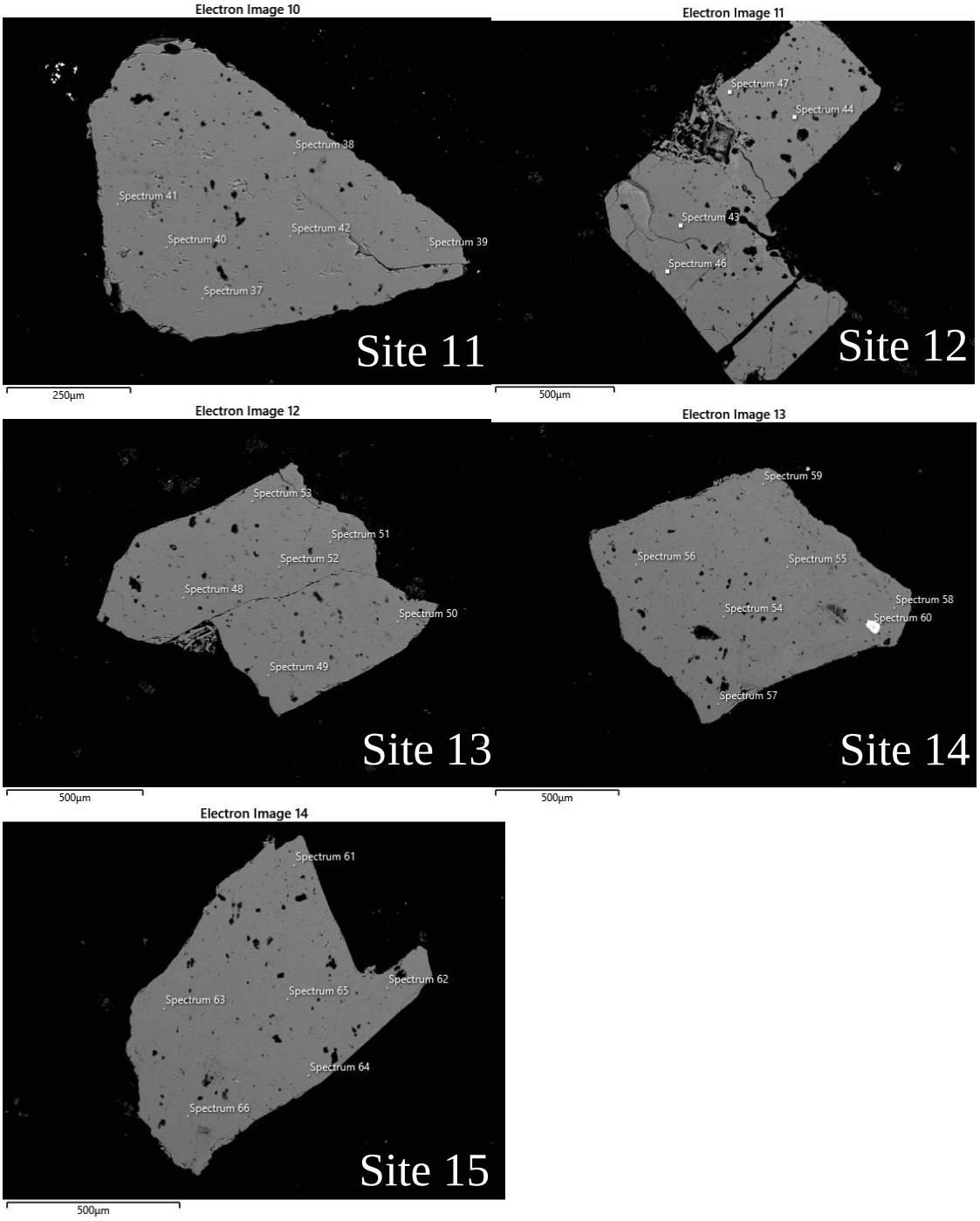

Plug 1: MC-73-16

Spectrum	Na	Al	Si	K	Ca	Ti	Mn	Fe	Ba	Total	Phase	Site
37	7.38	18.1	60.1	2.63	0.82				0.99	90.04	Anorthoclase	11
38	7.76	19	63	2.59	0.98				1.21	94.54	Anorthoclase	11
39	7.42	18.2	60.2	2.49	0.84				1.03	90.17	Anorthoclase	11
40	7.51	18.3	61.9	2.63	0.83				1.07	92.31	Anorthoclase	11
41	7.62	18.4	62.2	2.73	0.83				0.85	92.57	Anorthoclase	11
42	7.62	18.6	61.5	2.52	0.99				0.91	92.11	Anorthoclase	11
43	7.52	18.7	60.6	2.24	1.33				0.93	91.32	Anorthoclase	12
44	7.91	19.6	63.1	2.27	1.37				0.94	95.11	Anorthoclase	12
46	7.5	17.8	59.6	2.51	0.83				1	89.3	Anorthoclase	12
47	7.95	19.2	64	2.8	0.87				1.14	95.93	Anorthoclase	12
48	7.51	18.5	61.3	2.59	0.91				1.1	91.92	Anorthoclase	13
49	7.35	18.1	60.2	2.52	0.94				1.14	90.18	Anorthoclase	13
50	7.44	18.2	60.8	2.46	0.91				1.11	90.96	Anorthoclase	13
51	7.79	19.1	63.5	2.66	0.98				1.09	95.08	Anorthoclase	13
52	7.79	19	63.2	2.64	0.98				0.99	94.56	Anorthoclase	13
53	8.14	19.4	64.5	2.67	0.91				1.13	96.73	Anorthoclase	13
54	7.65	18.7	62.6	2.82	0.83				1.14	93.74	Anorthoclase	14
55	7.59	18.8	63.4	2.82	0.79				1.51	94.88	Anorthoclase	14
56	7.8	18.9	62.7	2.75	0.87				1.13	94.06	Anorthoclase	14
57	7.05	17.5	59.8	2.71	0.66				1.1	88.79	Anorthoclase	14
58	7.3	18.2	60.5	2.6	0.89				1.15	90.65	Anorthoclase	14
59	7.49	18.9	64.1	3.04	0.63				1.2	95.37	Anorthoclase	14
60		0.35				21.7	1.16	65.9		89.06	Ilmenite	14
61	7.88	19.3	63.9	2.84	0.81				0.95	95.65	Anorthoclase	15
62	7.65	18.7	62.1	2.55	1.01				1.05	93.05	Anorthoclase	15
63	7.83	18.9	62.4	2.78	0.81				1.12	93.81	Anorthoclase	15
64	7.27	18.3	60.3	2.58	0.91				1.07	90.47	Anorthoclase	15
65	7.81	18.9	62.9	2.74	0.94				1.11	94.44	Anorthoclase	15
66	7.36	18.1	59.7	2.52	0.76				0.99	89.35	Anorthoclase	15

Plug 1: MC-5-16

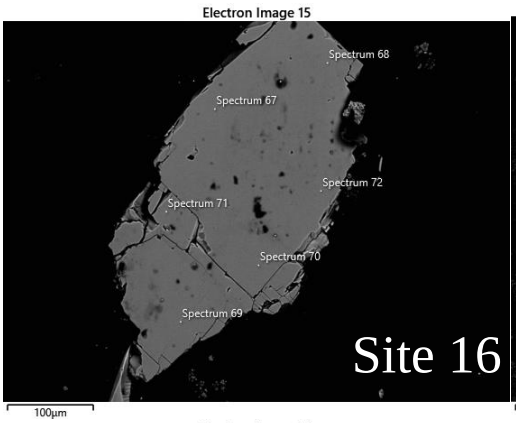
Electron Image 15
Spectrum 68
Spectrum 67
Spectrum 72
Spectrum 71
Spectrum 70
Spectrum 69
Site 16
100µm

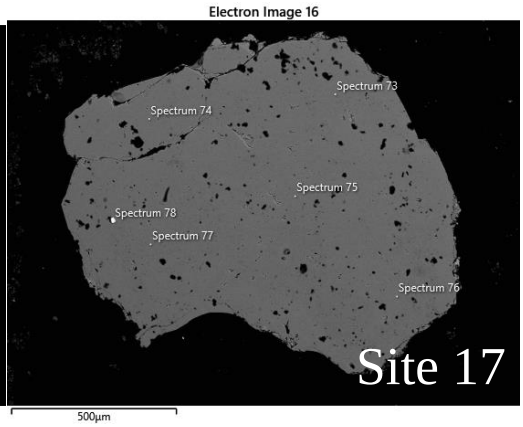
Electron Image 16
Spectrum 73
Spectrum 74
Spectrum 75
Spectrum 78
Spectrum 77
Spectrum 76
Site 17
500µm

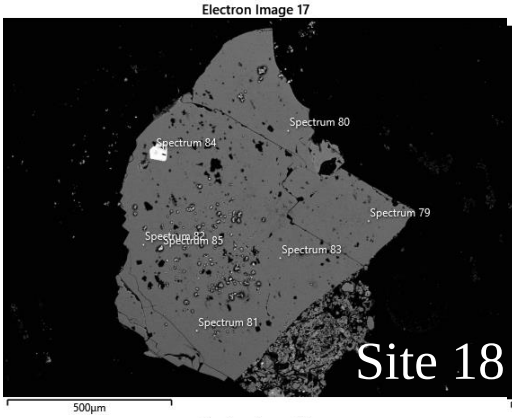
Electron Image 17
Spectrum 80
Spectrum 84
Spectrum 79
Spectrum 85
Spectrum 83
Spectrum 81
Site 18
500µm

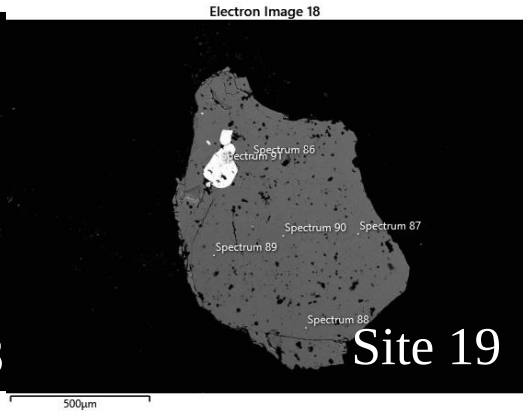
Electron Image 18
Spectrum 86
Spectrum 91
Spectrum 90
Spectrum 87
Spectrum 89
Spectrum 88
Site 19
500µm

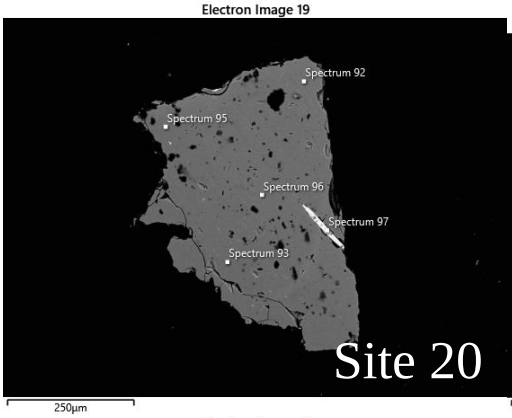
Electron Image 19
Spectrum 92
Spectrum 95
Spectrum 96
Spectrum 97
Spectrum 93
Site 20
250µm

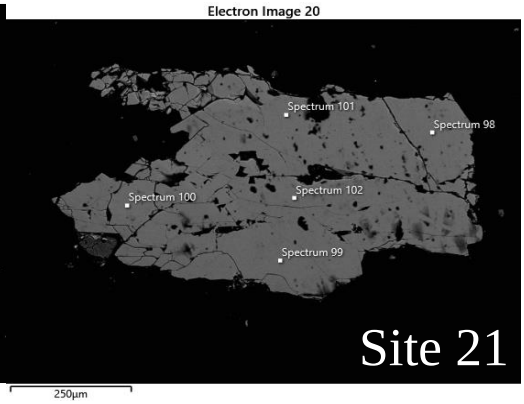
Electron Image 20
Spectrum 101
Spectrum 98
Spectrum 100
Spectrum 102
Spectrum 99
Site 21
250µm

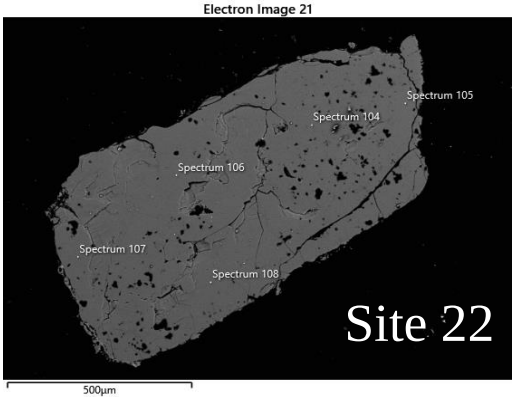
Electron Image 21
Spectrum 105
Spectrum 104
Spectrum 106
Spectrum 107
Spectrum 108
Site 22
500µm

Plug 1: MC-5-16

Spectrum	Na	Al	Si	P	K	Ca	Ti	Fe	Zr	Total	Phase	Site
67	7.57	21.8	60.3		0.66	4.26				94.57	Plagioclase	16
68	7.71	21.8	60.8		0.61	3.99				94.88	Plagioclase	16
69	7.44	21.2	58.8		0.66	4				92.13	Plagioclase	16
70	7.24	21	58.8		0.68	4.02				91.79	Plagioclase	16
71	7.68	21.3	60		0.62	3.7				93.26	Plagioclase	16
72	7.39	21.1	58.8		0.62	4.05				91.97	Plagioclase	16
73	7.66	21.2	60.4		0.65	4.03				94.37	Plagioclase	17
74	7.73	21.5	60.5		0.62	4.09				94.4	Plagioclase	17
75	7.48	21.6	59.6		0.52	4.17				93.37	Plagioclase	17
76	7.38	21.4	58.4		0.63	4.13				91.98	Plagioclase	17
77	7.32	21.2	58.4		0.67	4.06				91.61	Plagioclase	17
78			30.1						62.7	94	Zircon	17
79	7.36	21.3	59.1		0.66	4.06				92.49	Plagioclase	18
80	7.56	21.8	60		0.6	4.01				93.98	Plagioclase	18
81	7.14	20.7	57.4		0.64	4.06				89.92	Plagioclase	18
82	7.45	21.1	59.7		0.58	3.81				92.65	Plagioclase	18
83	7.6	21.2	59.9		0.65	3.9				93.2	Plagioclase	18
84		0.92					17.4	72.6		91.78	Ilmenite	18
86	7.55	21.7	59.6		0.66	4.33				93.87	Plagioclase	19
87	7.56	21.4	59.8		0.61	3.86				93.19	Plagioclase	19
88	7.26	20.8	58.1		0.67	4.02				90.82	Plagioclase	19
89	7.56	20.8	59.3		0.68	3.78				92.1	Plagioclase	19
90	7.52	21.2	59.1		0.58	3.96				92.35	Plagioclase	19
91		2.52	4.56			0.63	20.2	55.1		84.13	Ilmenite	19
92	2.2	11.2	71.7		4.42	0.64		1.27		91.47	Anorthoclase	20
93	2.16	11	70.5		4.43	0.51		1.15		89.79	Anorthoclase	20
95	2.09	11.3	71.7		4.57	0.55		1.13		91.3	Anorthoclase	20
96	2.11	11.1	71		4.35	0.61		1.89		90.98	Anorthoclase	20
97			1.21	37.1		49.5				87.8	Apatite	20
98	7.57	21.4	59.9		0.64	4.07		0.3		93.91	Plagioclase	21
99	7.43	20.5	59.4		0.78	3.48				91.58	Plagioclase	21
100	7.68	21.3	60.4		0.65	3.74				93.72	Plagioclase	21
101	7.93	21.5	61		0.63	3.66		0.37		95.05	Plagioclase	21
102	7.62	21.2	60.5		0.62	3.85				93.81	Plagioclase	21
104	7.46	21.3	59.6		0.59	3.93				92.83	Plagioclase	22
105	7.61	21.2	59.7		0.63	3.75				92.83	Plagioclase	22
106	7.72	20.8	59.2		0.82	3.47		0.28		92.33	Plagioclase	22
107	7.51	20.6	58.8		0.67	3.69				91.26	Plagioclase	22
108	7.88	21.2	60.5		0.65	3.59				93.76	Plagioclase	22

Plug 1: MC-3-BC

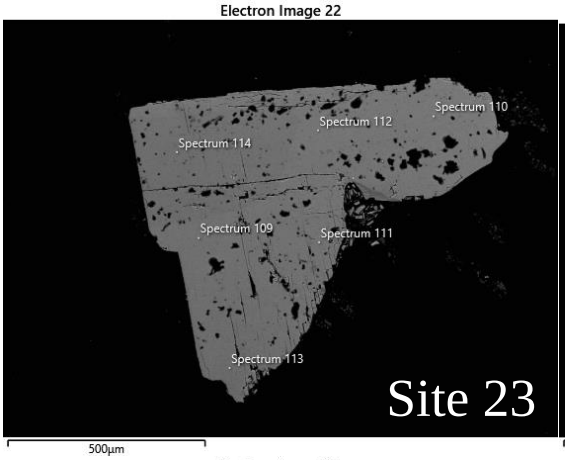
Electron Image 22
Spectrum 110
Spectrum 112
Spectrum 114
Spectrum 109
Spectrum 111
Spectrum 113
Site 23
500µm

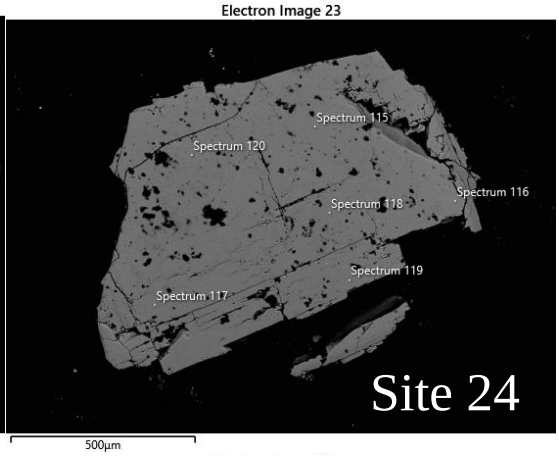
Electron Image 23
Spectrum 115
Spectrum 120
Spectrum 116
Spectrum 118
Spectrum 119
Spectrum 117
Site 24
500µm

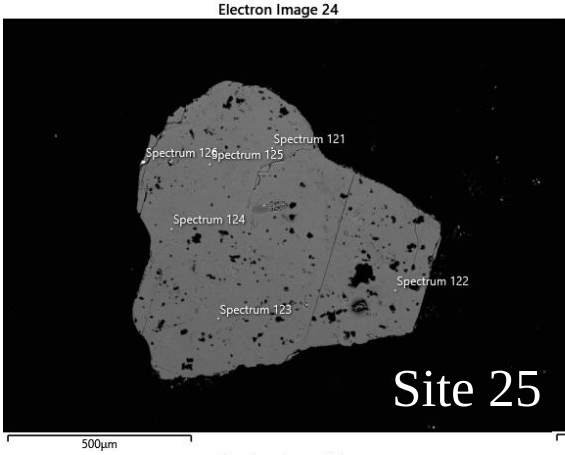
Electron Image 24
Spectrum 121
Spectrum 126
Spectrum 125
Spectrum 124
Spectrum 122
Spectrum 123
Site 25
500µm

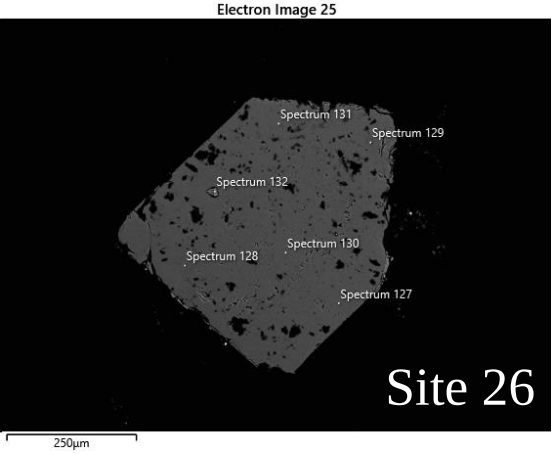
Electron Image 25
Spectrum 131
Spectrum 129
Spectrum 132
Spectrum 130
Spectrum 128
Spectrum 127
Site 26
250µm

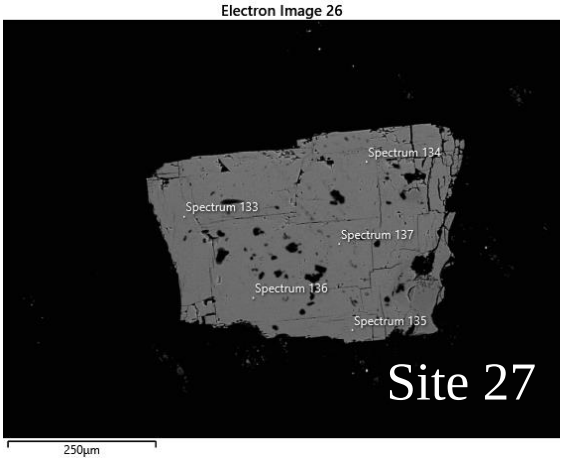
Electron Image 26
Spectrum 134
Spectrum 133
Spectrum 137
Spectrum 136
Spectrum 135
Site 27
250µm

Plug 1: MC-3-BC

Spectrum	Na	Al	Si	K	Ca	Fe	Zr	Ba	Total	Phase	Site
109	6.5	18.2	60.9	4.35	0.62	0.34		1.58	92.42	Anorthoclase	23
110	6.66	18.4	62.2	4.51	0.57	0.28		1.48	94.14	Anorthoclase	23
111	6.39	18	61	4.31	0.6			1.59	91.81	Anorthoclase	23
112	6.64	18.4	62.1	4.41	0.66			1.63	93.85	Anorthoclase	23
113	6.27	17.4	59.5	4.28	0.57			1.4	89.42	Anorthoclase	23
114	6.49	17.9	62.7	4.66				0.97	92.7	Anorthoclase	23
115	6.6	18.3	62.2	4.59	0.53			1.46	93.63	Anorthoclase	24
116	6.14	17.9	60.8	4.67	0.49			1.62	91.61	Anorthoclase	24
117	6.28	17.7	60.5	4.43	0.51			1.41	90.76	Anorthoclase	24
118	6.48	18.1	61.8	4.47	0.57			1.48	92.83	Anorthoclase	24
119	6.29	17.7	60.5	4.3	0.53			1.28	90.67	Anorthoclase	24
120	6.38	18.1	62.2	4.47				1.45	92.56	Anorthoclase	24
121	7.26	19	61.5	2.85	1.19			1.72	93.55	Anorthoclase	25
122	7.19	18.7	60.4	2.84	1.07			1.48	91.73	Anorthoclase	25
123	7.05	18.5	60.6	2.84	1.07			1.62	91.74	Anorthoclase	25
124	7.03	18.7	60.6	2.99	1.05			1.7	92.01	Anorthoclase	25
125	7.34	19.2	62	2.94	1.11			1.59	94.18	Anorthoclase	25
126			30.2				63.3		93.53	Zircon	25
127			93.6						93.59	Quartz	26
128			94.3						94.33	Quartz	26
129			96.1						96.14	Quartz	26
130			95.3						95.29	Quartz	26
131			96.2						96.15	Quartz	26
133	5.93	17.9	61.9	5.74				1.12	92.64	Anorthoclase	27
134	6.08	18.3	63	5.96				1.11	94.4	Anorthoclase	27
135	5.52	17.4	59.9	5.72				1.04	89.56	Anorthoclase	27
136	5.65	17.4	60.5	5.78				1	90.41	Anorthoclase	27
137	5.88	17.8	61.7	5.9		0.34		0.97	92.56	Anorthoclase	27

Plug 1: MC2B

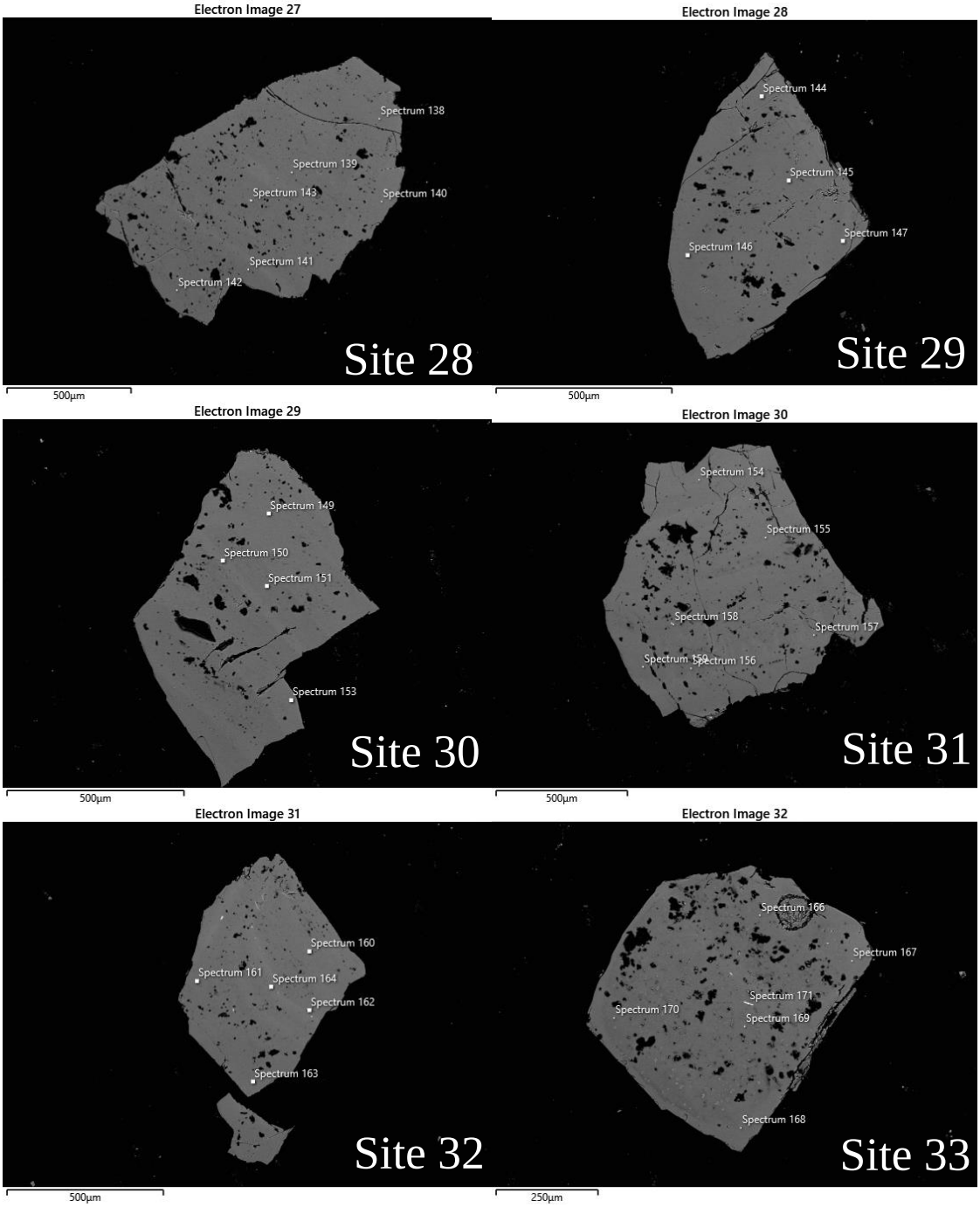
Electron Image 27
Spectrum 138
Spectrum 139
Spectrum 143
Spectrum 140
Spectrum 141
Spectrum 142
Site 28
500µm
Electron Image 28
Spectrum 144
Spectrum 145
Spectrum 147
Spectrum 146
Site 29
500µm
Electron Image 29
Spectrum 149
Spectrum 150
Spectrum 151
Spectrum 153
Site 30
500µm
Electron Image 30
Spectrum 154
Spectrum 155
Spectrum 158
Spectrum 157
Spectrum 159
Spectrum 156
Site 31
500µm
Electron Image 31
Spectrum 160
Spectrum 161
Spectrum 164
Spectrum 162
Spectrum 163
Site 32
500µm
Electron Image 32
Spectrum 166
Spectrum 167
Spectrum 171
Spectrum 170
Spectrum 169
Spectrum 168
Site 33
250µm

Plug 1: MC2B

Spectrum	Na	Mg	Al	Si	K	Ca	Ti	Fe	Total	Phase	Site
138	6.55		23.3	57.1	0.27	6.3			93.56	Plagioclase	28
139	6.2		23.9	55.9	0.27	6.91			93.14	Plagioclase	28
140	5.79		24.5	53	0.25	7.69		0.28	91.48	Plagioclase	28
141	6.23		22.7	54.7	0.31	6.34			90.28	Plagioclase	28
142	5.86		22.9	53.6	0.25	6.49			89.11	Plagioclase	28
143	6.28		23.8	55.7	0.27	7.06			93.1	Plagioclase	28
144	6.53		24.5	57.2	0.27	6.78			95.35	Plagioclase	29
145	6.09		23.7	55.2	0.28	7.13			92.43	Plagioclase	29
146	6.41		23.1	55.5	0.28	6.41			91.67	Plagioclase	29
147	6.02		23.3	54.6	0.28	6.82			91.03	Plagioclase	29
149	6.24		24.1	56	0.2	7.12			93.69	Plagioclase	30
150	5.39		25.3	53.6	0.16	8.46			92.9	Plagioclase	30
151	6.36		23.3	56.2	0.26	6.63			92.78	Plagioclase	30
153	5.95		24.1	54.5	0.23	7.21			91.9	Plagioclase	30
154	5.67		26.5	55.1	0.18	8.86			96.24	Plagioclase	31
155	6.08		24.9	55.9	0.21	7.27			94.41	Plagioclase	31
156	6.37		22.3	55.3	0.31	5.86			90.08	Plagioclase	31
157	5.32		24.5	52.8	0.19	7.99			90.83	Plagioclase	31
158	6.49		23	56.4	0.27	6.23			92.4	Plagioclase	31
159	6.41		22.7	55.1	0.26	6.05			90.52	Plagioclase	31
160	5.85		24.7	54.7	0.22	7.63			93.08	Plagioclase	32
161	6.02		24.3	55.3	0.36	7.49			93.53	Plagioclase	32
162	4.4	2.36	16	44.6	0.19	6.15		3.65	77.32	Pyroxene	32
163	5.26		24.6	51.7	0.18	8.36			90.07	Plagioclase	32
164	5.12		25.9	52.8	0.23	9.11			93.1	Plagioclase	32
166	6.22		24.2	55	0.22	7.25			92.79	Plagioclase	33
167	5.25		25.2	52.8	0.22	8.65			92.1	Plagioclase	33
168	5.91		23	52.9	0.32	6.86			88.98	Plagioclase	33
169	6.1		23.5	53.9	0.3	7.17			90.94	Plagioclase	33
170	6.52		23	54.3	0.32	6.69			90.86	Plagioclase	33
171			1.92	1.54		0.59	2.86	77.4	84.63	Ilmenite	33

Plug 2: MC1C

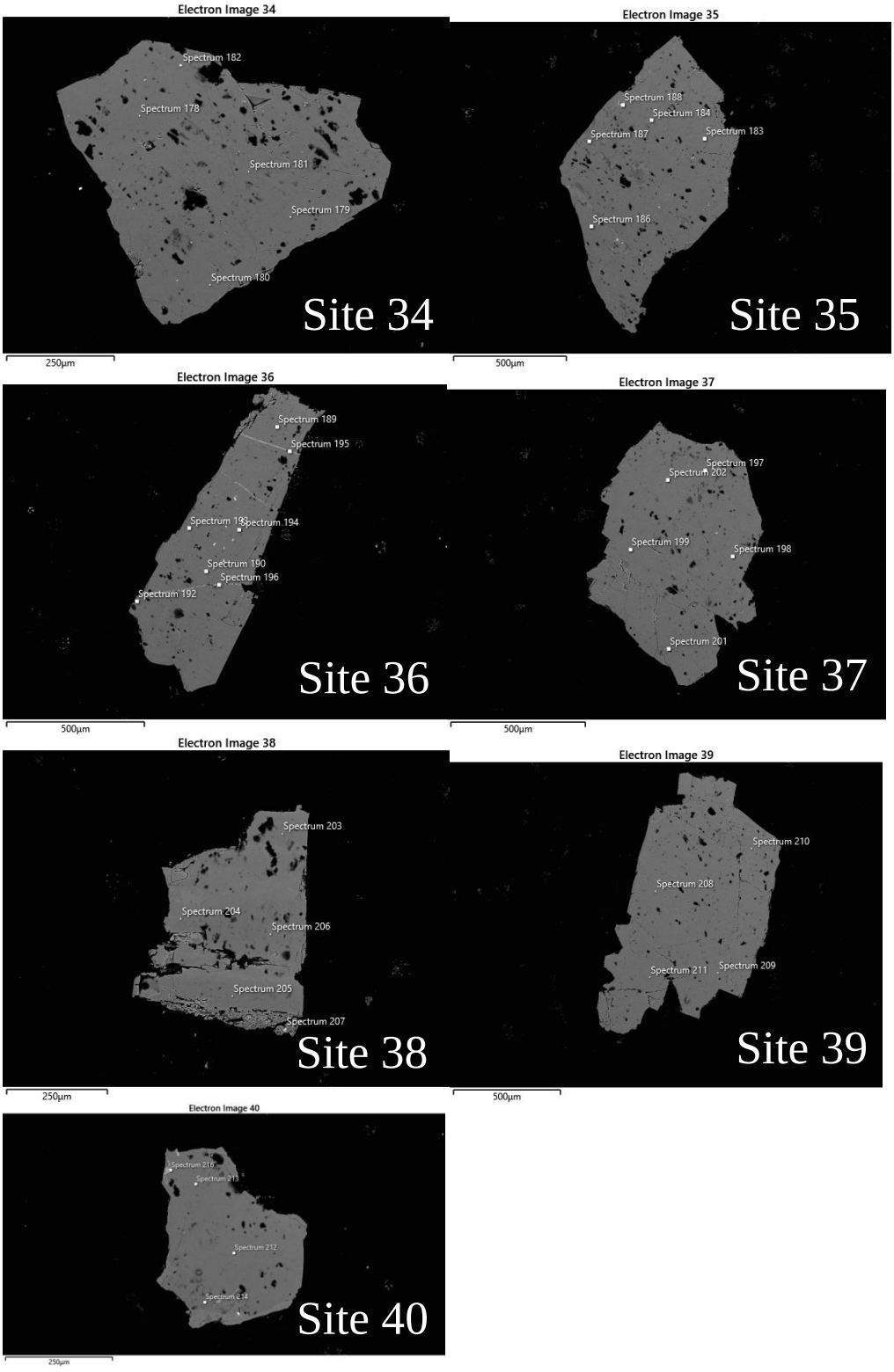
Electron Image 34
Spectrum 182
Spectrum 178
Spectrum 181
Spectrum 179
Spectrum 180
Site 34
250µm
Electron Image 35
Spectrum 188
Spectrum 184
Spectrum 187
Spectrum 183
Spectrum 186
Site 35
500µm
Electron Image 36
Spectrum 189
Spectrum 195
Spectrum 193
Spectrum 194
Spectrum 190
Spectrum 196
Spectrum 192
Site 36
500µm
Electron Image 37
Spectrum 197
Spectrum 202
Spectrum 199
Spectrum 198
Spectrum 201
Site 37
500µm
Electron Image 38
Spectrum 203
Spectrum 204
Spectrum 206
Spectrum 205
Spectrum 207
Site 38
250µm
Electron Image 39
Spectrum 210
Spectrum 208
Spectrum 211
Spectrum 209
Site 39
500µm
Electron Image 40
Spectrum 213
Spectrum 212
Site 40
250µm

Spectrum	Na	Mg	Al	Si	P	S	K	Ca	Ti	V	Mn	Fe	Ba	La	Ce	Nd	Total	Phase	Site
178	7.1		23.2	59.4			0.7	5.33									95.78	Plagioclase	34
179	7.17		21.8	58.6			0.73	4.64									92.89	Plagioclase	34
180	6.88		21.3	57.3			0.77	4.5									90.75	Plagioclase	34
181	7.51		21.7	60.9			0.82	4.16									95.01	Plagioclase	34
182	6.76		19.8	62.3	1.11		3.7	3.05									96.77	Plagioclase	34
183	7.48		22.6	60.4			0.75	4.88				0.36					96.54	Plagioclase	35
184	7.46		23.1	60.7			0.72	5.07									96.96	Plagioclase	35
186	7.18		21.3	57.3			1.19	4.02									90.97	Plagioclase	35
187	7.75		21.9	61.9			1.17	3.75									96.47	Plagioclase	35
188			2.07	5.43		30.8	0.87	0.38					60.8				100.35	Baryte	35
189	7.66		22.7	61.8			0.7	4.67									97.47	Plagioclase	36
190	7.2		22.7	59			0.67	5.06									94.58	Plagioclase	36
192	0.2		0.39	1.55	37.1			49				0.35					88.57	Apatite	36
193	7.38		23	60.6			0.73	5.26									96.94	Plagioclase	36
194				1.09	38.2			50.6									91.08	Apatite	36
195	1.95	0.86	6.08	32.6	0.47		0.72	1.06				41.6			0.44		85.79	Fe-oxide	36
196	3.77		10.8	36.8	0.62		0.48	1.88				32.1			0.63		87.04	Fe-oxide	36
197	7.27		23.2	60.2			0.67	5.34									96.71	Plagioclase	37
198	6.88		22.6	58			0.53	5.47									93.48	Plagioclase	37

Plug 2: MC1C

199	7.01		22.8	58.9		0.67	5.16						94.47	Plagioclase	37
201				0.75	35.7		47.8			0.35			84.54	Apatite	37
202	0.69		1.6	4.83	36.9		48.7					0.81	94.89	Apatite	37
203	7.09		24.4	59.2		0.31	6.34						97.26	Plagioclase	38
204	6.55		24.4	56.7		0.28	7						94.89	Plagioclase	38
205	6.39		22.4	55.1		0.37	5.93						90.15	Plagioclase	38
206	6.67		23.3	56.8		0.28	6.37						93.35	Plagioclase	38
207		0.87	1.13	0.49	1.31		1.82	3.55	0.68	0.28	72.4		82.53	Fe-oxide	38
208	7.26		22.9	60.7		0.8	5.07						96.73	Plagioclase	39
209	6.89		21.6	57.1		0.7	4.86						91.1	Plagioclase	39
210	7.71		22.3	61.5		0.83	4.27						96.58	Plagioclase	39
211	6.99		21.3	57.1		0.66	4.5						90.47	Plagioclase	39
212	7.23		22.9	59.2		0.68	5.23					0.43	95.6	Plagioclase	40
213	7.52		23.2	60.4		0.73	5.16						96.93	Plagioclase	40
214	6.96		21	58.2		1.14	4.21						91.54	Plagioclase	40
216	2.2		7.41	44.4	10.4	0.37	2.8					4.17	89.21	Quartz?	40

Plug 2: MC4C

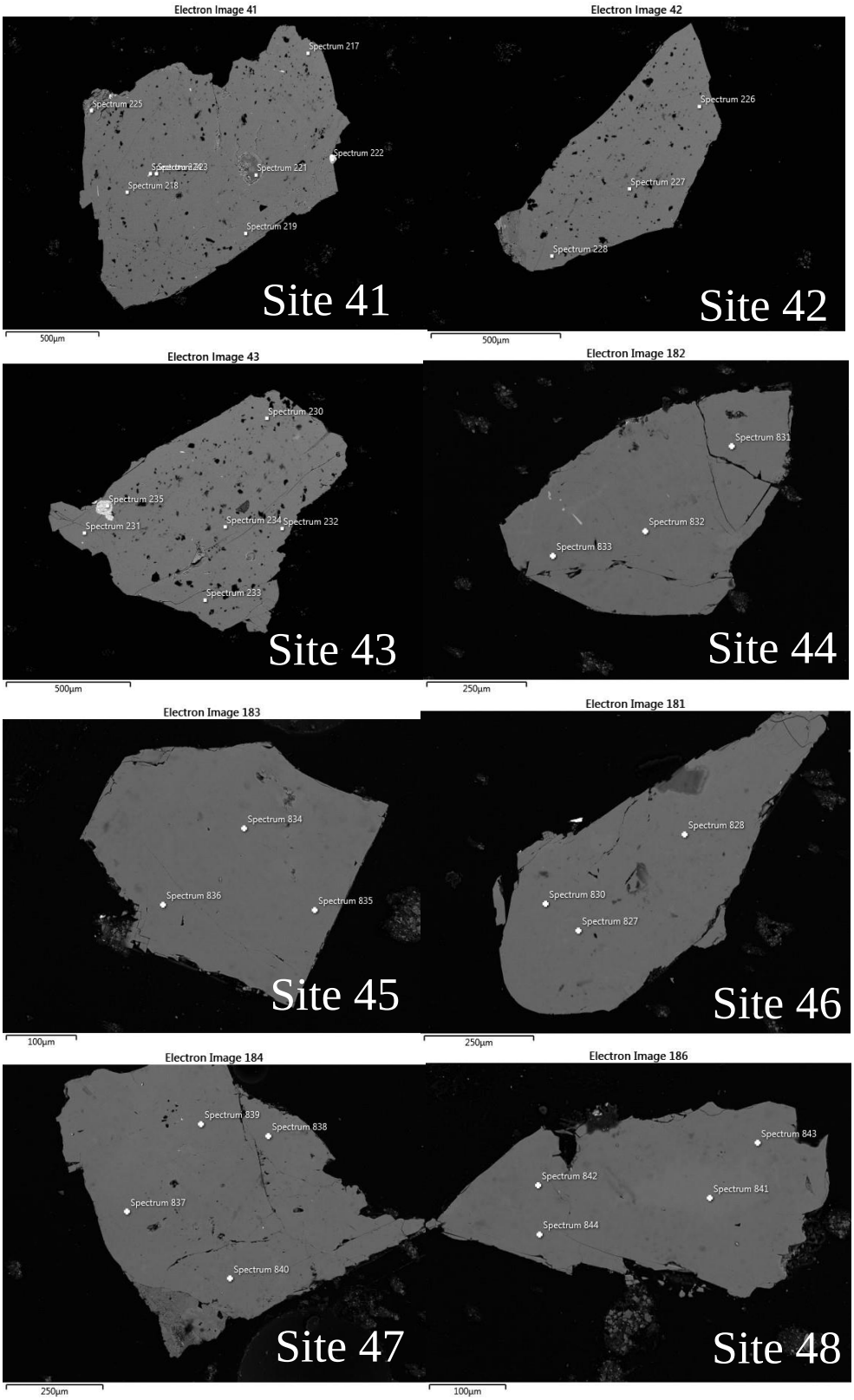
Electron Image 41
Spectrum 217
Spectrum 225
Spectrum 222
Spectrum 221
Spectrum 218
Spectrum 219
Site 41
500µm
Electron Image 42
Spectrum 226
Spectrum 227
Spectrum 228
Site 42
500µm
Electron Image 43
Spectrum 230
Spectrum 235
Spectrum 231
Spectrum 234
Spectrum 232
Spectrum 233
Site 43
500µm
Electron Image 182
Spectrum 831
Spectrum 832
Spectrum 833
Site 44
250µm
Electron Image 183
Spectrum 834
Spectrum 836
Spectrum 835
Site 45
100µm
Electron Image 181
Spectrum 828
Spectrum 830
Spectrum 827
Site 46
250µm
Electron Image 184
Spectrum 839
Spectrum 838
Spectrum 837
Spectrum 840
Site 47
250µm
Electron Image 186
Spectrum 843
Spectrum 842
Spectrum 841
Spectrum 844
Site 48
100µm

Plug 2: MC4C

Spectrum	Na	Al	Si	P	K	Ca	Ti	Fe	Total	Phase	Site
217	7.4	23.9	61.3		0.56	5.61			98.79	Plagioclase	41
218	6.82	22.1	57.2		0.54	5.25		0.33	92.25	Plagioclase	41
219	6.49	21.7	55.4		0.55	5.2		0.35	89.69	Plagioclase	41
221			96						95.98	Quartz	41
222		1.19	1				19.1	62.8	85.41	Ilmenite	41
223		0.97	0.19			0.18	22.8	66.8	91.74	Ilmenite	41
224			1.12	36.9		49.4			88.19	Apatite	41
225		4.38	14.3		0.15	0.56	0.53	64.5	84.46	Fe-oxide	41
226	7.12	23.5	59.8		0.57	5.59			96.64	Plagioclase	42
227	7.01	22.7	58.6		0.57	5.31			94.19	Plagioclase	42
228	6.61	21	54.7		0.55	5.04		0.28	88.14	Plagioclase	42
230	7.44	23.5	61.2		0.63	5.3		0.43	98.49	Plagioclase	43
231	6.7	22.2	56.7		0.54	5.38			91.57	Plagioclase	43
232	6.71	22.7	57.2		0.5	5.48			92.57	Plagioclase	43
233	6.28	21.4	54.6		0.52	5.25		0.28	88.38	Plagioclase	43
234	7	22.7	58.4		0.51	5.37			94	Plagioclase	43
235		3.04	17.1		0.12	1.13	51.8	6.89	80.93	Ilmenite	43
827	7.35	23.9	62.6		0.75	5.35			100	Plagioclase	44
828	7.49	23.2	63.6		0.77	4.95			100	Plagioclase	44
830	7.36	24	62.5		0.59	5.56			100	Plagioclase	44
831	7.24	23.7	62.8		0.63	5.58			100	Plagioclase	45
832	7.59	22.8	64.3		0.73	4.61			100	Plagioclase	45
833	7.31	23.6	62.5		0.63	5.53		0.4	100	Plagioclase	45
834	7.27	24.2	62.3		0.56	5.68			100	Plagioclase	46
835	7.28	24	62.5		0.57	5.72			100	Plagioclase	46
836	7.42	24	62.5		0.54	5.6			100	Plagioclase	46
837	7.18	24.8	61.2		0.41	6.48			100	Plagioclase	47
838	6.81	25.4	60.6		0.32	6.91			100	Plagioclase	47
839	6.47	25.8	59.6		0.3	7.82			100	Plagioclase	47
840	6.81	25.5	60.2		0.37	7.06			100	Plagioclase	47
841	7.64	23.6	62.5		0.59	5.26		0.48	100	Plagioclase	48
842	7.37	24	61.8		0.6	5.77		0.48	100	Plagioclase	48
843	7.27	23.7	62.7		0.65	5.31			100	Plagioclase	48
844	7.25	24.1	62.2		0.56	5.88			100	Plagioclase	48

Plug 2: MC-115-16

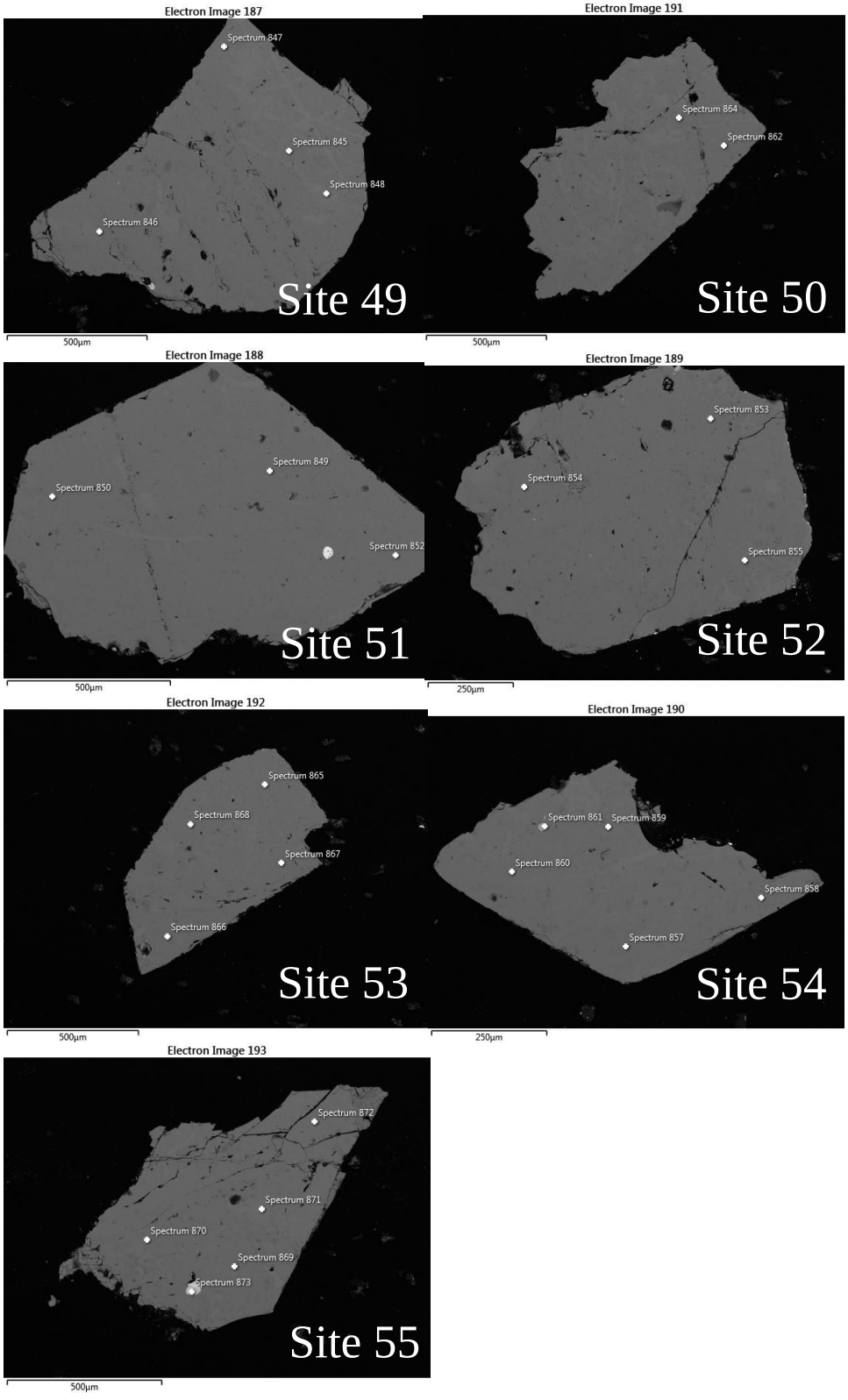

Plug 2: MC-115-16

Spectrum	Na	Al	Si	P	K	Ca	Ti	Mn	Fe	Total	Mineral	Site
845	7.18	24.2	61.8		0.58	5.87			0.44	100	Plagioclase	49
846	7.28	24.2	62.1		0.58	5.94				100	Plagioclase	49
847	7.42	23.8	62.6		0.57	5.61				100	Plagioclase	49
848	7.34	23.9	62		0.64	5.58			0.54	100	Plagioclase	49
862	7.43	23.8	62.7		0.6	5.53				100	Plagioclase	50
864	7.54	23.3	63		0.68	5			0.46	100	Plagioclase	50
849	7.19	24	62.6		0.6	5.66				100	Plagioclase	51
850	7.35	23.9	62		0.6	5.67			0.46	100	Plagioclase	51
852	7.33	24	62.6		0.63	5.42				100	Plagioclase	51
853	7.48	24.1	61.6		0.66	5.62			0.53	100	Plagioclase	52
854	7.43	24.2	62		0.7	5.72				100	Plagioclase	52
855	7.54	23.8	62.7		0.75	5.32				100	Plagioclase	52
865	7.59	23.4	63.1		0.66	5.22				100	Plagioclase	53
866	7.24	23.6	62.6		0.64	5.3			0.54	100	Plagioclase	53
867	7.56	23.7	62.7		0.6	5.46				100	Plagioclase	53
868	7.53	23.8	62.1		0.63	5.37			0.57	100	Plagioclase	53
857	7.48	23.7	62.8		0.64	5.41				100	Plagioclase	54
858	7.2	24.1	62.2		0.6	5.93				100	Plagioclase	54
859	7.15	24.3	61.9		0.65	5.97				100	Plagioclase	54
860	7.43	23.8	62.5		0.67	5.55				100	Plagioclase	54
861			0.69	41.9		54.9				97.44	Apatite	54
869	7.39	24.1	62.2		0.63	5.64				100	Plagioclase	55
870	7.43	23.8	62.5		0.58	5.7				100	Plagioclase	55
871	7.51	23.8	62.4		0.64	5.62				100	Plagioclase	55
872	7.2	24.2	62.1		0.63	5.83				100	Plagioclase	55
873		2.03	7.59			0.77	34.6	1.87	52.3	100	Ilmenite	55

Plug 2: MC4B

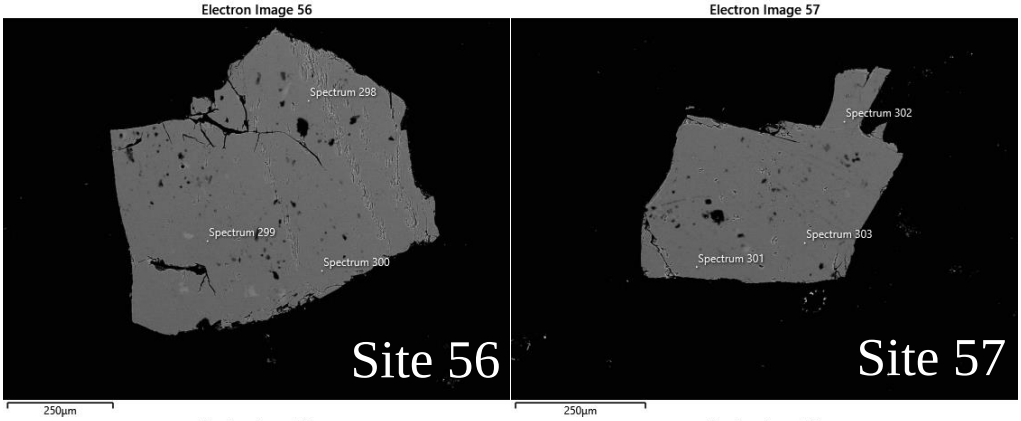
Electron Image 56
Spectrum 298
Spectrum 299
Spectrum 300
Site 56
250µm

Electron Image 57
Spectrum 302
Spectrum 303
Spectrum 301
Site 57
250µm

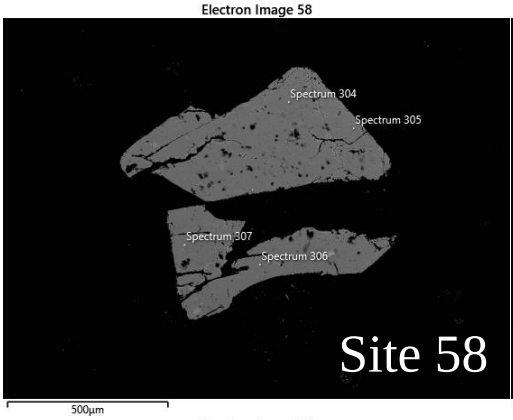
Electron Image 58
Spectrum 304
Spectrum 305
Spectrum 307
Spectrum 306
Site 58
500µm

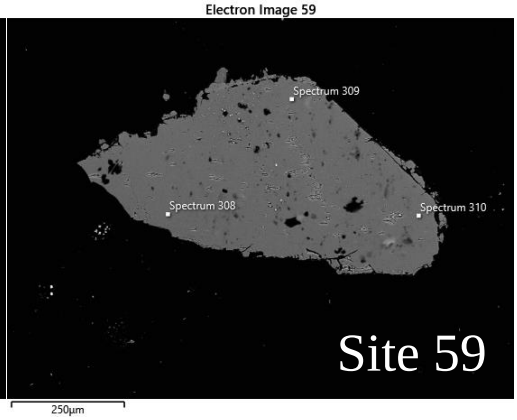
Electron Image 59
Spectrum 309
Spectrum 308
Spectrum 310
Site 59
250µm

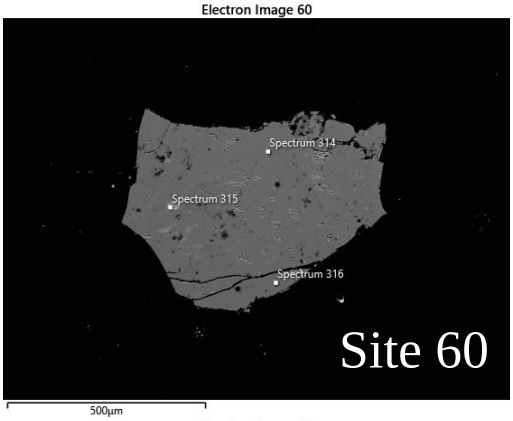
Electron Image 60
Spectrum 314
Spectrum 315
Spectrum 316
Site 60
500µm

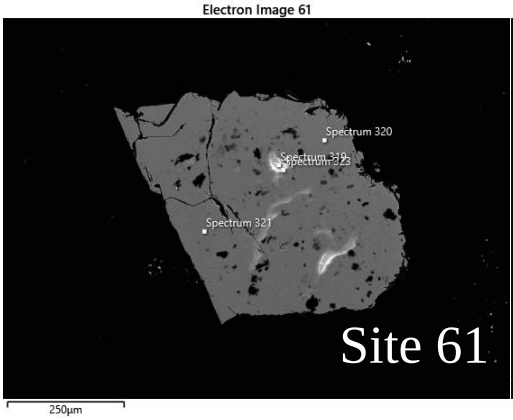
Electron Image 61
Spectrum 320
Spectrum 321
Site 61
250µm

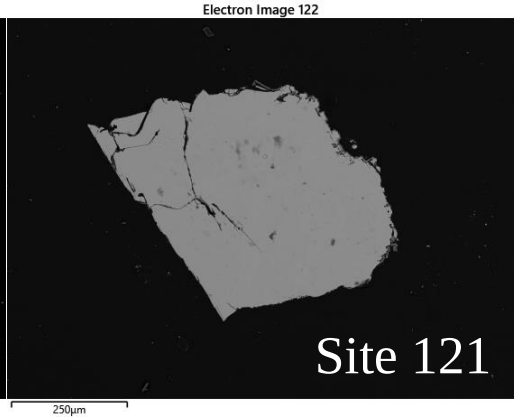
Electron Image 122
Site 121
250µm

Plug 2: MC4B

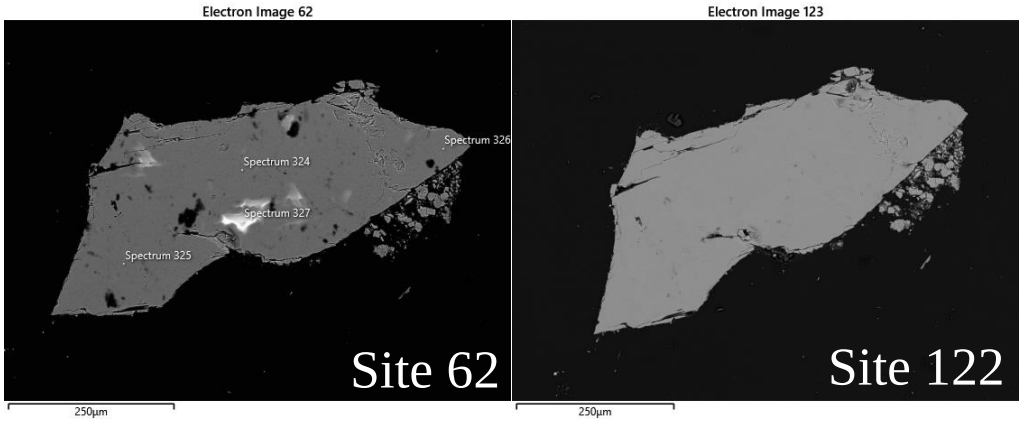

Spectrum	Na	Al	Si	K	Ca	Fe	Ba	Total	Phase	Site
298	8.04	20.4	64.7	1.51	2.09		0.56	97.24	Plagioclase	56
299	8.11	19.9	63	1.42	1.99	0.3	0.54	95.25	Plagioclase	56
300	7.78	19.5	61.7	1.38	1.88		0.45	92.65	Plagioclase	56
301	7.99	19.7	62	1.33	2.03	0.31	0.4	93.72	Plagioclase	57
302	8.65	20.4	64.6	1.5	1.94		0.56	97.59	Plagioclase	57
303	8.19	19.8	63.2	1.5	1.88	0.34	0.52	95.42	Plagioclase	57
304	8.54	20.4	65.4	1.62	1.87		0.7	98.48	Plagioclase	58
305	8.43	20.6	65.3	1.51	2.03	0.37	0.49	98.76	Plagioclase	58
306	8.14	19.6	63.2	1.48	1.92		0.76	95	Plagioclase	58
307	8.14	19.9	63.3	1.63	1.77		0.75	95.44	Plagioclase	58
308	7.66	19.7	62.9	1.39	1.8		0.46	93.88	Plagioclase	59
309	7.94	20.9	64.3	1.28	2.32		0.49	97.24	Plagioclase	59
310	8.03	20.3	62.4	1.21	2.42		0.5	94.85	Plagioclase	59
314	8.38	20.5	64.5	1.26	2.16			96.84	Plagioclase	60
315	8.06	19.2	59.1	1.22	1.88		0.37	89.89	Plagioclase	60
316	7.81	19.7	61.6	1.32	2.1		0.38	92.95	Plagioclase	60
319	8.09	18.7	58.5	1.24	1.72		0.41	88.73	Plagioclase	61
320	8.6	20.5	64.6	1.53	2.13		0.62	97.98	Plagioclase	61
321	8.24	19.8	63.3	1.33	2.05		0.41	95.1	Plagioclase	61
323	8.19	20.1	63.2	1.43	2.01		0.66	95.6	Plagioclase	61
324	7.9	20.3	64.2	1.45	2	0.31	0.63	96.79	Plagioclase	62
325	7.88	19.8	63.2	1.5	1.91			94.33	Plagioclase	62
326	7.49	20	64.3	1.44	1.71		0.57	95.48	Plagioclase	62
327	7.69	18.5	58.1	1.2	1.66			87.16	Plagioclase	62

Site 121 = Site 61, Site 122 = Site 62

Plug 2: MC-114-16

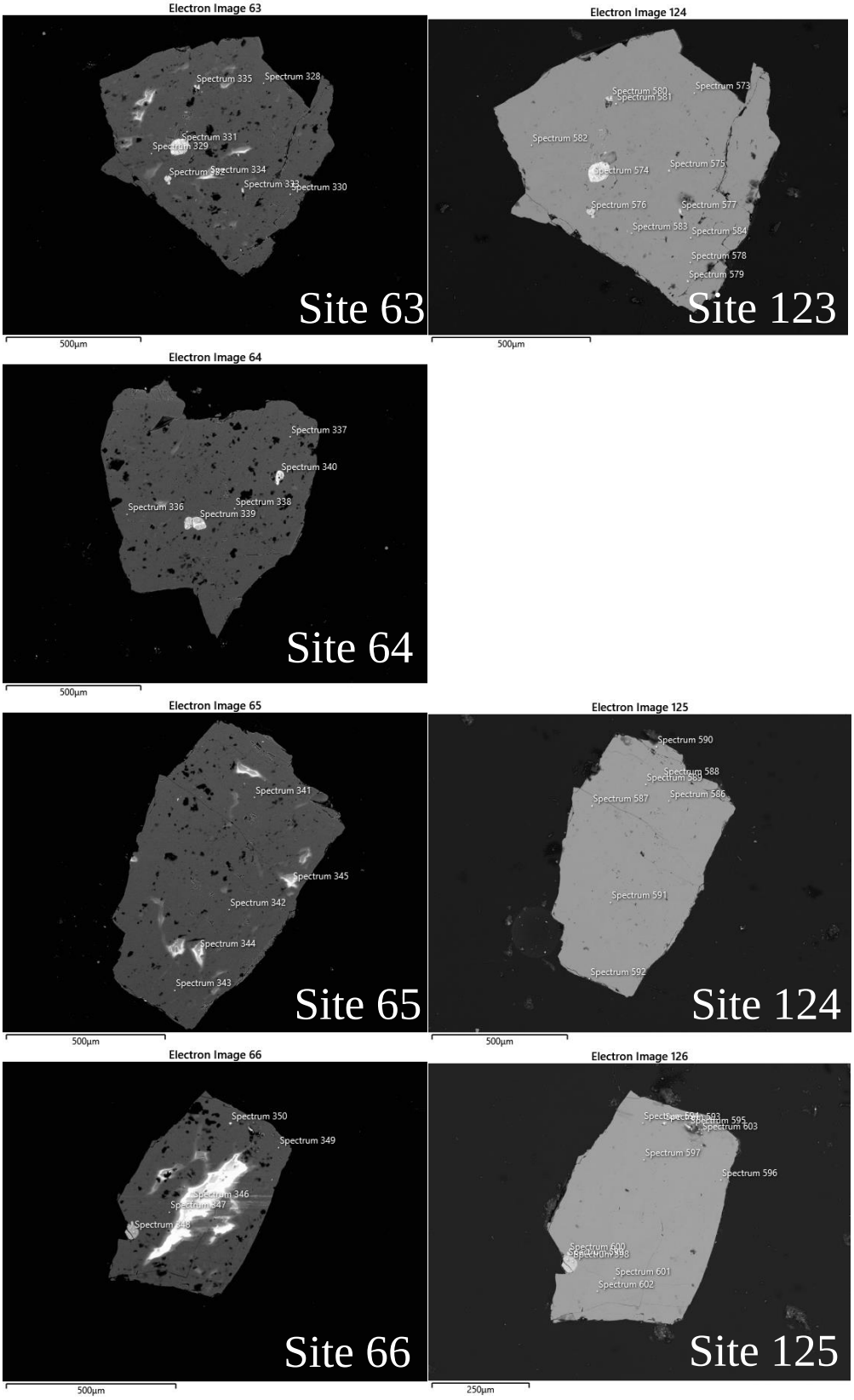

Plug 2: MC-114-16

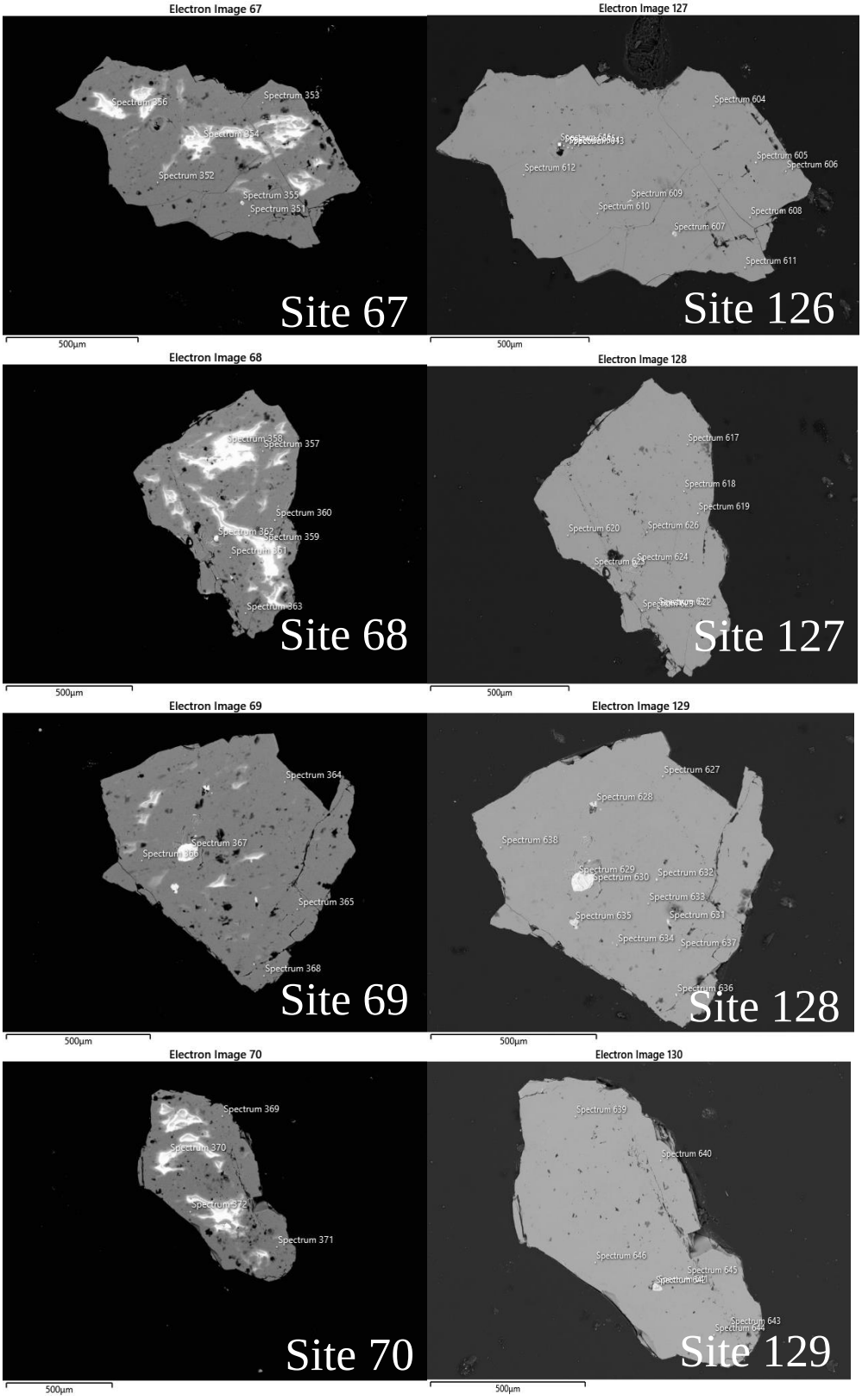

Plug 2: MC-114-16

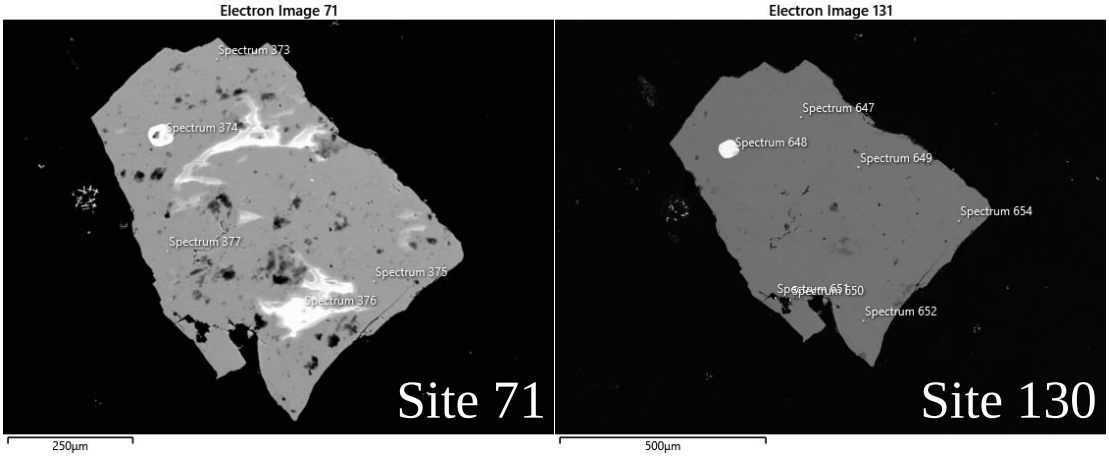

Spectrum	Na	Al	Si	P	K	Ca	Ti	Mn	Fe	Cu	Zn	Ba	Ce	Nd	Os	Total	Phase	Site
328	7.31	23.7	61.3		0.58	5.47			0.37							98.7	Plagioclase	63
329	7.21	23.3	59.2		0.59	5.67			0.32							96.26	Plagioclase	63
330	6.95	23.1	58.7		0.6	5.57										94.97	Plagioclase	63
331		1.72	11.2		0.16	1.84	35.8	1.65	37							89.38	Ilmenite	63
332			0.73	38.8		51.7										91.22	Apatite	63
333			0.7	38.5		51.1			0.56							90.85	Apatite	63
335			0.56	38.7		52.1										91.37	Apatite	63
336	7.08	23.1	59.4		0.62	5.44										95.62	Plagioclase	64
337	7.17	23.7	60.9		0.61	5.61										98.02	Plagioclase	64
338	7.42	23.6	60.5		0.6	5.54										97.63	Plagioclase	64
339		2.29	22.9		0.22	3.24	44.8	0.52	10.9		0.98					86.16	Ilmenite	64
340		1.62	7.3		0.14	0.94	30.7	1.03	49		1.12					91.86	Ilmenite	64
341	7.26	23.1	59.9		0.65	5.58										96.56	Plagioclase	65
342	7.21	22.9	59.5		0.54	5.25			0.31							95.72	Plagioclase	65
343	6.65	21.7	55.8		0.55	5.28			0.31							90.35	Plagioclase	65
346	7.3	21.5	56.3		0.51	4.54										90.21	Plagioclase	66
347	7.42	22.7	59.9		0.62	5.1										95.77	Plagioclase	66
348		2.31	24.1		0.21	3.98	45.9	0.38	2.04		0.75	1.85				81.53	Ilmenite	66
349	7.25	23.2	60.7		0.57	5.53										97.3	Plagioclase	66
350			1.06	39.3		51.6			0.39							92.38	Apatite	66
351	6.77	22.3	57.5		0.56	5.3										92.36	Plagioclase	67
352	6.82	23	58.6		0.56	5.56										94.52	Plagioclase	67
353	7.66	24	61.3		0.62	5.63										99.19	Plagioclase	67
355			0.8	38.2		50.9										89.87	Apatite	67
357	7.1	23.4	60.2		0.57	5.54			0.31							97.1	Plagioclase	68
358	7.26	21.2	55.3		0.52	4.36										88.57	Plagioclase	68
360	7.05	22.9	59.5		0.61	5.28										95.29	Plagioclase	68

361	7.07	22.7	58.7		0.6	5.26			0.33						94.73	Plagioclase	68
362		1.26	7.05		0.12	1.28	31.2	0.78	42.5		0.77	0.9			85.87	Ilmenite	68
363	6.6	21.6	56		0.56	4.96			0.36						90.11	Plagioclase	68
364	7.35	23.7	60.9		0.57	5.57									98.1	Plagioclase	69
365	6.99	22.8	58		0.46	5.56									93.76	Plagioclase	69
366	7.12	23.1	59.9		0.58	5.48									96.23	Plagioclase	69
367		1.61	12.2		0.16	2.24	37.4	1.27	31.9						86.78	Ilmenite	69
368	6.35	22.2	55.1		0.46	5.8									89.87	Plagioclase	69
369	7.55	24.1	61.7		0.59	5.63			0.34						99.81	Plagioclase	70
371	6.66	22.9	57.7		0.54	5.73									93.56	Plagioclase	70
372	6.88	22.7	57.8		0.49	5.62			0.34						93.89	Plagioclase	70
373	7.83	23.6	62.2		0.7	5.15									99.48	Plagioclase	71
374		0.88					25	0.93	67.7						94.48	Ilmenite	71
375	6.85	22.8	58		0.58	5.74									93.91	Plagioclase	71
377	7.4	22.3	60		0.67	4.63			0.3						95.27	Plagioclase	71
590	0.2	0.37	3.38	32.1		42.7			0.39				0.84	0.91	1.79	83.94	Apatite?	124
592		0.42	3.88			0.19		13.2	85							104.2	Fe-oxide	124
625		0.86	7.82	27.6	0.49	37.8			0.31				1.33	0.84	1.37	78.94	Apatite	127
626	4.87	15.3	35.4		0.3	2.75				44.9						103.56	Copper sulfide?	127
629		0.96	0.63			0.23	23	0.86	53.6							79.31	Ilmenite	128
634	3.54	9.66	19.6		0.14	1.42				56.9						91.57	Copper sulfide?	128

Site 123 = 63, Site 124 = 65, Site 125 = 66, Site 126 = 67, Site 127 = 68, Site 128 = 69, Site 129 = 70, Site 30 = 71

Plug 3: MC-1-16

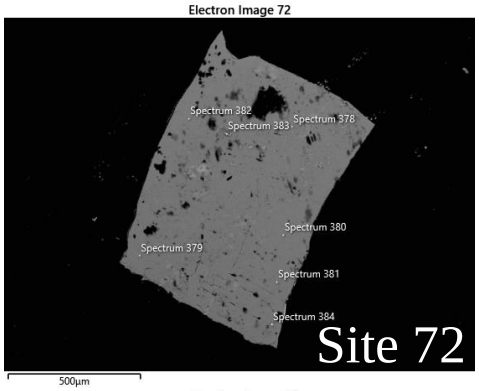
Electron Image 72
Spectrum 382
Spectrum 383
Spectrum 378
Spectrum 380
Spectrum 379
Spectrum 381
Spectrum 384
Site 72
500µm

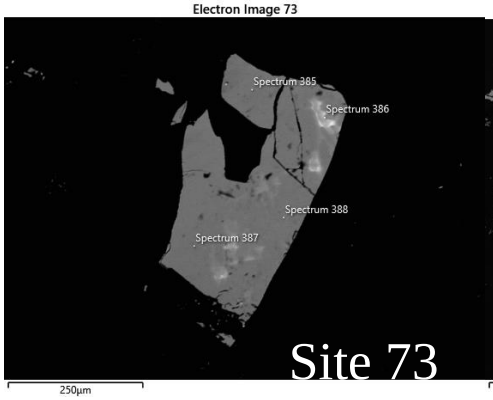
Electron Image 73
Spectrum 385
Spectrum 386
Spectrum 388
Spectrum 387
Site 73
250µm

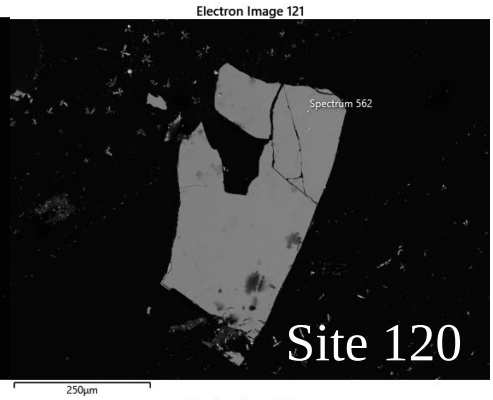
Electron Image 121
Spectrum 562
Site 120
250µm

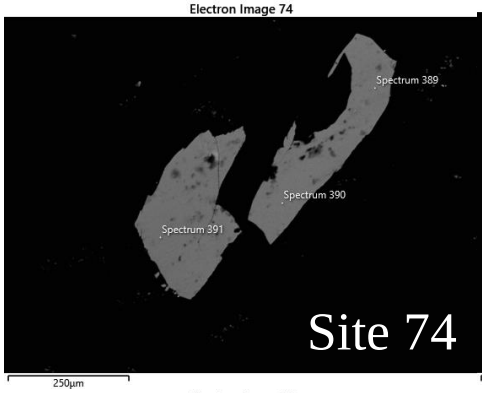
Electron Image 74
Spectrum 389
Spectrum 390
Spectrum 391
Site 74
250µm

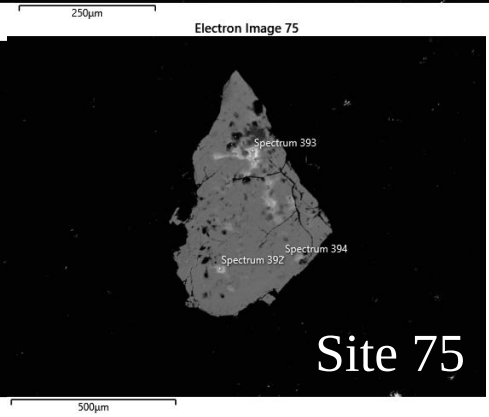
Electron Image 75
Spectrum 393
Spectrum 394
Spectrum 392
Site 75
500µm

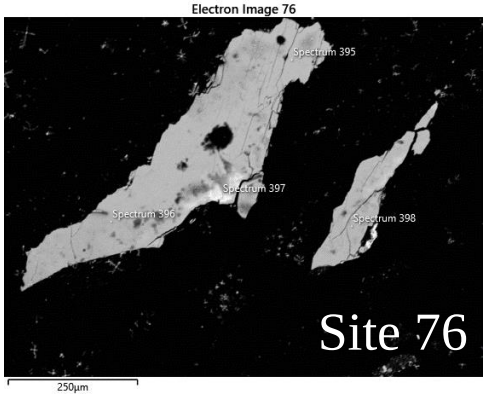
Electron Image 76
Spectrum 395
Spectrum 397
Spectrum 396
Spectrum 398
Site 76
250µm

Plug 3: MC-1-16

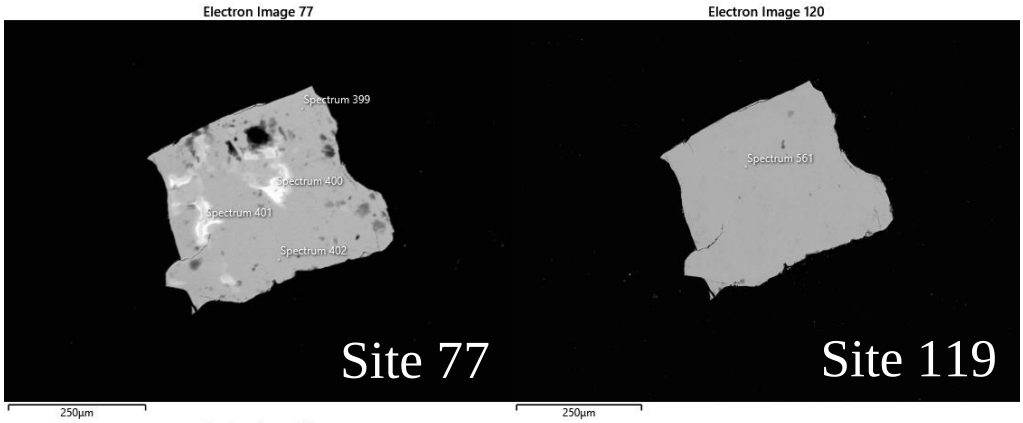
Electron Image 77
Spectrum 399
Spectrum 400
Spectrum 401
Spectrum 402
Site 77
250µm
Electron Image 120
Spectrum 561
Site 119
250µm

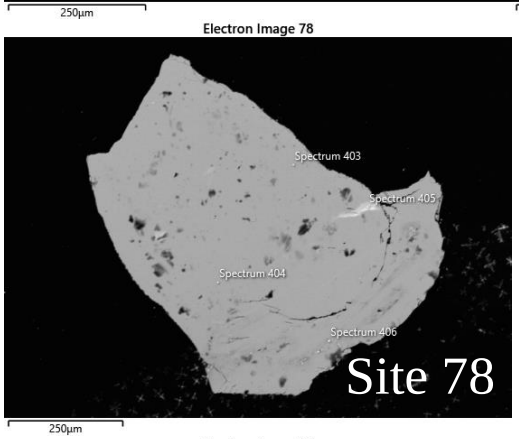
Electron Image 78
Spectrum 403
Spectrum 405
Spectrum 404
Spectrum 406
Site 78
250µm

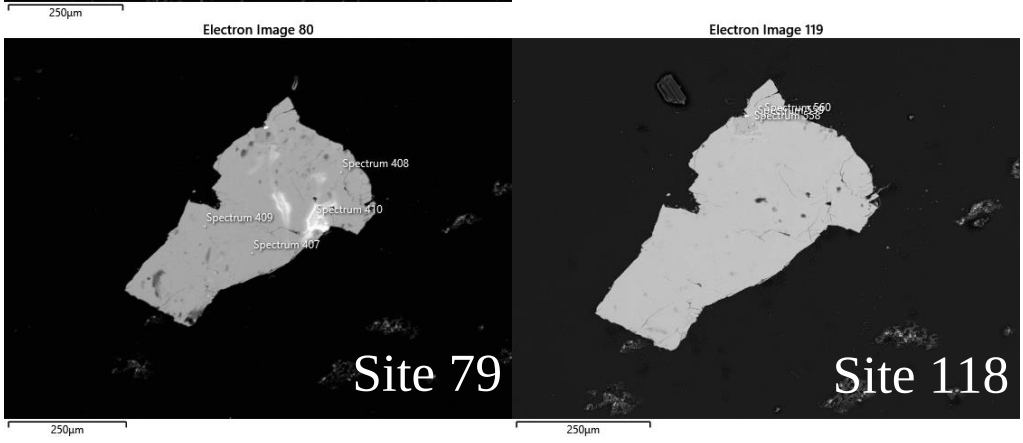
Electron Image 80
Spectrum 408
Spectrum 409
Spectrum 410
Spectrum 407
Site 79
250µm
Electron Image 119
Spectrum 560
Site 118
250µm

Plug 3: MC-1-16

Spectrum	Na	Al	Si	K	Ca	Fe	Ba	Total	Phase	Site
378	8.76	20.5	64.4	1.63	2.06		0.43	97.85	Plagioclase	72
379	8.34	20.4	63.7	1.48	2.06		0.71	96.61	Plagioclase	72
380	8.43	20.2	63.9	1.52	2.04	0.34	0.45	96.84	Plagioclase	72
381	8.26	20.2	63	1.5	2.01			94.98	Plagioclase	72
382	8.69	20.8	65.6	1.8	2.04		0.6	99.48	Plagioclase	72
385	8.6	20.7	65.5	1.71	1.93			98.36	Plagioclase	73
386	8.59	20.4	64.1	1.57	1.86		0.49	97.07	Plagioclase	73
387	8.02	20.2	61.9	1.36	2.1		0.51	94.07	Plagioclase	73
388	8.56	20.5	64	1.27	2.18		0.69	97.19	Plagioclase	73
389	8.56	20.6	65.4	1.68	2.01			98.2	Plagioclase	74
390	8.4	20.6	64.4	1.67	2.25	0.33	0.51	98.13	Plagioclase	74
391	8.2	19.9	63.3	1.71	1.96		0.53	95.61	Plagioclase	74
393	8.19	18.6	58.1	1.27	1.66		0.56	88.29	Plagioclase	75
394	8.33	20.2	63.2	1.81	2.01		0.53	96.1	Plagioclase	75
395	8.11	20.8	65	2.44	2.06		0.55	98.91	Plagioclase	76
396	8.15	20.3	63.3	2.68	1.84		0.57	96.77	Plagioclase	76
397	7.56	19.2	60.2	2.5	1.64		0.43	91.52	Plagioclase	76
398	7.71	19.8	62.3	2.42	2.01	0.34	0.47	95.1	Plagioclase	76
399	8.9	21	66.5	1.63	1.89	0.34	0.59	100.81	Plagioclase	77
401	8.23	19	59.7	1.47	1.79		0.47	90.58	Plagioclase	77
402	8.24	20	63.5	1.59	2.01		0.43	95.82	Plagioclase	77
403	8.83	21	64.5	1.17	2.61	0.33		98.45	Plagioclase	78
404	8.42	20	64.4	1.54	1.91		0.49	96.7	Plagioclase	78
405	8.47	20	58.7	0.88	2.36	0.34		90.82	Plagioclase	78
407	8.12	20.2	64.2	2.06	2.06		0.52	97.15	Plagioclase	79
408	8.34	20.8	65.4	2.49	2.05	0.29		99.37	Plagioclase	79
409	8.21	20.6	65	2.34	1.94			98.16	Plagioclase	79

Site 118 = 79, Site 119 = 77, Site 120 = 72

Plug 3: MC-68-16

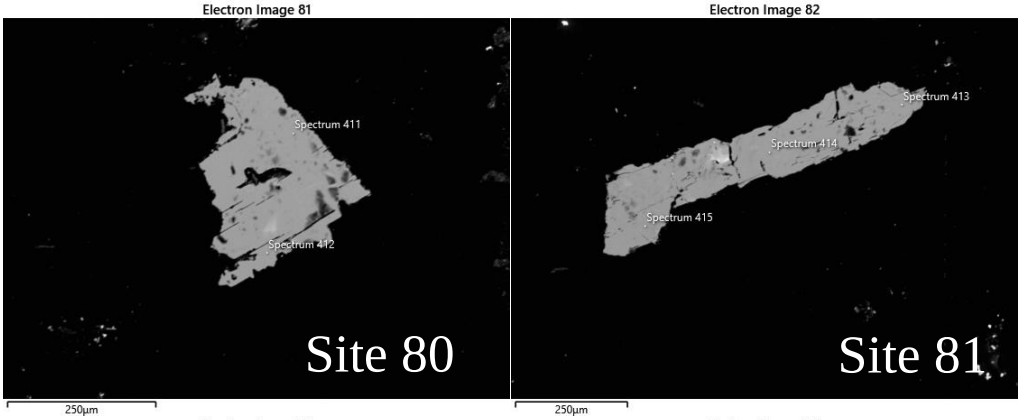

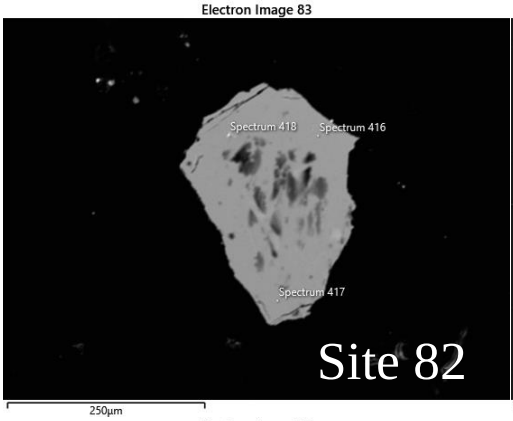

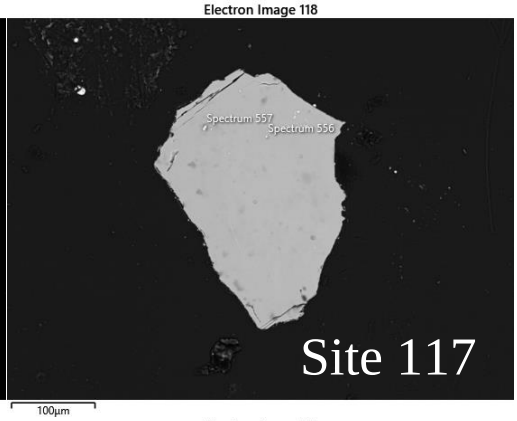

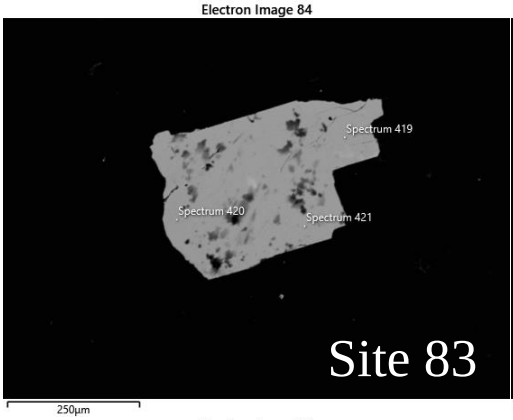

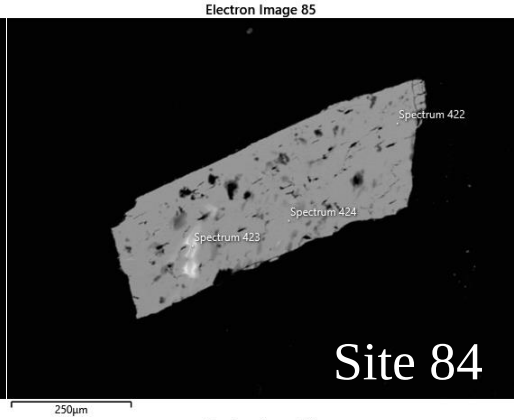

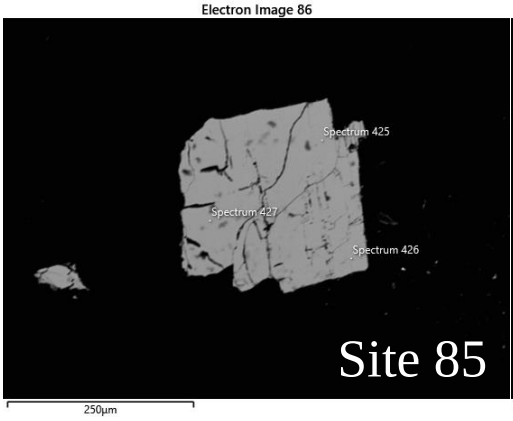

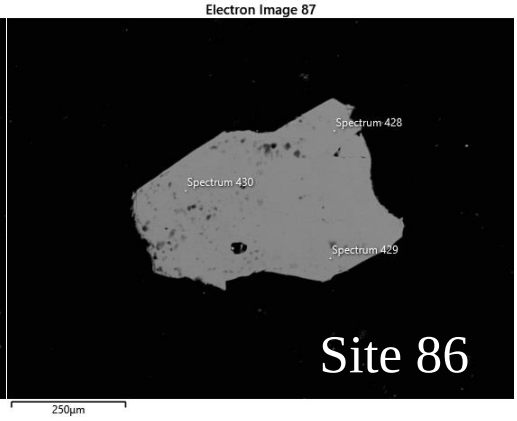

Plug 3: MC-68-16

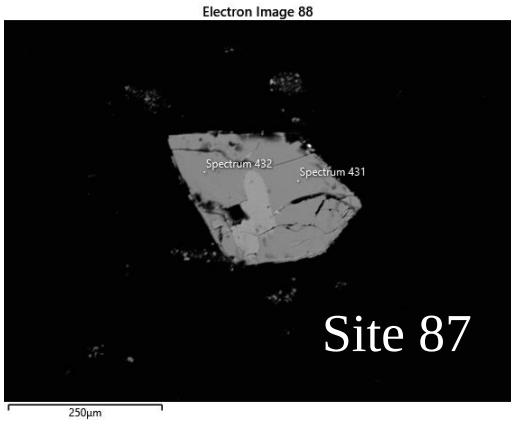

Spectrum	Na	Al	Si	K	Ca	Fe	Ba	Total	Phase	Site
411	8.91	22.1	64.3	0.88	3.25	0.33		99.71	Plagioclase	80
412	8.05	21	61.5	0.91	3.07	0.3		94.83	Plagioclase	80
413	9.4	20.9	66.3	1.46	1.79	0.36	0.43	100.7	Plagioclase	81
414	9.1	20.6	65.1	1.58	1.88			98.21	Plagioclase	81
415	8.94	20	63.8	1.27	1.7			95.72	Plagioclase	81
416	9.14	20.9	66	1.46	1.96			99.42	Plagioclase	82
417	8.26	19.8	62.8	1.34	1.89		0.52	94.58	Plagioclase	82
419	9.09	21.1	65.1	1.22	2.25			98.8	Plagioclase	83
420	8.56	20.4	62.7	1.15	2.36			95.1	Plagioclase	83
421	8.41	21	62.6	0.94	2.8		0.39	96.09	Plagioclase	83
422	9.19	20.8	65.6	1.39	1.85			98.73	Plagioclase	84
424	8.75	20	64	1.33	1.83		0.5	96.37	Plagioclase	84
425	8.77	20.8	66.5	2.28	1.65		0.58	100.6	Plagioclase	85
426	8.04	20	63.4	2.39	1.65	0.32	0.55	96.37	Plagioclase	85
427	8.54	20.3	64.5	1.59	1.99			96.9	Plagioclase	85
428			100					100.3	Quartz	86
429			97.2					97.22	Quartz	86
430			99.8					99.77	Quartz	86
431			99.4					99.42	Quartz	87
432			99.6					99.63	Quartz	87

Site 117 = 82

Plug 3: MC-84-16

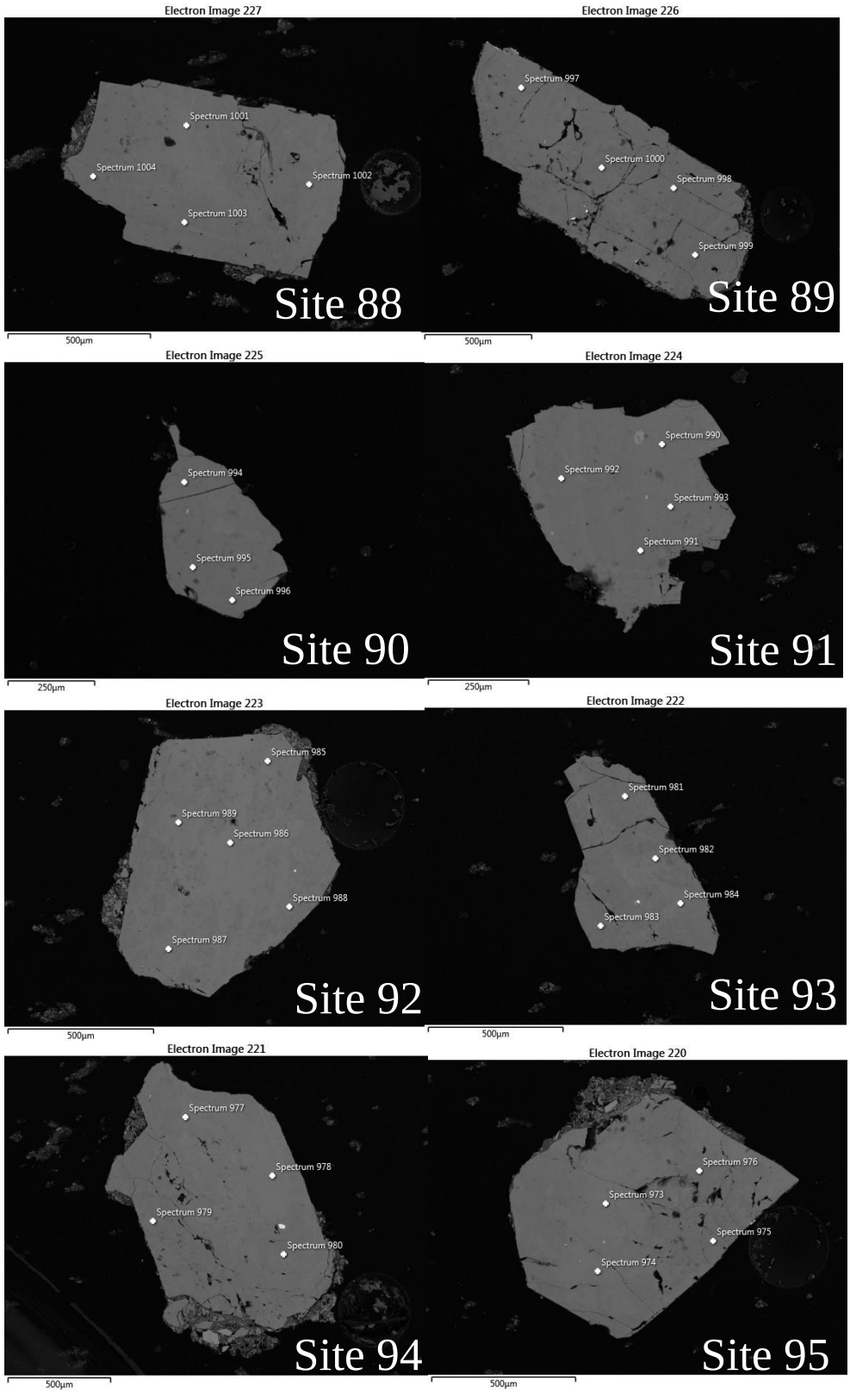

Plug 3: MC-84-16

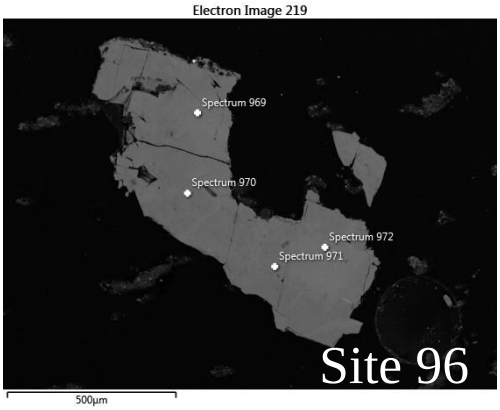

Spectrum	Na	Al	Si	K	Ca	Fe	Total	Mineral	Site
1001	7.06	40.4	48.9		15.4		111.8	Plagioclase	88
1002	8.55	36.7	51.5	0.43	11.8		109	Plagioclase	88
1003	7.76	36.2	49.7		12.1		105.8	Plagioclase	88
1004	8.01	36.7	49.8	0.37	12.3		107.2	Plagioclase	88
997	8.92	37	52.7	0.39	11.6		110.6	Plagioclase	89
998	7.77	37.4	49.9	0.36	12.7		108.1	Plagioclase	89
999	7.88	36	49	0.42	12		105.3	Plagioclase	89
1000	7.43	37.3	49	0.42	13.3		107.5	Plagioclase	89
994	9.07	35.2	52.4	0.4	10.6		107.7	Plagioclase	90
995	8.77	35.3	50.7	0.45	10.8		106.1	Plagioclase	90
996	8.54	34.9	50.8	0.32	10.7		105.2	Plagioclase	90
990	7.43	38.3	50	0.37	13.5		109.5	Plagioclase	91
991	7.74	36.6	49.3	0.34	12.5		106.5	Plagioclase	91
992	8.45	35.9	51.2	0.35	11.4		107.3	Plagioclase	91
993	7.23	37.8	49	0.26	14		108.2	Plagioclase	91
985	6.83	40.9	49.6	0.29	15.8	0.71	114.2	Plagioclase	92
986	6.54	41.2	48.9		16.4	0.63	113.6	Plagioclase	92
987	6.42	40.2	47.5		16	0.85	110.9	Plagioclase	92
988	6.46	39.5	47.5		16.1	0.79	110.3	Plagioclase	92
989	6.87	40.2	49		15.8	0.65	112.4	Plagioclase	92
981	8.87	36.4	52.2	0.49	11		109	Plagioclase	93
982	9.26	35.5	53	0.36	10.1		108.2	Plagioclase	93
983	8.72	34.1	51.3	0.42	9.91		104.4	Plagioclase	93
984	9	35	52.7	0.37	10.2		107.2	Plagioclase	93
977	8.68	37.3	52.5	0.33	12		110.8	Plagioclase	94
978	8.98	37.3	53	0.42	11.3		111	Plagioclase	94
979	9.04	33.9	51.5	0.32	9.69		104.5	Plagioclase	94
980	8.52	34.9	51.2	0.32	10.6		105.4	Plagioclase	94
973	7.93	38.3	51.1	0.3	13.4		111.1	Plagioclase	95
974	7.49	37.6	49.7	0.3	13.2		108.4	Plagioclase	95
975	8.34	35.7	51.1	0.43	10.8		106.4	Plagioclase	95
976	7.68	36.7	49.5	0.31	12.6		106.7	Plagioclase	95
969	8.55	37.5	52	0.49	12.3		110.8	Plagioclase	96
970	7.76	37.7	50.1	0.39	13.1		109.1	Plagioclase	96
971	5.99	40.3	46		16.5		108.9	Plagioclase	96
972	7.68	38.3	50.8	0.31	13.6		110.6	Plagioclase	96

Plug 3: MC-37-16

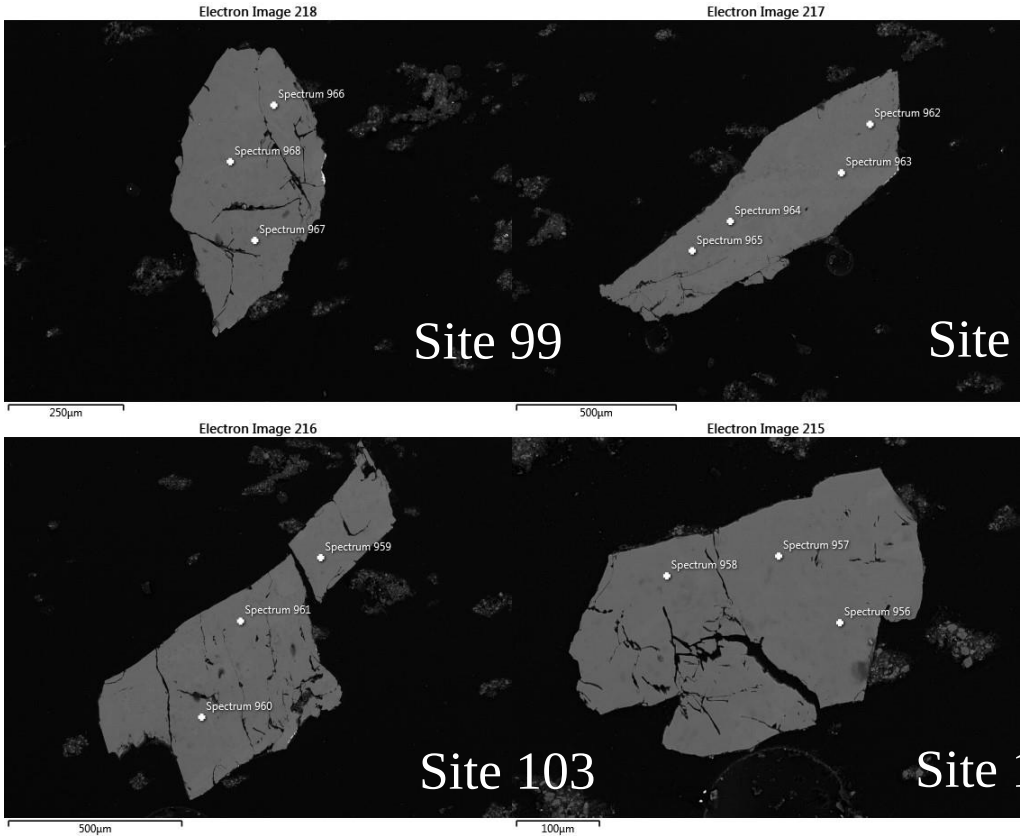

Spectrum	Na	Al	Si	K	Ca	Fe	Ba	Total	Mineral	Site
966	11.7	29.2	57.9	2.01	3.2			104	Plagioclase	99
967	10.7	27.3	55.8	2.28	2.49			98.49	Plagioclase	99
968	11.7	29	58.7	1.93	3.01		0.93	105.3	Plagioclase	99
962	11.5	29	57.9	1.95	3.17			103.4	Plagioclase	101
963	11.4	28.7	57.6	2	2.87	0.63		103.2	Plagioclase	101
964	11.6	28.6	57.1	1.99	3.8	0		103.2	Plagioclase	101
965	11.1	27.9	56	1.94	2.92		0.77	100.6	Plagioclase	101
959	11.4	28.8	57.6	2.03	2.95			102.8	Plagioclase	103
960	11.2	27.7	55.5	2.03	2.88			99.42	Plagioclase	103
961	11.4	29.1	57.7	2.13	2.9		1.12	104.4	Plagioclase	103
956	11.2	28.4	56.6	1.93	2.72			100.8	Plagioclase	104
957	11.7	29.3	57.9	1.89	3		0.82	104.6	Plagioclase	104
958	11.5	28.7	57.5	1.97	3.04			102.6	Plagioclase	104

Plug 3: MC-39-16

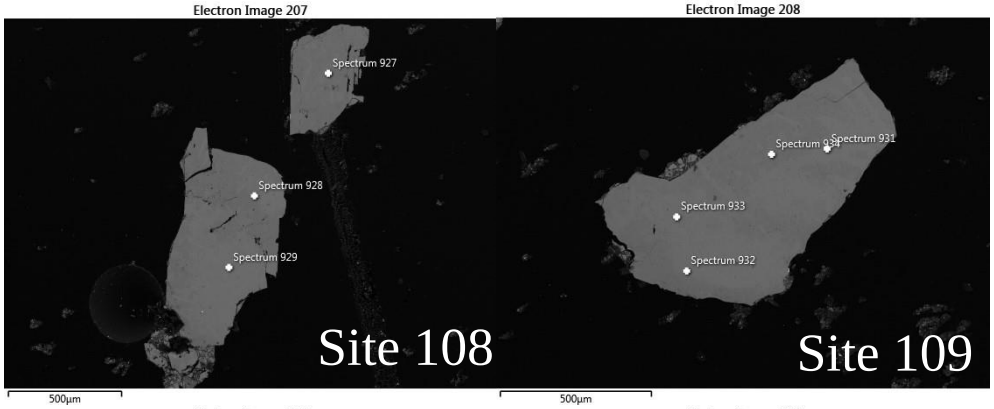

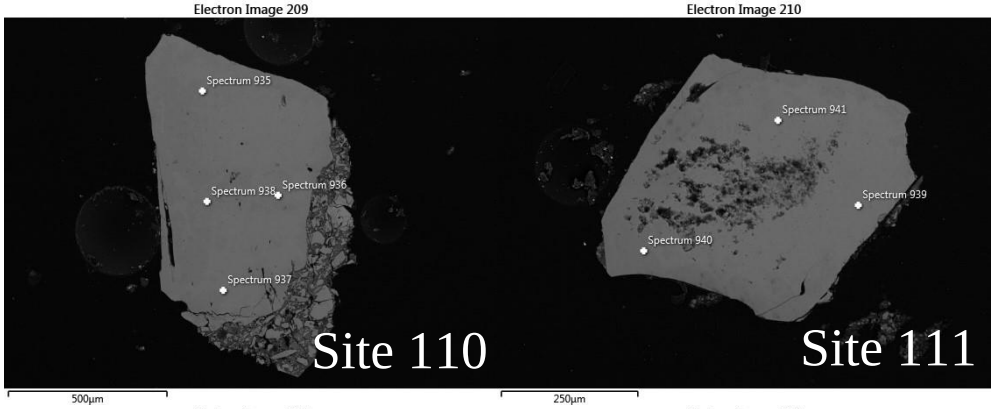

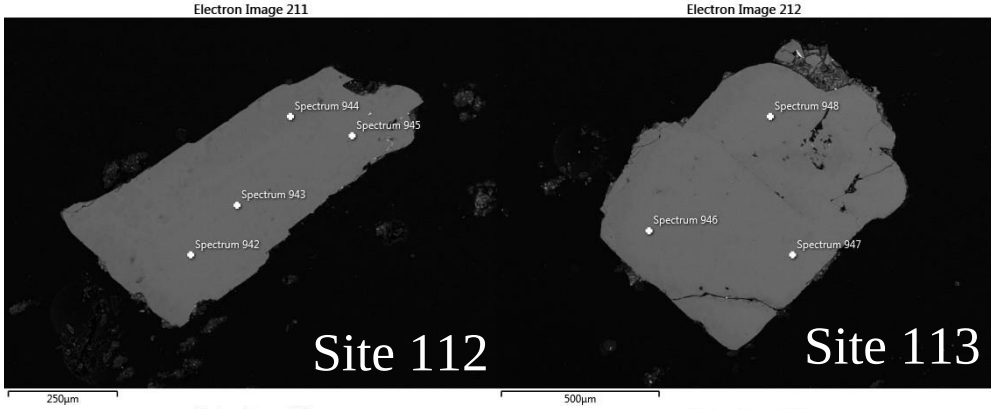

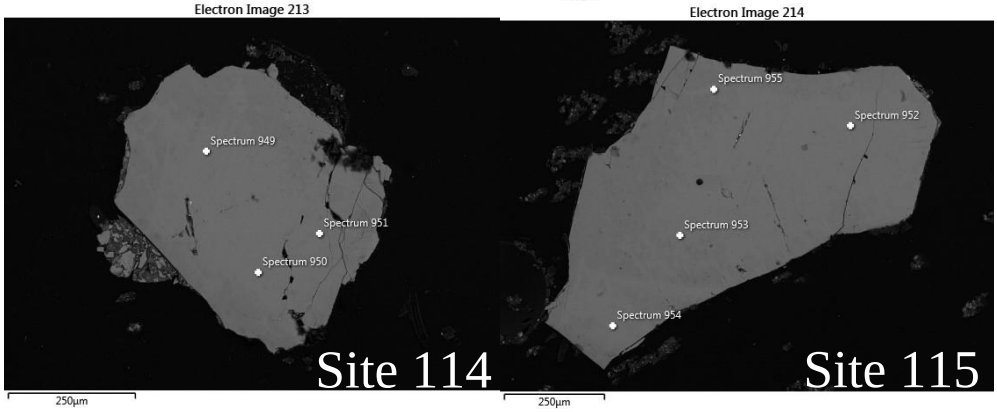

Plug 3: MC-39-16

Spectrum	Na	Al	Si	K	Ca	Total	Mineral	Site
927	11.6	31.1	58.7	1.65	4.29	107.3	Plagioclase	108
928	11.2	30.7	57.3	1.76	4.33	105.2	Plagioclase	108
929	11	29.2	55.1	1.63	3.79	100.7	Plagioclase	108
931	10.7	33.4	55.7	1.09	7.26	108.1	Plagioclase	109
932	10.6	30.1	55.5	1.62	5.07	102.9	Plagioclase	109
933	11.1	31.3	56.4	1.49	5.35	105.7	Plagioclase	109
934	10.6	32.9	56.1	1.22	6.85	107.7	Plagioclase	109
935	11.1	31.8	56.8	1.48	5.5	106.7	Plagioclase	110
936	11.2	30	57.2	1.78	4.14	104.3	Plagioclase	110
937	11.3	29.2	56.7	2.02	3.98	103.3	Plagioclase	110
938	10.9	30	56.2	1.75	4.18	103.1	Plagioclase	110
939	10.4	33.2	54.5	1.1	7.34	106.4	Plagioclase	111
940	10.2	30	53.7	1.23	5.57	100.7	Plagioclase	111
941	10.4	33.9	55.8	0.89	7.92	108.9	Plagioclase	111
942	11.3	30.2	56.8	1.74	4.46	104.5	Plagioclase	112
943	11.5	30.9	57.4	1.66	4.29	105.7	Plagioclase	112
944	11.3	30.7	57.5	1.46	4.06	104.9	Plagioclase	112
945	11.5	30.2	57.1	1.7	3.97	104.4	Plagioclase	112
946	10.9	30.8	56.8	1.82	4.67	105	Plagioclase	113
947	10.4	32.2	55.4	1.31	6.97	106.3	Plagioclase	113
948	10.8	32.7	56.3	1.35	6.81	107.9	Plagioclase	113
949	10.7	32.6	56.7	1.1	6.35	107.4	Plagioclase	114
950	10.7	31.3	55.8	1.47	5.71	105	Plagioclase	114
951	10.8	32.2	56.1	1.32	6.34	106.7	Plagioclase	114
952	10.7	31.6	56.2	1.4	5.57	105.4	Plagioclase	115
953	10.9	31.4	56.1	1.53	5.5	105.5	Plagioclase	115
954	10.6	29.2	54.9	1.77	4.45	100.9	Plagioclase	115
955	11.1	33.2	56.8	1.14	6.65	108.8	Plagioclase	115

Appendix E

Code to plot feldspar data in R

R is a free to use programming language that is specially designed to perform statistical analysis of data. The base program can be downloaded at www.r-project.org. While the base program does come with graphing commands and capabilities, a separate package is needed in order to plot data onto a ternary diagram. The package that was used is called 'ggtern', and can be downloaded at www.ggtern.com. Instructions for installing 'ggtern' and graphing the data are included below. Data files are saved in Excel as csv files prior to importing into R. For the thesis work, the feldspar data was analyzed altogether, and then broken up into separate cvs files based on the units. The cvs files had to be specially formatted in order to run in 'ggtern'. Columns for the individual crystals (Sites), the samples that they're from, and columns for the atomic % of Ab, Or, and An need to be defined for the program to be able to graph the data. Below is an example of the correct format for the data in order to plot in 'ggtern' using the crystal data for Dinner Creek Tuff Units 3 & 4, called unit3_4.csv. The code to create the graph in R can be found on the next page.

Site	Sample	Ab	Or	An
Site 23	MC-3-BC	0.6708099	0.3006084	0.0285817
Site 24	MC-3-BC	0.6657224	0.3088308	0.0254468
Site 25	MC-3-BC	0.7411855	0.1964056	0.0624088
Site 27	MC-3-BC	0.4995383	0.5004617	0
Site 1, 2	MC-63-16	0.5147456	0.018534	0.4667204
Site 3, 4	MC-63-16	0.7746909	0.1751047	0.0502045
Site 5	MC-63-16	0.7815045	0.1673332	0.0511623
Site 6	MC-63-16	0.7774977	0.1713361	0.0511663
Site 7	MC-63-16	0.7721313	0.1793088	0.0485599
Site 8	MC-63-16	0.675129	0.324871	0
Site 9	MC-63-16	0.7785144	0.1720202	0.0494654
Site 10	MC-63-16	0.7763502	0.1743143	0.0493355
Site 11	MC-73-16	0.7746035	0.1757312	0.0496653
Site 12	MC-73-16	0.7743964	0.1628351	0.0627684
Site 13	MC-73-16	0.7753459	0.1721476	0.0525065
Site 14	MC-73-16	0.7679442	0.1881415	0.0439143
Site 15	MC-73-16	0.7731622	0.1777813	0.0490566

```
# Clear R workstation

rm(list=ls(all=TRUE))

# Install 'ggtern' in R.

install.packages("ggtern")

# Load 'ggtern' after it installs

library(ggtern)

# Import data, saved as cvs file into R

data <- read.table("unit3_4.csv", header = TRUE, sep=",")

# Define the base graph and the name of the ends of the ternary

diagram.

base = ggtern(data=data,aes(Ab,Or,An))

# Create ternary diagram with data

base + geom_mask() +
  geom_point(aes(fill=Sample,shape=Sample, color=Sample)) +
```

```
 scale_shape_manual(values=c(1,2,3))

# In the above command, 'geom_mask()' tells R to allow data points to
overlap the boundaries of the plot. 'fill', 'shape', and 'color' are
commands that define the appearance of the data points. Setting them equal
to the Sample column will tell R to assign separate shapes and colors to
the different samples. 'scale_shape_manual(values=c(1,2,3))' defines the
total number of samples, which is three. All of this is included in the
'geom_point(aes())' command, which defines the points to be plotted in
the diagram. The result of all of this will be a graph that looks like
this:
```